



**PONTIFICIA UNIVERSIDAD CATÓLICA DE CHILE**  
**Facultad de Ciencias Biológicas**  
**Departamento de Fisiología**

**Role of endoplasmic reticulum stress on the insulin response in the  
fetoplacental vasculature from pregestational maternal obesity**

**Tesis entregada a la Pontificia Universidad Católica de Chile en cumplimiento parcial  
de los requisitos para optar al Grado de Doctor en Ciencias Biológicas con mención en  
Ciencias Fisiológicas**

**Por**

**ROBERTO ESTEBAN VILLALOBOS LABRA**

**Director de Tesis: Professor Luis Sobrevia**

Departamento de Obstetricia y Ginecología  
Facultad de Medicina

**Co-Director de Tesis: Professor Mauricio Boric**

Departamento de Fisiología  
Facultad de Ciencias Biológicas

**September 30, 2019**

*A mi hijo Benjamín*

## **i. Acknowledgements**

Recuerdo que el inicio de este camino estuvo lleno de entusiasmo y motivación por enfrentarme a nuevos desafíos; sin embargo, éste no estuvo exento de incertidumbre y miedos. Este viaje, que en un comienzo parecía ser largo y difícil, terminó siendo un viaje casi fugaz que me entregó herramientas personales y académicas invaluable; y que, a pesar de ser complejo en algunos momentos, el balance final fue siempre positivo gracias al apoyo de muchas personas. Agradezco a todas ellas por haber hecho posible que llegase a esta instancia.

En primer lugar, quiero agradecer a mis padres, mi hermana y su compañero de vida David, quienes fueron un gran apoyo en lo personal. Siempre estuvieron presentes y preocupados de mi bienestar. También quiero agradecer a mi pequeño hijo Benjamín, quien a su corta edad fue y seguirá siendo la mayor motivación para continuar este camino que he emprendido. Agradezco también a mis abuelos Raúl y Carmen, por recibirme cuando llegué a Santiago y por estar pendientes de mí durante estos años. Agradezco a Jose Luis, quien fue una compañía y apoyo incondicional durante los años del doctorado, y me comprendió en los momentos en los que el tiempo libre era escaso. También, a mi gran amigo Pedro Pichinao, quien me acompañó en mi venida a Santiago y luego fue un apoyo fundamental en los últimos años del doctorado.

Agradezco sinceramente el entusiasmo y la confianza depositada en mí por mi tutor y mentor, el profesor Luis Sobrevia, quien supo guiarme en cada paso que di durante estos años de doctorado; y que, gracias a su constancia, supo empujarme hacia horizontes que estaban más allá de lo que yo vislumbraba. También, al Dr. Marcelo Farías, con quien inicié mi trabajo como bioquímico en Santiago. Su apoyo y consejo fueron fundamentales para tomar la decisión de iniciar mis estudios de PhD, y ha continuado siendo una guía durante este tiempo. No puedo dejar de mencionar al profesor Marcelo González, quien, allá en Concepción, fue el que me abrió las puertas hacia la investigación y el primero en motivarme para que continuara en el camino de la ciencia; quien además, ha continuado siendo mi mentor durante estos años de doctorado.

Debo mencionar, sin duda, a Franciso Westermeier y Pablo Sáez, quienes fueron de gran apoyo en mi llegada a Santiago. Ambos incentivaron y fortalecieron en mí el desarrollo de un pensamiento científico crítico, y fueron fundamentales en los inicios de esta tesis. Pablo Sáez, además de gran amigo, ha sido también uno de mis mentores desde antes de iniciar mi tesis, quien aun estando fuera del país, se dedicó a aconsejar a este estudiante - a veces obstinado -, y fue fundamental en cada una de las decisiones importantes que tomé durante esta tesis.

Quiero agradecer también a toda la familia *CMPliana* - o personas ligadas al laboratorio -, quienes más que ser compañeros de trabajo, fueron mi familia en Santiago. Agradezco a Andrea Leiva y Fabián Pardo, quienes además de amigos fueron de gran apoyo profesional y personal. También agradezco especialmente a mis compañeros de laboratorio Lorena Carvajal, Bárbara Fuenzalida, Luis Silva, Rocío Salsoso y Susana Contreras por el

apoyo académico que me brindaron, quienes además de ser compañeros de trabajo, fueron amigos que me acompañaron de cerca día a día, desde pelearse por la campana de cultivo o las cámaras de western blot, hasta cafecitos a media mañana, idas post laboratorio al Danoi, o *carretes* en algún departamento. Gracias por todos los favores sin retribución – y, obviamente, solicitados a última hora - que hicieron por mí. No puedo dejar de mencionar en este grupo a Mario Subiabre, quien además de ser mi compañero de generación y de laboratorio, fue un gran amigo con el que compartí cada paso en esta carrera. Gracias *perrín* por toda la ayuda en el llenado de formularios, trámites del doctorado y Conicyt. También a Eric Barros, por los consejos siempre oportunos en lo académico y personal, por todos los *breaks* y conversaciones fuera del laboratorio, y por toda la ayuda desinteresada en la elaboración de este escrito. A Andreína Arias e Indira Chiarello, por las conversaciones y risas fuera del laboratorio, el apoyo en los momentos difíciles, y la ayuda y preocupación que mostraron en el desarrollo de mi trabajo. A Tamara Sáez, quien siempre estuvo disponible a distancia para cada consejo que necesité. A Amparo Pacheco, por ser una excelente persona y amiga, colaborando siempre para hacer el trabajo más agradable. También a Javier Ustariz y su compañero de vida Ramiro Guerrero, por ser buenos amigos que siempre estuvieron preocupados por mi bienestar. Agradezco además a Katherinne Bugueño y Carolina Pizarro, quienes estuvieron en el laboratorio en los inicios de mis estudios y se convirtieron en grandes amigas. Gracias, además, a Gonzalo Fuentes y Carolina Oliva, quienes se integraron en este último tiempo al laboratorio, pero aun así supieron dejar una huella en mí.

Todos ustedes llegaron a ser sumamente especiales para mí y atesoraré siempre los buenos momentos en mi memoria.

A todos, sinceramente, gracias.

## ii. Publications

### Articles and Reviews ISI

- Villalobos-Labra R**, Westermeier F, Pizarro C, Sáez PJ, Toledo F, Pardo F, Kusanovic JP, Mardones F, Poblete JA, Sobrevia L, Farías M, Neonates from women with pregestational maternal obesity show reduced umbilical vein endothelial response to insulin, *Placenta*, 2019 (In Press). DOI:10.1016/j.placenta.2019.07.007
- Cabalín C, **Villalobos-Labra R**, Toledo F, Sobrevia L. Involvement of A2B adenosine receptors as anti-inflammatory in gestational diabetes, *Mol Aspects Med.*, 2019: 31-39. DOI:10.1016/j.mam.2019.01.001
- Subiabre M, **Villalobos-Labra R**, Silva L, Fuentes G, Toledo F, Sobrevia L. Role of insulin, adenosine, and adipokine receptors in the foetoplacental vascular dysfunction in gestational diabetes mellitus, *BBA - Mol Basis Dis*, 2019 (In Press). DOI:10.1016/j.bbadis.2018.12.021
- Villalobos-Labra R**, Subiabre M, Toledo F, Pardo F, Sobrevia L. Endoplasmic reticulum stress and development of insulin resistance in adipose, skeletal, liver, and foetoplacental tissue in diabetes, *Mol Aspects Med.*, 2019: 49-61. DOI:10.1016/j.mam.2018.11.001
- Villalobos-Labra R**, Subiabre M, Silva L, Toledo F, Saez PJ, Westermeier F, Pardo F, Farias-Jofre M, Sobrevia L. Pre-pregnancy maternal obesity associates with endoplasmic reticulum stress in umbilical vein endothelium, *BBA - Mol Basis Dis*, 2018: 3195-3210. DOI:10.1016/j.bbadis.2018.07.007
- Pardo F, **Villalobos-Labra R**, Sobrevia B, Toledo F, Sobrevia L. Extracellular vesicles in obesity and diabetes mellitus, *Mol. Aspects Med.*, 2017: 81-91. DOI:10.1016/j.mam.2017.11.010
- Villalobos-Labra R**, Silva L, Subiabre M, Araos J, Salsoso R, Fuenzalida B, Sáez T, Toledo F, González M, Quezada CA, Pardo F, Chiarello D, Leiva A, Sobrevia L. Akt/mTOR role in human foetoplacental vascular insulin resistance in diseases of pregnancy, *J Diab Res*, 2017:5947859. DOI:10.1155/2017/5947859
- Subiabre M, Silva L, **Villalobos-Labra R**, Toledo F, Paublo M, López M, Salsoso R, Pardo F, Leiva A, Sobrevia L. Maternal insulin therapy does not restore foetoplacental endothelial dysfunction in gestational diabetes mellitus, *BBA - Mol Basis Dis*, 2017: 2987-2998. DOI:10.1016/j.bbadis.2017.07.022
- Pardo F, **Villalobos-Labra R**, Chiarello D, Salsoso R, Toledo F, Gutiérrez J, Leiva A, Sobrevia L. Molecular implications of adenosine in obesity, *Mol Aspects Med*, 2017: 90-101. DOI:10.1016/j.mam.2017.01.003
- Sobrevia L, Salsoso R, Fuenzalida B, Barros E, Toledo L, Silva L, Pizarro C, Subiabre M, **Villalobos R**, Araos J, Toledo F, González M, Gutiérrez J, Farías M, Chiarello D, Pardo F, Leiva A. Insulin is a key modulator of fetoplacental endothelium metabolic

disturbances in gestational diabetes mellitus, *Front Physiol*, 2016: 119.  
DOI:10.3389/fphys.2016.00119

Leiva A, Fuenzalida B, Barros E, Sobrevia B, Salsoso R, Sáez T, **Villalobos R**, Silva L, Chiarello I, Toledo F, Gutiérrez J, Sanhueza C, Pardo F, Sobrevia L. Nitric oxide is a central common metabolite in vascular dysfunction associated with diseases of human pregnancy, *Curr Vasc Pharmacol*, 2016: 237-259.  
DOI:10.2174/1570161114666160222115158

Sanhueza C, Araos J, Naranjo L, **Villalobos R**, Westermeier F, Salomon C, Beltrán A, Ramírez MA, Gutiérrez J, Pardo F, Leiva A, Sobrevia L. Modulation of intracellular pH in human ovarian cancer, *Curr Mol Med*, 2016: 23-32.  
DOI:10.2174/1566524016666151222143437

González M, Rojas S, Avila P, Cabrera L, **Villalobos R**, Palma C, Aguayo C, Peña E, Gallardo V, Guzmán-Gutiérrez E, Sáez T, Salsoso R, Sanhueza , Pardo F, Leiva A, Sobrevia L. Insulin reverses D-glucose-increased nitric oxide and reactive oxygen species generation in human umbilical vein endothelial cells, *PLoS One*, 2015.  
DOI:10.1371/journal.pone.01223983

Sáez PJ, **Villalobos-Labra R**, Westermeier F, Sobrevia L, Farías-Jofré M. Modulation of endothelial cell migration by ER stress and insulin resistance: A role during maternal obesity?, *Front in Pharmacol*, 2014. DOI:10.3389/fphar.2014.00189

Westermeier F, Sáez PJ., **Villalobos-Labra R**, Sobrevia L, Farías-Jofré M. Programming of fetal insulin resistance in pregnancies with maternal obesity by ER stress and inflammation, *BioMed Res Internat.*, 2014. DOI:10.1155/2014/917672

### Articles and Reviews Not ISI

Pardo F, Silva L, Salsoso R, Sáez T, Farías M, **Villalobos R**, Leiva A, Sanhueza C, Sobrevia L. Fetoplacental endothelial dysfunction in maternal hypercholesterolemia and obesity in pregnancy. *Physiology Mini-Reviews* 7:60-76, 2014

### Book chapters

Subiabre M, **Villalobos-Labra R**, Silva L, Pardo F, Sobrevia L. Insulin therapy and foetoplacental endothelial dysfunction in gestational diabetes mellitus. In: *Frontiers in Clinical Drug Research-Diabetes & Obesity (FCDR-DO)*. Eds. Atta-ur-Rahman. Ed. Bentham Science Publishers (In press).

### iii. Index of contents

i.	Acknowledgements .....	1
ii.	Publications .....	3
iii.	Index of contents .....	5
iv.	Index of figures .....	8
v.	Index of tables .....	11
vi.	Index of schemes .....	12
vii.	List of abbreviations.....	13
viii.	Resumen .....	16
ix.	Abstract .....	19
1.	Introduction .....	21
1.1	Endothelial dysfunction and vascular insulin response.....	23
1.1.1	The endothelium.....	23
1.1.2	Structure and function of eNOS .....	24
1.1.3	Endothelial dysfunction in PGMO .....	27
1.1.4	Vascular insulin resistance in PGMO .....	29
1.2	Endoplasmic Reticulum Stress .....	31
1.2.1	ER stress and the unfolded protein response .....	34
1.2.2	Association of ER stress with insulin resistance and endothelial dysfunction.....	37
1.2.3	ER stress in fetoplacental vasculature from PGMO.....	41
2.	Hypothesis.....	43
3.	Objectives.....	44
3.1	General objectives .....	44
3.2	Specific objectives.....	44
4.	Methods.....	46
4.1	Study groups.....	46
4.2	Collection of umbilical cords and isolation of HUVECs .....	49
4.3	Experimental conditions.....	50
4.4	Isolation and quantification of proteins.....	50
4.5	Western blot .....	51
4.6	Umbilical vein reactivity .....	53
4.7	Total RNA extraction and reverse transcription.....	54

4.8	Non-quantitative PCR .....	54
4.9	Quantitative PCR.....	54
4.10	L-Arginine transport.....	57
4.11	Intracellular NO determination .....	59
4.12	L-Citrulline determination.....	59
4.13	Arginase activity.....	60
4.14	Quantification of proteins in lysates extracted with KOH .....	61
4.15	Immunofluorescence and confocal microscopy .....	61
4.16	IRE1 $\alpha$ suppression.....	62
4.17	Sample size estimation .....	63
4.18	Statistical analysis .....	64
5.	Results.....	65
5.1	Patients .....	65
5.1.1	Study groups.....	65
5.1.2	Association of GWG and birth weight with the pre-pregnancy BMI .....	65
5.2	Endothelial dysfunction and insulin resistance .....	69
5.2.1	Characteristics of the umbilical vein rings .....	69
5.2.2	Vascular reactivity in response to insulin.....	69
5.2.3	Vascular reactivity in response to CGRP .....	69
5.2.4	NO production by HUVECs in response to insulin .....	76
5.2.5	L-Arginine transport and hCAT-1 .....	82
5.2.6	Insulin signaling .....	86
5.3	Activation of UPR .....	91
5.3.1	Activation of the master UPR sensors.....	91
5.3.2	Pharmacologic modulation of ER stress .....	91
5.3.3	Activity of PERK branch .....	105
5.3.4	Activity of the IRE1 $\alpha$ branch .....	112
5.3.5	Activation of ATF6 .....	113
5.4	ER stress, endothelial dysfunction, and insulin resistance .....	120
5.4.1	ER stress and endothelial dysfunction.....	120
5.4.2	ER stress and insulin response .....	135
5.4.3	Pharmacological inhibition of PERK, IRE1 $\alpha$ , and knockdown of IRE1 $\alpha$ .....	148
5.4.4	PERK and IRE1 $\alpha$ involvement in the impairment of the insulin response .....	159
6.	Discussion .....	169
6.1	Pregestational maternal obesity.....	170
6.2	Insulin desensitization and endothelial dysfunction in fetoplacental vasculature .....	174

6.2.1	PGMO effect on umbilical vein reactivity .....	175
6.2.2	PGMO effect on endothelial function and insulin response in HUVECs .....	177
6.2.3	PGMO effect on L-arginine transport in HUVECs .....	178
6.2.4	PGMO effect on the insulin signaling pathway in HUVECs .....	180
6.3	Endoplasmic reticulum stress in HUVECs from PGMO pregnancies .....	181
6.3.1	PERK signaling branch in HUVECs from PGMO pregnancies .....	182
6.3.2	IRE1 $\alpha$ signaling branch in HUVECs from PGMO pregnancies .....	183
6.3.3	ATF6 activation in HUVECs from PGMO .....	185
6.4	PGMO-associated ER stress and endothelial dysfunction .....	187
6.4.1	PGMO-associated ER stress and NO production.....	187
6.4.2	PGMO-associated ER stress and eNOS activation state .....	188
6.4.3	PGMO-associated ER stress and L-arginine transport.....	189
6.4.4	PGMO-associated ER stress and arginases activity .....	190
6.5	PGMO-associated ER stress and desensitization to insulin .....	191
6.5.1	PGMO-associated ER stress and impaired insulin response.....	191
6.5.2	PERK and IRE1 $\alpha$ involvement in the impairment of the insulin response .....	192
6.6	Final comments .....	195
7.	Conclusions .....	199
8.	Appendix .....	200
9.	References .....	204

#### iv. Index of figures

Figure 1	Endoplasmic reticulum stress and unfolded protein response. ....	36
Figure 2	Relationship of the dependence of gestational weight gain and birth weight on the maternal pre-pregnancy BMI.....	68
Figure 3	Stretching at the optimal diameter. ....	70
Figure 4	KCl-induced contraction at the optimal diameter. ....	71
Figure 5	SNP-induced vasodilation.....	72
Figure 6	Insulin-induced relaxation in human umbilical vein rings.....	73
Figure 7	CGRP-induced relaxation in human umbilical vein rings. ....	74
Figure 8	DAF-FM fluorescent signal in HUVECs.....	78
Figure 9	Total and NOS-dependent NO generation in response to insulin by HUVECs.....	79
Figure 10	Abundance and activation status of eNOS.....	81
Figure 11	L-arginine transport in HUVECs. ....	83
Figure 12	Protein abundance of hCAT-1 in HUVECs.....	85
Figure 13	Abundance and insulin-induced activation of IR.....	88
Figure 14	Abundance and activation status of IRS1. ....	89
Figure 15	Abundance and insulin-induced activation of Akt.....	90
Figure 16	Abundance and activation status of PERK. ....	94
Figure 17	Abundance and activation state of eIF2 $\alpha$ . ....	95
Figure 18	Abundance and activation status of IRE1 $\alpha$ . ....	96
Figure 19	Cellular localization of ATF6. ....	97
Figure 20	Time curve for inactivation of eIF2 $\alpha$ in response to tunicamycin in HUVECs from PGMN pregnancies.....	98
Figure 21	Time curve for inactivation of eIF2 $\alpha$ in response to tunicamycin in HUVECs from PGMO pregnancies.....	99

Figure 22	Time curve for inactivation of eIF2 $\alpha$ in response to TUDCA in HUVECs from PGMN pregnancies. ....	100
Figure 23	Time curve for inactivation of eIF2 $\alpha$ in response to TUDCA in HUVECs from PGMO pregnancies. ....	101
Figure 24	eIF2 $\alpha$ activation state in response to different concentrations of tunicamycin and TUDCA in HUVECs. ....	103
Figure 25	Modulation of PERK phosphorylation by tunicamycin and TUDCA. ....	107
Figure 26	Modulation of eIF2 $\alpha$ phosphorylation by tunicamycin and TUDCA. ....	108
Figure 27	Modulation of CHOP expression by tunicamycin and TUDCA. ....	109
Figure 28	Modulation of TRB3 expression by tunicamycin and TUDCA. ....	110
Figure 29	Modulation of BiP mRNA levels by tunicamycin and TUDCA. ....	111
Figure 30	Modulation of IRE1 $\alpha$ by tunicamycin and TUDCA. ....	115
Figure 31	Modulation of JNK by tunicamycin and TUDCA. ....	116
Figure 32	Processing of XBP1 mRNA by Tunicamycin and TUDCA. ....	117
Figure 33	Effect of tunicamycin and TUDCA treatment on the cellular localization of ATF6. ....	119
Figure 34	ER stress modulation of NO generation in HUVECs. ....	123
Figure 35	ER stress modulation of L-citrulline content in HUVECs. ....	124
Figure 36	Modulation of eNOS abundance and activation state by ER stress. ....	126
Figure 37	Modulation of Akt abundance and activation state by ER stress. ....	127
Figure 38	ER stress effect on arginases activity. ....	130
Figure 39	ER stress effect on L-arginine transport. ....	132
Figure 40	Modulation of hCAT-1 expression in HUVECs by ER stress. ....	134
Figure 41	Involvement of ER stress in the insulin-induced relaxation in umbilical vein rings. ....	137
Figure 42	ER stress modulation of NO generation in response to insulin by HUVECs. .	140

Figure 43	Modulation of the abundance and activation state of eNOS in response to inulin by ER stress. ....	143
Figure 44	Modulation of the abundance and activation state of eNOS in response to inulin by ER stress. ....	145
Figure 45	Modulation of Akt abundance and activation in response to insulin by ER stress .....	146
Figure 46	Modulation of Akt abundance and activation state by ER stress.....	147
Figure 47	Inhibition of PERK by GSK2606114. ....	150
Figure 48	PERK-induction of eIF2 $\alpha$ activation in HUVECs. ....	151
Figure 49	Inhibition of IRE1 $\alpha$ by KIRA6. ....	153
Figure 50	IRE1 $\alpha$ -inhibition effect on JNK and XBP1 processing. ....	155
Figure 51	Knockdown of IRE1 $\alpha$ . ....	156
Figure 52	Effect of IRE1 $\alpha$ Knockdown on the activation of JNK. ....	157
Figure 53	Inhibition of JNK by SP600125.....	158
Figure 54	PERK-inhibition effect on the NOS-dependent NO production in response to insulin. ....	162
Figure 55	Effect of IRE1 $\alpha$ inhibition on the NOS-dependent NO production in response to insulin. ....	163
Figure 56	Effect of IRE1 $\alpha$ inhibition on the NOS-dependent NO production in response to insulin. ....	164
Figure 57	Effect of IRE1 $\alpha$ Knockdown on the activation of IRS1. ....	165
Figure 58	JNK-inhibition effect on the IRS1 activation state. ....	166
Figure 59	IRE1 $\alpha$ involvement in the insulin-induced eNOS activation in HUVECs from PGMO. ....	167
Figure 60	IRE1 $\alpha$ involvement in the insulin-induced Akt activation in HUVECs from PGMO. ....	168
Figure 61	The potential involvement of pre-pregnancy maternal obesity-induced endoplasmic reticulum stress in human umbilical vein endothelial cell dysfunction and insulin desensitization. ....	198

**v. Index of tables**

Table 1 UPR activation in metabolic tissues of patients with obesity..... 33

Table 2 ER stress and induction of endothelial dysfunction and insulin resistance  
in the vasculature ..... 39

Table 3 Selection criteria of biological samples..... 48

Table 4 Antibodies used in Western blot..... 52

Table 5 Oligonucleotide sequences for non-quantitative and quantitative PCR ..... 56

Table 6 Clinical characteristics of pregnant women and newborns ..... 66

Table 7 Parameters for NOS-dependent relaxation to insulin and CGRP in human  
umbilical vein rings..... 75

Table 8 Kinetic parameters for the L-arginine transport in HUVECs..... 84

Table 9 Tunicamycin and TUDCA concentrations and incubation times used in the  
treatment of cells cultures ..... 104

Table 10 Kinetic parameters for the L-arginine transport in HUVECs..... 133

Table 11 Parameters dose-response of NOS-dependent relaxation in response to  
insulin in human umbilical vein rings treated with tunicamycin or TUDCA .... 138

## vi. Index of schemes

Scheme 1. L-arginine uptake and NO generation.....	77
Scheme 2. Insulin signaling pathway in endothelium .....	87
Scheme 3. Key proteins of the unfolded protein response .....	93
Scheme 4. ER stress and endothelial function.....	122
Scheme 5. ER stress and insulin signaling pathway.....	139
Scheme 6. PERK and IRE1 $\alpha$ involvement in the insulin signaling pathway .....	161

## vii. List of abbreviations

ACOG	American College of Obstetricians and Gynecologists
ATF4	Activating transcription factor 4
ATF6	Activating transcription factor 6
BAECs	Bovine aortic endothelial cells
BH <sub>4</sub>	Tetrahydrobiopterin
BiP	Binding immunoglobulin protein
BMI	Body mass index
CaM	Calmodulin
CARE	CCAAT-enhancer binding protein-activating transcription factor response elements
CAT-1	Cationic amino acid transporter isoform 1
CAT-2B	Cationic amino acid transporter isoform 2B
Cav-1	Caveolin 1
cDNA	Complementary DNA
cGMP	Cyclic guanosine monophosphate
CGRP	Calcitonin gene-related peptide
CHOP	CCAAT-enhancer-binding protein homologous protein
CNX	Calnexin
CRT	Calreticulin
DAF-FM	4-Amino-5-methylamino-2',7'-difluorofluorescein diacetate
db/db	Leptin receptor deficient mice
DIO	Diet-induced obesity
DMG	Diabetes mellitus gestational
DMT1	Diabetes mellitus type 1
DMT2	Diabetes mellitus type 2
EC	Endothelial cells
EC <sub>50</sub>	Half maximal effective concentration
EDR	Endothelium-dependent response
eGWG	Excessive gestational weight gain
eIF2 $\alpha$	Subunit $\alpha$ of the eukaryotic translation initiator factor 2
eNOS	Endothelial nitric oxide synthase
ER	Endoplasmic reticulum
ERAD	ER-associated degradation
FMD	Flow-mediated dilation
GWG	Gestational weight gain
HAECs	Human aortic endothelial cells
hCAT-1	Human cationic amino acid transporter isoform 1
hCAT-2B	Human cationic amino acid transporter isoform 2B
HEPES	4-(2-hydroxyethyl)-1-piperazineethanesulfonic acid buffer
HFD	High-fat diet
HG	Hyperglycemia
HOMA-IR	Homeostatic model assessment for insulin resistance
HUVECs	Human umbilical vein endothelial cells
ICAM	Intercellular Adhesion Molecule 1

IL-6	Interleukin 6
iNOS	Inducible nitric oxide synthase
IOM	Institute of Medicine (US)
IR	Insulin receptor
IRE1 $\alpha$	Inositol-requiring enzyme 1 $\alpha$
IRS-1	Insulin receptor substrate 1
IUGR	Intrauterine growth restriction
JNK	c-jun N-terminal kinase 1
K <sub>m</sub>	Michaelis-Menten constant
MAECs	Mouse aortic endothelial cells
MAPK	Mitogen-activated protein kinases
MCEC	Mouse coronary endothelial cells
MINSAL	Ministerio de Salud de Chile
MRA	Mesenteric resistance arteries
mRNA	Messenger ribonucleic acid
NADPH	Nicotinamide adenine dinucleotide phosphate hydrogenated
nNOS	Neuronal nitric oxide synthase
NO	Nitric oxide
NOS	Nitric oxide synthase
NO <sub>x</sub>	Nitrite/nitrate levels
O <sub>2</sub>	Molecular oxygen
OAT	Omental adipose tissue
OCTT	Oral glucose tolerance test
PBS	Phosphate-buffered saline
PCM	Primary culture medium
PCR	Polymerase Chain Reaction
PDI	Protein disulfide isomerase A3
PDK1	3-phosphoinositide-dependent protein kinase 1
PERK	Protein kinase RNA-like endoplasmic reticulum kinase
PGMO	Pre-gestational maternal obesity
PI3K	Phosphatidylinositol 3-kinase
PIP3	Phosphatidylinositol 3,4,5-trisphosphate
PKA	Protein kinase A
PKC	Protein kinase C
QUICKI	Quantitative insulin sensitivity check index
Rh	Rhesus D antigen
RIDD	IRE1-dependent decay
R <sub>max</sub>	Maximum relaxation
SAT	Subcutaneous adipose tissue
Ser	Serine residue
sGC	Soluble guanylate cyclase
Sh2	Src homology 2
SNP	Sodium nitroprusside
Thr	Threonine residue
TNF $\alpha$	Tumor necrosis factor $\alpha$
TRAF2	Tumor necrosis factor receptor-associated factor 2
TRB3	Tribbles-like protein 3

TUDCA	Tauroursodeoxycholic acid
Tyr	Tyrosine residue
UPR	Unfolded protein response
VAT	Visceral adipose tissue
VCAM	Vascular cell adhesion protein 1
$v_i$	Initial velocity
$V_{max}$	Maximum velocity
$V_{max}/K_m$	Maximum transport capacity
XBP1	X-box binding protein 1
XBP1s	Spliced X-box binding protein 1
XBP1u	Unspliced X-box binding protein 1

## **viii. Resumen**

La prevalencia de mujeres con obesidad en Chile ha aumentado drásticamente en las últimas décadas, alcanzando un 38,4% de las mujeres mayores de 18 años en el año 2017. La obesidad en el embarazo es un factor de riesgo independiente tanto para la madre como para el feto, quienes presentan mayor riesgo para el desarrollo de diabetes gestacional, preeclampsia, anomalías congénitas, macrosomía y mortalidad materna o fetal. Además, se ha demostrado que los efectos adversos inducidos por la obesidad durante el embarazo sobre el feto perduran durante toda su vida. Estudios epidemiológicos muestran que la obesidad materna pre-gestacional (PGMO) es un factor de riesgo para el desarrollo de resistencia a la insulina y disfunción endotelial en neonatos y adolescentes, las cuales son condiciones fisiopatológicas consideradas como los primeros estados que conducen al desarrollo de síndrome metabólico y complicaciones cardiovasculares. En cuanto a los mecanismos involucrados, se ha mostrado que la disfunción endotelial y la resistencia a la insulina presentes en obesidad están estrechamente asociadas con estrés del retículo endoplásmico (RE). Por otro lado, estudios sugieren que PGMO induce disfunción endotelial y resistencia a la insulina en vasculatura fetoplacentaria. Sin embargo, se desconoce si el estrés de RE está presente en el endotelio fetoplacentario de embarazos PGMO y si está involucrado en la disfunción endotelial y la alterada respuesta a la insulina. Así, la hipótesis de este estudio propone que "la obesidad materna pre-gestacional genera una menor respuesta a la insulina en la vasculatura fetoplacentaria humana debido a una disfunción endotelial asociada al estrés del retículo endoplásmico".

En esta tesis se demostró que PGMO se asoció con disfunción endotelial y resistencia a la insulina en venas umbilicales, la cuales no mostraron vasodilatación en

respuesta a CGRP o insulina. La menor respuesta vascular se asoció con una producción reducida de óxido nítrico (NO) debido a una menor activación de la sintasa del NO endotelial (eNOS) en las células endoteliales de vena umbilical humana (HUVECs). Además, la insulina no activó la vía de señalización metabólica post-IR, eNOS y no aumentó la producción de NO en respuesta a la insulina en estas células. Los resultados muestran que el transporte de L-arginina estaba aumentado, sugiriendo un mecanismo compensatorio que parece no ser suficiente para recuperar la producción de NO. Por otro lado, PGMO se asoció con un aumento de la actividad de UPR en HUVECs. Se encontró un aumento en la actividad de las vías de señalización asociados a PERK e IRE1 $\alpha$ , así como de la translocación de ATF6 al núcleo. La reducción del estrés de ER mediante TUDCA (100  $\mu$ M) redujo la actividad de las tres vías de la UPR y generó una reducción del transporte de L-arginina, un aumento de la actividad eNOS basal e inducida por insulina, de la producción de NO, y sensibilizó la activación de la vía de señalización de insulina en respuesta a insulina. Así, el estrés del RE asociado a PGMO se asoció con la disfunción endotelial y la desensibilización a la insulina presentadas por HUVECs. Por otro lado, las alteraciones observadas en HUVECs PGMO fueron reproducidas en HUVECs de embarazos PGMN al inducir ER stress con tunicamicina (5  $\mu$ ). Finalmente, el aumento de la expresión de TRB3 inducida por PERK, una pseudoquinasa que inhibe Akt, no parece estar involucrado en la menor respuesta de insulina presentada por las HUVECs de embarazos de madres con PGMO. Sin embargo, el aumento en la actividad de IRE1 $\alpha$  y la consiguiente activación de JNK generó inhibición de IRS1, reducción de Akt, activación de eNOS y producción de NO en respuesta a la insulina. Por lo tanto, la vía IRE1 $\alpha$ /JNK/IRS1 se propone como un probable mecanismo en el deterioro de la vía de señalización de insulina producida por el estrés de RE en las HUVEC de embarazos PGMO. Así, este estudio plantea que PGMO produce disfunción endotelial y

desensibilización a la insulina en el endotelio de la vena umbilical a través de la generación de estrés de RE.

## **ix. Abstract**

The prevalence of women with obesity has rapidly increased in Chile, reaching 38.4% of women over 18 years in 2017. Obesity during pregnancy is an independent risk factor to both the mother and the fetus, who are at higher risk to develop gestational diabetes, preeclampsia, congenital anomalies, macrosomia, and maternal or fetal mortality. Moreover, the obesity-induced adverse effects during pregnancy on the fetus remain throughout the offspring lifespan. Epidemiological studies indicated that pre-gestational maternal obesity (PGMO) is a risk factor for the development of insulin resistance and endothelial dysfunction in neonates and adolescents, which are pathophysiological states considered as the first steps leading to the development of metabolic syndrome and cardiovascular complications. On the other hand, studies suggest that PGMO induces endothelial dysfunction and insulin resistance in fetoplacental vasculature. Among the mechanisms, it has been shown that in obesity the endothelial dysfunction and insulin resistance are closely associated with endoplasmic reticulum (ER) stress. However, whether ER stress is present in the fetoplacental endothelium from PGMO pregnancies and whether it is involved in endothelial dysfunction and altered insulin response is unknown. Therefore, we hypothesized that ‘Pre-gestational maternal obesity generates a lower response to insulin in the human fetoplacental vasculature due to endoplasmic reticulum stress-associated endothelial dysfunction’.

In this thesis we demonstrated that PGMO was associated with endothelial dysfunction and insulin resistance in umbilical veins, which did not show vasodilation in response to calcitonin gene-related peptide or insulin. This deficient vascular response was associated with reduced nitric oxide (NO) production due to reduced activation of the endothelial nitric oxide synthase (eNOS) in human umbilical vein endothelial cells (HUVECs). Moreover,

insulin did not activate the post-IR metabolic signaling pathway, eNOS and did not increase the NO production in response to insulin in these cells. The transport of L-arginine was found increased, suggesting a compensatory mechanism that seems unable to recover the NO production. On the other hand, PGMO was associated with higher UPR activity in HUVECs. The activity of the signaling pathways activated by PERK and IRE1 $\alpha$  was increased, as well as the translocation of ATF6 to the nucleus. The amelioration of ERS by TUDCA (100  $\mu$ M) reduced the activity of the three pathways of the UPR and resulted in a reduction of the L-arginine transport, an increase of the basal and insulin-induced eNOS activity, the NO production, and sensitized the activation of the insulin signaling pathway in response to insulin. Thus, the PGMO-associated ERS was related to the endothelial dysfunction and the insulin desensitization seen in HUVECs. On the other hand, the impairment seen in HUVECs from PGMO was reproduced in HUVECs from PGMN pregnancies by the induction of ER stress with tunicamycin. Finally, the increased PERK-induced TRB3 expression, a pseudokinase that inhibits Akt, was not involved in the lower insulin response by HUVECs from PGMO. However, the increased IRE1 $\alpha$  activity and the consequent activation of JNK, resulted in inhibition of IRS1, inhibition of Akt, eNOS activation and NO production in response to insulin. Thus, the IRE1 $\alpha$ /JNK/IRS1 pathway is a likely mechanism in the deterioration of the insulin signaling pathway produced by the ER stress in the HUVECs from PGMO pregnancies. Therefore, this study shows that PGMO resulted in endothelial dysfunction and insulin desensitization in the endothelium of the umbilical vein through the generation of ER stress.

## 1. Introduction

Obesity is a metabolic disease whose prevalence is increasing worldwide (World Health Organization (WHO), 2018). More than 650 million adults were obese in 2016, three times the worldwide prevalence in 1975 (WHO, 2018). According to the latest report from the Ministry of Health (MINSAL) of Chile, the prevalence of obesity is 9% higher than in 2011, reaching 34.4% of the population. The percentage among women reached 38.4% are women (MINSAL, 2017). Epidemiologic evidence shows that pre-gestational maternal obesity (PGMO) (body mass index (BMI)  $\geq 30$  kg/m<sup>2</sup>) is an independent risk factor for the development of gestational diabetes mellitus or preeclampsia (American College of Obstetricians and Gynecologists (ACOG), 2005). Furthermore, the offspring of PGMO mothers are predisposed to develop obesity, cardiovascular disease and metabolic disorders in childhood and adulthood (Gaillard et al., 2014; Godfrey et al., 2017; Mamun et al., 2009; Pirkola et al., 2010; Roberts et al., 2015; Stuebe et al., 2012, 2009). The latter support the possibility that some risk factor could be ‘transferable’ from the mothers to their children. Indeed, newborns from insulin-resistant obese mothers showed increased insulin resistance at birth (Catalano et al., 2009; Desoye, 2018). The possibility that harmful factors would be transferred from obese mothers to children has been addressed in the literature (Penfold and Ozanne, 2015); however the mechanism(s) involved are not fully understood.

The transference of risk factors occur during pregnancy (Longtine and Nelson, 2011; Sobrevia et al., 2014), in a phenomenon referred to as “fetal programming” (Barker, 1998; Gluckman et al., 2008). This is supported by findings showing that after weight loss following bariatric surgery, children born to these mothers presented lower incidence of obesity and insulin resistance compared to their siblings born before the intervention

(Guenard et al., 2013; Kral et al., 2006; Smith et al., 2009). Fetoplacental tissues play a vital role in this phenomenon since they are the structural and functional connection of the fetus with the mother (Griffiths and Campbell, 2015). The placenta is an organ specialized in vital processes including gas exchange, transport of ions, nutrients, and waste products between the maternal and fetal plasma. Maternal substances are transferred from the maternal blood through the chorionic villous into the fetal capillaries. Blood flows through chorionic veins and reaches the umbilical vein returning the freshly oxygenated blood to the fetal circulation (Griffiths and Campbell, 2015; Villalobos-Labra et al., 2018b). Even when the fetoplacental tissues are a transient organ, altered function of this tissue is crucial in the fetal outcome with lifetime lasting consequences (Howell and Powell, 2017; Longtine and Nelson, 2011; Sobrevia et al., 2014).

Obesity in adults associated with endothelial dysfunction and vascular insulin resistance, both of which are critical conditions in the early stages of the development of cardiovascular disease (Janus et al., 2016; Prieto et al., 2014; Versari et al., 2009). Reports available in the literature showed that, among the alterations associated to obesity, there is a strong correlation with abnormal endoplasmic reticulum (ER) homeostasis resulting in accumulation of misfolded proteins, a condition referred to as 'ER stress' (Battson et al., 2017; Cnop et al., 2012; Lenna et al., 2014). Obesity during pregnancy associates with endothelial dysfunction in human umbilical vein endothelial cells (HUVECs), umbilical veins (Pardo et al., 2015; Schneider et al., 2015), chorionic arteries (Schneider et al., 2015), and vascular (Pardo et al., 2015) and systemic (Catalano et al., 2009; Desoye, 2018) insulin desensitization in the fetus. Indeed, fetoplacental tissues from mothers with obesity showed high plasma level of inflammatory and oxidative markers (Bar et al., 2012; Ferretti et al.,

2014; Saben et al., 2014), which are in close association with ER stress (Flamment et al., 2012). Thus, the occurrence of ER stress appears to be a direct factor in the development of endothelial dysfunction and insulin resistance in fetoplacental tissues from PGMO mothers.

## **1.1 Endothelial dysfunction and vascular insulin response**

### *1.1.1 The endothelium*

The endothelium is a continuous monolayer of cells covering the inner side of the blood vessels. This tissue not only acts as a barrier of separation and exchange between intra and extravascular spaces, but it is also a major player in the control of the vascular tone, blood fluidity, platelet aggregation, regulation of immunity, inflammation, angiogenesis, and is considered to act as an endocrine organ (Félétou, 2011). Thus, the endothelium participates in the signaling to and from the vascular lumen by directly interacting with blood cells (such as leukocytes, platelets or erythrocytes) and with other cells from the vascular wall (smooth muscle cells, fibroblasts, immune cells). Alterations of these endothelial functions result in a condition known as ‘endothelial dysfunction’. The endothelial dysfunction is defined as ‘the shift of the properties of the endothelium toward a phenotype characterized by impaired vasodilation and a proinflammatory and prothrombic status’ (Soriano et al., 2017). It is characterized by ‘an imbalance between vasodilating and vasoconstricting substances produced by (or acting on) endothelium’ (Deanfield et al., 2005). This condition is considered one of the main and first factors leading to the initiation, development and perpetuation of cardiovascular pathologies (Sandoo et al., 2015). The endothelial dysfunction appears even decades before a clinical outcome associated with a cardiovascular disease (Davignon and Ganz, 2004). Therefore, studying endothelial dysfunction is crucial to understand the cellular and molecular mechanisms underlying the development of cardiovascular disease.

Endothelial dysfunction associates with abnormal generation of nitric oxide (NO), one of the main vasodilators released by the endothelium and critical in the regulation of vasomotor tone (Gimbrone and García-Cardeña, 2016). Once NO is produced, it diffuses from the endothelium reaching the underlying layer of smooth muscle cells. At this site, NO activates the soluble guanylyl cyclase (sGC) leading to the relaxation of smooth muscle cells (Gimbrone and García-Cardeña, 2016). Moreover, the deficiency of NO generation has been associated with peripheral vasoconstriction, which is a typical characteristic of metabolic syndrome (Mendizábal et al., 2013). Therefore, understanding the mechanisms leading to abnormal NO synthesis in pathological conditions turns out to be crucial to study the contribution of endothelial dysfunction in the development of cardiovascular disease.

### *1.1.2 Structure and function of eNOS*

NO is synthesized from L-arginine via the nitric oxide synthases (NOS), releasing L-citrulline as a byproduct. There are three mammalian isoforms of NOS: inducible (iNOS), neuronal (nNOS) and endothelial (eNOS). The eNOS is the dominant isoform expressed in the vasculature, being the main enzyme synthesizing the endothelium-derived NO in physiological conditions. It is constitutively expressed but its abundance can be up- or downregulated at a transcriptional and post-transcriptional level. Its activity is modulated at a post-translational level by  $\text{Ca}^{2+}$ /calmodulin (CaM) binding, L-arginine uptake, availability of cofactors and activating and inhibiting phosphorylations (Balligand et al., 2009; Fleming, 2010; Förstermann and Sessa, 2012; Mas, 2009; Rafikov et al., 2011).

eNOS is mainly located in the caveolae and the peri-area of the Golgi apparatus. It is an enzyme with two domains that functions as a dimer. Each subunit is formed by an N-terminal oxygenase domain that binds to heme, L-arginine, tetrahydrobiopterin ( $\text{BH}_4$ ) and

Ca<sup>2+</sup>/calmodulin (CaM), and a C-terminal reductase domain that binds to nicotinamide adenine dinucleotide phosphate (NADPH), flavin mononucleotide (FMN), and flavin adenine dinucleotide (FAD). In its inactive state, eNOS is coupled to caveolin-1 (Cav-1) decreasing its activity by preventing the binding of CaM (Michel et al., 1997). Besides, eNOS is constitutively phosphorylated in Thr 495 by PKC, which also prevents the binding to CaM. Its activation occurs by an increase in the intracellular calcium level resulting in dissociation of eNOS from Cav-1 and formation of a multi-protein complex with CaM, the chaperone heat shock protein 90 (HSP-90), and the recruiting of Akt and protein kinase A (PKA). These kinases enhance the NO production by phosphorylating the enzyme in serine 1177 (Balligand et al., 2009; Fleming, 2010; Gimbrone and García-Cardena, 2016).

The mechanism of NO synthesis starts by the delivery of electrons from NADPH to the flavins in the reductase domain of one subunit, which are then transferred to the heme in the oxygenase domain of the other subunit. Finally, the heme iron binds oxygen (O<sub>2</sub>) and catalyzes the NO synthesis from L-arginine. The CaM-binding is crucial for the eNOS activation, since it dimerizes the enzyme and enables the electron transference from the reductase to the oxygenase domain (Balligand et al., 2009; Fleming, 2010; Hellermann and Solomonson, 1997; Mas, 2009). Moreover, the calcium level is crucial to activate the enzyme, but it is only necessary to maintain the basal NO production. The maximal capacity of NO production does not depend on the calcium level, but on post-translational modifications. Several eNOS activity-modulatory phosphorylations have been reported, but the phosphorylation in threonine 495 and serine 1177 are considered the central modulators (Fleming, 2010). The phosphorylation in threonine 495 disrupts the binding of CaM to the reductase domain, blocking the enzyme activation and reducing the basal eNOS activity by

about 10-20 times. On the other hand, phosphorylation in serine 1177 enhances the electron flux at the reductase domain increasing the efficiency of NO production by about 2-3 times over the basal (Fleming, 2010).

It is reported that extracellular L-arginine availability is also crucial to eNOS activity in endothelial cells (Casanello et al., 2007; Hardy and May, 2002; Mann et al., 2003; Toral et al., 2018). However, while the extracellular L-arginine level is around 50-200  $\mu\text{M}$ , the intracellular level in endothelial cells can reach 800  $\mu\text{M}$  or higher. Moreover, the affinity of purified eNOS for L-arginine is lower than the intracellular level ( $K_m = 2.9 \mu\text{M}$ ) (Hardy and May, 2002), suggesting that the enzyme is operating under a saturated level of its substrate. Despite this, the NO production by endothelium is highly dependent on the extracellular L-arginine, as reported in animal models (Cooke et al., 1992), humans (Clarkson et al., 1996; Cooke and Dzau, 1997; Drexler et al., 1991; Mirmiran et al., 2016), and in human endothelial cell cultures (Toral et al., 2018; Wyatt et al., 2002). The dependence of eNOS activity on the extracellular level of L-arginine, even when its intracellular level is higher, is described as the 'L-arginine paradox' (Hardy and May, 2002; Kurz and Harrison, 1997). This apparent controversy could be explained by 'L-arginine compartmentalization' (Casanello et al., 2007; Closs et al., 2004; Cynober, 2002), where the L-arginine contained in caveolae, which is used by eNOS for the synthesis of NO, is dependent on the amino acid transport from the extracellular medium and independent on other intracellular pools (Casanello et al., 2007).

L-Arginine is taken up from the extracellular space via several plasma membrane transport systems, including the system  $y^+$  (Mann et al., 2003). System  $y^+$  is a family of proteins referred to as human cationic amino acids transporters (hCATs). hCATs members include hCAT-1, hCAT-2A, hCAT-2B, hCAT-3, and hCAT-4 (Mann et al., 2003). The

transport of L-arginine in HUVECs is mainly mediated by hCAT1 and hCAT-2B (Rajapakse et al., 2016; Vásquez et al., 2004), whose affinities for L-arginine are 100-200  $\mu$ M and 200-400  $\mu$ M, respectively (Casanello et al., 2007). The NO synthesized by eNOS requires the expression and activity of CAT-1, since CAT-1 co-localizes with eNOS in caveolae (García-Cardena et al., 1996; McDonald et al., 1997). Indeed, a direct interaction of eNOS with CAT-1, which reduces the affinity of eNOS for cav-1 and stimulates its activation, has been reported (Li et al., 2005). Moreover, the transport activity of CAT-2B is required for iNOS activation in other cell types (Cynober, 2002). Thus, a structural and functional association of eNOS with CAT-1 more than CAT-2B is suggested (Casanello et al., 2007).

### *1.1.3 Endothelial dysfunction in PGMO*

Endothelial dysfunction is described in the vasculature of pregnant women with PGMO (Stewart et al., 2007). The occurrence of endothelial dysfunction in fetoplacental tissues from PGMO women has also been reported. Chorionic arteries from mothers with exceeded weight (overweight and obesity) during pregnancy show impaired vasodilation in response to calcitonin gene-related peptide (CGRP) (Schneider et al., 2015), an endothelial-dependent vasodilator (Brain, 2004; Dong et al., 2004). In addition, umbilical veins from mothers with normal pre-pregnancy weight ending the pregnancy with obesity presented lower NOS-dependent vasodilation. An increased threonine 495 phosphorylation but reduced serine 1177 phosphorylation, eNOS expression and L-citrulline production was found in HUVECs from that condition (Pardo et al., 2015). These findings suggest a deficient activity of eNOS giving a mechanistic explanation for the impaired endothelium-dependent vasodilation seen in these vessels (Pardo et al., 2015). Likewise, the umbilical arteries from PGMO mothers present higher resistance to blood flow, a finding that may relate to the occurrence of endothelial

dysfunction in these vessels (Sarno et al., 2015). Altogether, the described results suggest the occurrence of endothelial dysfunction in fetoplacental vessels from PGMO mothers and raise NO deficiency as one of the potential causes of the altered endothelial function.

The altered transport of L-arginine in the fetoplacental endothelium has been seen in several metabolic pregnancy complications associated with obesity. Among these are preeclampsia, intrauterine growth restriction (IUGR) or in gestational diabetes mellitus (GDM). HUVECs from GDM showed increased hCAT-1 expression and L-arginine transport, which correlated with higher NO production (Vásquez et al., 2004). Meanwhile, HUVECs from mothers with preeclampsia showed higher hCAT-1 expression and L-arginine transport but lower NO synthesis (Salsoso et al., 2015). Conversely, HUVECs from IUGR show reduced hCAT-1 expression, L-arginine transport, and NO synthesis (Casanello et al., 2009). However, there is no information addressing whether L-arginine and hCAT-1 expression are altered in the fetal endothelium from PGMO pregnancies. Interestingly, increased L-arginine level and reduced L-citrulline and nitrite/nitrate levels (NO<sub>x</sub>, an index of NO bioavailability) is reported in the serum from subjects with obesity (Giam et al., 2016; Gruber et al., 2008). It is also reported that after weight reduction by bariatric surgery there is a decrease in the plasma level of L-arginine and increase in the NO<sub>x</sub> level, suggesting that overweight reduced the transport of L-arginine and NO production (Sledzinski et al., 2010). On the other hand, obese mice show reduced CAT-1 expression, and the overexpression of CAT-1 in the endothelium resulted in preventing obesity-reduced NO<sub>x</sub> (Rajapakse et al., 2014). The obesity-induced hypertension was also reduced in these mice (Rajapakse et al., 2015, 2014). Therefore, the endothelial dysfunction in the fetoplacental vasculature of PGMO may involve altered CAT-1 expression and L-arginine transport.

#### *1.1.4 Vascular insulin resistance in PGM0*

Obesity also associates with systemic insulin resistance, a condition related to endothelial dysfunction and chronic cardiometabolic disorders (Flamment et al., 2012; Georgescu et al., 2011; Mather et al., 2013; Muniyappa and Sowers, 2013). Insulin resistance characterizes by low sensitivity and responsiveness to insulin in target tissues, including the vasculature (Kim et al., 2006; M. Breen and Giacca, 2011; Savage et al., 2005). Insulin resistance becomes more important in the vasculature since the endothelial insulin resistance contributes to induce endothelial dysfunction (Duncan et al., 2008).

One of the most relevant effects of insulin in the control of vascular tone is the stimulation of NO synthesis by the endothelium (Muniyappa et al., 2007; Zeng and Quon, 1996). The biological effects of insulin in the vasculature starts with the activation of the insulin receptor (IR) in the endothelium. The activation of this tyrosine kinase type receptor results in a parallel and balanced activation of two major signaling pathways: the phosphoinositide 3-kinase (PI3K)/Akt pathway, known as the metabolic branch and has been described to induce vasodilation; and the Ras/mitogen-activated protein kinases (MAPK) pathway, known as the mitogenic branch and has been described to induce vasoconstriction. The activation of both branches promotes cardiovascular and endothelial growth, cell metabolism, and a healthy vascular function (D'Oria et al., 2017; Muniyappa and Sowers, 2013). The state of insulin resistance is characterized by impaired metabolic branch resulting in excessive activation of the mitogenic branch, leading to impaired insulin-induced vasodilation, thus, contributing to the endothelial dysfunction (Clark et al., 2003; D'Oria et al., 2017; Mather et al., 2013).

The activation of the metabolic branch results in vasodilation via increased NO production (Muniyappa et al., 2007). The activation of this pathway begins with the IR

activation and subsequent activation of the isoform 1 of the insulin receptor substrate 1 (IRS1) through phosphorylation of tyrosine residues. The phosphorylation of IRS1 exposes Src homology 2 (Sh2) domain-binding motifs that bind to Sh2-containing proteins such as PI3K. The docking of PI3K to IRS1 activates the protein which produces phosphatidylinositol 3,4,5-trisphosphate (PIP3) inducing the phosphorylation and activation of phosphoinositide-dependent kinase-1 (PDK1). Subsequently, PDK1 phosphorylates the serine residue 473 of Akt which, after being recruited by dimerized eNOS, phosphorylates the enzyme in serine 1177 and leads to the increased production of NO (Manrique et al., 2014; Muniyappa et al., 2007). In this context, the insulin resistance occurs by the phosphorylation of IRS1 in serine residues, thus reducing the affinity of the protein for the IR and the scaffolding proteins and leading to the inhibition of insulin signaling (Muniyappa et al., 2007).

Patients with obesity show vascular insulin resistance, which is evidenced by lower insulin-induced vasodilation (Farb et al., 2016; Georgescu et al., 2011). Insulin resistance impaired the metabolic branch, in several tissues in obese patients, such as adipose tissue, liver, or skeletal muscle. Therefore, we speculate that the reduced insulin-induced vasodilation in the vasculature from obese patients is due to its associated blunted metabolic branch (Huang, 2009; Huang et al., 2018; Mather et al., 2013). There is evidence supporting this idea from studies in animal models showing that the vasculature from obese mice show lower insulin-induced activation of IRS1, Akt, and eNOS (Naruse et al., 2006; Symons et al., 2009).

It is also reported that newborns (Catalano et al., 2009), children and adults (Mingrone et al., 2008; O'Reilly and Reynolds, 2013; Tan et al., 2015) born to mothers with PGMO also

showed systemic insulin resistance. In a study of the transcriptome of trophoblast cells from the first trimester of pregnancy in mothers with PGMO, the insulin-induced gene expression was lower compared with cells from normal pregnancies (Lassance et al., 2015). These findings suggest lower insulin sensitivity in these cells from obese mothers. In another set of studies the fetoplacental vasculature from mothers with obesity also shows signs of insulin resistance since a genetic profile associated to insulin resistance in umbilical cords from PGMO mothers was found (Thakali et al., 2014). Additionally, a null response to insulin was reported by umbilical veins from mother that started pregnancy with normal weight and ended with obesity (Pardo et al., 2015). Thus, although there are no reports directly addressing it, the occurrence of insulin resistance in the fetoplacental vasculature from PGMO mothers is strongly suggested.

## **1.2 Endoplasmic Reticulum Stress**

Several factors in obesity contribute to the dysfunction of metabolic organs, including the vasculature, such as systemic proinflammatory state, increased concentration of circulating free fatty acids in blood, or hyperlipidemia (Hardy et al., 2012; Noakes, 2018). Interestingly, all these factors are involved in the induction of ER stress (Alhusaini et al., 2010; Boden et al., 2014; Esser et al., 2014; Mandal et al., 2017; Villalobos-Labra et al., 2018b) and obesity associated-metabolic dysfunction (Table 1) (Villalobos-Labra et al., 2018b; Yilmaz, 2017). Indeed, ER stress shows a strong relationship with insulin resistance and endothelial dysfunction in obesity (Table 2), and with other metabolic syndrome-associated diseases (Battson et al., 2017; Cnop et al., 2012; Flamment et al., 2012). Thus, ER stress is proposed as a key factor in the mechanism of obesity-induced insulin resistance and endothelial dysfunction (Cnop et al., 2012; Flamment et al., 2012; Yilmaz, 2017). However,

the cellular mechanisms linking ER stress with endothelial dysfunction and vascular insulin resistance in PGMO are not described. Hence, this thesis focused on the understanding of the effect of ER stress on endothelial dysfunction and insulin resistance in the fetoplacental vasculature from PGMO mothers.

**Table 1. UPR activation in metabolic tissues of patients with obesity**

<i>Pathology</i>	<i>Tissue/cell</i>	<i>Effect</i>	<i>Protein abundance</i>	<i>mRNA level</i>	<i>Reference</i>
Obesity	SAT	Increased	PDI CRT CNX P~JNK1	XBP1s	Boden et al., 2008
Obesity	Antecubital vein EC	Increased	PERK IRE1 $\alpha$ ATF6		Kaplon et al., 2013
PGMO	OAT	Increased	IRE1 $\alpha$ BiP	XBP1s	Liong and Lappas, 2015
Obesity	Adipose tissue	Increased	P~eIF2	XBP1s ATF6	Sharma et al., 2008
Obesity	Abdominal SAT	Increased	P~eIF2 BiP P~JNK1	XBP1s	Gregor et al., 2009
Obesity	Abdominal SAT	Increased	IRE1 $\alpha$ BiP	ATF6	Alhusaini et al., 2010
Obesity	SAT	Increased	CHOP P~JNK1	–	Díaz-Ruiz et al., 2015
PGMO	Skeletal muscle	Increased	IRE1 $\alpha$ BiP	XBP1s	Liong and Lappas, 2016
PGMO	Placenta	Increased	P~eIF2	XBP1s	Yung et al., 2016
Severe obesity <sup>a</sup>	VAT, SAT	Increased	BiP	XBP1s	Vendrell et al., 2010

EC, endothelial cells; SAT, subcutaneous adipose tissue; OAT, omental adipose tissue; VAT, visceral adipose tissue; P~PERK, phosphorylated protein kinase RNA-like endoplasmic reticulum kinase; TRB3, tribbles-like protein 3; PDI, protein disulfide isomerase A3; CRT, calreticulin; CNX, calnexin; P~JNK1, phosphorylated c-jun N-terminal kinase 1; XBP1s, spliced X-box binding protein 1 mRNA; IRE1 $\alpha$ , inositol-requiring enzyme 1 $\alpha$ ; BiP, binding immunoglobulin protein; P~eIF2, phosphorylated eukaryotic translation initiator factor 2; ATF6, activating transcription factor 6; CHOP, CCAAT-enhancer-binding protein homologous protein. –, not reported. <sup>a</sup> Severe obesity refers to BMI  $\geq$  40 kg/m<sup>2</sup>.

### *1.2.1 ER stress and the unfolded protein response*

ER is an organelle responsible for the synthesis and processing of secretory and membrane proteins, Ca<sup>2+</sup> storage and lipid biosynthesis (Cnop et al., 2012; Flamment et al., 2012). The ER homeostasis is maintained by a variety of modulatory mechanisms to ensure cell survival, proliferation, and growth, among others. A disturbance of this state results in the accumulation of misfolded proteins that leads to ER stress and the unfolded protein response (UPR). The latter is intended to restore the homeostasis of the endoplasmic reticulum and results in the alteration of the cellular metabolism. UPR is the starting point for activation of three canonical ER stress transducers at the ER membrane, i.e. the protein kinase RNA-like endoplasmic reticulum kinase (PERK), inositol-requiring enzyme 1-alpha (IRE1 $\alpha$ ), and activating transcription factor 6 (ATF6) (Ghemrawi et al., 2018; Hetz et al., 2015; Mukherjee et al., 2015) (Figure 1). One major modulator described to UPR activation after ER stress is the ER chaperone binding immunoglobulin protein (BiP) (Flamment et al., 2012). During unstressed conditions, PERK, IRE1 $\alpha$  and ATF6 are inactivated by binding to BiP at the lumen side of the ER. Under ER stress, BiP is displaced from the transducers to bind with misfolded luminal proteins, which releases PERK, IRE1 $\alpha$  and ATF6 and leads to their activation (Cnop et al., 2012; Flamment et al., 2012).

PERK is a tyrosine kinase-like protein which is activated by phosphorylation in threonine 981. This kinase phosphorylates the alpha subunits of the eukaryotic initiation factor 2 (eIF2 $\alpha$ ) in serine 51, leading to its inactivation and thus to a rapid decrease of cap-dependent translation, causing the attenuation of the global protein synthesis. However, that alteration results in the selective translation of specific proteins that are translated by other mechanisms. One of them is cap-independent, which do not require the eIF2-protein complex because they

have internal ribosome entry sites (IRESs) (Komar and Hatzoglou, 2011). Other mechanism is for proteins containing more than one upstream open reading frame in their mRNA sequence (Chambers and Marciniak, 2014; Kilberg et al., 2009), as for the activating transcription factor 4 (ATF4). ATF4 is a key transcription factor for PERK-modulated gene expression, which triggers the transcription by binding to CCAAT-enhancer binding protein-activating transcription factor response elements (CARE).

IRE1 $\alpha$  is activated by trans-autophosphorylation and shows kinase and endoribonuclease activity catalyzing the processing of X-box binding protein 1 (XBP1) mRNA cleaving a 26-nucleotide intron and shifting the reading frame to translate the processed form of the transcription factor XBP1 (XBP1s). Additionally, IRE1 $\alpha$  degrades other RNA targets by a process known as regulated IRE1-dependent decay (RIDD). The cytosolic domain of IRE1 $\alpha$  binds to tumor necrosis factor receptor-associated factor 2 (TRAF2), activating the c-jun N-terminal kinase (JNK) pathway through IRE1 $\alpha$  kinase domain. Meanwhile, ATF6 translocates to the Golgi where is cleaved. The cleaved-off cytoplasmic domain acts as a transcription factor leading to the suppression and expression of several genes. Through phenomena such as expression of chaperones, foldases, and proteins involved in ER-associated degradation (ERAD) machinery, redox metabolism, autophagy, and apoptosis (e.g. CCAAT-enhancer-binding protein homologous protein (CHOP)), among others, the UPR reduces the unfolded protein load and increases the size and the folding capacity of ER to restore its homeostasis (Cnop et al., 2012; Dufey et al., 2014; Ghemrawi et al., 2018).

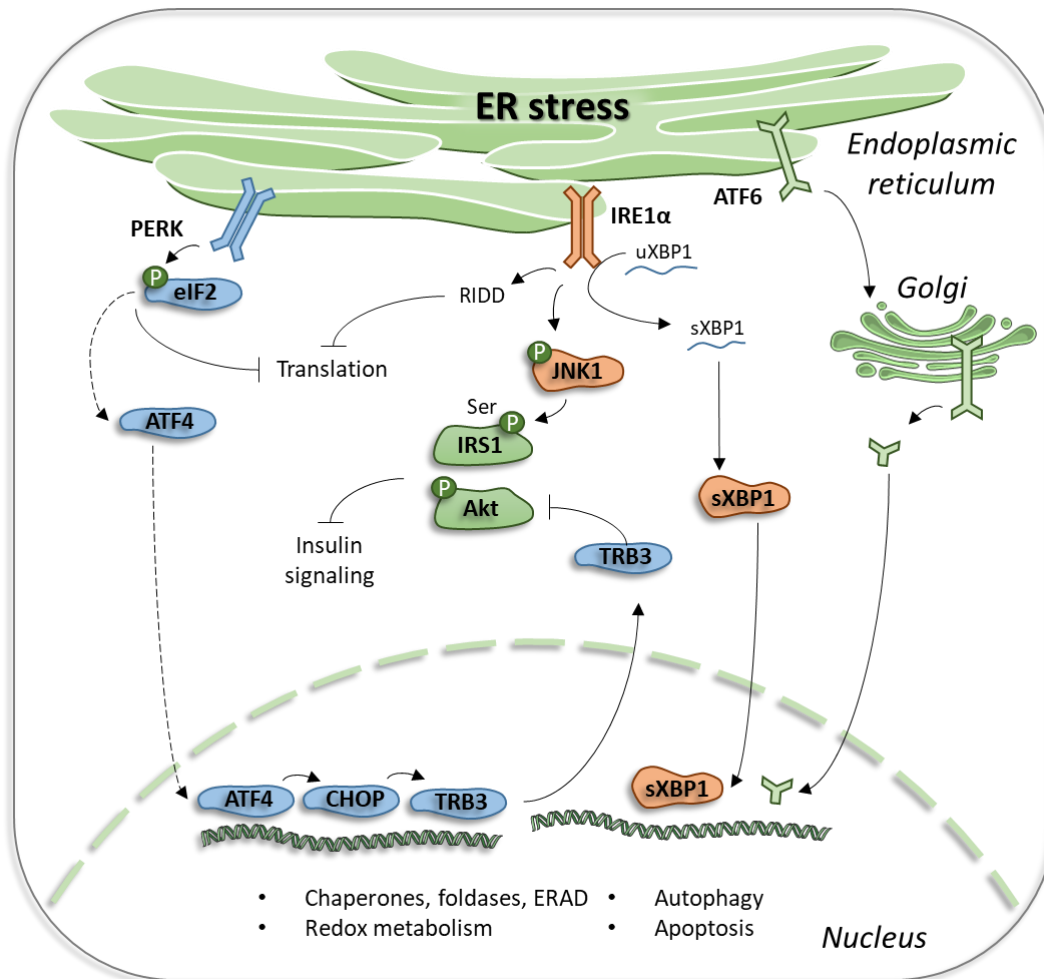


**Figure 1. Endoplasmic reticulum stress and unfolded protein response.** Endoplasmic reticulum (ER) stress leads to the activation of the unfolded protein response through the activation of protein kinase RNA-like endoplasmic reticulum kinase (PERK), inositol-requiring enzyme 1- $\alpha$  (IRE1 $\alpha$ ) and activating transcription factor 6 (ATF6). PERK phosphorylates the  $\alpha$  subunit of eukaryotic translation initiator factor 2 (eIF2), attenuating the general translation and enhancing the expression of activating transcription factor 4 (ATF4), CCAAT-enhancer-binding protein homologous protein (CHOP) and ultimately tribbles-like protein 3 (TRB3), which alters insulin signaling by inhibiting Akt. IRE1 $\alpha$  activates c-jun N-terminal kinase (JNK) by phosphorylation, which reduces insulin signaling by phosphorylating insulin receptor substrate 1 (IRS1) in serine residues. IRE1 $\alpha$  also produces an unconventional splicing of the unspliced X-box binding protein 1 (uXBP1) mRNA, shifting the reading frame to translate a more stable protein known as spliced XBP1 (sXBP1). Besides, IRE1 $\alpha$  contributes to the attenuation of the general translation by the regulated IRE1-dependent decay (RIDD) of mRNA. ATF6 migrates to the Golgi where is cleaved, releasing a fraction that works as transcription factor. ATF4, sXBP1 and the cleaved fraction of ATF6 work as transcription factors addressed to modulate genes involved in ER metabolism, ER-associated degradation (ERAD), redox metabolism, autophagy and apoptosis, among others, leading to restore the ER homeostasis or, ultimately, cell death.

### 1.2.2 Association of ER stress with insulin resistance and endothelial dysfunction

Several mechanisms linking ER stress with insulin resistance are described in obesity. The most studied are the IRE1 $\alpha$ -dependent activation of JNK and the activation of PERK/eIF2/ATF4 signaling (Figure 1). JNK phosphorylates IRS1 in serine residues, inhibiting the enzyme and contributing to the obesity associated-systemic insulin resistance (Flamment et al., 2012; Hirosumi et al., 2002; Ozcan et al., 2004). It is also reported that JNK is involved in reducing the vasodilation in response to insulin of visceral arterioles from obese subjects (Farb et al., 2016). The activation of PERK/eIF2/ATF4 signaling results from ATF4 inducing the expression of CHOP, a transcription factor that together with ATF4 leads to the expression of tribbles-like protein 3 (TRB3) (Ohoka et al., 2005). TRB3 is a pseudokinase that inhibits Akt activity promoting insulin resistance (Du et al., 2003; Flamment et al., 2012; Koh et al., 2013; Marinho et al., 2015; Ozcan et al., 2013). TRB3 expression is increased in the blood (Nourbakhsh et al., 2017) and skeletal muscle (Koh et al., 2013) from obese subjects, as well as in other metabolic tissues affected by obesity in mice (Du et al., 2003; Lima et al., 2009; Liu et al., 2010; Ozcan et al., 2013). Thus, JNK and TRB3 are factors involved in the obesity-induced insulin resistance and both are potential candidates in the development of insulin resistance in the fetoplacental vasculature from PGMO.

ER stress is also related to the development of endothelial dysfunction (Battson et al., 2017) (Table 2). The treatment of mouse coronary artery endothelial cells with tunicamycin, which induces ER stress by the inhibition of *N*-glycosylation of proteins (Mahoney and Duksin, 1980), reduced the levels of mRNA, protein, serine 1177 phosphorylation of eNOS and nitrite. Co-incubation of these cells with tauroursodeoxycholic acid (TUDCA), a bile

acid that acts as a chaperone reducing ER stress (Kraskiewicz and Fitzgerald, 2012), blocked tunicamycin-induced ER stress (Galán et al., 2014). Furthermore, HUVECs treated with tunicamycin showed reduced serine 1177 phosphorylation of eNOS and null production of NO in response to a calcium ionophore (Murugan et al., 2015), as described in mouse aortic endothelial cells (Cheang et al., 2014). Thus, ER stress has been linked with lower eNOS activity in endothelial cells.

On the other hand, ER stress is proposed to affect endothelial function by affecting the L-arginine transport. CAT-1 expression is shown to increase following the activation of the PERK/eIF2/ATF4 signaling pathway (Kilberg et al., 2009). CAT-1 expression is increased after eIF2 $\alpha$  phosphorylation (Fernandez et al., 2002b) since its gene contains an IRES region (Fernandez et al., 2002a). Moreover, the sequence of hCAT-1 has a CARE region whose expression is regulated by ATF4 (Kilberg et al., 2009; Lopez et al., 2007; Majumder et al., 2009). Thus, the expression of CAT-1 depends on the levels of phosphorylated eIF2 $\alpha$  and ATF4 (Huang et al., 2010; Lopez et al., 2007) suggesting a key role of the PERK/eIF2/ATF4 signaling as an inductor of L-arginine transport. Since the structural interaction (Li et al., 2005) and the L-arginine transport by CAT-1 is crucial to eNOS activity, and because the ER stress reduced the expression and activity of eNOS, it is likely that the ER stress in the endothelium results in endothelial dysfunction. Therefore, the occurrence of endothelial dysfunction could be due to ER stress in the fetoplacental vasculature from PGMO mothers.

**Table 2. ER stress and induction of endothelial dysfunction and insulin resistance in the vasculature**

	<i>Tissue/EC</i>	<i>ER stress modulation</i>		<i>UPR protein evaluated</i>	<i>Effect</i>	<i>Parameter evaluated</i>	<i>Reference</i>
		<i>Induction</i>	<i>Reduction</i>				
Endothelial function	Mouse aorta MCEC	Tunicamycin	TUDCA	P~PERK P~eIF2 $\alpha$ CHOP BiP ATF6	Decrease	P~eNOS NO production Endothelium-dependent response	Galán et al., 2014
	Mouse aorta MRA	Angiotensin II Tunicamycin	TUDCA PBA	P~eIF2 $\alpha$ ATF4 CHOP BiP	Decrease	P~eNOS Endothelium-dependent response	Kassan et al., 2012
	Mouse aorta HUVECs	Angiotensin II Tunicamycin	TUDCA PBA	P~eIF2 $\alpha$ CHOP BiP ATF6	Decrease	P~eNOS NO production Endothelium-dependent response	Murugan et al., 2015
	Mouse aorta MAECs	HFD <sup>a</sup> Tunicamycin	Metformin	P~eIF2 $\alpha$ ATF6	Decrease	P~eNOS NO production Nitrite levels Endothelium-dependent response	Cheang et al., 2014
	Rat aorta	Homocysteine	TUDCA PBA	P~eIF2 $\alpha$ ATF6	Decrease	Endothelium-dependent response	Cheang et al., 2015
	Mouse aorta MAECs	db/db <sup>b</sup> Hyperglycemia	TUDCA PBA	P~eIF2 $\alpha$ ATF6 XBP1s P~JNK	Decrease	P~eNOS NO production Endothelium-dependent response	Cheang et al., 2017
	Mouse aorta MRA HUVECs	Tunicamycin	TUDCA	BiP P~PERK P~eIF2 $\alpha$ CHOP	Decrease	Endothelium-dependent response	Kassan et al., 2017

				ATF6			
Coronary artery	db/db <sup>b</sup>	TUDCA	BiP P~PERK P~eIF2 $\alpha$ P~IRE1 $\alpha$	Decrease	Endothelium-dependent response ICAM VCAM	Choi et al., 2016	
Human brachial artery	Hyperglycemia	TUDCA	–	Decrease	FMD	Walsh et al., 2016	
Insulin response	HUVECs	Plasma <sup>c</sup> Thapsigargin Tunicamycin	TUDCA PBA BiP P~PERK P~eIF2 $\alpha$ P~IRE1 $\alpha$ XBP1s	Decrease	Insulin-induced P~eNOS NO production	Di Pietro et al., 2017	
	Mesentery arterioles HAECs BAECs	Palmitate HFD <sup>a</sup>	TUDCA BiP CHOP XBP1s JNK	Decrease	Insulin-induced P~IRS1 P~Akt P~eNOS Vasodilation	Kim et al., 2015	
	Human EC <sup>d</sup>	Diabetes	Liraglutide P~IRE1 $\alpha$ P~PERK P~JNK CHOP	Decrease	Insulin-induced P~eNOS	Bretón-Romero et al., 2018	

EC, endothelial cell; ER stress, endoplasmic reticulum stress; UPR, unfolded protein response; MCECs, mouse coronary endothelial cells; TUDCA, Tauroursodeoxycholic acid; MRA, mesenteric resistance arteries; HUVECs, human umbilical vein endothelial cells; MAECs, mouse aortic endothelial cells; FMD, flow-mediated dilation; HAECs, human aortic endothelial cells; BAECs, bovine aortic endothelial cells. –, not reported. <sup>a</sup>High-fat diet-fed mouse as a model of obesity; <sup>b</sup>leptin receptor deficient db/db mouse as a model for obesity and type 2 diabetes; <sup>c</sup>Plasma from obese young patients; <sup>d</sup>Human peripheral venous endothelial cells from forearm veins of diabetic and non diabetic patients.

### *1.2.3 ER stress in fetoplacental vasculature from PGMO*

Obese subjects show over-activation of the UPR in the antecubital vein endothelial cells suggesting a condition of ER stress (Kaplun et al., 2013). Also, skeletal muscle from PGMO women shows ER stress (Liong and Lappas, 2015). Moreover, offspring from pregnant mice with obesity presented with ER stress in liver and adipose tissue, suggesting a likely transference of this metabolic alteration from mothers with PGMO to their offspring. However, there is not information addressing whether the fetoplacental vasculature from PGMO mothers presents ER stress.

The occurrence of some alterations associated with ER stress in the fetoplacental tissue from obese women suggest the occurrence of ER stress in this tissue. Placentas from mothers with obesity showed higher levels of tumor necrosis factor  $\alpha$  (TNF $\alpha$ ) and interleukin 6 (IL-6) (Bar et al., 2012; Ferretti et al., 2014; Saben et al., 2014), two pro-inflammatory cytokines that induce ER stress in different cell types (Denis et al., 2010; Hardy et al., 2012; Hu et al., 2006; McArdle et al., 2013; Xue et al., 2005). Oxidative stress, which is also tightly associated with ER stress (Flamment et al., 2012), was also detected in these placentas. Moreover, other studies showed that placentas from PGMO mothers exhibit higher expression of phosphorylated JNK (Saben et al., 2013), suggesting activation of IRE1 $\alpha$  and JNK as probable candidate in the induction of insulin resistance in this tissue. The latter, along with the occurrence of endothelial dysfunction and insulin resistance in the fetoplacental vasculature, suggests that ER stress might be present and participate in vascular dysfunction in the fetoplacental vasculature from PGMO mothers.

The available information strongly suggests that the fetoplacental vasculature from PGMO mothers shows endothelial dysfunction and insulin resistance. Also, ER stress could

be crucial in the transference of risk from the mother to the fetus. Thus, this thesis proposes that PGMO induces endothelial dysfunction and insulin resistance in the fetoplacental vasculature via a mechanism involving ER stress in the vascular endothelium.

## **2. Hypothesis**

Pre-gestational maternal obesity causes a lower response to insulin in the fetoplacental vasculature due to endoplasmic reticulum stress-associated endothelial dysfunction.

### **3. Objectives**

#### **3.1 General objectives**

1. To establish whether PGMO pregnancy resulted in endothelial dysfunction and reduced fetoplacental vasculature response to insulin.
2. To establish whether PGMO pregnancy caused endoplasmic reticulum stress in the fetoplacental endothelium.
3. To evaluate whether PGMO-associated endoplasmic reticulum stress caused endothelial dysfunction and insulin resistance in fetoplacental vasculature.

#### **3.2 Specific objectives**

*For general objective 1*

1. To assess whether the human umbilical veins from PGMO pregnancy show reduced endothelium-dependent dilation in response to insulin.
2. To demonstrate whether PGMO reduces the eNOS expression and activity in HUVECs.
3. To demonstrate whether PGMO alters the L-arginine transport and hCAT-1 expression in HUVECs.
4. To evaluate whether HUVECs from PGMO present reduced insulin-induced activation of the insulin signaling pathway and eNOS.

*For general objective 2*

1. To assess whether HUVECs from PGMO pregnancy show increased activation of the PERK signaling pathway.
2. To evaluate whether HUVECs from PGMO pregnancy show increased endoribonuclease and kinase activity of IRE1 $\alpha$ .
3. To assay whether ATF6 is activated in HUVECs from PGMO pregnancy.

*For general objective 3*

1. To assay whether the repression of endoplasmic reticulum stress restores the vasodilation in response to insulin in umbilical veins from PGMO pregnancy.
2. To determine whether the repression of endoplasmic reticulum stress restores L-arginine transport, eNOS activity, and insulin-induced activation of the insulin signaling pathway in HUVECs from PGMO pregnancy.
3. To evaluate whether the inhibition of PERK restores the insulin response in HUVECs from PGMO pregnancy.
4. To evaluate whether the inhibition of IRE1 $\alpha$  restores insulin response in HUVECs from PGMO pregnancy.
5. To propose a model for the causal relationship between endoplasmic reticulum stress, endothelial dysfunction, and insulin signaling in the fetoplacental vasculature from PGMO pregnancy.

## 4. Methods

### 4.1 Study groups

This study included patients from the Hospital Clínico UC-CHRISTUS and San Juan de Dios Hospital (Santiago, Chile). The umbilical cords were collected at birth from pregnant women with pre-pregnancy normal weight ( $n = 48$ ) (hereafter referred to as 'PGMN', BMI 18.5-24.9 kg/m<sup>2</sup>) or with pre-pregnancy obesity ( $n = 64$ ) (hereafter referred to as 'PGMO', BMI  $\geq 30$  kg/m<sup>2</sup>) (IOM and NRC, 2009; WHO, 2018). PGMN and PGMO groups were selected based on the inclusion and exclusion criteria listed in Table 3. Pregnant women included in this study did not smoke or consume drugs or alcohol and had no intrauterine infection or any other medical or obstetrical complications. The ethnicity of patients included in this study was Hispanic. The investigation conforms to the principles outlined in the Declaration of Helsinki and counts with Ethics Committee approval from the Faculty of Medicine of the Pontificia Universidad Católica de Chile. Patient written and informed consents were obtained 12-24 h before delivery.

Weight of women before pregnancy was self-reported. All pregnant women were evaluated for weight and height, and BMI was recorded at the first interview with the treating obstetrician (i.e. 5-12 weeks of gestation, 1<sup>st</sup> trimester of pregnancy) and at delivery (37.1-41.0 weeks of gestation). Pregnant women with normal glycaemia at the first trimester of pregnancy were also evaluated by the oral glucose tolerance test (OGTT) with a unique glucose load (75 g fasting) at 24-28 weeks of gestation to discard GDM (according to the Perinatal Guide 2015 from the Health Ministry of Chile) (Ministerio de Salud; Gobierno de Chile, 2015). Basal glycemia  $<5.55$  mM ( $<100$  mg/dL) after 8-9 hours from the last feeding

and  $<7.9$  mM ( $<140$  mg/dL) at two hours after glucose load was considered as normal (Ministerio de Salud; Gobierno de Chile, 2015).

**Table 3. Selection criteria of biological samples**

<b>Inclusion</b>	<b>Exclusion</b>
PGMN, Pre-gestational BMI 18.5-24.9 kg/m <sup>2</sup>	GDM
PGMO, Pre-gestational BMI $\geq$ 30 kg/m <sup>2</sup>	DMT1 or DMT2
Single fetus	Pre-eclampsia
Gestational age $\geq$ 37 weeks	IUGR
	Clinical chorioamnionitis
	Intrahepatic cholestasis of pregnancy
	Rh isoimmunization
	Renal alteration
	Hypertension
	Autoimmune alteration
	Presence of meconium in the amniotic fluid
	Chronic pathology
	Consumption of cigarettes, alcohol or any other drug during pregnancy

PGMN, pre-gestational maternal normal weight; PGMO, pre-gestational maternal obesity; BMI, body mass index; GDM, gestational diabetes mellitus; DMT1, diabetes mellitus type 1; DMT2, diabetes mellitus type 2; IUGR, intrauterine growth restriction; Rh, Rhesus D antigen.

## 4.2 Collection of umbilical cords and isolation of HUVECs

Placentas were collected at delivery on ice and transferred to the laboratory until use 15-30 minutes later. Middle sections of umbilical cords (100-120 mm length) were dissected into 200 mL phosphate-buffered saline (PBS) solution (mM: 130 NaCl, 2.7 KCl, 0.8 Na<sub>2</sub>HPO<sub>4</sub>, 1.4 KH<sub>2</sub>PO<sub>4</sub>, pH 7.4, 4°C) and kept in this solution until use 6-12 hours later for the isolation of the endothelial cells.

HUVECs were obtained from the umbilical cord vein by the method described initially by Jaffe and colleagues (Jaffe et al., 1973) and adapted in the laboratory (Villalobos-Labra et al., 2018a). The protocol consisted of cannulating the umbilical vein, replenishing the venous lumen with type II collagenase (0.25 mg/mL; Collagenase Type II from *Clostridium histolyticum*, Boehringer, Mannheim, Germany) dissolved in M199 medium (Gibco, Gibco Life Technologies, Carlsbad, CA), and incubating the umbilical cord at 37°C for 15 minutes. After digestion, the cord was gently massaged and the cell suspension was removed by centrifugation at 1200 rpm for 10 minutes. The resulting pellet was resuspended in primary culture medium (PCM: M199 supplemented with 3.2 mM L-glutamine, 100 U/mL penicillin/streptomycin (Gibco, Gibco Life Technologies, Carlsbad, CA), 10% fetal bovine serum (FBS) (Gibco) and 10% newborn calf serum (NBCS) (Gibco)). The cell suspension was transferred to cell culture dishes (25 cm<sup>2</sup> surface) previously covered with 1% gelatin (Merck Millipore, Billirica, MA, USA). Cells were kept in a humidified environment at 37°C with an atmosphere of 5% CO<sub>2</sub> equilibrated with air. The whole PCM was completely replaced every 48 hours. The cell culture was expanded to passage 3. Each passage was made upon reaching 100% confluence (i.e. endothelial monolayer).

### **4.3 Experimental conditions**

Cells at 90% confluence in passage 3 were incubated with M199 supplemented with 1% FBS and 1% NBCS sera (deprivation medium) for 12 hours. To evaluate the involvement of ER stress, the cells were incubated with or without tunicamycin (5  $\mu$ M, Merck Millipore, inducer of ER stress) (Osowski and Urano, 2011), TUDCA (100  $\mu$ M, Merck Millipore, redactor of ER stress) (Yoon et al., 2016), GSK2606115 (3  $\mu$ M, Merck Millipore, PERK inhibitor), KIRA6 (3  $\mu$ M, Merck Millipore, IRE1 $\alpha$  inhibitor), or SP600125 (30  $\mu$ M, Merck Millipore, JNK inhibitor) by 8 hours, or different periods and concentrations as indicated for curves. Cells were first incubated for 1 hour with TUDCA, GSK2606115, KIRA6 or SP600125, followed by tunicamycin for further 8 hours. Thirty minutes before the end of the 8 hours incubation period, L-NAME (100  $\mu$ M, NOS inhibitor) (Fleming and Busse, 2003) was added to evaluate the involvement of NOS activity in the NO production. After the 8 hours of incubation with the drugs, the cells were exposed to 1 nM insulin (20 min). The  $K_i$  values for each inhibitor are listed in Table 3.

### **4.4 Isolation and quantification of proteins**

Total protein was obtained from confluent cells at passage three 3, washed twice with ice-cold PBS and harvested in 100  $\mu$ L of lysis buffer composed by 63.7 mM Tris/HCl (pH 6.8), 10% glycerol, 2% sodium dodecyl sulphate (SDS), 1 mM sodium orthovanadate, 50 mg/mL leupeptin, and 5% 2-mercaptoethanol. Cells were sonicated (6 cycles, 5 s, 100 Watts, 4°C) and total protein was separated by centrifugation (14000 g, 15 min, 4°C). Since the use of detergent in the protein extraction protocol, the protein quantification was performed by the bicinchoninic acid (BCA) assay (Smith et al., 1985) (BCA Protein Assay Kit, Thermo Fisher Scientific, Waltham, MA, USA). This method is based on the biuret reaction

(reduction of  $\text{Cu}^{2+}$  to  $\text{Cu}^+$  by protein bonds) and the chelation of the  $\text{Cu}^+$  by BCA forming an intense purple complex with a peak absorbance at 562 nm. The protocol was performed according to the recommendations provided by the manufacturer. Aliquotes of 10  $\mu\text{L}$  of the total protein lysate were prepared and 5 times diluted. Also, a standard curve was prepared with bovine serum albumin (BSA) containing 0, 31.3, 62.5, 125, 250, 500, and 1000 ng/mL. Aliquotes of 25  $\mu\text{L}$  of each standard or unknown sample were transferred in duplicate into 96-well plates. Then, 200  $\mu\text{L}$  of the working reagent were added and the plate was incubated for 30 minutes at 37°C. From the standard curve, the values were interpolated with the absorbances measured at 560 nm wavelength for each sample in a spectrophotometer (Multiskan EX, Thermo LabSystems).

#### **4.5 Western blot**

Proteins (40  $\mu\text{g}$ ) were separated by SDS-polyacrylamide gel (10%) electrophoresis and transferred onto Immobilon-P polyvinylidene difluoride membranes (BioRad Laboratories, Hertfordshire, UK). The membranes were blocked for 1 hour in blocking solution (5% skim milk or 5% BSA + Tris Tween saline solution (TBS-T): 50 mM Tris/HCl, 150 mM NaCl, 0.02% v/v Tween 20, 4°C, pH 7.4), and then incubated with the antibodies listed in table 4. The membranes were rinsed in TBS-T and incubated (1 h) in blocking solution containing secondary horseradish peroxidase-conjugated goat *anti-rabbit* or *anti-mouse* antibodies. Proteins were detected by enhanced chemiluminescence (SuperSignal West Femto, SuperSignal West Dura, Thermo Fisher Scientific) in a ChemiDoc-It 510 Imagen System (UVP, LCC Upland, CA, USA), analysed and quantified by densitometry using the ImageJ version 1.51j8 (National Institutes of Health, Bethesda, MD, USA).

**Table 4. Antibodies used in Western blot**

Company	Host	Against	Dilution	Incubation time (h)	Temperature
Santa Cruz Biotechnology, Santa Cruz, CA, USA	Mouse	eNOS	1:1000	8	4°C
	Rabbit	PERK	1:500	8	4°C
	Rabbit	P~Thr981 PERK	1:500	8	4°C
	Rabbit	CHOP	1:1000	8	4°C
	Goat	IgG-Fc rabbit	1:2500	1	RT
	Goat	IgG-Fc mouse	1:5000	1	RT
BD Transduction Laboratories, New Jersey, USA	Mouse	P~Ser1177 eNOS	1:1000	8	4°C
	Mouse	P~Thr495 eNOS	1:1000	8	4°C
Cell Signaling, Technology Inc, Danvers, MA, USA	Rabbit	Akt	1:1000	8	4°C
	Rabbit	P~Ser473 Akt	1:1000	8	4°C
	Rabbit	eIF2 $\alpha$	1:1000	8	4°C
	Rabbit	P~Ser51 eIF2 $\alpha$	1:1000	8	4°C
Thermo Fisher Scientific, Waltham, MA, USA	Rabbit	IRS1	1:1000	8	4°C
	Rabbit	P~Ser307 IRS1	1:1000	8	4°C
Abcam, Cambridge, UK	Rabbit	IRE1 $\alpha$	1:1000	8	4°C
	Rabbit	P~Ser724 IRE1 $\alpha$	1:1000	8	4°C
	Rabbit	JNK1	1:1000	1	RT
	Rabbit	P~Thr <sup>183</sup> /Tyr <sup>185</sup> JNK	1:1000	8	4°C
Merck Millipore	Rabbit	TRB3	1:1000	8	4°C
Sigma-Aldrich	Mouse	$\beta$ -actin	1:4000	1	RT

eNOS, endothelial nitric oxide synthase; PERK, protein kinase RNA-like endoplasmic reticulum kinase; CHOP, CCAAT-enhancer-binding protein homologous protein; P~, phosphorylated at (residue); IgG-Fc, fragment crystallisable region of immunoglobulin G; eIF2 $\alpha$ , eukaryotic initiation factor 2  $\alpha$ ; IRS1, insulin receptor substrate 1; IRE1 $\alpha$ , inositol-requiring enzyme 1-alpha; JNK, c-jun N-terminal kinase; TRB3, tribbles-like protein 3.

#### 4.6 Umbilical vein reactivity

Umbilical vein rings (2-4 mm in diameter) from PGMN or PGMO pregnancies were dissected and stored in sterile PBS. The rings were mounted in a myograph (610M Multiwire Myograph System, Danish Myo Technology A/S, Denmark) for the measurement of isometric force in Krebs solution (mM: 118.5 NaCl, 4.7 KCl, 25 NaHCO<sub>3</sub>, 1.2 MgSO<sub>4</sub>, 1.2 KH<sub>2</sub>PO<sub>4</sub>, 2.5 CaCl<sub>2</sub>, 5.5 D-glucose, 37°C, pH 7.4) maintained with constant bubbling of a 95% O<sub>2</sub>/5% CO<sub>2</sub> mixture.

For determination of the role of ER stress in the vascular reactivity, the rings were incubated in M199 (5% CO<sub>2</sub>, 37°C) for 8 hours in the absence or presence of tunicamycin (5 µM), TUDCA (100 µM) or both, prior to mounting on the myograph. After a 30 minutes equilibration period in Krebs solution, vein rings were stretched to their optimal lumen diameter for active tension development determined by the maximum contraction response to KCl (62.5 mM). After a second period of 30 minutes for equilibration, vascular reactivity in response to insulin (0.1-1000 nM), CGRP (0.01-100 nM), or sodium nitroprusside (SNP, 1 µM, NO donor) (Sigma-Aldrich, St Louis, MO, USA) was measured in vessel rings pre-contracted with KCl (37.5 mM) in the absence or presence of L-NAME (100 µM). Changes in isometric tension were recorded using the LabChart computer program (LabChart 7Pro for Windows, ADInstruments, Australia) coupled with a PowerLab device (PowerLab 8/30 Data Acquisition System, ADInstruments, Australia). The response of the vessel rings was expressed as a percentage of maximal contraction in response to KCl (37.5 mM) (Villalobos-Labra et al., 2019).

#### **4.7 Total RNA extraction and reverse transcription**

The total RNA was isolated using the TRIzol reagent. The RNA was quantified by spectrophotometry ( $OD_{260}$  nm) and its quality and integrity were evaluated by agarose gel (2 %m/V) visualization and spectrophotometric analysis ( $OD_{260/280}$ ). For the reverse transcription reaction, aliquots of 1  $\mu$ g of total RNA were used with oligo (dT), random primers and the enzyme MMLV-RT (Moline Murine Leukaemia Virus-Reverse Transcriptase, Promega) according to the recommendations provided by the manufacturers.

#### **4.8 Non-quantitative PCR**

The cDNAs of XBP1 unspliced or spliced were amplified using the primers (0.2  $\mu$ M) described in Table 5 in a solution containing dNTP (0.5 mM each), Taq DNA polymerase (1 IU/ $\mu$ L), MgCl<sub>2</sub> (25 mM) (González et al., 2011, 2004). The incubation cycle was carried out at 95°C for 5-7 minutes, 40 cycles including a denaturation step for 30 seconds at 95°C, alignment at 56°C and an elongation phase by the polymerase at 72°C for 7 minutes. The PCR reactions were carried out in an I-Cycler thermocycler from BioRad.

The amplified cDNA was separated by electrophoresis on a 1.5% agarose gel in Tris-borate-EDTA buffer solution (Winkler, Santiago, Chile), containing 0.5  $\mu$ g/mL of GelRed (Biotium, Hayward, CA, USA) to differentiate the spliced and unspliced XBP1 cDNA as described (Uemura et al., 2009). The amplification products were observed by the exposure of the gel to UV light in a transilluminator. Images were captured and digitized by a NIKON camera (USA) and analyzed by the ImageJ software.

#### **4.9 Quantitative PCR**

Experiments were performed using a StepOne Real-Time PCR system (Applied Biosystems, Foster City, CA, USA) in a reaction mix containing 0.2  $\mu$ M primers and master

mix provided in the brilliant SYBR green qPCR Master Mix (Stratagene, La Jolla, CA, USA). Hot-start DNA polymerase was activated (20 s, 95°C), and the PCR cycling profile included a 95°C denaturation (3 s), annealing (30 s) at 56°C (CHOP, TRB3, BIP, XBP1s, and  $\beta$ -actin) and 54°C (28S), and extension (30 s) at 72°C. Product melting temperature values were 79.3°C (CHOP), 83.7°C (TRB3), 73.8°C (BIP), 80.2°C ( $\beta$ -actin), and 80°C (28S). Primers efficiency were 101.5% (CHOP), 91.3% (TRB3), 103.1% (BIP), 93.3% ( $\beta$ -actin), and 109.3% (28S). The sequences of the oligonucleotide primers are listed in Table 5. The relative gene expression was estimated by the  $2^{-\Delta\Delta Ct}$  method (Antonov et al., 2005). The 28S and  $\beta$ -actin cDNA were used as internal standards.

**Table 5. Oligonucleotide sequences for non-quantitative and quantitative PCR**

<i>Primer</i>	<i>DNA strand</i>	<i>Sequence</i>
TRB3	Sense	5'-ATT AGG CAG GGT CTG TCC TGT G-3'
	Antisense	5'-AGT ATG GAC CTG GGA TTG TGG A-3'
CHOP	Sense	5'-AAT GAA CGG CTC AAG CAG GA-3'
	Antisense	5'-TGC AGA TTC ACC ATT CGG TCA-3'
BiP/GRP78	Sense	5'-CCA CCA AGA TGC TGA CAT TG-3'
	Antisense	5'-AGG GCC TGC ACT TCC ATA GA-3'
XBP1u and s (Variant 1 and 2)	Sense	5'-GGA GTT AAG ACA GCG CTT GGG GA-3'
	Antisense	5'-TGT TCT GGA GGG GTG ACA ACT GGG-3'
XBP1s (Variant 2)	Sense	5'-TGC TGA GTC CGC AGC AGG TG-3'
	Antisense	5'-GCT GGC AGG CTC TGG GGA AG-3'
hCAT-1	Sense	5'-GAG TTA GAT CCA GCA GAC CA-3'
	Antisense	5'-TGT TCA CAA TTA GCC CAG AG-3'
28S	Sense	5'-TTG AAA ATC CGG GGG AGA G-3'
	Antisense	5'-ACA TTG TTC CAA CAT GCC AG-3'
$\beta$ -actin	Sense	5'-GCC GGG ACC TGA CTG ACT AC-3'
	Antisense	5'-TTC TCC TTA ATG TCA CGC ACG AT-3'

TRB3, tribbles-like protein 3; CHOP, CCAAT-enhancer-binding protein homologous protein; BiP, binding immunoglobulin protein; XBP1u; unspliced X-box binding protein 1 mRNA; XBP1s, spliced X-box binding protein 1 mRNA; hCAT-1, human cationic amino acids transporter 1; 28S, ribosomal RNA of the 28S subunit.

#### 4.10 L-Arginine transport

The transport of L-arginine was carried out in confluent cells (~90%) in passage 3 in 96-plates as described (Guzmán-Gutiérrez et al., 2016). After 12 hours of incubation with deprivation medium, the culture medium was removed and the cells were washed (x2) with 200  $\mu\text{L}$ /well of Krebs solution (mM: 31 NaCl, 5.6 KCl, 25 NaHCO<sub>3</sub>, 1 NaH<sub>2</sub>PO<sub>4</sub>, 5 D-glucose, 20 HEPES, 2.5 CaCl<sub>2</sub>, 1 MgCl<sub>2</sub>, pH 7.4). The cells were exposed to 62.5 to 1000  $\mu\text{M}$  L-arginine mixed with L-[<sup>3</sup>H]arginine (NEN, Dreieich, FRG) (3  $\mu\text{Ci}/\text{mL}$ ) for 1 minute (initial velocity) at 37°C in Krebs solution. The transport of L-arginine was stopped by removing the uptake medium and washing (x2) with Krebs solution at 4°C. Cells were then digested with 100  $\mu\text{L}$  of 0.5 N KOH. Aliquotes of 80  $\mu\text{L}$  of the cell digest were transferred to plastic tubes and mixed with scintillation liquid (2 mL). The remaining 20  $\mu\text{L}$  were used for protein determination (Salsoso et al., 2015; Guzmán-Gutiérrez et al., 2016). The kinetic parameters of the L-arginine transport (apparent constant of Michaelis-Menten and maximal velocity,  $K_m$  and  $V_{max}$ , respectively) were determined using the data obtained after quantifying the samples with a scintillation counter.

The calculations for the transport of L-arginine were made according to the following expression:

$$\text{Saturable component} = (\text{overall uptake}) - (\text{non-saturable component}) \quad (\text{Equation 1})$$

in which, overall uptake (CT) was defined by

$$CT = \frac{V_{max} \cdot [Arg]}{K_m + [Arg]} + (m \cdot [Arg]) \quad (\text{Equation 2})$$

where  $[Arg]$  was the concentration of L-arginine in the medium and  $m \cdot [Arg]$  was the non-saturable (linear) component of transport in the range of concentrations used in this study.

From the graphical representation of the overall transport data, the slope value of the linear phase corresponding to the non-saturable transport component was calculated. By subtracting the non-saturable component of the overall transport, the saturable transport data was obtained and represented by the Michaelis-Menten equation:

$$v = \frac{V_{max} \cdot [Arg]}{K_m + [Arg]} \quad (\text{Equation 3})$$

where  $v$  corresponds to the initial transport velocity at different concentrations of L-arginine. The kinetic parameter  $V_{max}$  was expressed as pmol/ $\mu$ g protein/minute and the apparent  $K_m$  as  $\mu$ M. The maximum transport capacity of L-arginine was estimated by the  $V_{max}/K_m$  ratio (Deves and Boyd, 1998; Mann et al., 2003).

The initial rate of uptake (i.e. linear uptake up to 1 minute) was derived from the slope of the linear phases of L-arginine uptakes. Values for uptake were adjusted to the one phase exponential association equation considering the least squares fit:

$$v_i = V_m \cdot (1 - e^{-(k \cdot t)}) \quad (\text{Equation 4})$$

where  $v_i$  is initial velocity,  $V_m$  is the highest velocity reached at a given time ( $t$ ) and L-arginine concentration, and  $e$  and  $k$  are constants.

#### **4.11 Intracellular NO determination**

Intracellular NO was determined using the fluorescent dye 4-amino-5-methylamino-2',7'-difluorofluorescein diacetate (DAF-FM, Merck Millipore). Confluent cells grown on black 96-well plates in passage 3 were incubated in the absence or presence of tunicamycin (5  $\mu$ M, 8 h) and/or TUDCA (100  $\mu$ M, 8 h), and then exposed (1 h, 37°C) to 5  $\mu$ M DAF-FM in the absence or presence of 100  $\mu$ M L-NAME in Krebs buffer (37°C, pH 7.4). The fraction of NOS-activity derived NO was estimated by the difference between the fluorescence in the presence and absence of L-NAME. The fluorescence ( $\lambda_{exc}/\lambda_{em}$  : 485/538 nm) was determined in an Infinite M200PRO Tecan (Männedorf, Zürich, Switzerland). After the experiment, aliquots of 100  $\mu$ L of 0.5 N KOH were added to lyse the cells for protein quantification.

#### **4.12 L-Citrulline determination**

The intracellular content of L-citrulline was determined by high-performance liquid chromatography (HPLC) (Pardo et al., 2015). The cells were incubated (60 min) in HEPES buffer (1 mL) supplemented with 100  $\mu$ M L-arginine in the absence or presence of 100  $\mu$ M of L-NAME. The cells were then washed (x2) with PBS (4°C), scraped and collected in 600  $\mu$ L of PBS containing 1  $\mu$ M L-arginine. The cell suspension was homogenized by sonication (6 cycles, 5 s, 100 W, 4°C) and centrifuged (13,500 g, 15 min, 4°C). Aliquots of 100  $\mu$ L were used for determination of proteins by the BCA method (see above). The remaining 500  $\mu$ L of HUVECs extracts were centrifuged (10,000 g, 2 min, 4°C), and the resulting pellet was resuspended with 200  $\mu$ L of HClO<sub>4</sub> (1.5 M) and vigorously mixed in vortex (1 min). The suspension was mixed with 100  $\mu$ L of K<sub>2</sub>CO<sub>3</sub> (2 M), centrifuged (3,000 g, 5 min, 4°C) and aliquots of 100  $\mu$ L of supernatant were collected for amino acid determination. The supernatant was subjected to derivatization reactions by mixing with 20  $\mu$ L of 0.1 M sodium

borate and 20  $\mu\text{L}$  of *o*-phthalaldehyde (30 mM in 0.2%  $\beta$ -mercaptoethanol). Samples were filtered with a filter attached to a syringe and loaded onto the analytical column (C18: 4.6 mm  $\times$  250 mm) coupled to the HPLC system (PU2089s; JASCO, Tokyo, Japan). The columns were equilibrated with 0.1 M  $\text{NaH}_2\text{PO}_4$  (mobile phase: 17% acetonitrile, pH 5.0, 40 min, flow 0.7 mL/min). The fluorescence was monitored by wavelengths of 340 nm excitation and 455 nm emission, using the fluorescence detector (FP 2020 Plus, JASCO) of the HPLC system. The L-citrulline concentration was determined as a function of a standard curve of L-citrulline (0-3 nM). The chromatograms obtained were analyzed using the ChromPass 1.7 Software (JASCO).

#### **4.13 Arginase activity**

Total urea production from L-arginine was measured as previously described in HUVECs (Prieto et al., 2011). Confluent HUVECs on Petri dishes (100 mm diameter) in passage 3 were incubated in the absence or presence of tunicamycin (5  $\mu\text{M}$ ) or TUDCA (100  $\mu\text{M}$ ), or both, and 20  $\mu\text{M}$  *S*-(2-boronoethyl)-L-cysteine (BEC, arginases inhibitor) (Kim et al., 2001). The cells were then washed twice with cold PBS (4°C, pH 7.4) and incubated (5 min, on ice) with lysis buffer (1  $\mu\text{M}$  pepstatin A, 1  $\mu\text{M}$  leupeptin, 200  $\mu\text{M}$  phenylmethylsulfonyl fluoride (PMSF), 50 mM Tris-HCl (pH 7.5), 0.2% Triton X-100). Cell lysate was sonicated (20 pulses, 150 Watts, x3) and total protein content was determined by Bradford method. The total cell protein aliquotes (70  $\mu\text{g}$  contained in 90  $\mu\text{L}$ ) obtained from the lysates were preincubated (10 min, 55°C) with 100 mM  $\text{MnCl}_2$  in 50 mM Tris-HCl buffer (pH 7.5) and then mixed with L-arginine (50 mM, 60 min, 37°C). The reaction was stopped by addition (400  $\mu\text{L}$ ) of an acid mix ( $\text{H}_2\text{SO}_4:\text{H}_3\text{PO}_4:\text{H}_2\text{O} = 1:3:7$  v/v) and incubated (45 min, 100°C) with 9%  $\alpha$ -isonitrosopropiophenone (25  $\mu\text{L}$ ) for colorimetric determination of urea

(absorbance at 540 nm) in a microplate reader (Multiskan EX, Thermo LabSystems). Arginases activity was calculated from the urea formation in the absence of BEC minus the urea formation in the presence of this inhibitor (Prieto et al., 2011). The activity was expressed as pmol urea/ $\mu$ g protein/minute.

#### **4.14 Quantification of proteins in lysates extracted with KOH**

Because basicity interferes with protein quantification by the BCA method, proteins extracted with KOH were quantified by the Bradford method (Bradford, 1976). This method is based on the change in coloration of Coomassie brilliant blue at different protein concentrations. The lysate of proteins extracted by KOH method were homogenized by agitation and then 20  $\mu$ L of the sample were transferred to 96-well plates. Bradford's commercial solution (Bio-Rad Protein Assay) was diluted 1:5 (v/v) and aliquots of 200  $\mu$ L were added to each well. Additionally, a standard curve was prepared with BSA containing 0, 20, 30, 50, 80 and 100 ng/mL. From this standard curve, the values were interpolated with the absorbances measured at 595 nm wavelength for each sample in a spectrophotometer (Multiskan EX, Thermo LabSystems).

#### **4.15 Immunofluorescence and confocal microscopy**

HUVECs were grown on glass coverslips ( $6 \times 10^4$  cells per slide) (Sail Brand, Shanghai, China) in PCM up to 100% confluence. Cells were then cultured in medium M199 containing 1% FCS and 1% NBCS in the absence or presence of tunicamycin (5  $\mu$ M, 8 h), TUDCA (100  $\mu$ M, 8 h), or both molecules. The cells were then fixed in 4% paraformaldehyde (5 min), rinsed (x3) with PBS, permeabilized, and blocked with 1% BSA-containing blocking solution (50 mM  $\text{NH}_4\text{Cl}$ , and 0.05% Triton X-100 in PBS (2 h) (Sáez et al., 2013). ATF6 was immunolocalized by incubating the cells with primary monoclonal rabbit *anti*-ATF6 (1:30

dilution) (Spring Bioscience, Pleasanton, CA, USA) overnight at 4°C in 1% BSA-blocking solution. The cells were then washed (x3) with PBS, followed by incubation (1 h, 22°C) with the secondary antibody Alexa Fluor 568 goat *anti*-rabbit IgG (H+L,  $\lambda_{exc}/\lambda_{em}$ : 578/603 nm, 1:500 dilution) (Life Technologies) in 1% BSA-blocking solution. Nuclei were counterstained with DAPI (5  $\mu$ M, Life Technologies) and the coverslips mounted with Fluoromount G (Electron Microscopy Sciences, Washington, PA, USA).

Images were acquired under an inverted Eclipse C2 confocal Nikon microscope using a 60x oil immersion objective lens (numerical aperture 1.4) and the confocal acquisition software NIS-Elements C (Nikon, Tokyo, Japan). Each sample was examined through successive 0.3  $\mu$ m optical slices along the z-axis to capture 15 slices per cell. Relative fluorescence was measured using ImageJ version 1.52b and the ratio between the ATF6 fluorescence at the nuclear region and the perinuclear region of each cell was determined. Nuclear regions defined by DAPI fluorescence were also analysed for the optical slide number 7, i.e.  $\sim$ 2.1  $\mu$ m from the cell culture surface. ATF6 fluorescence at the perinuclear area (*pnA*) was derived from the expression:

$$pnA = (1.9 \cdot nA) - nA \quad (\text{Equation 5})$$

where *nA* is the nuclear area corresponding to DAPI fluorescence and 1.9 is the increase in the *nA* fixed for each cell.

#### **4.16 IRE1 $\alpha$ suppression**

Suppression of IRE1 $\alpha$  expression was done using the commercially available short interference RNAs (siRNA) IRE1 $\alpha$  siRNA (h) or control sequence (siC) (Santa Cruz Biotechnology) following the manufacturer's instructions. HUVECs in passage 3 ( $2 \times 10^5$

cells) were seeded into six-well culture plates with antibiotic-free PCM and incubated at 37°C for 18 hours until reaching a confluence of 60-70%. Cells were washed (x2) with transfection medium and incubated for 8 hours with 1 mL of transfection medium mixed with transfection reagent plus IRE1 $\alpha$  siRNA or siRNA negative control. Then, 1 mL of PCM with double the concentration of the antibiotic and NBCS and FBS sera was added, and cells were left incubating further 12 hours. The medium was removed and replaced with PCM, and the cells left incubating for 18 hours. After this period of 18 hours cells were exposed to deprived medium for further 12 hours. Finally, cells were incubated in the absence or presence of tunicamycin (5  $\mu$ M) for 8 hours. After the experiments the cells were washed with cold PBS (4°C) and proteins were extracted for Western blot.

#### 4.17 Sample size estimation

The insulin-induced relaxation values in the umbilical veins and the protein abundance of eIF2 $\alpha$  in HUVECs were used to calculate the sample size. The sample size to be used for each variable was calculated with the expression:

$$n = \frac{2(Z\alpha + Z\beta)^2 * S^2}{d^2} \quad (\text{Equation 6})$$

Where,

n = study subjects

Z $\alpha$  = value of Z corresponding to the desired risk for unilateral test (1,645)

Z $\beta$  = value of Z corresponding to the power of 90% (1,282)

S = variance of the control group (1,028)

d = minimum value of the difference to be detected (1,664)

Thus, at least 7 samples per group should be included by analysis to determine differences in relation to insulin effect and UPR activation.

#### **4.18 Statistical analysis**

Values for clinical parameters are as mean  $\pm$  S.D. (range). For *in vitro* assays the values are mean  $\pm$  S.E.M., where *n* indicates the number of different biological samples (48 umbilical cords from PGMN, 64 umbilical cords from PGMO). The normal distribution of the data was tested by the D'Agostino-Pearson omnibus test. Comparisons between two groups were performed using Student's unpaired *t*-test or Mann-Whitney test for parametric or non-parametric data, respectively. The differences between more than two groups were performed by analysis of variance (ANOVA, one or two-ways). If the ANOVA demonstrated a significant interaction between variables, *post hoc* analyses were performed by the multiple-comparison Tukey test. In case of data presented as a percentage, an arcsin transformation was first performed, and then ANOVA analysis was applied. The statistical software GraphPad Prism 8.2.0 (GraphPad Software Inc., San Diego, CA, USA) was used for data analysis. All tests used a confidence interval of 95% (95%CI) and  $P < 0.05$  was considered significant.

## 5. Results

### 5.1 Patients

#### 5.1.1 Study groups

Pregnancies were with a single fetus and pregnant women showed similar age and height, were normotensive, with similar OGTT and normal glycemia at delivery (Table 6). The pre-pregnancy weight and BMI were higher (~1.5 fold) in PGMO compared with PGMN. The gestational weight gain (GWG) was lower (~17%) in PGMO than PGMN. There were no differences in birth weight, height and ponderal index in newborns from both conditions. The glycemia in the umbilical vein did not show significant differences; however, insulin (~1.7 fold) and C-peptide (~1.5 fold) levels and HOMA-IR (2.4 fold) were higher, and QUICKI was lower (~10%) in umbilical vein blood from PGMO mothers.

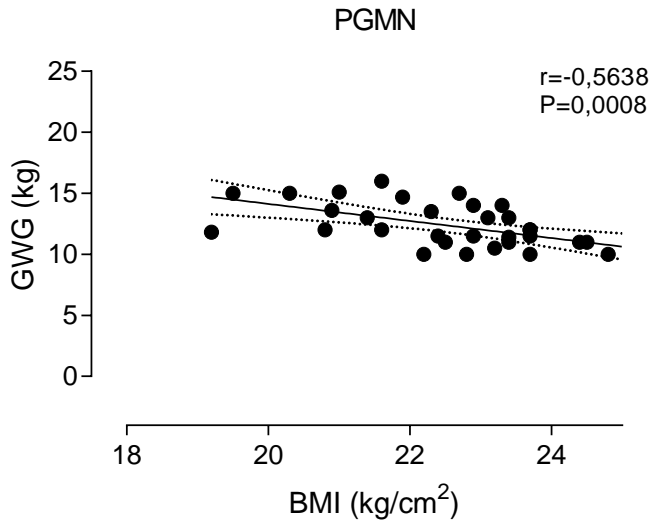
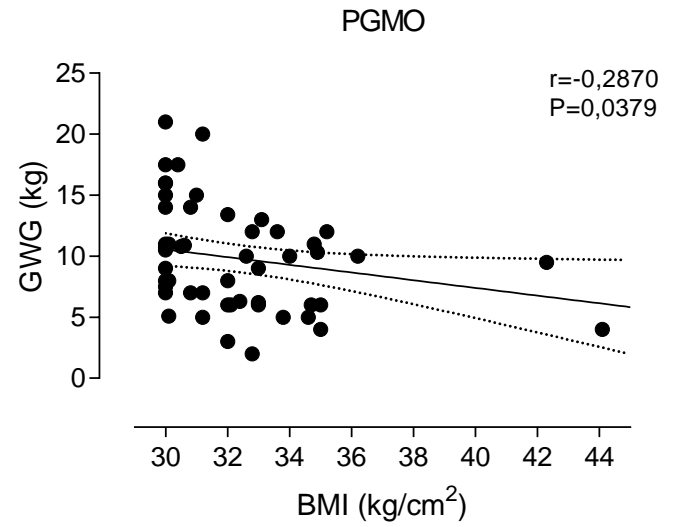
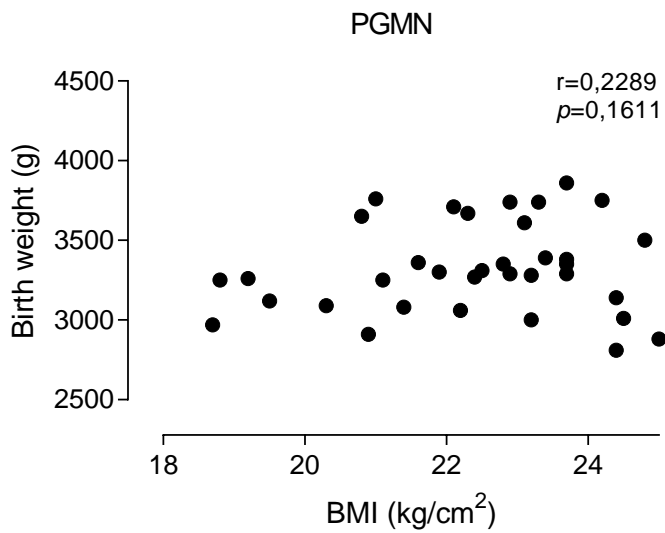
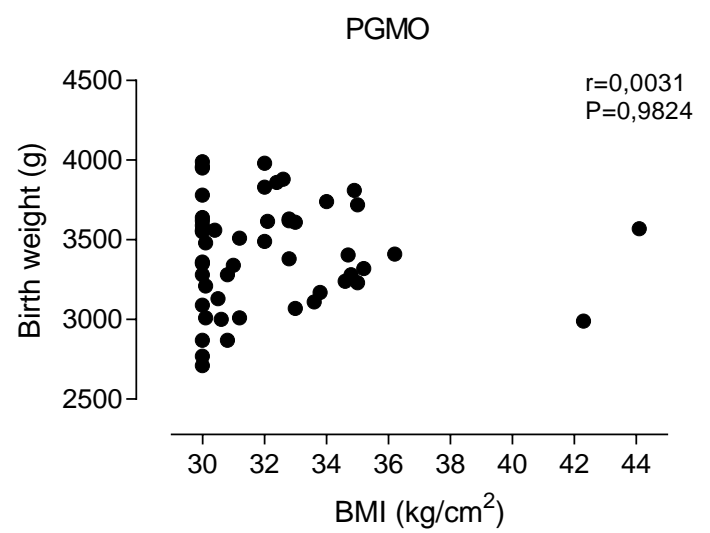
#### 5.1.2 Association of GWG and birth weight with the pre-pregnancy BMI

Pre-pregnancy BMI showed a negative correlation to gestational weight gain in PGMN ( $r = -0.5638$ ) and PGMO ( $r = -0.2870$ ) mothers (Figure 2A,B). On the other hand, the birth weight did not show dependence on the pre-pregnancy BMI (Figure 2C,D) or GWG of the mother (Figure 2E and 2F).

**Table 6. Clinical characteristics of pregnant women and newborns**

Variables	PGMN (n = 48)	PGMO (n = 64)
<i>Maternal variables</i>		
Age (years)	29.5 ± 5.5 (21–40)	30.9 ± 3.8 (24–38)
Height (cm)	160.9 ± 4.7 (149–170)	159.6 ± 6.3 (146–175)
Weight (kg)		
Pre-pregnancy <sup>a</sup>	57.0 ± 6.5 (45–65)	83.5 ± 16.6 * (70–127)
Delivery	70.6 ± 5.1 (57–83)	90.2 ± 14.8 * (72–135)
GWG (kg) <sup>b</sup>	12.3 ± 1.8 (9.4–16.0)	9.6 ± 4.2 * (2.0–21.0) <sup>c</sup>
BMI (kg/m <sup>2</sup> )		
Pre-pregnancy (0–12 wg)	22.6 ± 1.5 (19.2–24.9)	32.8 ± 4.0 * (30.0–44.1)
Delivery	27.2 ± 1.3 (24.0–28.7)	35.7 ± 4.8 * (33.0–48.1)
Blood pressure at 3 <sup>rd</sup> trimester (mmHg)		
Systolic	108 ± 11 (90–125)	113 ± 9 (100–120)
Diastolic	70 ± 8 (60–85)	72 ± 7 (60–80)
Mean	89 ± 8 (75–105)	92 ± 7 (80–100)
Basal glycaemia at delivery (mg/dL)	79 ± 4 (73–85)	78 ± 6 (69–94)
OGTT (mg/dL)		
Glycemia basal	76 ± 6 (68–85)	77 ± 9 (67–95)
Glycemia 2 h after glucose load	94 ± 15 (56–125)	98 ± 17 (60–135)
<i>Newborn variables</i>		
Sex (female/male)	25/23	25/39
Gestational age (weeks)	39.2 ± 0.9 (37.1–41.0)	39.1 ± 0.9 (37.1–40.9)
Birth weight (grams)	3384 ± 335 (2810–3860)	3489 ± 398 (2710–3990)
Height (cm)	50.5 ± 1.7 (47.0–54.0)	50.7 ± 1.7 (47.5–55.0)
Ponderal index (grams/cm <sup>3</sup> x 100)	2.6 ± 0.2 (2.2–3.2)	2.7 ± 0.2 (2.3–3.3)
Umbilical vein glycaemia (mg/dL)	64.8 ± 1.8 (48.6–73.9)	68.5 ± 1.8 (57.7–77.5)
Umbilical vein insulin (μU/mL)	5.01 ± 0.36 (2.6–6.4)	8.36 ± 1.78 (4.6–19.7) *
Umbilical vein C-peptide (ng/mL)	0.65 ± 0.03 (0.50–0.90)	0.94 ± 0.12 (0.58–1.50) *
HOMA-IR	0.44 ± 0.02 (0.37–0.57)	1.05 ± 0.28 (0.52–2.64) *
QUICKI	0.40 ± 0.02 (0.36–0.47)	0.36 ± 0.04 (0.31–0.41) *

Pregnant women were with a normal pre-pregnancy body mass index (BMI 18.5–24.9 kg/m<sup>2</sup>) (PGMN) or with pre-pregnancy obesity (BMI ≥ 30 kg/m<sup>2</sup>) (PGMO) according to the US Institute of Medicine (IOM, 2009). <sup>a</sup>Pre-pregnancy weight corresponds to self-reported weight by the pregnant women at their first interview with the medical specialist (i.e., 4–12 weeks of pregnancy), the annotated weight in clinical charts after routine medical screening (i.e. 1–3 months before pregnancy) or the weight measured at the 1<sup>st</sup> (0–14 weeks of gestation) trimester. <sup>b</sup>The gestational weight gain (GWG) corresponds to the difference between the weight at pre-pregnancy and delivery. <sup>c</sup> 46.2% of the patients were out of the IOM recommended range. Oral glucose tolerance test (OGTT, 75 g glucose load) was measured between 24–28 weeks of gestation. HOMA-IR, Homeostatic Model Assessment for Insulin Resistance; QUICKI, Quantitative Insulin Sensitivity Check Index. Values are mean ± S.D. (range). *P* < 0.05. \* vs corresponding values in PMGN.

**A****B****C****D**

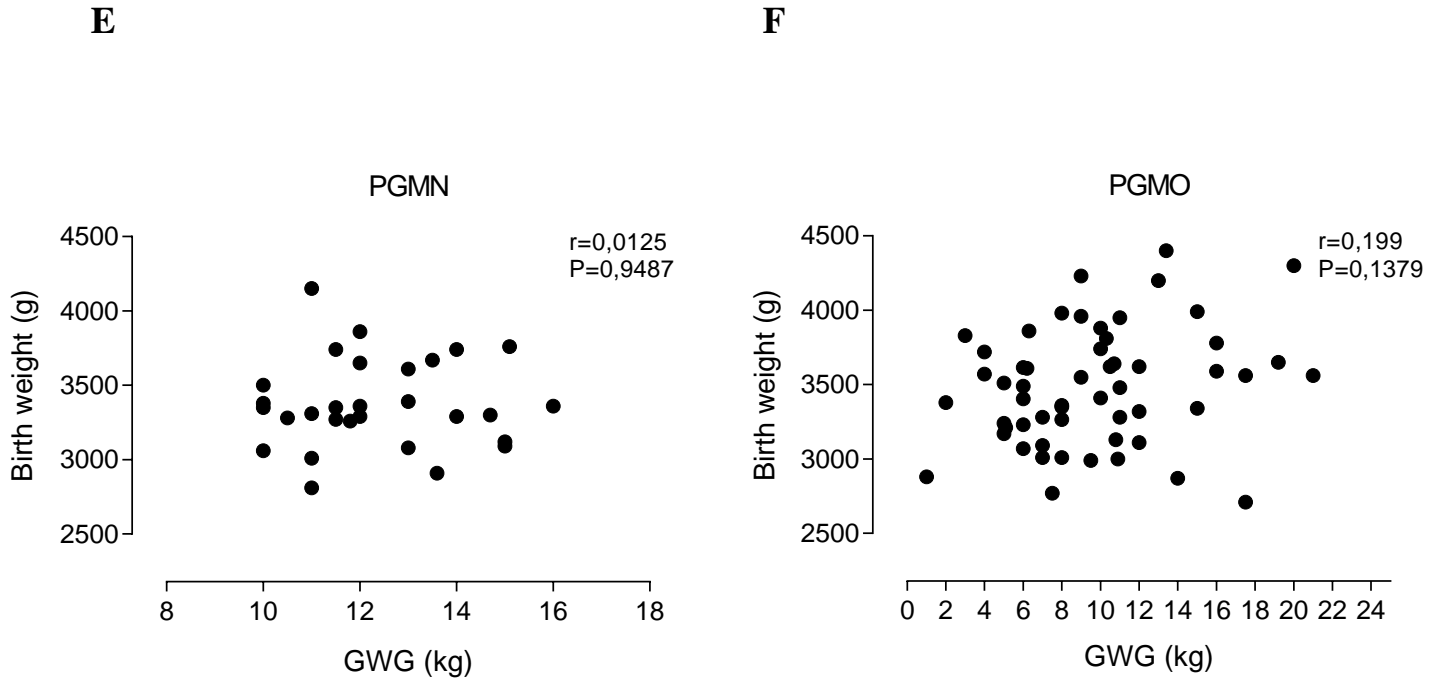


**Figure 2. Relationship of the dependence of gestational weight gain and birth weight on the maternal pre-pregnancy BMI.** Pregnant women were with normal pre-pregnancy body mass index (BMI 18.5–24.9 kg/m<sup>2</sup>) (PGMN) or with pre-pregnancy obesity (BMI ≥30 kg/m<sup>2</sup>) (PGMO) according to the US Institute of Medicine guidelines (IOM and NRC, 2009). **A** and **B**, scatter plots of gestational weight gain (GWG) vs pre-gestational body mass index (BMI) of the mothers. The best fitting line and the 95% confidence level envelopes are shown in the graph with a significant correlation. **C** and **D**, scatter plots of fetal birth weight vs BMI of mothers. **E** and **F**, scatter plots of birthweight vs GWG of the mother. Correlations were computed by the Pearson correlation coefficients.  $r$  and  $P$ -value are shown.

## 5.2 Endothelial dysfunction and insulin resistance

### 5.2.1 Characteristics of the umbilical vein rings

The stretch needed to reach the optimal diameter was higher ( $\Delta \sim 1,1$  mm) in umbilical veins from PGMO than from PGMN pregnancies (Figure 3). On the other hand, the contraction induced by KCl (32,5 mM) once the optimal diameter was reached was lower ( $\sim 56\%$ ) in rings from PGMN than the contraction in rings from PGMO (Figure 4). In a parallel set of assays, the incubation with SNP caused a comparable dilation in umbilical veins from both conditions (PGMN  $\sim 33\%$ , PGMO  $\sim 29\%$ ) (Figure 5).

### 5.2.2 Vascular reactivity in response to insulin

The umbilical vein response to insulin was assayed in a wire myograph using an increasing concentration of insulin (0.1 to 1  $\mu\text{M}$ ). Insulin induced relaxation ( $R_{\text{max}} \sim 21\%$ ) in umbilical vein rings from PGMN pregnancies. However, umbilical veins from PGMO did not respond to insulin. The preincubation with L-NAME blocked the effect of insulin on PGMN rings. The  $R_{\text{max}}$  for the NOS-dependent vasodilation in response to insulin in umbilical veins from PGMN was  $\sim 14\%$  (Figure 6, Table 7).

### 5.2.3 Vascular reactivity in response to CGRP

CGRP was used to evaluate the endothelium status of the umbilical veins. CGRP caused relaxation in umbilical veins from PGMN pregnancies ( $R_{\text{max}} \sim 26,6\%$ ) but not in umbilical veins from PGMO pregnancies (Figure 7). Pre-incubation with L-NAME blocked the CGRP-induced vasodilation in umbilical veins from PGMN and did not induce changes in rings from PGMO pregnancies. The  $R_{\text{max}}$  for the NOS-dependent relaxation was  $\sim 23\%$  (Figure 7, Table 7)

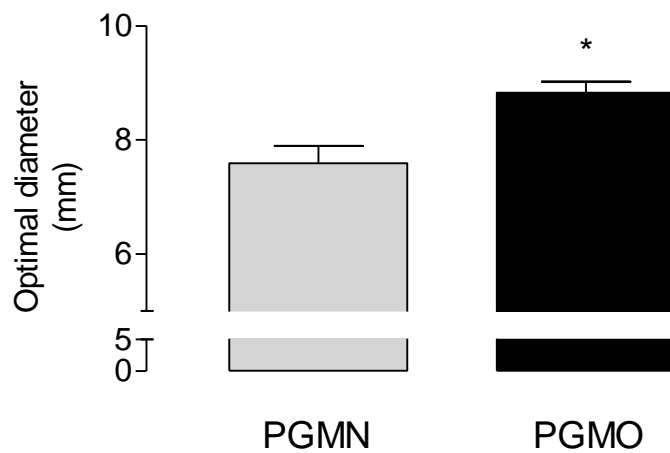


**Figure 3. Stretching at the optimal diameter.** The stretch necessary to achieve the maximum contraction in response to KCl 65 mM (optimal diameter) of the human umbilical vein rings from pregnancies where the mother showed pre-gestational maternal normal weight (PGMN) or pre-gestational maternal obesity (PGMO) mounted on a myograph was measured. Values are mean  $\pm$  S.E.M.  $P < 0.05$ . \* *vs* PGMN (n = 5 PGMN, 7 PGMO).

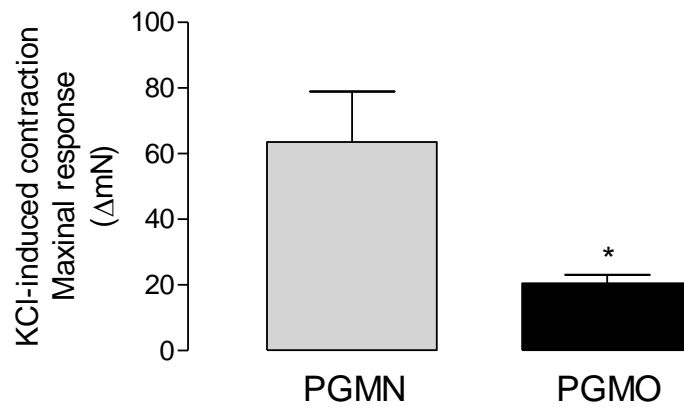


**Figure 4. KCl-induced contraction at the optimal diameter.** The maximum strain induced by 65 mM KCl at the optimal diameter of human umbilical vein rings from PGMN or PGMO pregnancies was measured in a myograph. The response is shown as the delta ( $\Delta$ ) between the force after incubation with KCl and the force induced in resting condition. Values are mean  $\pm$  S.E.M.  $P < 0.05$ . \* vs PGMN (n = 5 PGMN, 7 PGMO).

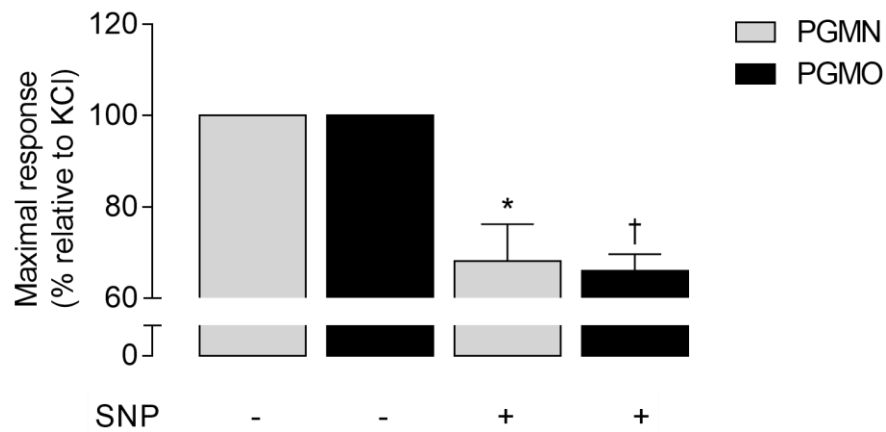


**Figure 5. SNP-induced vasodilation.** The maximal response of human umbilical vein rings from pregnancies where the mother showed pre-gestational maternal normal weight (PGMN) or pre-gestational maternal obesity (PGMO) pre-contracted with KCl (32.5 mM) was measured in a myograph. Vein rings were in the absence (-) or presence (+) of sodium nitroprusside (SNP, 10  $\mu$ M, 5 min) (see Methods). Values are mean  $\pm$  S.E.M.  $P < 0.05$ . \* vs control PGMN, † vs control PGMO (n = 5 PGMN, 7 PGMO).

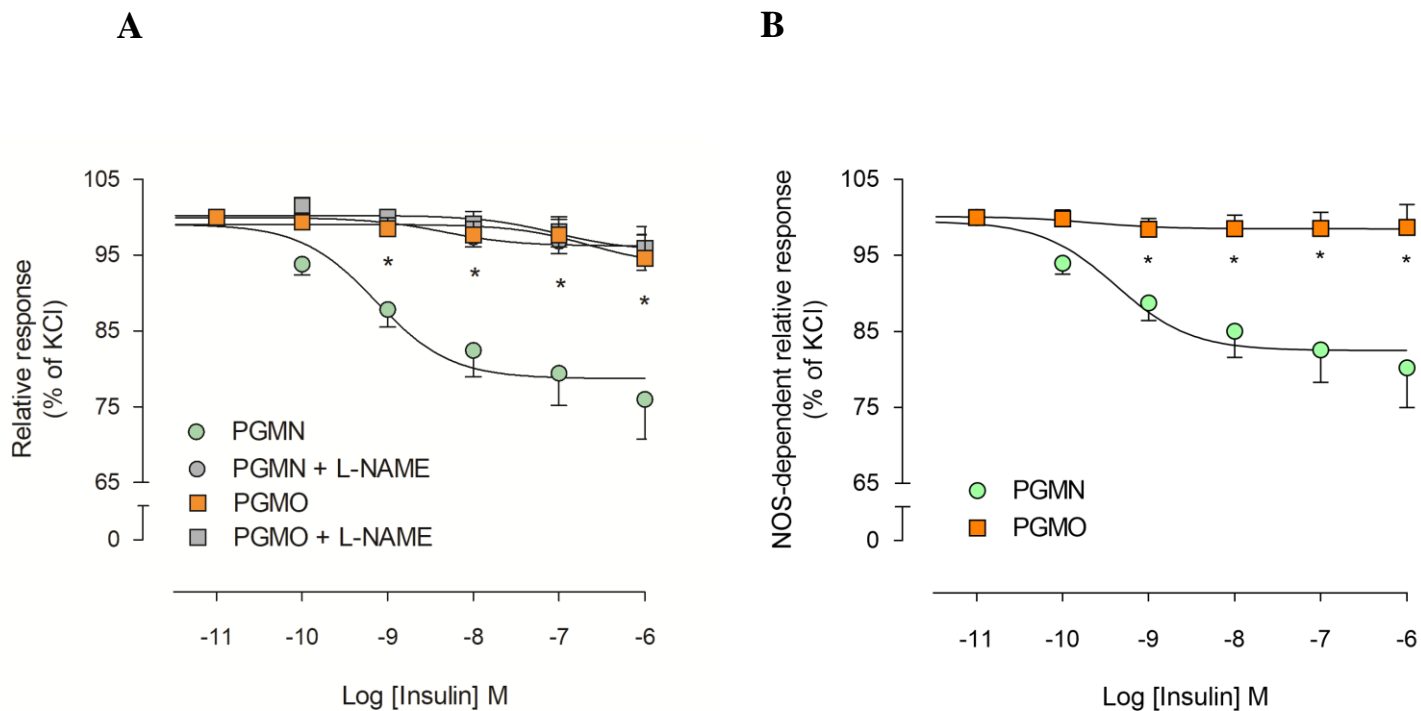


**Figure 6. Insulin-induced relaxation in human umbilical vein rings.** **A**, Human umbilical vein rings from pregnancies where the mother showed pre-gestational maternal normal weight (PGMN) or pre-gestational maternal obesity (PGMO) were pre-contracted with KCl 32.5 mM and incubated without or with L-NAME (30 minutes, 100  $\mu$ M) and then exposed (5 minutes) to insulin (see Methods). **B**, NOS-dependent vasodilation determined by the subtraction of the total insulin response minus the response in the presence of L-NAME. Values are mean  $\pm$  S.E.M.  $P < 0.05$ . \* vs the corresponding values in PGMN (n = 5 PGMN, 7 PGMO).

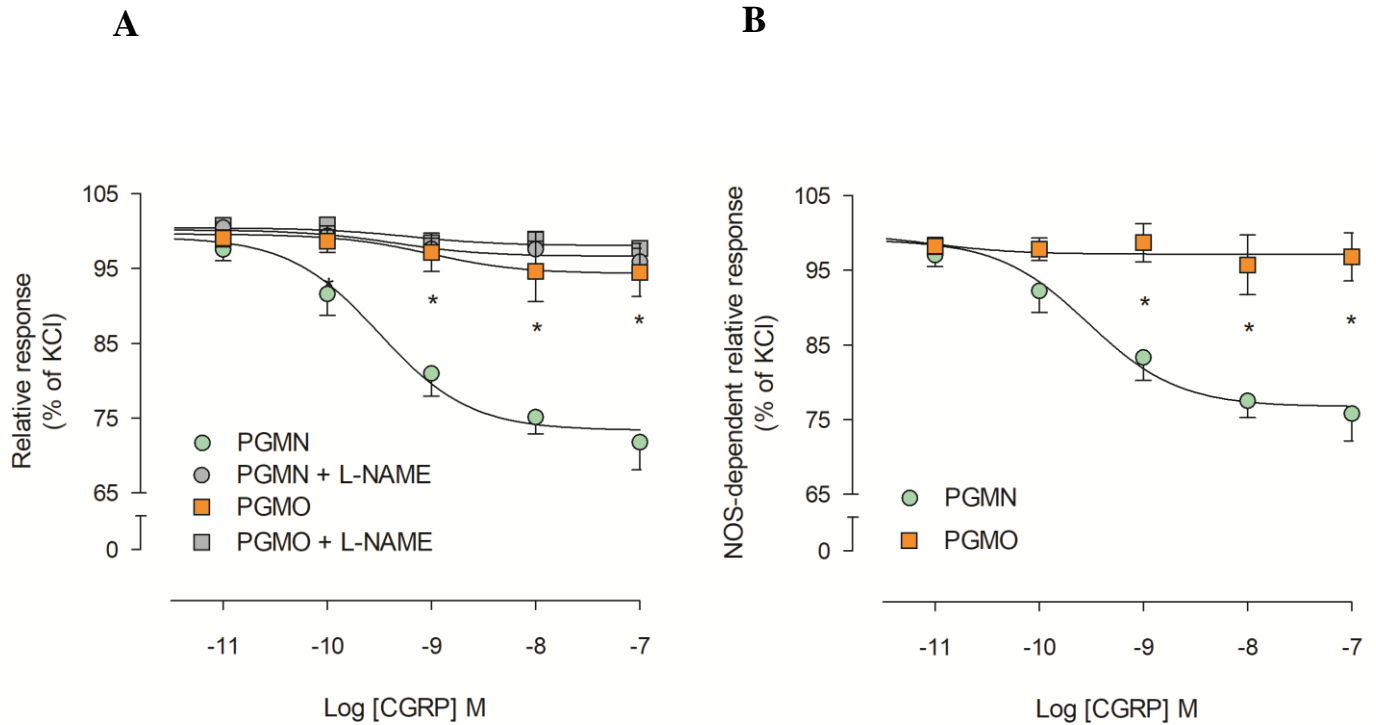


**Figure 7. CGRP-induced relaxation in human umbilical vein rings.** **A**, Human umbilical vein rings from pregnancies where the mother showed pre-gestational maternal normal weight (PGMN) or pre-gestational maternal obesity (PGMO) were pre-contracted with KCl 32.5 mM without or with L-NAME (30 minutes, 100  $\mu$ M), and then exposed (5 minutes) to CGRP (see Methods). **B**, NOS-dependent vasodilation determined by the subtraction of the total CGRP response minus the response in the presence of L-NAME. Values are mean  $\pm$  S.E.M.  $P < 0.05$ . \* vs the corresponding values in PGMN (n = 3 PGMN, 3 PGMO).

**Table 7. Parameters for NOS-dependent relaxation to insulin and CGRP in human umbilical vein rings.**

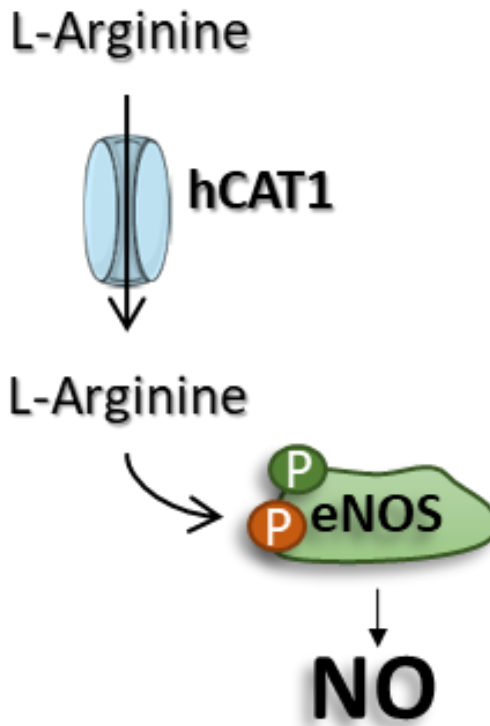
	<i>Condition</i>	<i>EC<sub>50</sub> (nM)</i>	<i>R<sub>max</sub></i>	<i>R<sub>max</sub>/EC<sub>50</sub></i>
<i>Insulin</i>	PGMN	0.42 ± 0.04	17.5 ± 1.7	43.7 ± 7.0
	PGMO	-	-	-
<i>CGRP</i>	PGMN	0.30 ± 0.02	23.3 ± 1.9	77.5 ± 3.5
	PGMO	-	-	-

CGRP, Calcitonin gene-related peptide; EC<sub>50</sub>, half maximal effective concentration. R<sub>max</sub>, maximum response. Values are mean ± S.E.M. (n in insulin was 5 PGMN and 7 PGMO, n in CGRP was 3 PGMN and 3 PGMO)

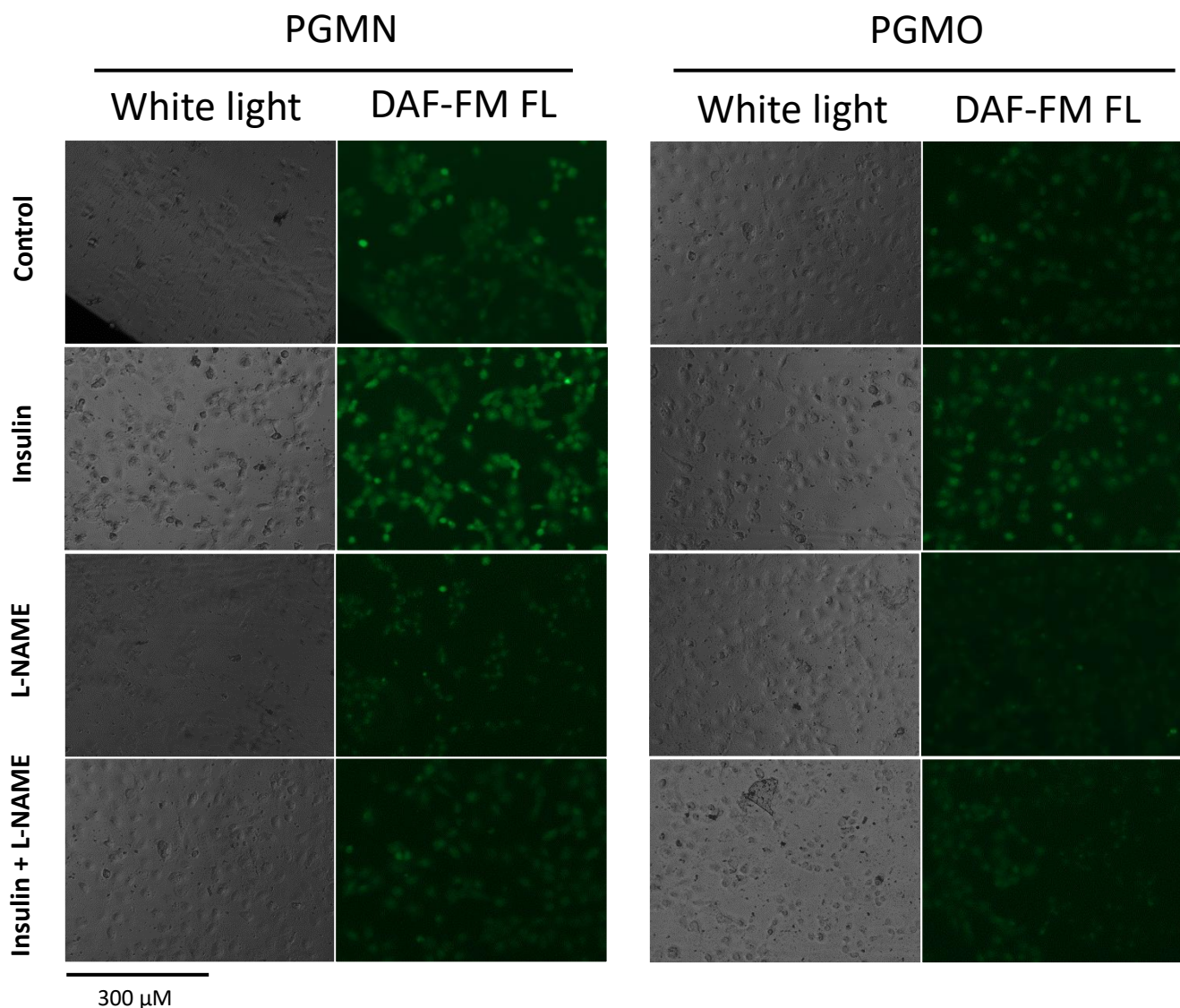
#### 5.2.4 *NO production by HUVECs in response to insulin*

Since the vasodilation in response to insulin is mediated by the endothelium-derived NO, the expression and activity of eNOS in HUVECs from PGMN or PGMO pregnancies was determined. Scheme 1 shows a representation of the key elements evaluated in sections 5.2.4 and 5.2.5. Insulin increased (~2.0 fold) the relative fluorescence for NO in HUVECs from PGMN but it was unaltered in HUVECs from PGMO (Figures 8 and 9A). L-NAME blocked the action of insulin in HUVECs from PGMN. The production of NOS-dependent NO was calculated from the subtraction between the overall production of NO and that inhibited by L-NAME. The basal NOS-dependent NO production was lower (~55%) in HUVECs PGMO than HUVECs PGMN (Figure 9B). The increase in the NOS-dependent NO production in response to insulin (~2.7 fold) in HUVECs from PGMN was similar to the overall production, with no changes in HUVECs from PGMO.

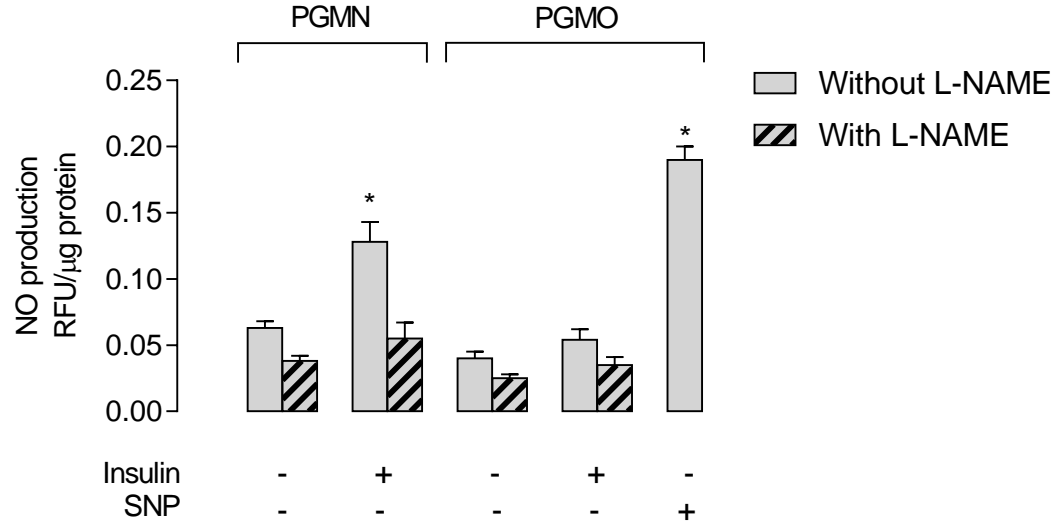
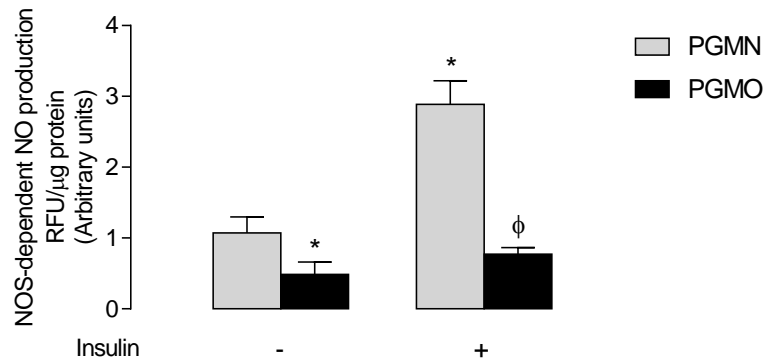
The analysis of protein abundance showed that there was no change in the total expression of eNOS (Figure 10A). However, HUVECs from PGMO showed lower activating phosphorylation of eNOS (serine 1177, ~34%) compared with HUVECs from PGMN, and the incubation with insulin increased the phosphorylation of this residue only in cells from PGMN pregnancies (Figure 10B). Conversely, the inhibiting phosphorylation of eNOS in Thr 495 was higher (~1,5 fold) in HUVECs from PGMO, and the incubation with insulin did not alter this phosphorylation in cells from both groups (Figure 10C). Thus, the lack of insulin response in umbilical veins and HUVECs from PGMO might also be due to a lower activation of eNOS.



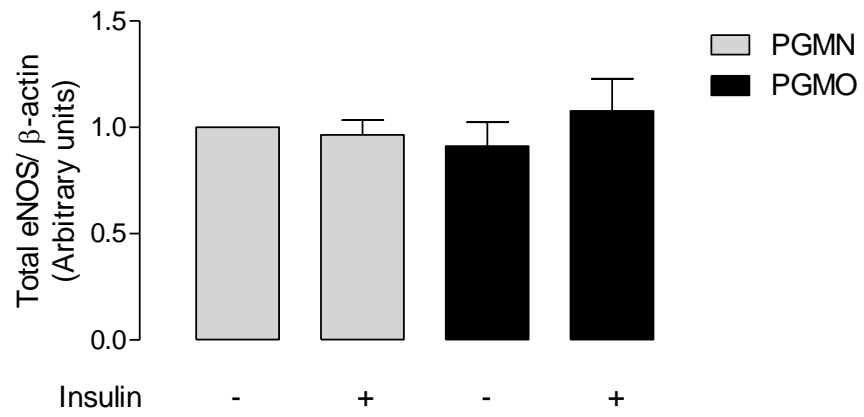
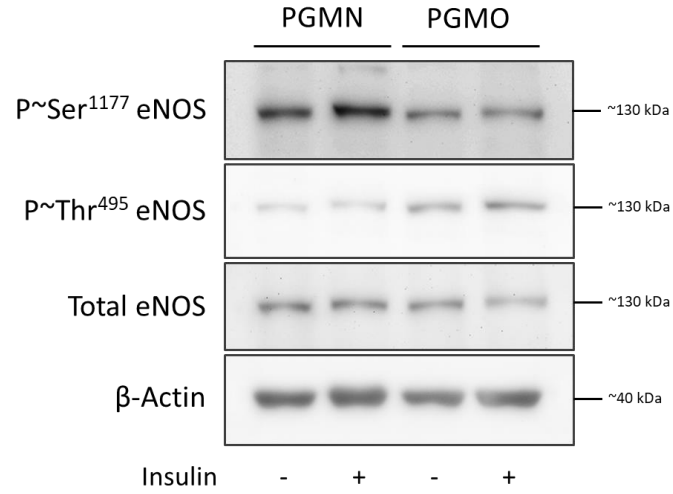
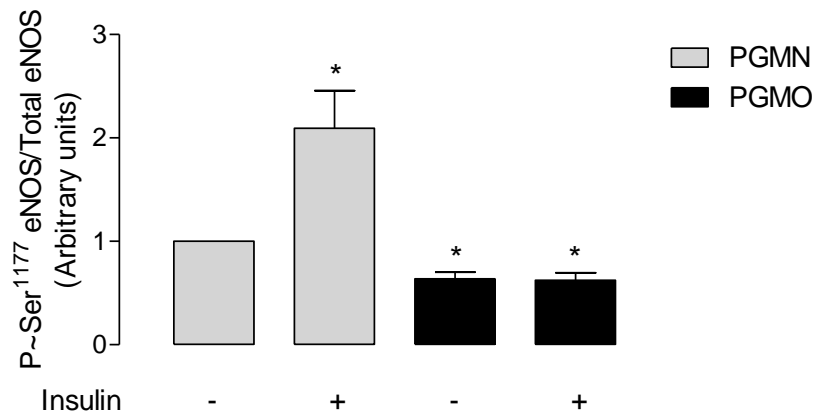
**Scheme 1. L-arginine uptake and NO generation.** hCAT1, human cationic amino acid transporter 1; eNOS, endothelial nitric oxide synthase; P in green, activating phosphorylation in serine 1177; P in orange, inhibiting phosphorylation in threonine 495; NO, nitric oxide.



**Figure 8. DAF-FM fluorescent signal in HUVECs.** The level of intracellular NO was evaluated by loading HUVECs from pregnancies where the mother showed pre-gestational maternal normal weight (PGMN) or pre-gestational maternal obesity (PGMO) with the probe sensitive to NO, DAF-FM, in the absence or presence of L-NAME (NOS inhibitor, pre-incubated 30 minutes, 100  $\mu$ M) and insulin (1 nM) (see Methods). The images are photographs taken by an epifluorescence microscope with white light and green fluorescence in cultures of HUVECs. Representative of other 7 experiments.

**A****B****Figure 9. Total and NOS-dependent NO generation in response to insulin by HUVECs.**

The level of intracellular NO in HUVECs from pregnancies where the mother showed pre-gestational maternal normal weight (PGMN) or pre-gestational maternal obesity (PGMO) was evaluated in cells loaded with DAF-FM (1 hour, 5  $\mu$ M) in the absence (-) or presence (+) of L-NAME (pre-incubated 30 minutes, 100  $\mu$ M), insulin (1 nM) and SNP (100  $\mu$ M) (see Methods). **A**, total fluorescence. **B**, NOS-dependent fraction of NOS calculated by subtracting the signal from cells treated with L-NAME. The values are the mean  $\pm$  S.E.M. Two ways ANOVA denoted significant differences between PGMN and PGMO groups, insulin treatment and interaction.  $P < 0.05$ . \* vs PGMN in basal condition.  $\phi$  vs PGMN + insulin. (n = 5 PGMN, 6 PGMO).

**A****B**

C

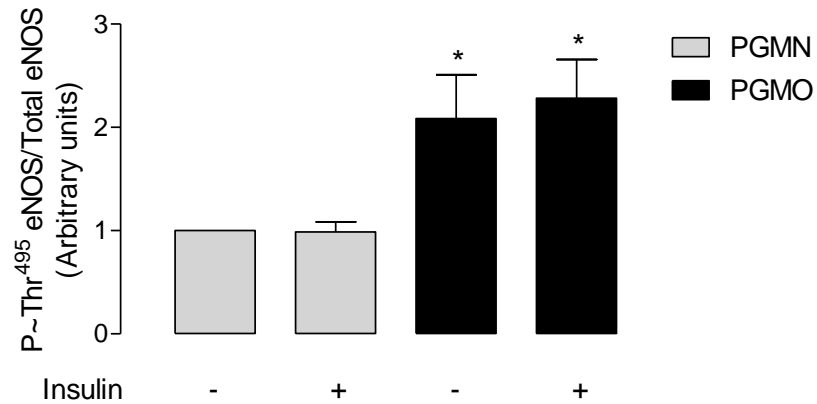


**Figure 10. Abundance and activation status of eNOS.** The protein abundance and the activating and inhibiting phosphorylations of eNOS in HUVECS from pregnancies where the mother showed pre-gestational maternal normal weight (PGMN) or pre-gestational maternal obesity (PGMO) incubated without (-) or with (+) insulin (1 nM) were evaluated by western blot (see Methods). **A**, Representative western blot for the eNOS. **B**, Densitometry for the total protein abundance of eNOS relative to  $\beta$ -actin. **C**, Densitometry for eNOS phosphorylated in serine 1177 over eNOS total. **D**, Densitometry for eNOS phosphorylated in threonine 495 over eNOS total. The densitometry was normalized to 1 with the data in HUVECS PGMN in absence of insulin. Values are mean  $\pm$  S.E.M. In **B**, two ways ANOVA denoted significant differences between PGMN and PGMO groups, insulin treatment and interaction. In **C**, two ways ANOVA denoted significant differences between PGMN and PGMO groups.  $P < 0,05$ . \* vs PGMN control. (n = 6 PGMN, 7 PGMO).

### 5.2.5 *L-Arginine transport and hCAT-1*

The  $v_i$  for the overall transport was higher (~1.4 fold) in cells from PGMO than PGMN with  $K_D$  values that were lower in PGMO compared with PGMN (Table 8). Overall transport data was semisaturable and showed a non-linear behavior in the Eadie-Hofstee plot representation (Figure 11).

After subtracting the linear, non-saturable transport component from the overall transport, the remaining L-arginine transport was saturable and adjusted to a single Michaelis-Menten equation and a linear representation in the Eadie-Hofstee plot (Figure 11C,D). The saturable transport in cells from PGMO showed higher  $V_{max}$  and maximal transport capacity ( $V_{max}/K_m$ ) compared with cells from PGMN pregnancies (Table 8). The apparent  $K_m$  values were not significantly altered in cells from these two study groups in all experimental conditions. Concordant with the L-arginine transport, the hCAT-1 protein abundance was higher (~1.5 fold) in cells from PGMO compared with PGMN (Figure 12).

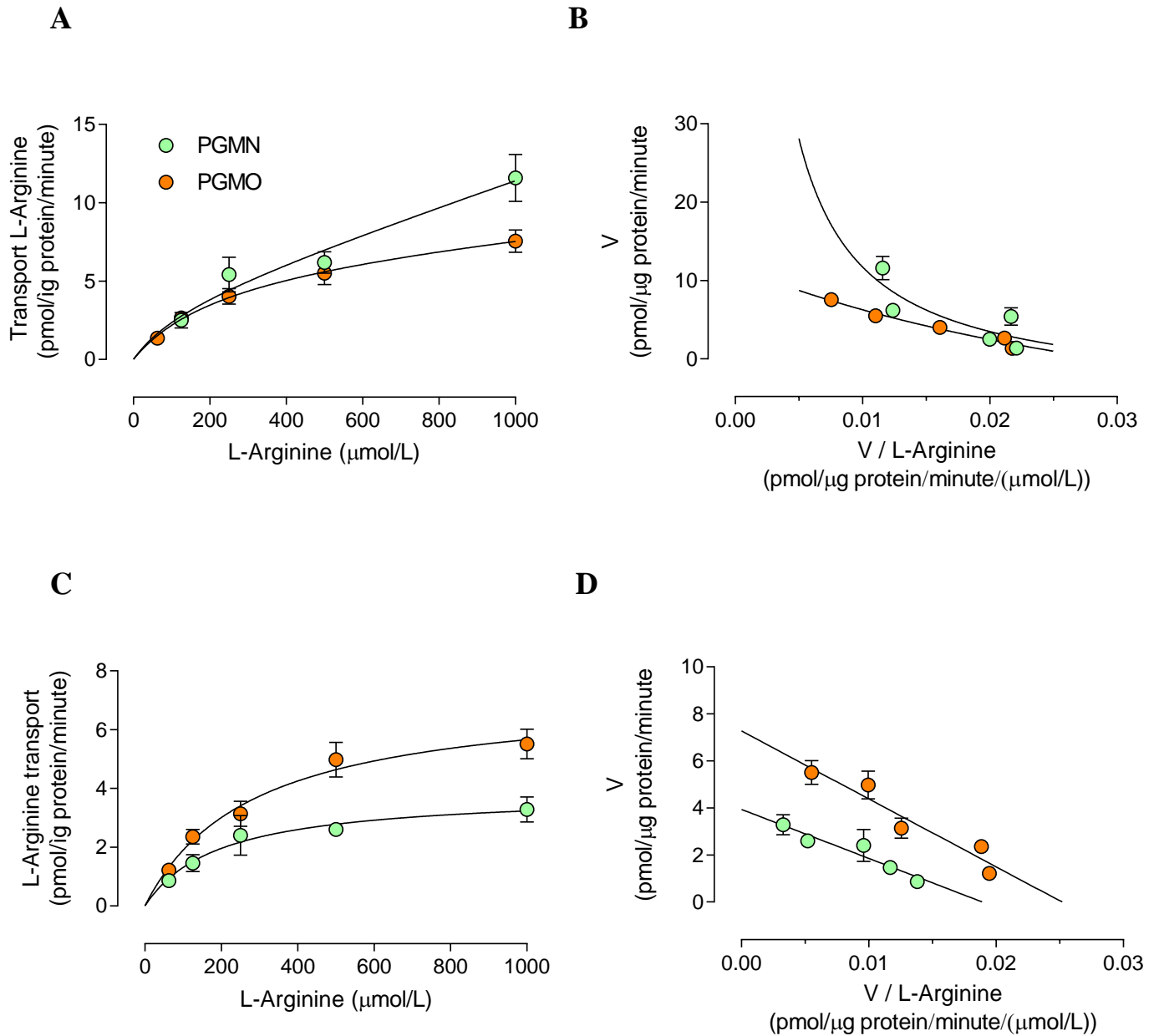


**Figure 11. L-arginine transport in HUVECs.** The overall L-arginine transport was determined in HUVECs from pregnancies where the mother showed pre-gestational maternal normal weight (PGMN) or pre-gestational maternal obesity (PGMO). The cells were incubated with L-arginine (0-1000  $\mu\text{M}$ , 3  $\mu\text{Ci/mL}$  of L- $^3\text{H}$ arginine, 37°C, 1 minute) (see Methods). **A**, overall L-arginine transport. Data were adjusted to the Michaelis-Menten hyperbola plus a nonsaturable, linear component. **B**, Eadie-Hofstee plots for overall transport data. **C**, Saturable transport of L-arginine derived from data in A adjusted to a single Michaelis-Menten equation. **D**, Eadie-Hofstee plots for saturable transport data. Values are mean  $\pm$  S.E.M. (n = 12 PGMN, 12 PGMO).

**Table 8. Kinetic parameters for the L-arginine transport in HUVECs**

	<i>Saturable transport</i>			<i>Overall transport</i>	
	$V_{\max}$ (pmol/ $\mu$ g protein/ minute)	$K_m$ ( $\mu$ M)	$V_{\max}/K_m$ (pmol/ $\mu$ g protein/ minute/ $\mu$ M)	$K_D$ (pmol/ $\mu$ g protein/ minute/ $\mu$ M)	$v_i$ (pmol/ $\mu$ g protein/ 0.5 s)
PGMN	3.86 $\pm$ 0.29	195 $\pm$ 42	0.0198 $\pm$ 0.0029	0.0081 $\pm$ 0.0042	0.0069 $\pm$ 0.0001
PGMO	7.26 $\pm$ 0.59 *	253 $\pm$ 58	0.0287 $\pm$ 0.0043 *	0.0021 $\pm$ 0.0010 *	0.0099 $\pm$ 0.0001 *

L-Arginine transport (0–1000  $\mu$ mol/L, 1 min, 37 °C) was measured in HUVECs from women PGMN or PGMO (see Methods). Maximal velocity ( $V_{\max}$ ) and apparent Michaelis-Menten constant ( $K_m$ ) of saturable transport were calculated assuming a single Michaelis-Menten hyperbola. The  $V_{\max}/K_m$  represents maximal L-arginine transport capacity. The lineal phase of overall transport of L-arginine ( $K_D$ ) was obtained from transport data fitted to a Michaelis-Menten equation increased in a lineal component. Initial velocity ( $v_i$ ) was calculated for 0.5 s with 100  $\mu$ mol/L L-arginine transport.  $P < 0.05$ . \* vs the PGMN control. Values are mean  $\pm$  S.E.M. (n = 12 PGMN, 12 PGMO).

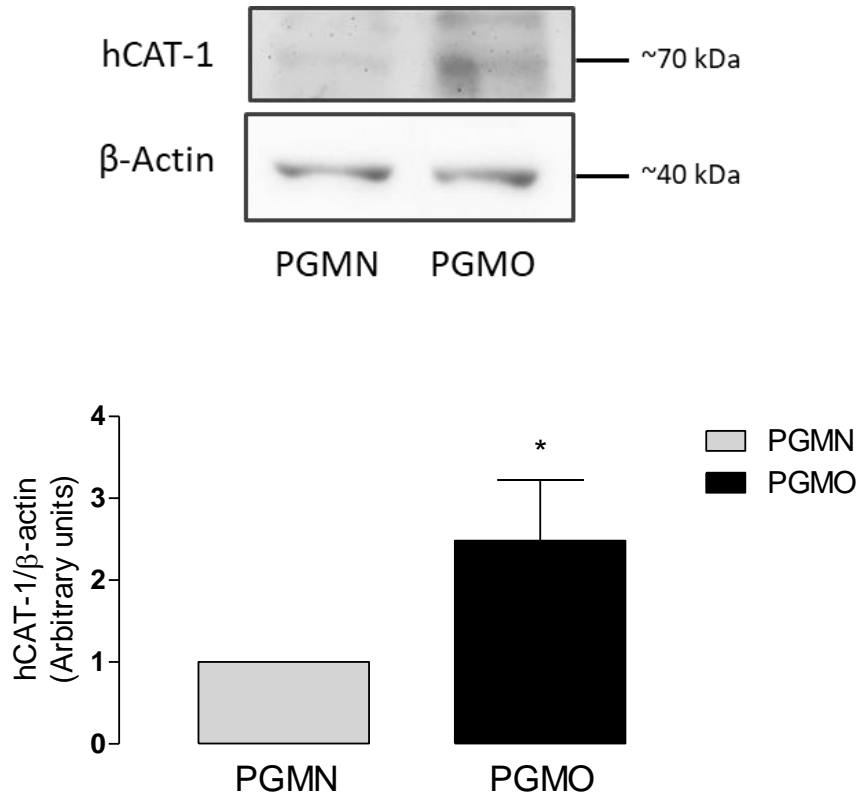
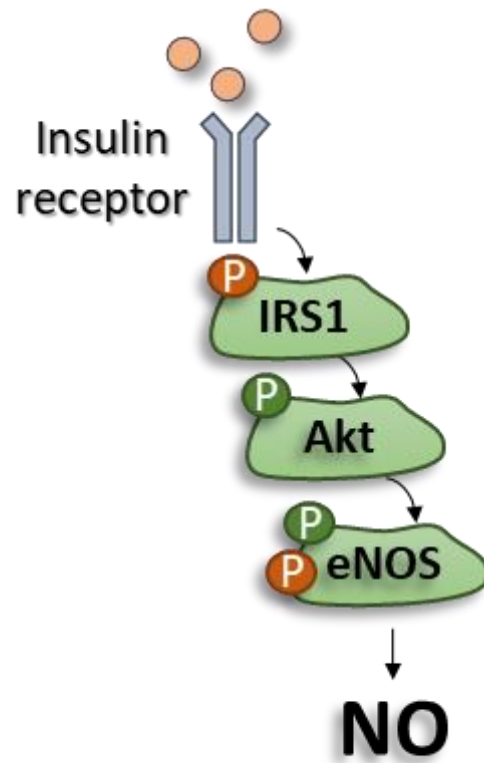


**Figure 12. Protein abundance of hCAT-1 in HUVECs.** Western blot for hCAT-1 and  $\beta$ -actin protein abundance in HUVECs from pregnancies where the mother showed pre-gestational maternal normal weight (PGMN) or pre-gestational maternal obesity (PGMO). Lower panel: hCAT-1/ $\beta$ -actin ratio densitometry normalized to 1 in PGMN. Values are mean  $\pm$  S.E.M.  $P < 0.05$ . \* vs PGMN (n = 9 PGMN, 9 PGMO).

### 5.2.6 *Insulin signaling*

Insulin signaling pathway was evaluated by the activation of IR, IRS1, and Akt in basal conditions and in response to insulin (see Scheme 2). There were no significant differences in the total protein abundance of  $\beta$ -IR (Figure 13A), IRS1 (Figure 14A), and Akt (Figure 15A). Also, there were no changes in the activating phosphorylation in tyrosine 1361 of the  $\beta$ -IR at basal conditions but insulin increased the phosphorylation at this residue which was similar (~7.5 fold) in cells from PGMN or PGMO pregnancies (Figure 13B). However, the inhibiting phosphorylation of IRS1 on serine 307 was higher (~2.0 fold) in HUVECs from PGMO compared with cells from PGMN (Figure 14B). The phosphorylation of IRS1 on serine 307 was unaltered by insulin in cells from both study groups. Consistent with higher inhibition of IRS1, the activating phosphorylation of Akt in serine 473 was reduced (~31%) in HUVECs from PGMO compared with PGMN, and the treatment with insulin resulted in higher (~1.7 fold) Akt phosphorylation only in HUVECs from PGMN (Figure 15B).



**Scheme 2. Insulin signaling pathway in endothelium.** IRS1, insulin receptor substrate 1; eNOS, endothelial nitric oxide synthase; P in orange, inhibiting phosphorylation; P in green, activating phosphorylation.

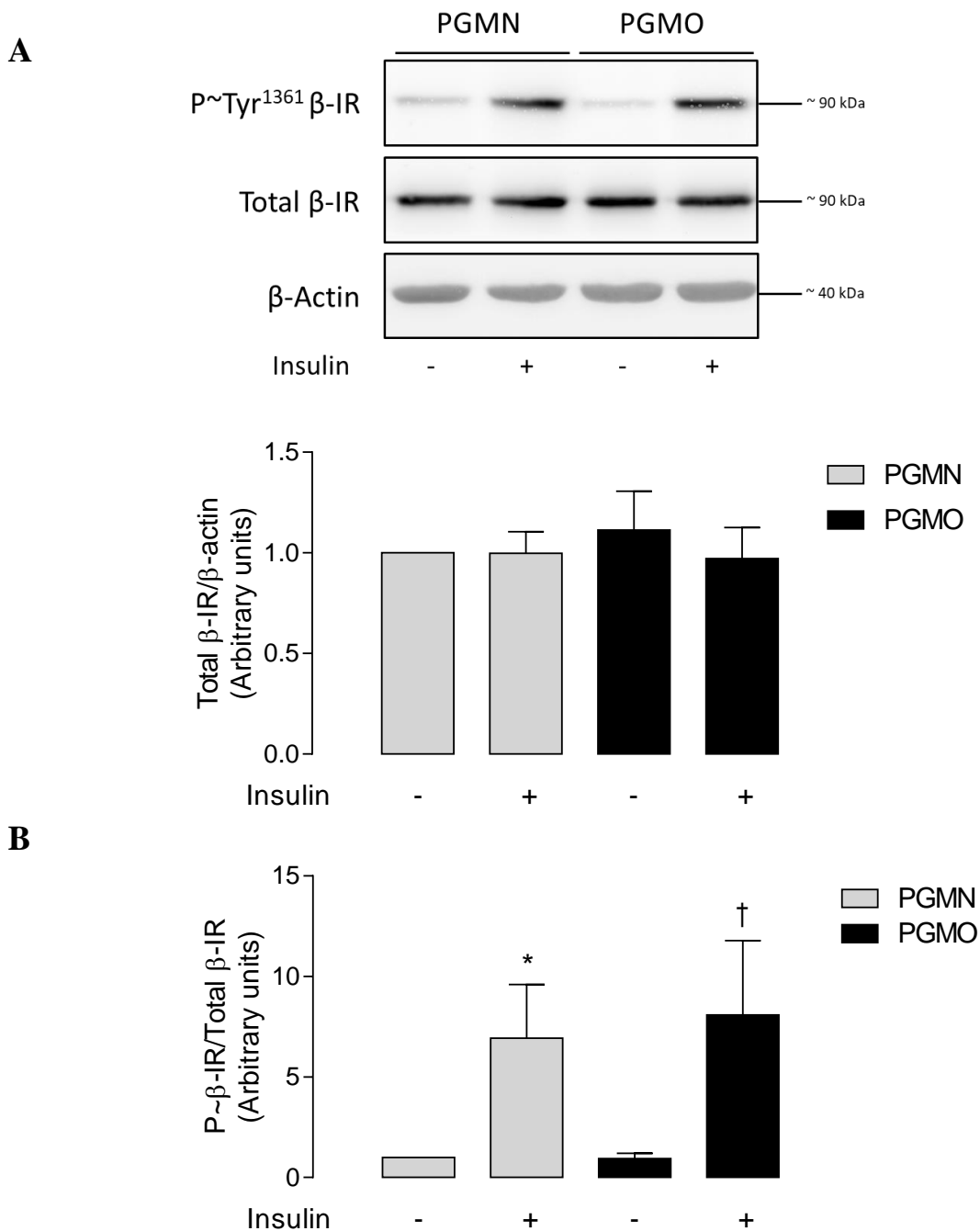


**Figure 13. Abundance and insulin-induced activation of IR.** **A**, Western blot for total β-IR, phosphorylated β-IR, and β-actin protein abundance in HUVECs from pregnancies where the mother showed pre-gestational maternal normal weight (PGMN) or pre-gestational maternal obesity (PGMO). Cells were incubated without (–) or with (+) insulin (20 min) (see Methods). Lower graphs show Total β-IR/β-actin and (**B**) phosphorylated β-IR/total β-IR ratio densitometries normalized to 1 in PGMN without insulin. Values are mean ± S.E.M. Two ways ANOVA denoted significant differences for insulin treatment. *P*<0,05. \* vs PGMN control. † vs PGMO control (n = 4 PGMN, 4 PGMO).

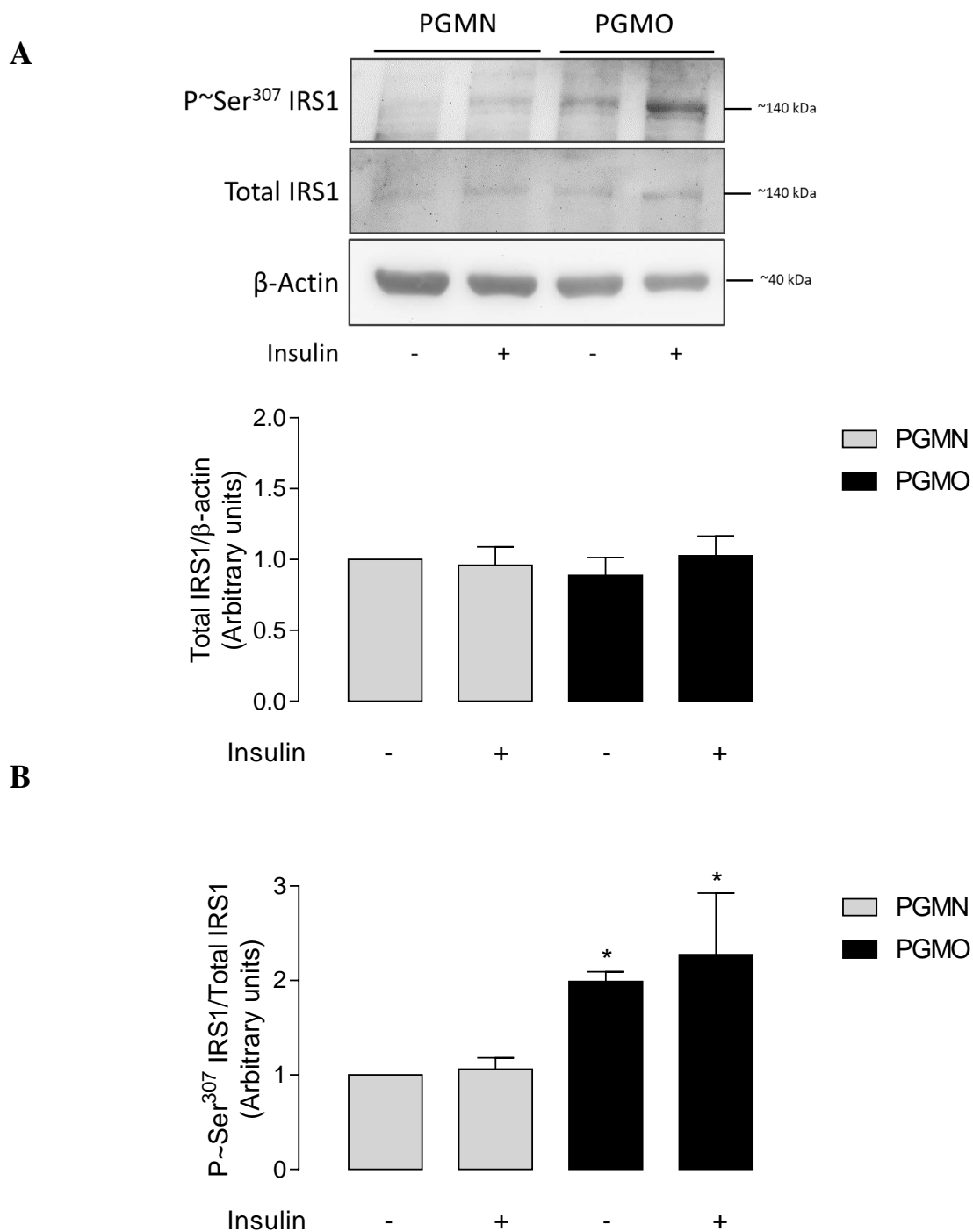


**Figure 14. Abundance and activation status of IRS1.** A, Western blot for total IRS-1, phosphorylated IRS-1, and  $\beta$ -actin protein abundance in HUVECs from pregnancies where the mother showed pre-gestational maternal normal weight (PGMN) or pre-gestational maternal obesity (PGMO). Cells were incubated without (-) or with (+) insulin (20 min) (see Methods). Lower graphs show Total IRS-1/ $\beta$ -actin and (B) phosphorylated IRS-1/total IRS-1 ratio densitometries normalized to 1 in PGMN without insulin. Values are mean  $\pm$  S.E.M. Two ways ANOVA denoted significant differences between groups.  $P < 0,05$ . \* vs PGMN control. (n = 4 PGMN, 4 PGMO).

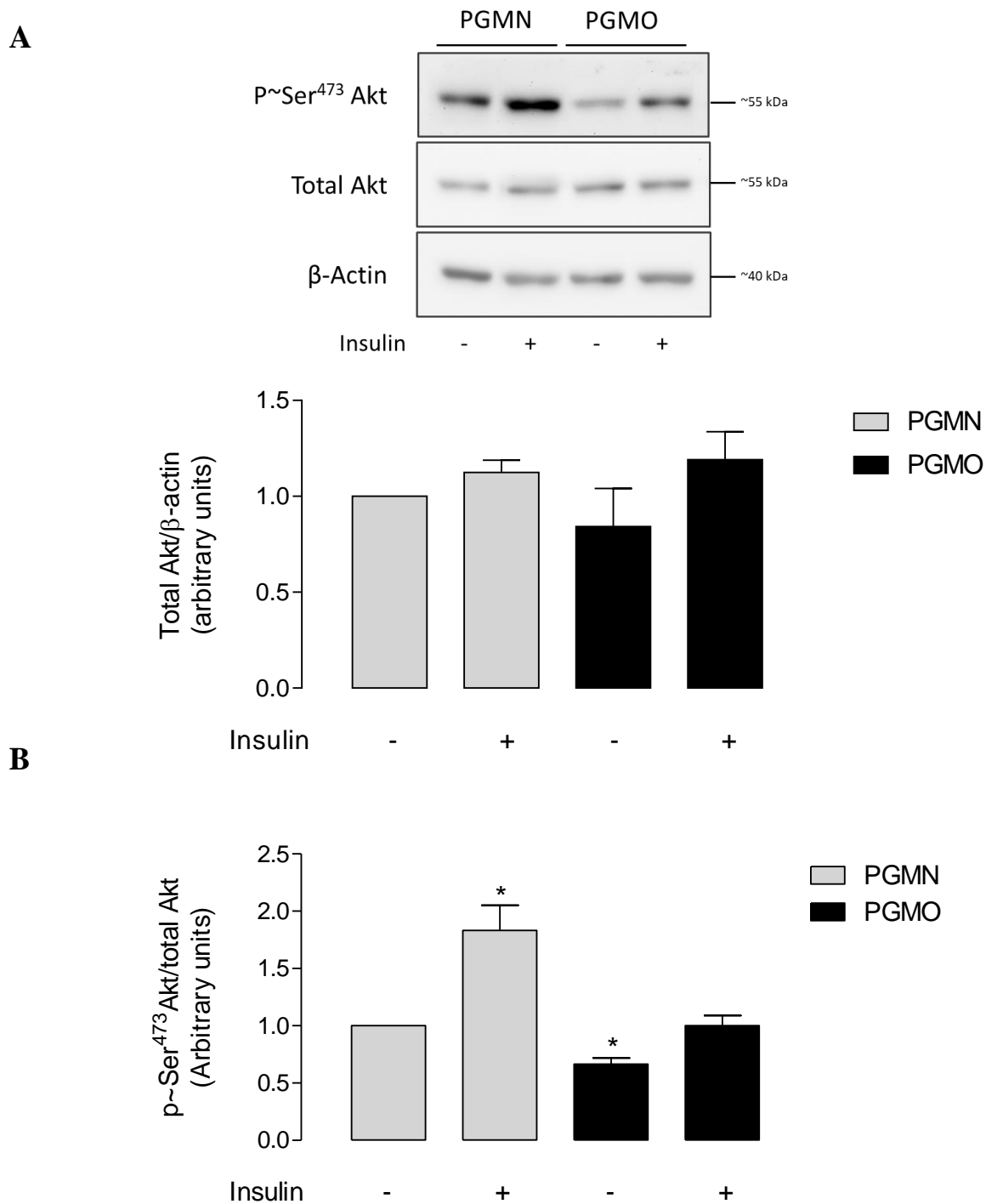


**Figure 15. Abundance and insulin-induced activation of Akt.** **A**, Western blot for total Akt and phosphorylated Akt, and  $\beta$ -actin protein abundance in HUVECs from pregnancies where the mother showed pre-gestational maternal normal weight (PGMN) or pre-gestational maternal obesity (PGMO). Cells were incubated without (-) or with (+) insulin (20 min) (see Methods). Lower graphs show Total Akt/ $\beta$ -actin and **(B)** phosphorylated Akt/total Akt ratio densitometries normalized to 1 in PGMN without insulin. Values are mean  $\pm$  S.E.M.  $P < 0,05$ . Two ways ANOVA denoted significant differences between PGMN and PGMO groups and insulin treatment. \* vs PGMN control. (n = 10 PGMN, 13 PGMO).

### 5.3 Activation of UPR

The occurrence of ER stress was evaluated through the activation of key proteins of the UPR, whose are represented in the Scheme 3.

#### 5.3.1 Activation of the master UPR sensors

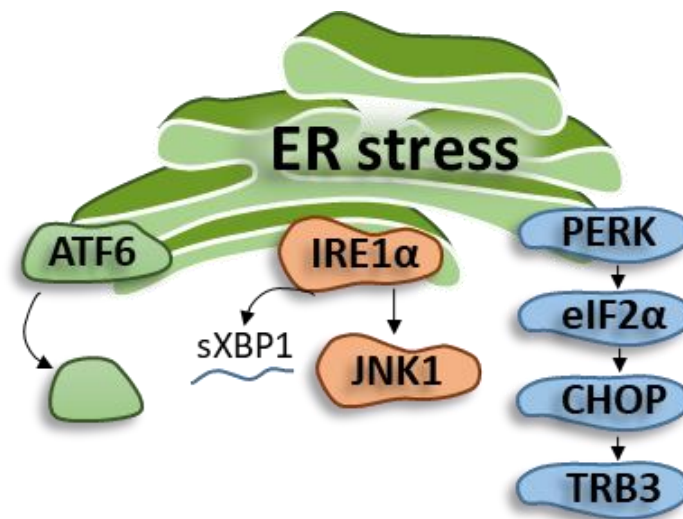
The activating phosphorylation of PERK at threonine 981 (Figure 16) and eIF2 at serine 51 (Figure 17) in the  $\alpha$  subunit were higher in HUVECs from PGMO than PGMN pregnancies (~2.0 and ~2.7 fold, respectively); however, there were no significant differences in total protein abundance. Conversely, there was an increase (~1.9 fold) in the total protein abundance of IRE1 $\alpha$  in cells from PGMO, but the activating phosphorylation in serine 724 was unaltered (Figure 18). Parallel assays in HUVECs from PGMO showed a higher localization of ATF6 at the nucleus (~2,6 fold) compared with cells from PGMN (Figure 19).

#### 5.3.2 Pharmacologic modulation of ER stress

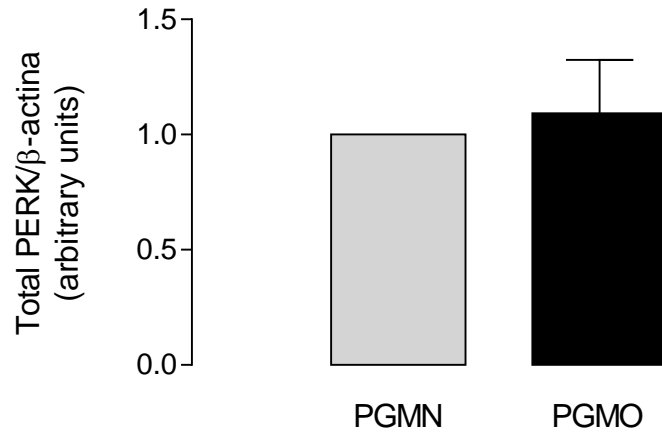
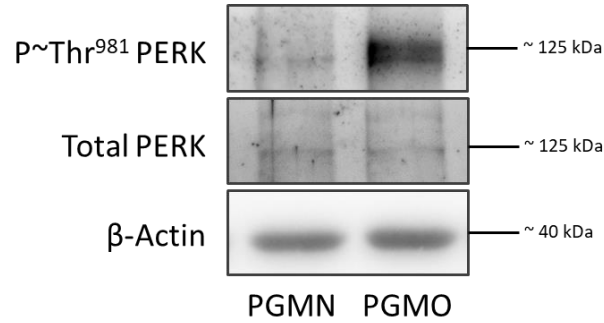
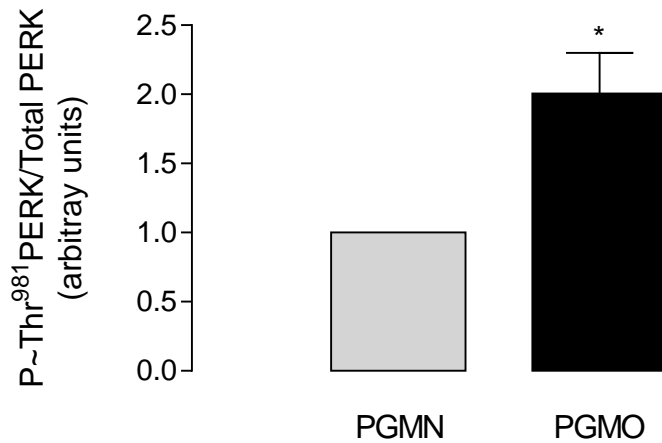
Tunicamycin and TUDCA were used to modulate ER stress in HUVECs from both conditions. The standardization of the time and concentration were determined by evaluating the inhibiting phosphorylation of eIF2 $\alpha$ . Tunicamycin (5  $\mu$ M, 0-12 h) increased (2.9 fold) the eIF2 $\alpha$  phosphorylation in HUVECs from PGMN (Figure 20) but did not change it in cells from PGMO (Figure 21). Meanwhile, TUDCA (100  $\mu$ M, 0-12 hours) did not change the phosphorylation of eIF2 $\alpha$  in cells from PGMN (Figure 22) but reduced it (~73%) in HUVECs from PGMO at 8 hours of incubation (Figure 23).

The concentration curve (8 h, 0-10  $\mu$ M) showed that tunicamycin treatment at 5  $\mu$ M increased the phosphorylation of eIF2 $\alpha$  with an EC<sub>50</sub> of  $2.3 \pm 1.9 \mu$ M (Figure 24A). According to the available literature (see Table 9), the concentration of tunicamycin used in order to induce ER stress is between 1 to 10  $\mu$ M. Therefore, in this study, a concentration of

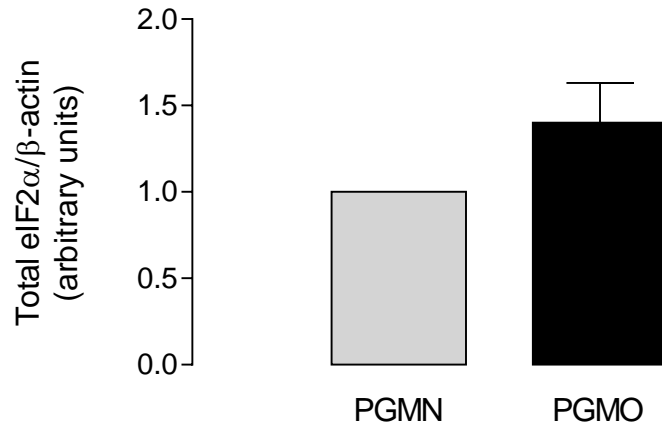
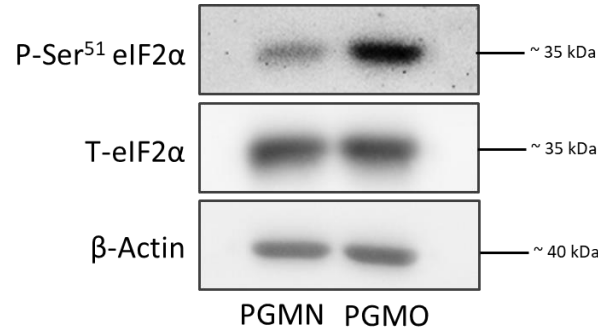
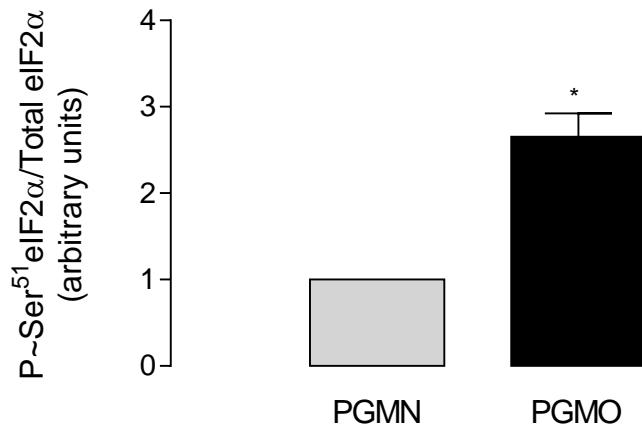
5  $\mu\text{M}$  tunicamycin for 8 hours incubation was used for the induction of ER stress in HUVECs. On the other hand, the treatment with TUDCA (8 h, 0-1000  $\mu\text{M}$ ) at 100  $\mu\text{M}$  reduced the phosphorylation of eIF2 $\alpha$  ( $\sim 37\%$ ,  $\text{EC}_{50}$  was  $46,7 \pm 56.5$   $\mu\text{M}$ ) to a similar level to that reached by 500  $\mu\text{M}$  and 1000  $\mu\text{M}$  TUDCA in HUVECs from PGMO (Figure 24 C), but not in cells from PGMN. The concentrations of TUDCA described in the literature to reduce ER stress in cultured cells are from 20  $\mu\text{M}$  to 10 mM (Table 9). Thus, the concentration and time chosen for the treatment of cells with TUDCA were 100  $\mu\text{M}$  and 8 hours.



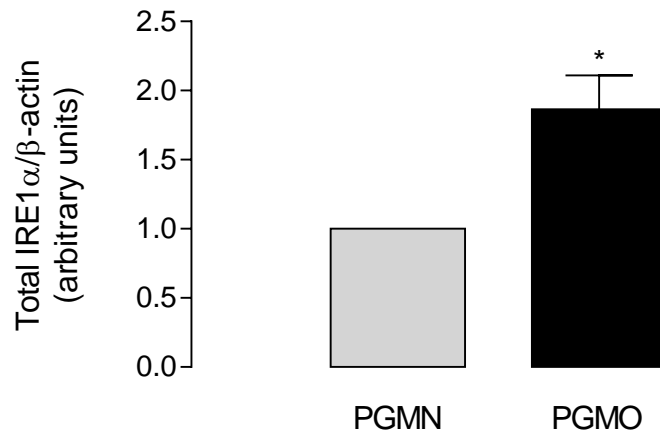
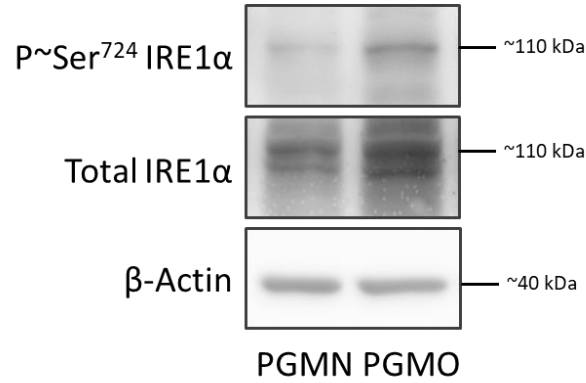
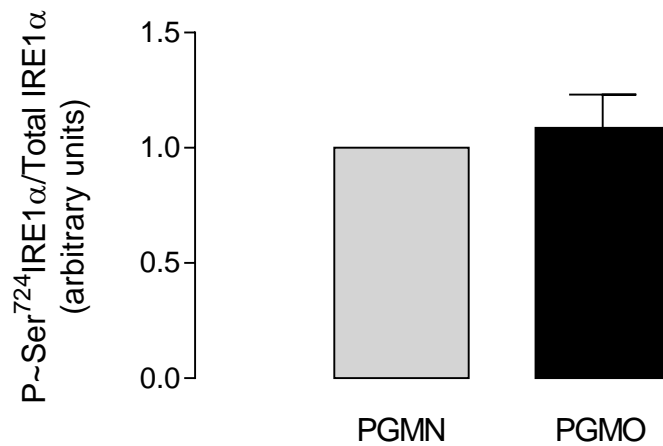
**Scheme 3. Key proteins of the unfolded protein response.** ER, endoplasmic reticulum; ATF6, activating transcription factor 6; IRE1 $\alpha$ , Inositol-requiring enzyme 1 $\alpha$ ; JNK, c-jun N-terminal kinase 1; sXBP1, spliced X-box binding protein 1 mRNA; PERK, Protein kinase RNA-like endoplasmic reticulum kinase; eIF2 $\alpha$ , subunit  $\alpha$  of the eukaryotic translation initiator factor 2; CHOP, CCAAT-enhancer-binding protein homologous protein; TRB3, Tribbles-like protein 3.

**A****B**

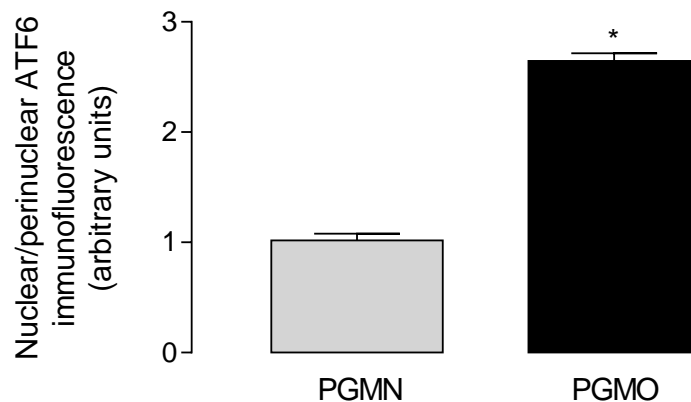
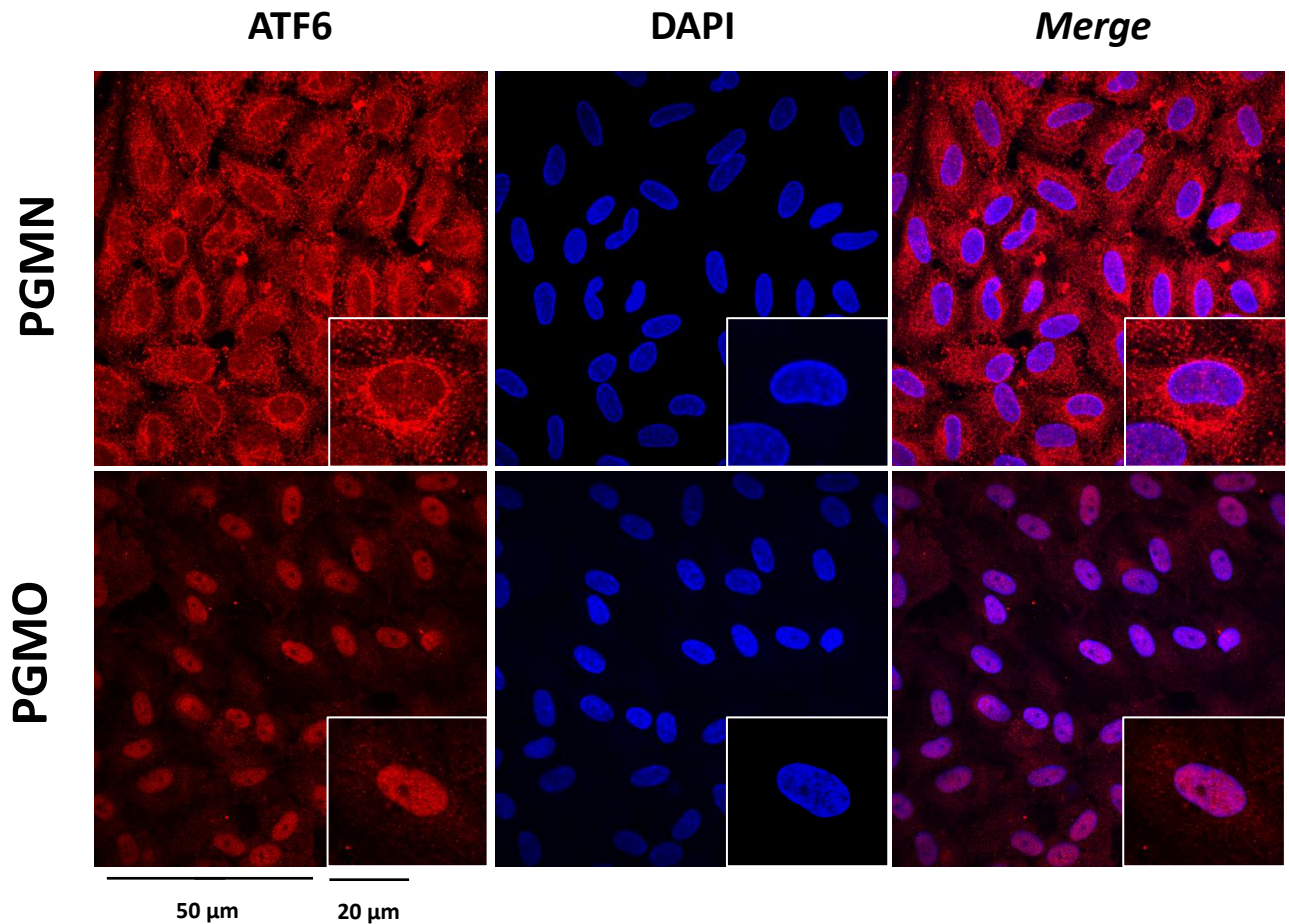
**Figure 16. Abundance and activation status of PERK.** **A**, Western blot for total and phosphorylated PERK, and β-actin protein abundance in HUVECs from pregnancies where the mother showed pre-gestational maternal normal weight (PGMN) or pre-gestational maternal obesity (PGMO). Lower graphs show Total PERK/β-actin and **(B)** phosphorylated PERK/total PERK ratio densitometries normalized to 1 in PGMN. Values are mean ± S.E.M.  $P < 0.05$ . \* vs PGMN. (n = 9 PGMN, 9 PGMO).

**A****B**

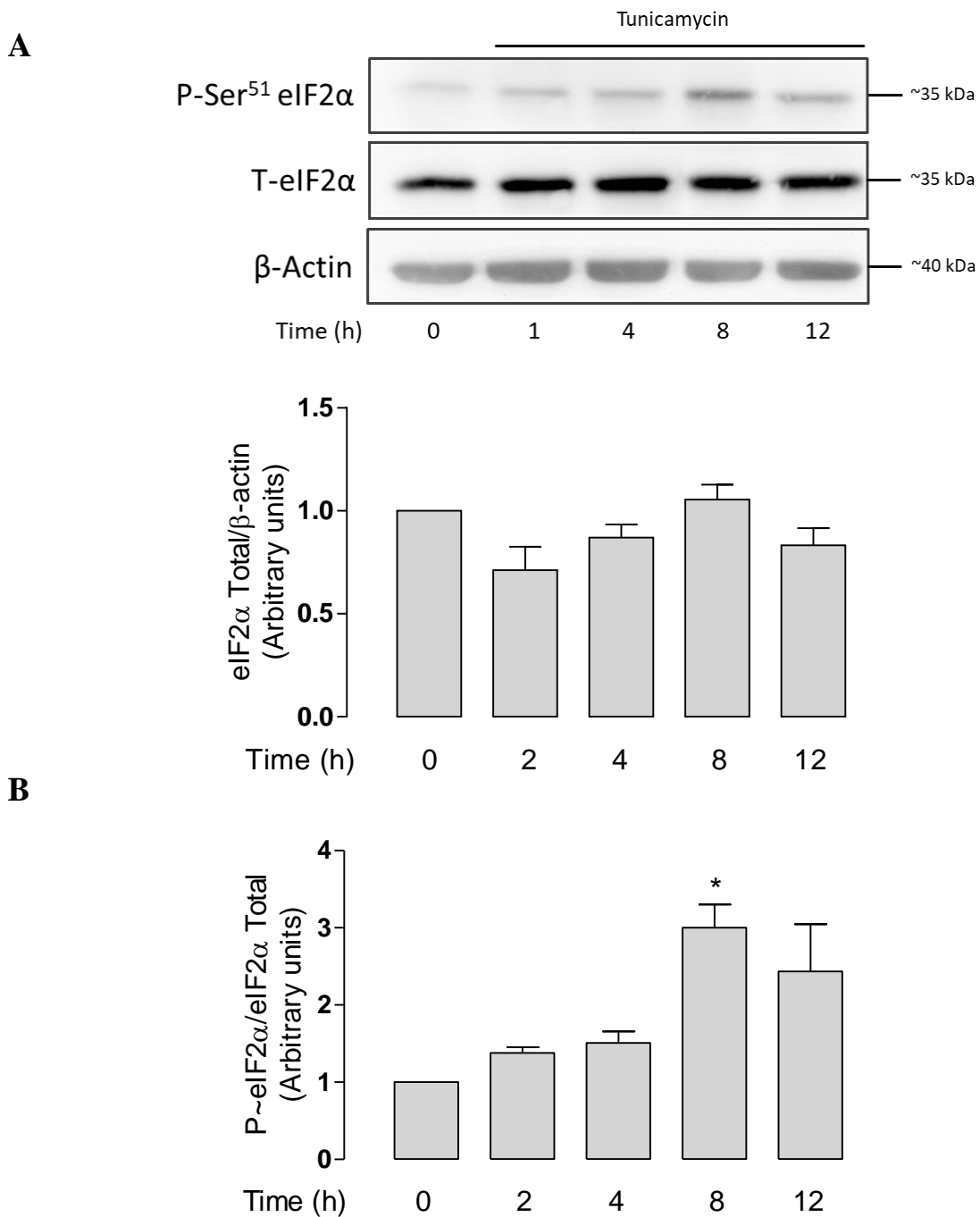
**Figure 17. Abundance and activation state of eIF2 $\alpha$ .** **A**, Western blot for total eIF2 $\alpha$  and phosphorylated eIF2 $\alpha$ , and  $\beta$ -actin protein abundance in HUVECs from pregnancies where the mother showed pre-gestational maternal normal weight (PGMN) or pre-gestational maternal obesity (PGMO). Lower graphs show Total eIF2 $\alpha$ / $\beta$ -actin and **(B)** phosphorylated eIF2 $\alpha$ /total eIF2 $\alpha$  ratio densitometries normalized to 1 in PGMN. Values are mean  $\pm$  S.E.M.  $P < 0.05$ . \* vs PGMN. (n = 9 PGMN, 9 PGMO).

**A****B**

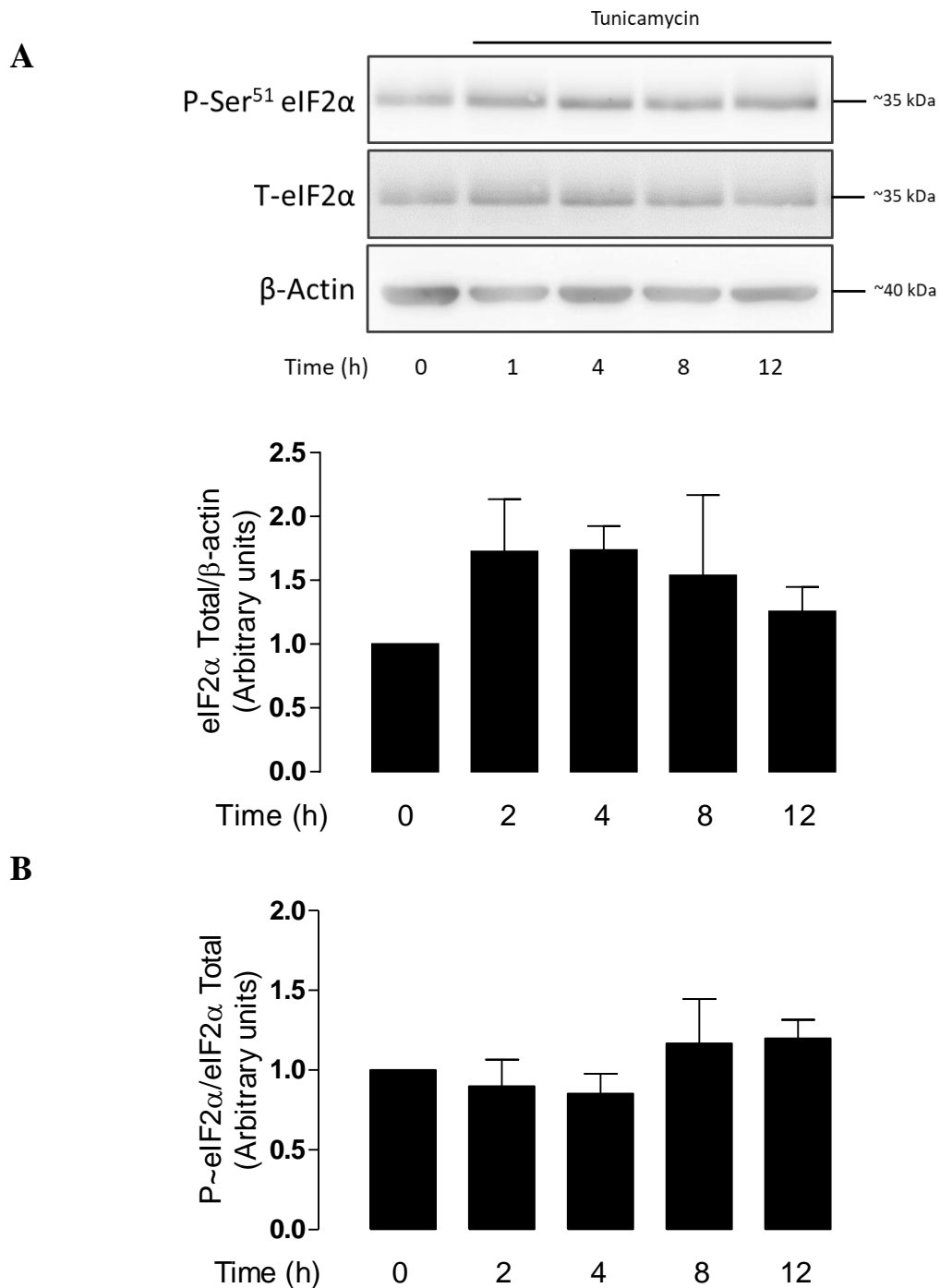
**Figure 18. Abundance and activation status of IRE1α.** **A**, Western blot for total IRE1α and phosphorylated IRE1α, and β-actin protein abundance in HUVECs from pregnancies where the mother showed pre-gestational maternal normal weight (PGMN) or pre-gestational maternal obesity (PGMO). Lower graphs show Total IRE1α/β-actin and **(B)** phosphorylated IRE1α/total IRE1α ratio densitometries normalized to 1 in PGMN. Values are mean ± S.E.M.  $P < 0,05$ . \* vs PGMN. (n = 8 PGMN, 8 PGMO).



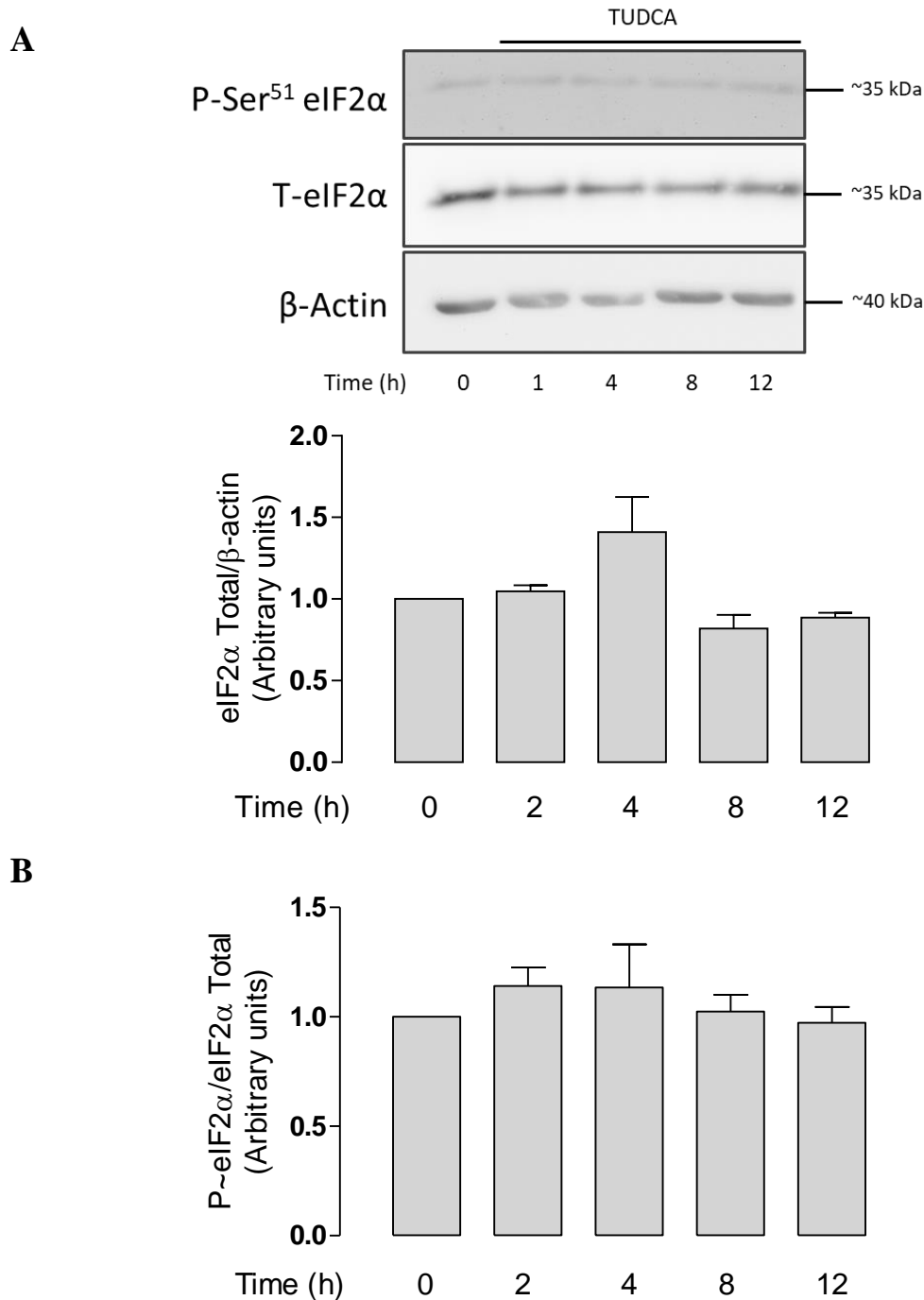
**Figure 19. Cellular localization of ATF6.** The localization of ATF6 was evaluated by immunofluorescence in confocal microscopy (see Methods). Images show the immunofluorescence for cellular localization of ATF6 (representative of other 7 experiments) in HUVECs from pregnancies where the mother showed pre-gestational maternal normal weight (PGMN) or pre-gestational maternal obesity (PGMO). ATF6 is shown in red and the nuclei in blue (DAPI). The graph shows the Nuclear/perinuclear ratio of the localization of ATF6. The values were normalized to 1 with data in HUVECs PGMN.  $P < 0.05$ . \* vs PGMN. Values are mean  $\pm$  S.E.M. (n = 8 PGMN, 8 PGMO).



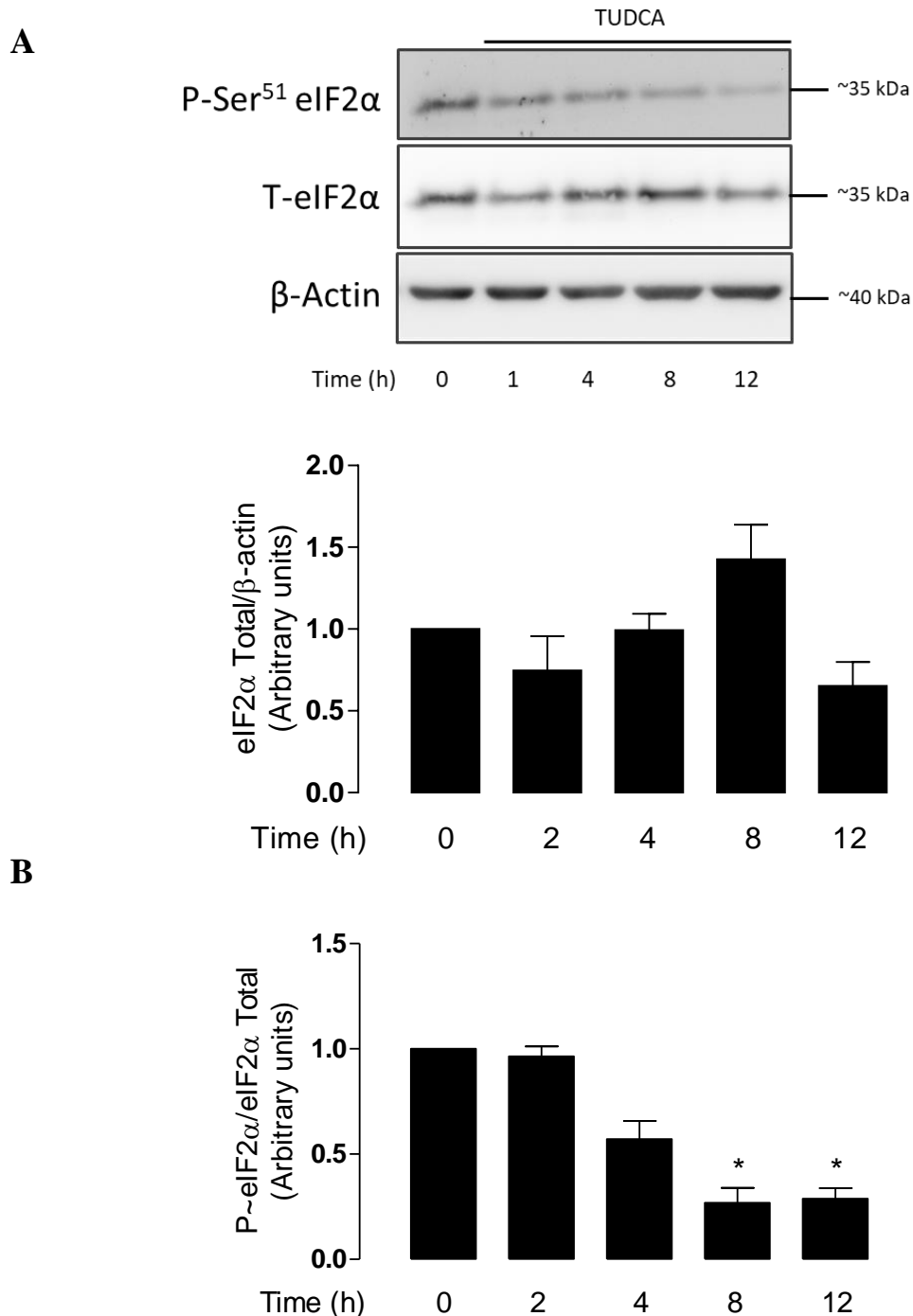
**Figure 20. Time curve for inactivation of eIF2 $\alpha$  in response to tunicamycin in HUVECs from PGMN pregnancies.** The effect of tunicamycin (5  $\mu$ M) on the inactivating phosphorylation of eIF2 $\alpha$  was evaluated by western blot at the indicated times in HUVECs from pregnancies where the mother showed pre-gestational maternal normal weight (PGMN) (see Methods). **A**, Western blot for total eIF2 $\alpha$  and phosphorylated eIF2 $\alpha$ , and  $\beta$ -actin protein abundance. Lower graphs show Total eIF2 $\alpha$ / $\beta$ -actin and **(B)** phosphorylated eIF2 $\alpha$ /total eIF2 $\alpha$  ratio densitometries normalized to 1 in control. Values are mean  $\pm$  S.E.M.  $P < 0,05$ . \* vs control. (n = 3).



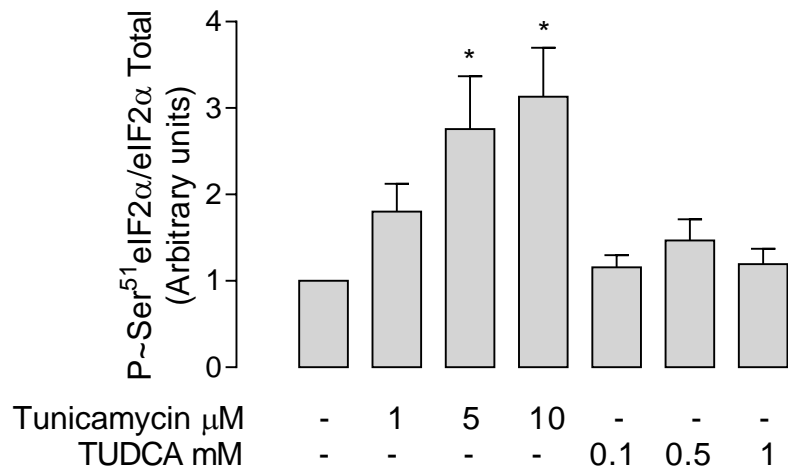
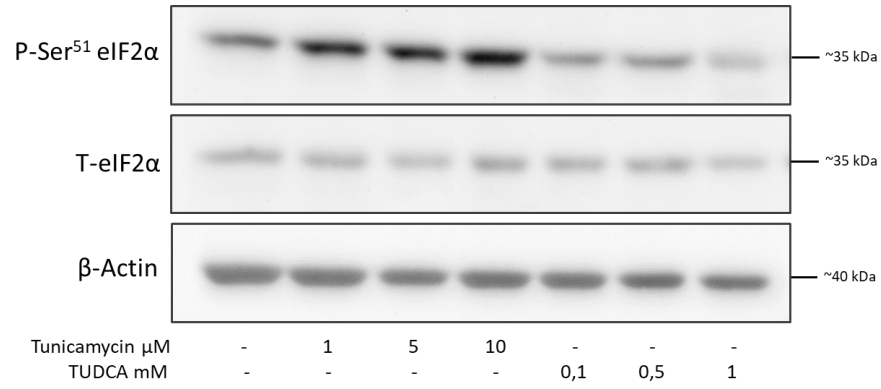
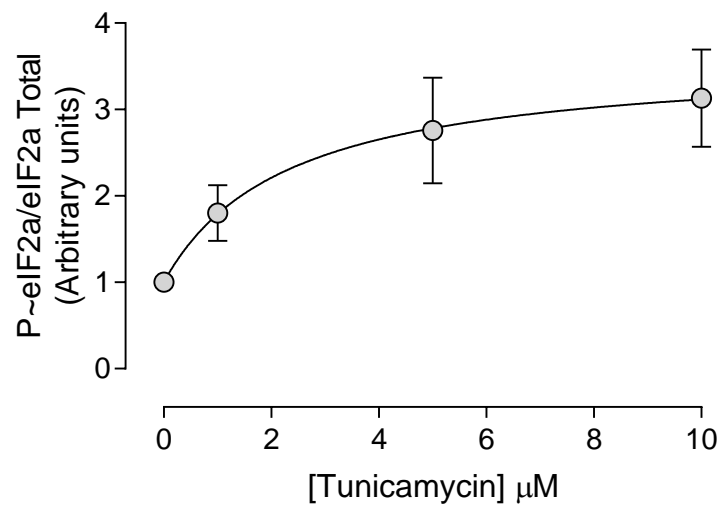
**Figure 21. Time curve for inactivation of eIF2 $\alpha$  in response to tunicamycin in HUVECs from PGMO pregnancies.** The effect of tunicamycin (5  $\mu$ M) on the inactivating phosphorylation of eIF2 $\alpha$  was evaluated by western blot at the indicated times abundance in HUVECs from pregnancies where the mother showed pre-gestational maternal obesity (PGMO) (see Methods). **A**, Western blot for total and phosphorylated eIF2 $\alpha$ , and  $\beta$ -actin protein abundance. Lower graphs show Total eIF2 $\alpha$ / $\beta$ -actin and **(B)** phosphorylated eIF2 $\alpha$ /total eIF2 $\alpha$  ratio densitometries normalized to 1 in control. Values are mean  $\pm$  S.E.M.  $P < 0,05$ . \* vs control. (n = 3).



**Figure 22. Time curve for inactivation of eIF2α in response to TUDCA in HUVECs from PGMN pregnancies.** The effect of TUDCA (100 μM) on the inactivating phosphorylation of eIF2α was evaluated by western blot at the indicated times in HUVECs from pregnancies where the mother showed pre-gestational maternal normal weight (PGMN) (see Methods). **A**, Western blot for total and phosphorylated eIF2α, and β-actin protein abundance. Lower graphs show Total eIF2α/β-actin and **(B)** phosphorylated eIF2α/total eIF2α ratio densitometries normalized to 1 in control. Values are mean ± S.E.M. *P* < 0.05. \* vs control. (n = 3).



**Figure 23. Time curve for inactivation of eIF2 $\alpha$  in response to TUDCA in HUVECs from PGMO pregnancies.** The effect of TUDCA (100  $\mu$ M) on the inactivating phosphorylation of eIF2 $\alpha$  was evaluated by western blot at the indicated times in HUVECs from pregnancies where the mother showed pre-gestational maternal obesity (PGMO) (see Methods). **A**, Western blot for total and phosphorylated eIF2 $\alpha$ , and  $\beta$ -actin protein abundance. Lower graphs show Total eIF2 $\alpha$ / $\beta$ -actin and (**B**) phosphorylated eIF2 $\alpha$ /total eIF2 $\alpha$  ratio densitometries normalized to 1 in control. Values are mean  $\pm$  S.E.M.  $P < 0.05$ . \* vs control. (n = 3).

**A****B**

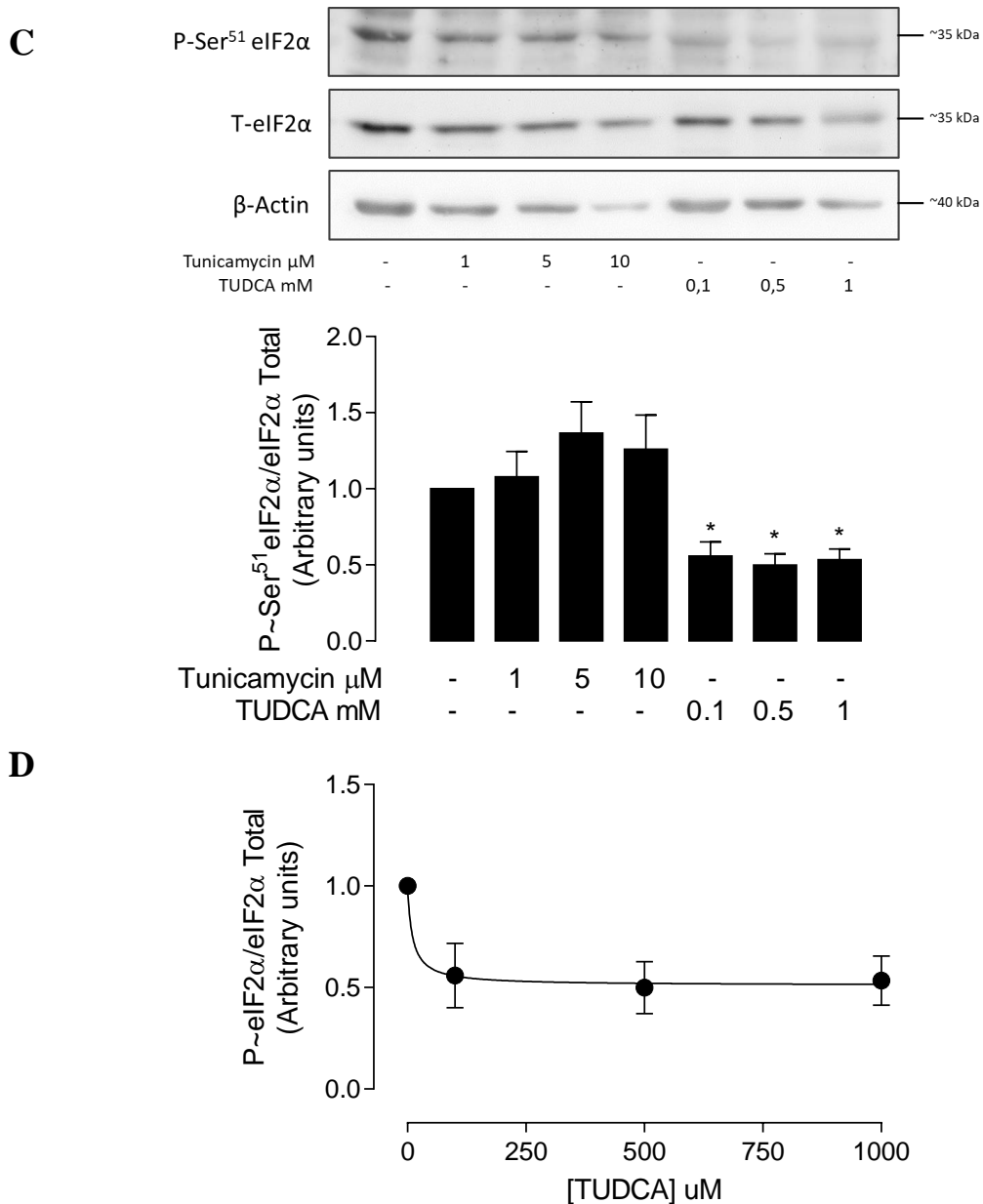


**Figure 24. eIF2 $\alpha$  activation state in response to different concentrations of tunicamycin and TUDCA in HUVECs.** The effects of tunicamycin (8 hours) and TUDCA (8 hours) on the inactivating phosphorylation of eIF2 $\alpha$  were evaluated by western blot at the indicated concentrations in HUVECs from pregnancies where the mother showed pre-gestational maternal normal weight (PGMN) or pre-gestational maternal obesity (PGMO) (see Methods). **A**, Representative western blot for the phosphorylation of eIF2 $\alpha$  in HUVECs from PGMN pregnancies. The graph shows the densitometry for phosphorylation of eIF2 $\alpha$  over total eIF2 $\alpha$ . The densitometry was normalized to 1 with data in control. **B**, Dose-response curve representation for cells treated with tunicamycin. **C**, Representative western blot for the phosphorylation of eIF2 $\alpha$  in HUVECs from PGMO pregnancies. The graph shows the densitometry for phosphorylation of eIF2 $\alpha$  over total eIF2 $\alpha$ . **D**, Dose-response curve representation for cells treated with TUDCA. Values are mean  $\pm$  S.E.M. \*  $P < 0.05$  vs cells in control. (n = 3 PGMN; 3 PGMO).

**Table 9. Tunicamycin and TUDCA concentrations and incubation times used in the treatment of cells cultures**

	Cellular type	Concentration ( $\mu$ M)	Incubation time (h)	Parameter	Reference
Tunicamycin	HUVECs	2,5-5	48	N-glycosilation	Ghoshal et al., 2014
	HUVECs	1	6	N-glycosilation	Kothari et al., 2013
	MCAECs	1	8	ER stress, eNOS	Galán et al., 2014
	HUVECs	0,75	24	GRP78 (BiP)/CHOP	Suganya et al., 2014
	HUVECs	10	8	GRP78 (BiP)	Matsushita et al., 2011
	HUVECs	2,2	16	NO production	Murugan et al., 2015
TUDCA	MCAECs	1,000	9	eNOS, NO, ER stress	Galán et al., 2014
	HUVECs	10,000	5	GRP78 (BiP), CHOP	Yang et al., 2013
	HUVECs	20	24	ER stress	Murugan et al., 2015
	HRMECs	125	24	NO content	Wang et al., 2016
	HUVECs	1,000	50	NO production	Wu et al., 2015
	Astrocytes	200	24	P~eIF2 $\alpha$	Yanguas-Casás et al., 2014

Concentrations and incubation times of tunicamycin and TUDCA reported in the literature for the treatment of endothelial cell cultures. HUVECs: human umbilical vein endothelial cells; MCAECs: mouse coronary artery endothelial cell, HRMECs: human retinal microvascular endothelial cell; ER: endoplasmic reticulum; eNOS: endothelial nitric oxide synthase; GRP78: glucose-regulated protein 78 (also known as binding immunoglobulin protein, BiP); CHOP: CCAAT-enhancer-binding protein homologous protein; NO: nitric oxide; P~eIF2 $\alpha$ : Inhibiting phosphorylation of the  $\alpha$  subunit of the eukaryotic initiation factor 2.

### 5.3.3 Activity of *PERK* branch

#### *PERK*

The treatment of cells with tunicamycin increased the level of activating phosphorylation of *PERK* (~2.2 fold) in HUVECs from PGMN pregnancies, but did not alter its phosphorylation in cells from PGMO pregnancies (Figure 25A). The co-incubation with TUDCA prevented the increase caused by tunicamycin in cells from PGMN. On the other hand, TUDCA reduced the PGMO-increased phosphorylation of *PERK* (~42%) in the absence and presence of tunicamycin. There were no significant changes in the total protein abundance of *PERK* in cells from PGMN or PGMO pregnancies (Figure 25A,B).

#### *eIF2 $\alpha$*

The total protein abundance of *eIF2 $\alpha$*  did not show significant differences between the experimental conditions in PGMN or PGMO pregnancies (Figure 26A). Tunicamycin increased the phosphorylation of *eIF2 $\alpha$*  (~1.6 fold) in HUVECs from PGMN pregnancies, an effect prevented by the co-incubation with TUDCA (Figure 26B). The PGMO-increased phosphorylation was reduced by TUDCA, either in the presence or absence of tunicamycin.

#### *CHOP, TRB3, and BiP*

Since *CHOP* and *TRB3* are transcription factors involved in the ER stress-associated insulin resistance, their total protein abundance were evaluated. Both *CHOP* and *TRB3* protein abundance were found elevated (~2.3 and ~1.8 fold, respectively) along with their mRNA (~28.6 and ~4.6 fold) in HUVECs from PGMO compared to cells from PGMN pregnancies (Figures 27 and 28, respectively). Tunicamycin increased the abundance of both proteins in HUVECs from PGMN and the mRNA but did not alter their expression in HUVECs from PGMO. TUDCA decreased the *CHOP* and *TRB3* protein abundance (~44%

and ~41%, respectively) and their mRNA (~89% and ~84%, respectively) in cells from PGMO pregnancies (Figure 27 and 28). However, TUDCA was not effective in cells from PGMO treated with tunicamycin for the protein and mRNA expression of CHOP and TRB3. Finally, the BiP mRNA showed a pattern similar to that presented by CHOP and TRB3 mRNA (Figure 29).

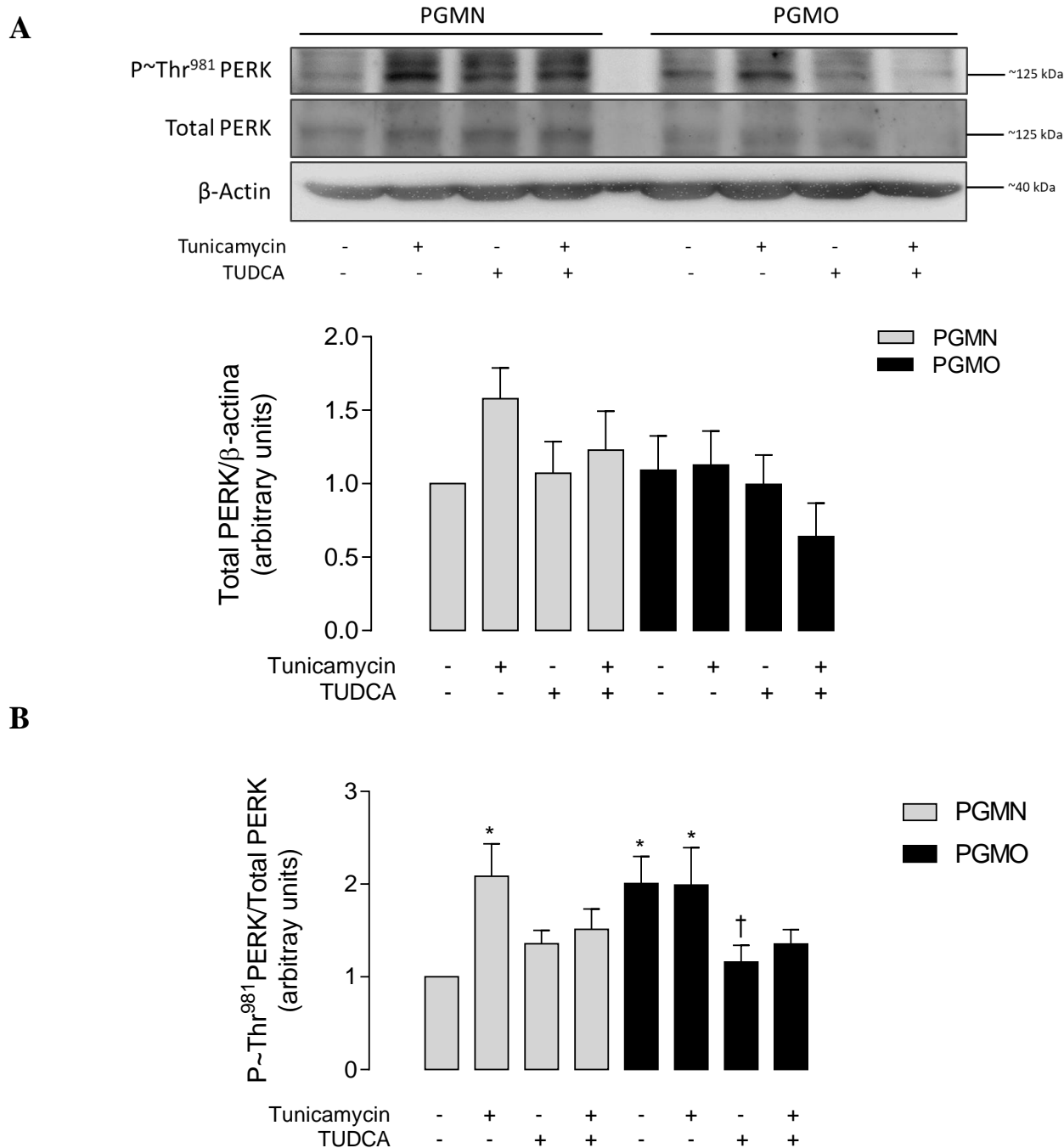


**Figure 25. Modulation of PERK phosphorylation by tunicamycin and TUDCA.** **A**, Western blot for total PERK and phosphorylated PERK, and  $\beta$ -actin protein abundance in HUVECs from pregnancies where the mother showed pre-gestational maternal normal weight (PGMN) or pre-gestational maternal obesity (PGMO). Cells were incubated without (-) or with (+) tunicamycin (5  $\mu$ M, 8 hours) and TUDCA (100  $\mu$ M, 8 hours) (see Methods). Lower graphs show Total PERK/ $\beta$ -actin and (**B**) phosphorylated PERK/total PERK ratio densitometries normalized to 1 in PGMN control. Values are mean  $\pm$  S.E.M.  $P < 0,05$ .  $P < 0,05$ . \* vs PGMN control; † vs PGMO control (n = 9 PGMN, 9 PGMO).

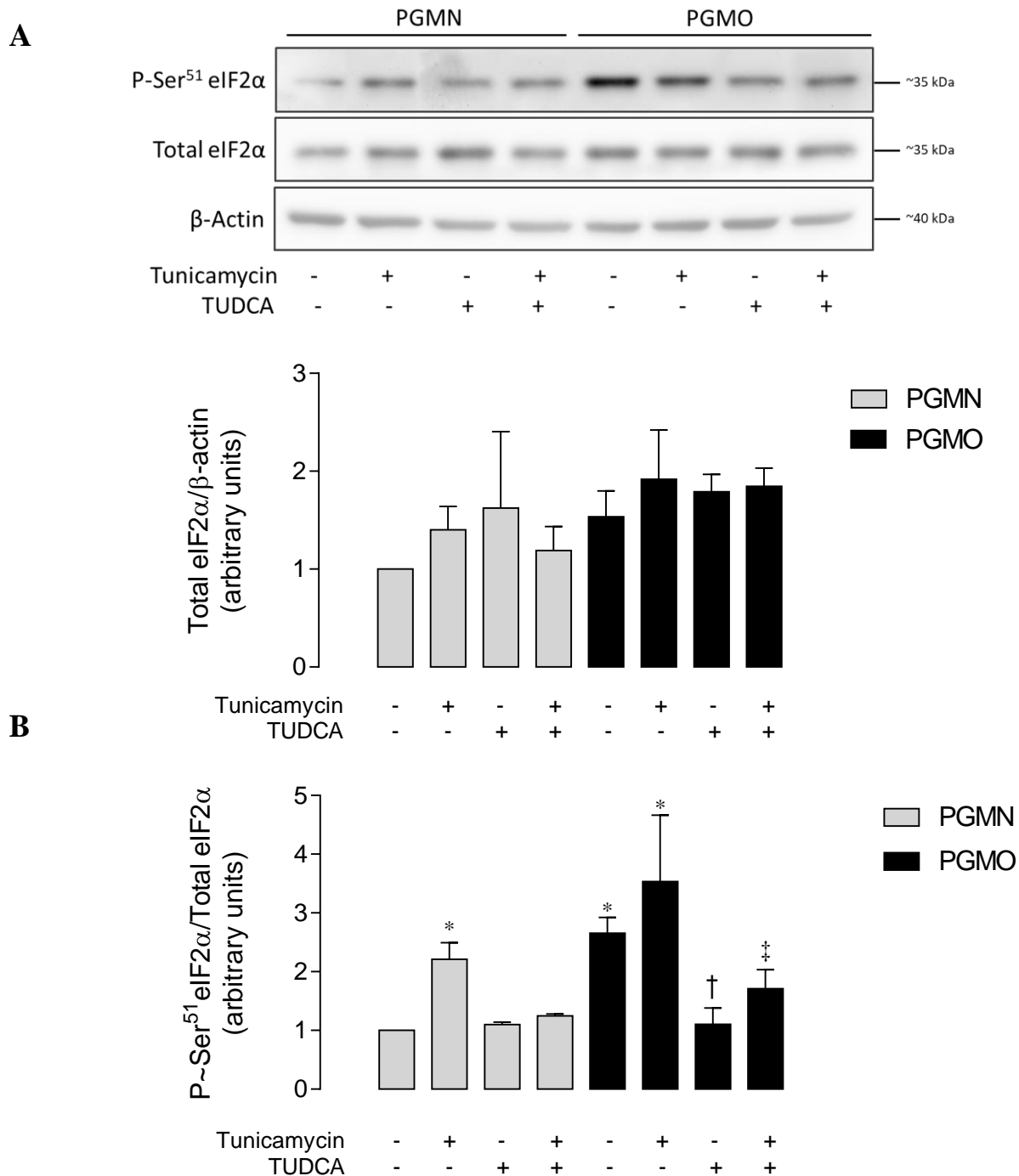


**Figure 26. Modulation of eIF2α phosphorylation by tunicamycin and TUDCA. A,** Western blot for total eIF2α and phosphorylated eIF2α (P~eIF2), and β-actin protein abundance in HUVECs from pregnancies where the mother showed pre-gestational maternal normal weight (PGMN) or pre-gestational maternal obesity (PGMO). Cells were incubated without (–) or with (+) tunicamycin (5 μM, 8 hours) and TUDCA (100 μM, 8 hours) (see Methods). Lower graphs show Total eIF2α/β-actin and (B) phosphorylated eIF2α/total eIF2α ratio densitometries normalized to 1 in PGMN control. Values are mean ± S.E.M. *P* < 0.05. \* vs PGMN control. † vs PGMO control. ‡ vs PGMO + tunicamycin (n = 9 PGMN, 9 PGMO).

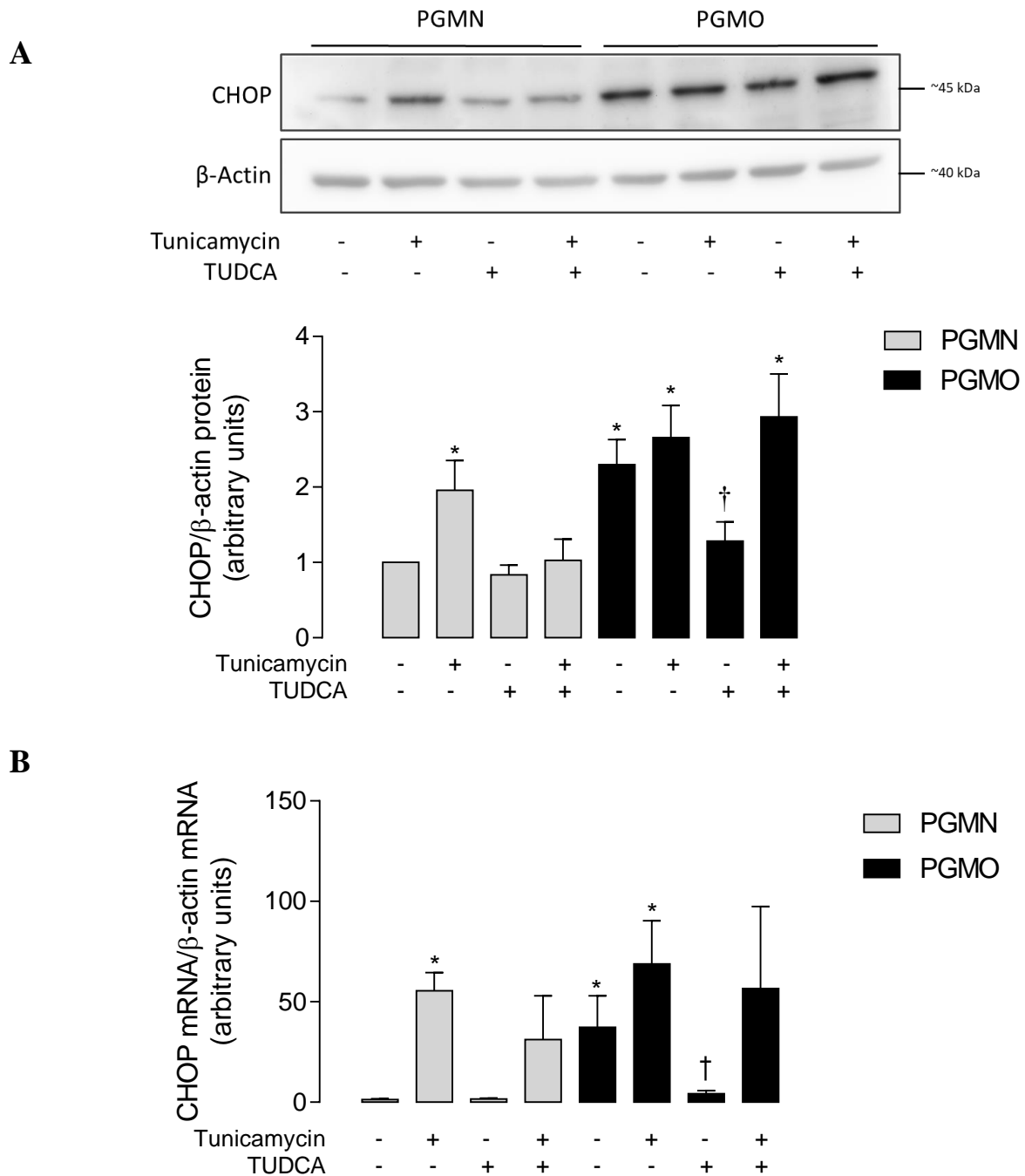


**Figure 27. Modulation of CHOP expression by tunicamycin and TUDCA.** **A**, Western blot for CHOP and  $\beta$ -actin protein abundance in HUVECs from pregnancies where the mother showed pre-gestational maternal normal weight (PGMN) or pre-gestational maternal obesity (PGMO). Cells were incubated without (-) or with (+) tunicamycin (5  $\mu$ M, 8 hours) and TUDCA (100  $\mu$ M, 8 hours) (see Methods). Lower panel shows CHOP/ $\beta$ -actin ratio densitometry normalized to 1 in PGMN control (n = 9 PGMN, 9 PGMO). **B**, Relative mRNA expression for CHOP in HUVECs as in A (n = 5 PGMN, 8 PGMO). Values are mean  $\pm$  S.E.M.  $P < 0.05$ . \* vs PGMN. † vs PGMO in the baseline condition.

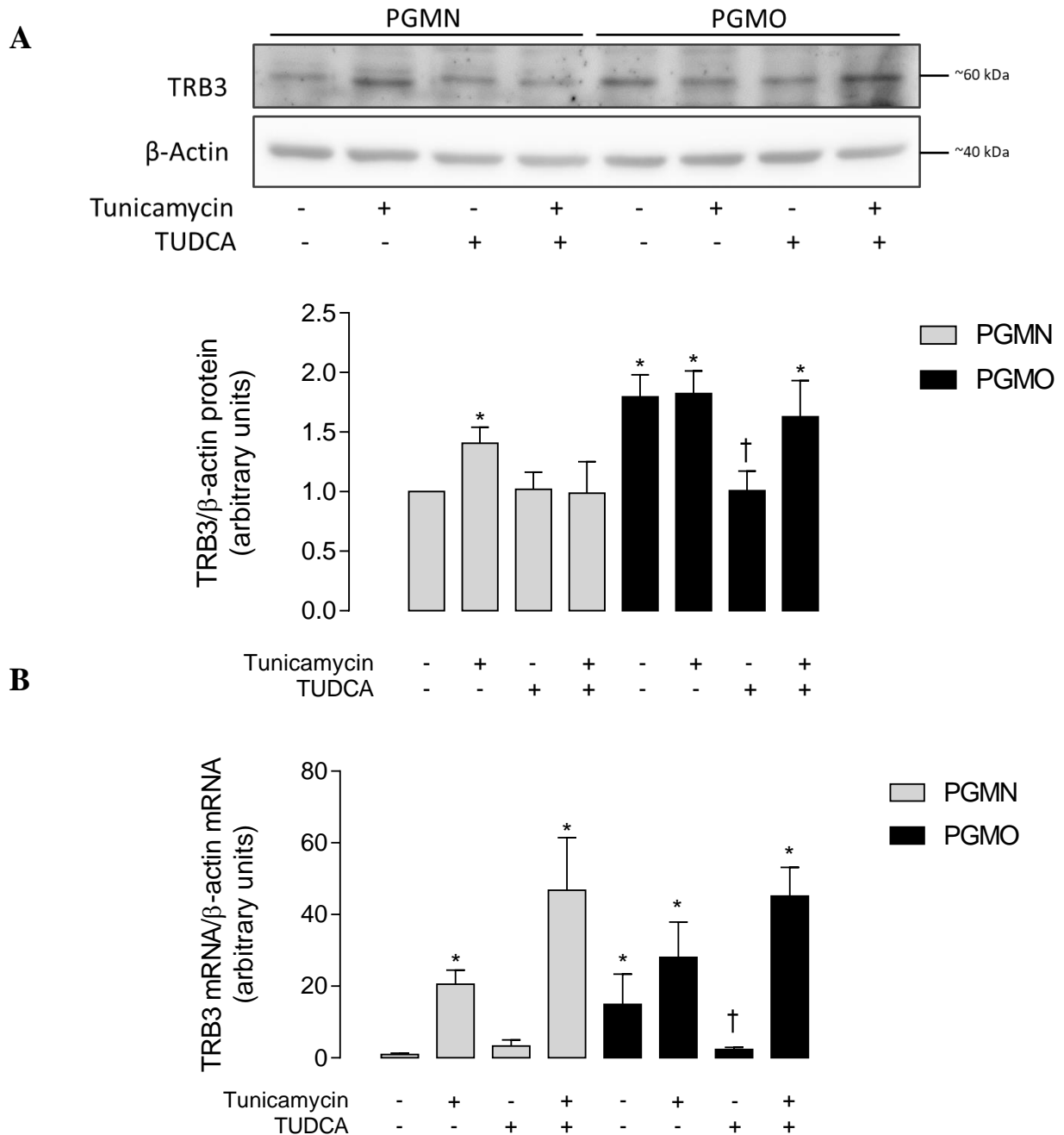


**Figure 28. Modulation of TRB3 expression by tunicamycin and TUDCA.** **A**, Western blot for TRB3 and  $\beta$ -actin protein abundance in HUVECs from pregnancies where the mother showed pre-gestational maternal normal weight (PGMN) or pre-gestational maternal obesity (PGMO). Cells were incubated without (-) or with (+) tunicamycin (5  $\mu$ M, 8 hours) and TUDCA (100  $\mu$ M, 8 hours) (see Methods). Lower panel shows TRB3/ $\beta$ -actin ratio densitometry normalized to 1 in PGMN control (n = 9 PGMN, 9 PGMO). **B**, Relative mRNA expression for TRB3 in HUVECs as in A (n = 5 PGMN, 8 PGMO). Values are mean  $\pm$  S.E.M.  $P < 0.05$ . \* vs PGMN control. † vs PGMO control.

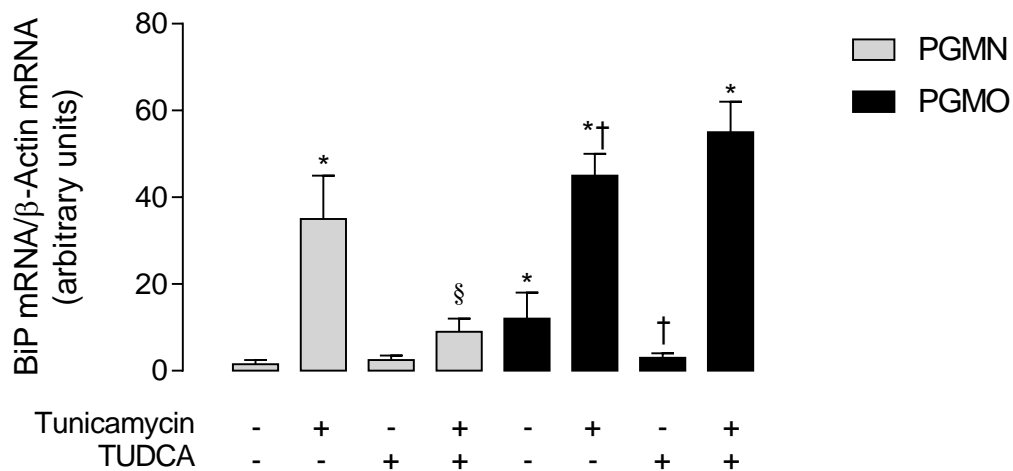


**Figure 29. Modulation of BiP mRNA levels by tunicamycin and TUDCA.** The mRNA abundance of BiP in HUVECs from PGMN and PGMO pregnancies treated or not with tunicamycin (5  $\mu$ M, 8 hours) and TUDCA (100  $\mu$ M, 8 hours) was evaluated by RT-qPCR (see Methods). The graph shows the relative abundance of BiP mRNA analyzed by the  $\Delta\Delta C_T$  method. Values are mean  $\pm$  S.E.M.  $P < 0,05$ . \* vs PGMN in the baseline condition. § vs PGMN + tunicamycin. † vs PGMO in the baseline condition. ( $n = 5$  PGMN, 8 PGMO).

#### 5.3.4 Activity of the IRE1 $\alpha$ branch

##### *IRE1 $\alpha$*

Tunicamycin increased the total protein abundance of IRE1 $\alpha$  (~2.3 fold) in HUVECs from PGMN but did not affect the level of this protein in cells from PGMO (Figure 30A). Conversely, TUDCA decreased the total IRE1 $\alpha$  protein abundance (~33%) in HUVECs from PGMO and did not induce a change in HUVECs from PGMN in the absence or presence of tunicamycin. There were no significant changes in the ratio of activating phosphorylation of IRE1 $\alpha$  protein abundance (Figure 30B).

##### *JNK*

There were no significant differences in the total protein abundance of JNK in cells from PGMN or PGMO pregnancies (Figure 31A). The activating phosphorylations of JNK in threonine 183 and tyrosine 185 were measured since it is activated after ER stress by IRE1 $\alpha$  kinase activity. The activating phosphorylation of JNK was increased in HUVECs from PGMO (~1.5 fold) compared with cells from PGMN pregnancies, an effect that was reduced (~32%) by TUDCA (Figure 31B). Meanwhile, tunicamycin increased the level of phosphorylated JNK in HUVECs from PGMN (~1.8 fold) but not in cells from PGMO. The co-incubation with TUDCA prevented the tunicamycin-increased phosphorylation of JNK in HUVECs from PGMN, and tunicamycin did not change the reduction caused by TUDCA in HUVECs from PGMO pregnancies.

##### *XBPI*

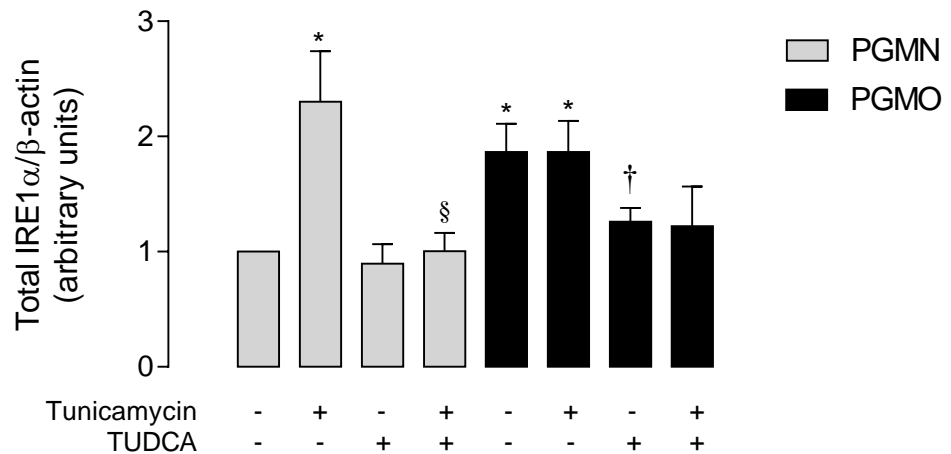
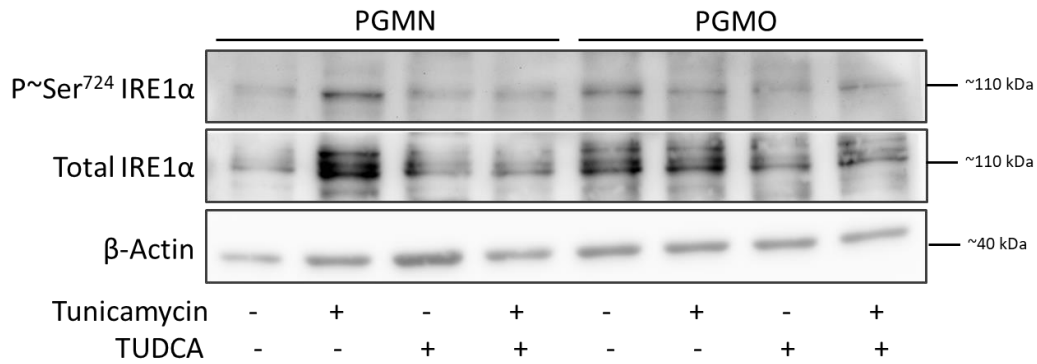
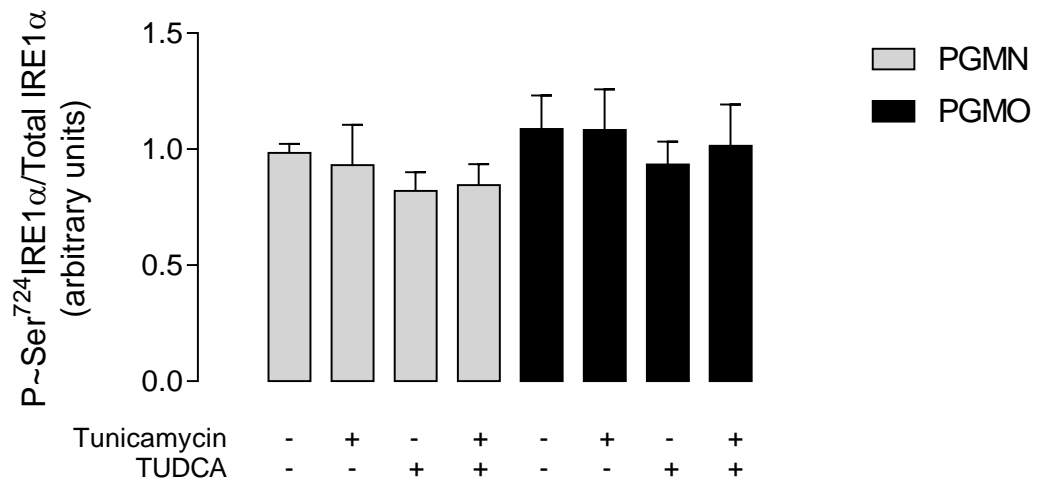
The processing of the XBPI mRNA was measured in order to evaluate the endoribonuclease activity of IRE1 $\alpha$ . Assays using conventional PCR showed similar abundance of the processed form of XBPI mRNA in cells from both conditions (Figure 32A).

Tunicamycin increased the processing of XBP1 mRNA (product of 138 bp) at similar levels (~12.0 fold) in cells from both conditions. The RT-qPCR assay was performed with specific primers for the processed form of the mRNA confirming that there were no differences in the processing of XBP1 mRNA between HUVECs from PGMN and PGMO pregnancies (Figure 32B). On the other hand, tunicamycin increased its level in both conditions (~48.1 fold), an effect blocked by TUDCA in HUVECs from PGMN but not in cells from PGMO pregnancies. TUDCA alone did not induce changes in the level of the processed mRNA in cells from both conditions (Figure 32B).

#### 5.3.5 Activation of ATF6

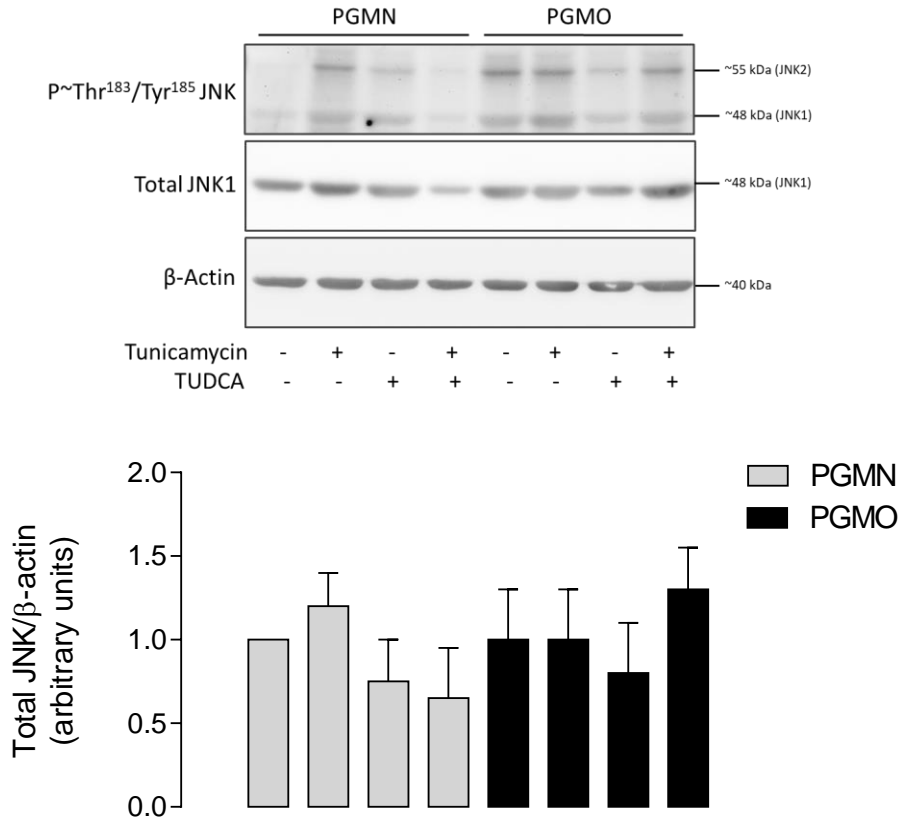
Activation of ATF6 was determined by the ratio for nuclear/cytoplasmic fluorescence in HUVECs from both conditions. In the absence of tunicamycin or TUDCA, ATF6 was detected mainly at the perinuclear region in cells from PGMN pregnancies (Fig. 33). However, ATF6 was detected in the nuclear region in cells from PGMO pregnancies. Tunicamycin increased (~2.6 fold) the ATF6 signal at the nuclear region in cells from PGMN but did not alter the nuclear signal for this protein in cells from PGMO. presence of ATF6 in the nucleus than in cells from PGMN (Figure 33). The treatment of cells with tunicamycin increased the ATF6 nuclear localization in HUVECs from PGMN (~2.1 fold), but it did not alter the localization in the HUVECs from PGMO. TUDCA did not alter the perinuclear distribution of ATF6 signal in cells from PGMN but abolished the ATF6 signal at the nuclear region in cells from PGMO pregnancies. TUDCA also reduced the tunicamycin-increased signal at the nuclear region resulting in higher perinuclear signal for this protein in cells from PGMN pregnancies. In cells from PGMO pregnancies treated with

tunicamycin, TUDCA reduced (~40%) the nuclear signal for ATF6 protein, which was prevented by co-incubation with tunicamycin (Figure 33).

**A****B**

**Figure 30. Modulation of IRE1 $\alpha$  by tunicamycin and TUDCA.** **A**, Western blot for total and phosphorylated IRE1 $\alpha$ , and  $\beta$ -actin protein abundance in HUVECs from pregnancies where the mother showed pre-gestational maternal normal weight (PGMN) or pre-gestational maternal obesity (PGMO). Cells were incubated without (–) or with (+) tunicamycin (5  $\mu$ M, 8 hours) and TUDCA (100  $\mu$ M, 8 hours) (see Methods). Lower graphs show Total IRE1 $\alpha$ / $\beta$ -actin and **(B)** phosphorylated IRE1 $\alpha$ /total IRE1 $\alpha$  ratio densitometries normalized to 1 in PGMN control. Values are mean  $\pm$  S.E.M.  $P < 0,05$ . \* *vs* PGMN in the baseline condition. † *vs* PGMO in the baseline condition. § *vs* PGMN + tunicamycin (n = 8 PGMN, 8 PGMO).

**A**



**B**

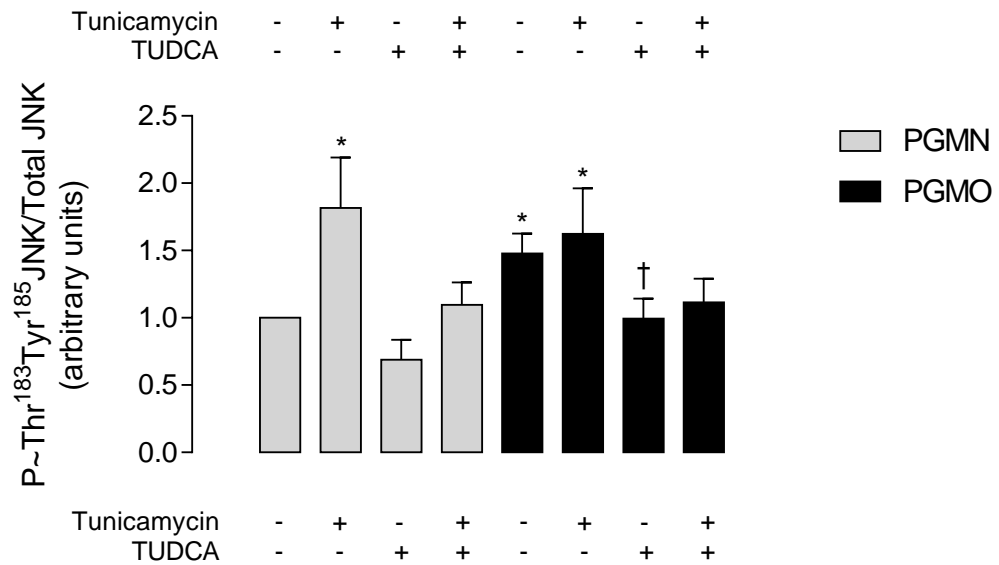


**Figure 31. Modulation of JNK by tunicamycin and TUDCA.** **A**, Western blot for total and phosphorylated JNK, and β-actin protein abundance in HUVECs from pregnancies where the mother showed pre-gestational maternal normal weight (PGMN) or pre-gestational maternal obesity (PGMO). Cells were incubated without (–) or with (+) tunicamycin (5 μM, 8 hours) and TUDCA (100 μM, 8 hours) (see Methods). Lower graphs show Total JNK1/β-actin and **(B)** phosphorylated Thr<sup>183</sup>/Tyr<sup>185</sup> JNK/total JNK1 ratio densitometries normalized to 1 in PGMN control. Values are mean ± S.E.M. *P* < 0,05. \* vs PGMN in the baseline condition. † vs PGMO in the baseline condition (n = 8 PGMN, 8 PGMO).

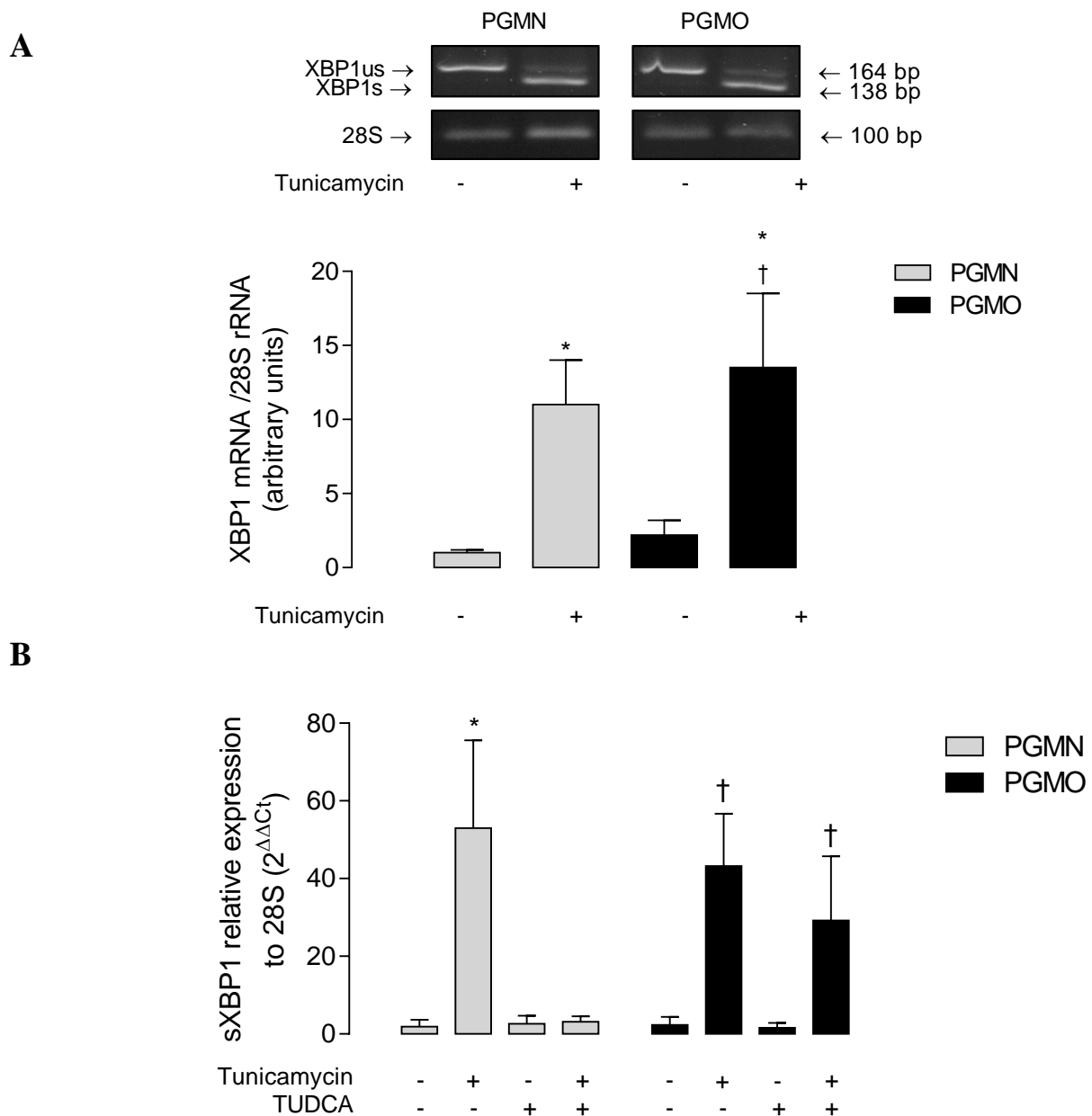
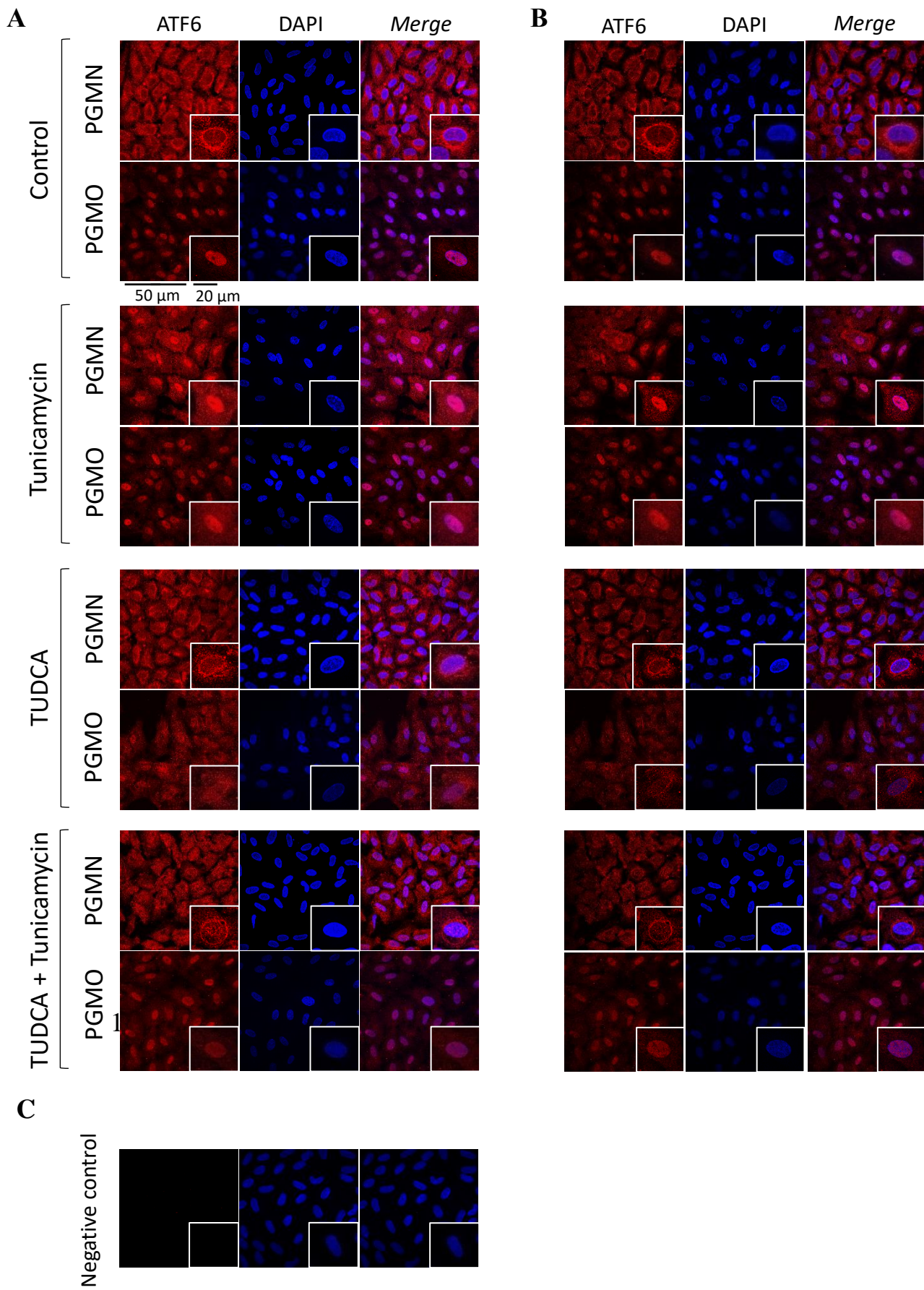


**Figure 32. Processing of XBP1 mRNA by Tunicamycin and TUDCA.** The processing and abundance of XBP1 mRNA in HUVECs from PGMN and PGMO pregnancies treated or not with tunicamycin (5  $\mu$ M, 8 hours) and TUDCA (100  $\mu$ M, 8 hours) were evaluated by PCR and RT-qPCR (see Methods). **A**, Photograph of an agarose gel representative of the unprocessed XBP1 amplified cDNA (XBP1<sub>us</sub>, 164 bp) and processed (XBP1<sub>s</sub>, 138 bp) and 28S rRNA in HUVECs from PGMN and PGMO pregnancies treated or not with tunicamycin. The graph shows the XBP1<sub>s</sub> mRNA/28S rRNA ratio of the densitometries normalized to 1 in PGMN in the absence of tunicamycin. **B**, Graph showing the relative abundance of XBP1<sub>s</sub> mRNA analyzed by the  $\Delta\Delta C_T$  method. Values are mean  $\pm$  S.E.M.  $P < 0.05$ . \* vs PGMN in baseline condition. † vs PGMO in the baseline condition. (n = RT-PCR: 8 PGMN, 8 PGMO; RT-qPCR: 4 PGMN, 10 PGMO).



**D**

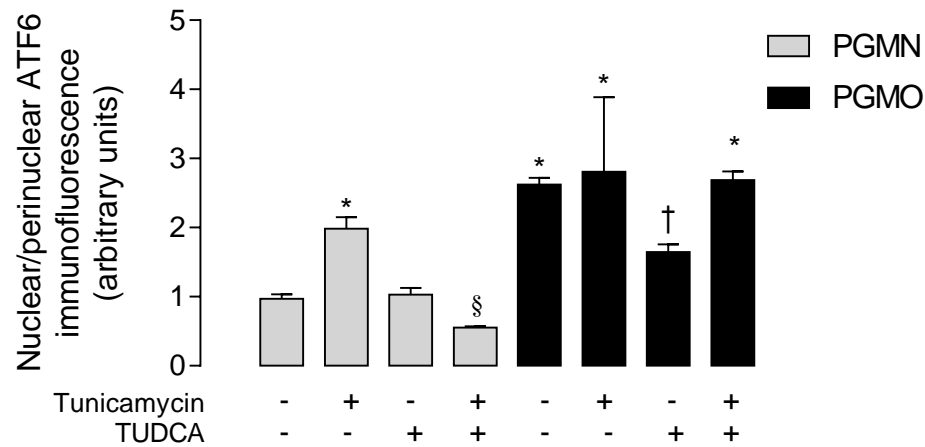


**Figure 33. Effect of tunicamycin and TUDCA treatment on the cellular localization of ATF6.** The localization of ATF6 was evaluated by immunofluorescence in a confocal microscope in HUVECs from pregnancies where the mother showed pre-gestational maternal normal weight (PGMN) or pre-gestational maternal obesity (PGMO). Cells were exposed (8 h) to the culture medium without (Control) or with tunicamycin (5  $\mu$ M), TUDCA (100  $\mu$ M), or both (see Methods). Confocal microscopy immunofluorescence of ATF6 (red fluorescence) and nuclei (blue fluorescence, counterstained with DAPI) was assayed. Fifteen confocal images were taken through the Z-axis (each 0.3  $\mu$ m) from the bottom to the top of the cells. **A**, Pictures represent Z-stacked images (15 images, 40X). **B**, Pictures show the Z-plane for the optical slide number 7, i.e., ~2.1- 2.4  $\mu$ m from cell culture surface. An amplification is shown at the inserts in each picture. **C**, Negative control for ATF6 in cells from PGMN. **D**, Immunofluorescent signal at the nuclear over the perinuclear region. Values are mean  $\pm$  S.E.M.  $P < 0.05$ . \* vs control in PGMN. † vs control and tunicamycin in PGMO. § vs tunicamycin in PGMN (n= 8 PGMN, 8 PGMO).

## 5.4 ER stress, endothelial dysfunction, and insulin resistance

### 5.4.1 ER stress and endothelial dysfunction

The ER stress involvement in endothelial function was evaluated by the induction of reduction of ER stress and its effect on key elements of the endothelial function, as represented in Scheme 4.

#### *ER stress and basal NO generation*

The basal production of NOS-dependent NO was lower in HUVECs from PGMO (~35%) than HUVECs from PGMO pregnancies (Figure 34). The incubation with tunicamycin reduced the level of NO in HUVECs PGMN (~33%), but this molecule did not affect the basal production in HUVECs from PGMO. Conversely, TUDCA increased (~1.4 fold) the basal level of NO in HUVECs PGMO and did not change the NO level in HUVECs from PGMN (Figure 34).

The NOS-dependent L-citrulline formation was lower (~77%) in HUVECs from PGMO in comparison to cells from PGMN (Figure 35). Tunicamycin reduced the content of L-citrulline in cells from both conditions (~59 and ~75%, respectively), and TUDCA increased the content of L-citrulline (~6.5 fold) in cells from PGMO but did not induce changes in cells from PGMN pregnancies. The co-incubation of both compounds prevented the tunicamycin-induced decrease of L-citrulline in HUVECs from PGMN and the TUDCA-induced increase of L-citrulline in HUVECs from PGMO (Figure 35).

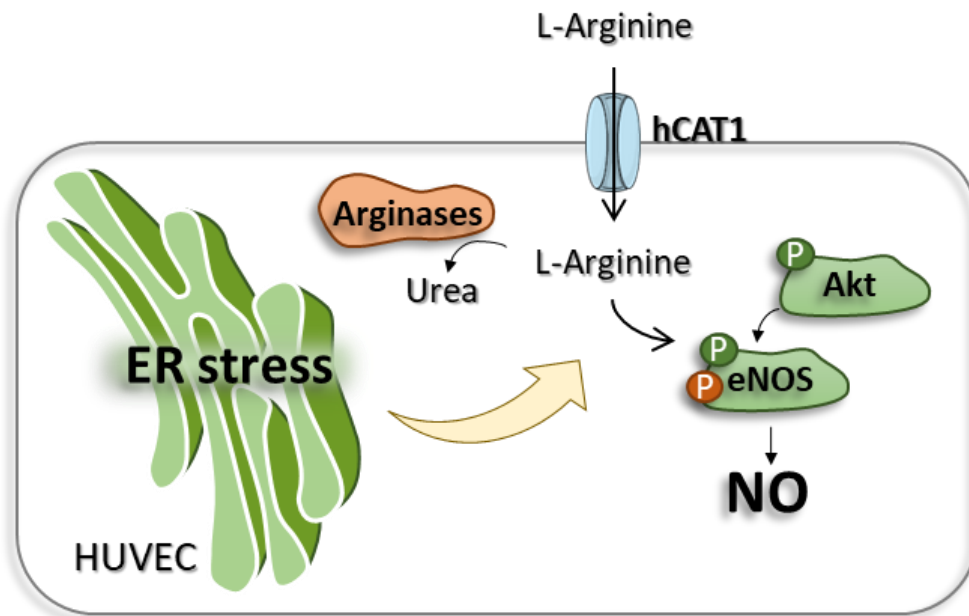
#### *ER stress and eNOS*

Tunicamycin, TUDCA, or both did not change the total protein abundance of eNOS (Figure 36A). The level of eNOS phosphorylated in serine 1177 decreased (~52%) in HUVECs from PGMN pregnancies treated with tunicamycin but there were no changes in

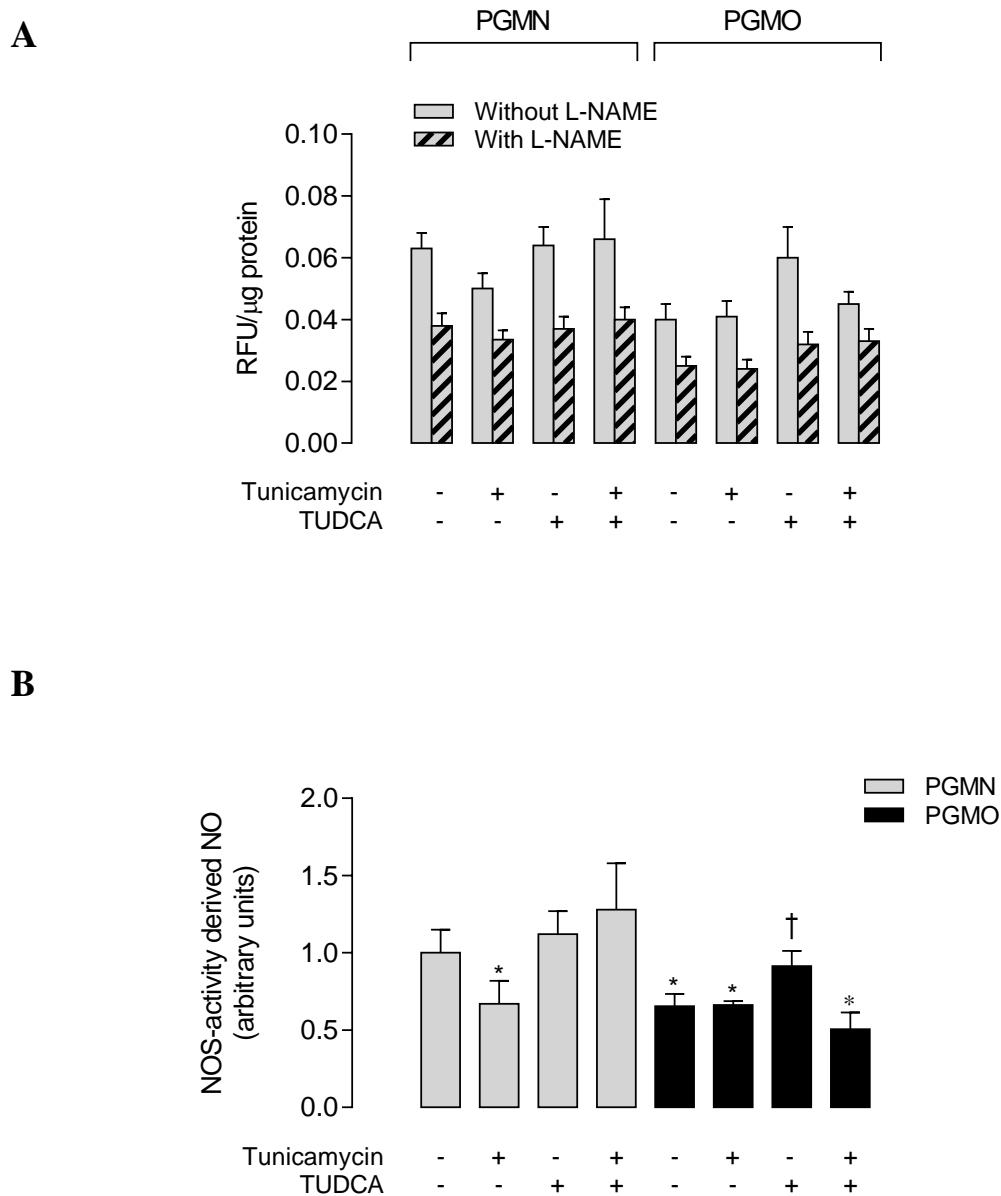
HUVECs from PGMO pregnancies (Figure 36B). On the other hand, TUDCA increased (~1.7 fold) this phosphorylation in HUVECs PGMO to levels that were similar to those detected in HUVECs of PGMN pregnancies. Tunicamycin did not change the inhibiting phosphorylation (threonine 495) of eNOS in HUVECs from both conditions (Figure 36C). TUDCA did not change the threonine 495 phosphorylation of eNOS in HUVECs from PGMN but reduced it (~56%) in HUVECs from PGMN to a level that was similar to HUVECs from PGMN at basal conditions. The treatment of cells with both compounds prevented the effect of tunicamycin alone on the phosphorylation in serine 1177 in HUVECs from PGMN and the effect of TUDCA alone on phosphorylations in serine 1177 and threonine 495 in HUVECs from PGMO pregnancies (Figure 36).

#### *ER stress and Akt*

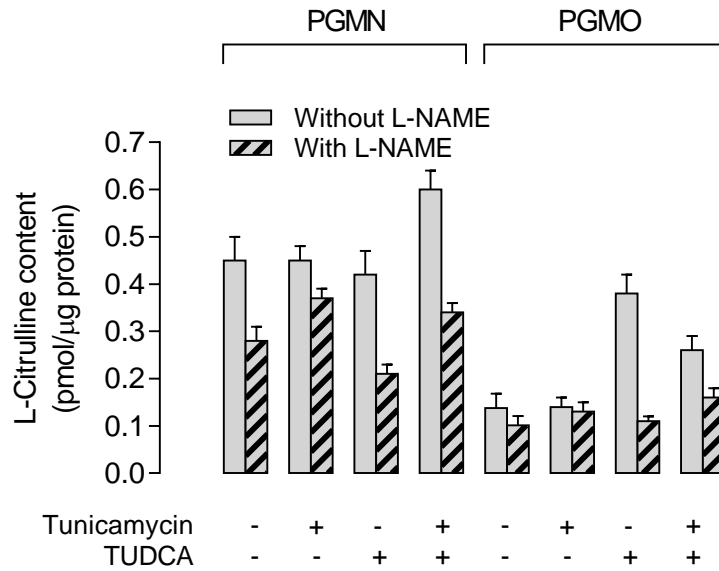
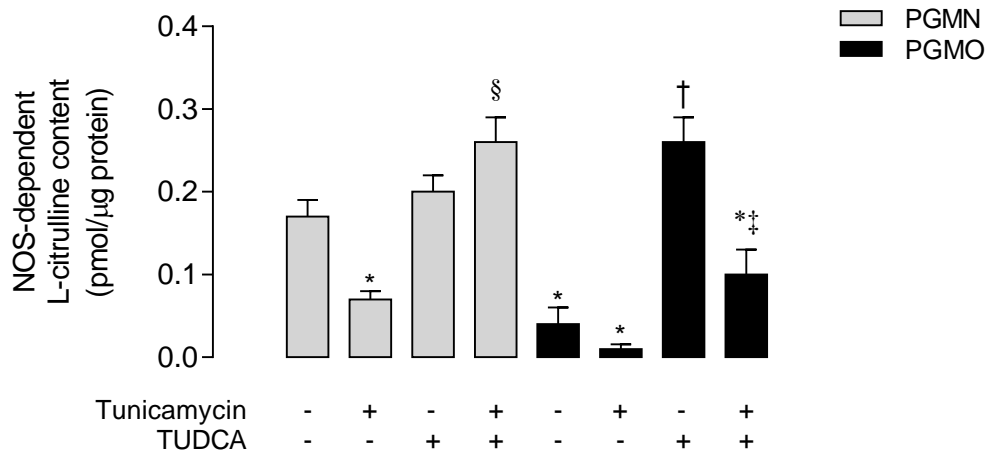
The basal activation status of Akt was evaluated since it is one of the eNOS activating kinases that are described to be altered either in a state of endothelial dysfunction or ER stress. There was no significant change in the total protein abundance of Akt after treatment of cells with tunicamycin, TUDCA, or both in HUVECs from both conditions (Figure 37A). Tunicamycin reduced (~33%) the activating phosphorylation of Akt in HUVECs from PGMN, but did not generate changes in HUVECs from PGMO. TUDCA did not change Akt phosphorylation in HUVECs from PGMN but increased (~1.9 times) the phosphorylation of Akt in PGMO pregnancies similar levels as those in HUVECs from PGMN pregnancies. The treatment with both compounds prevented the tunicamycin-induced decrease in HUVECs from PGMN and the TUDCA-induced increase in HUVECs from PGMO of the activating phosphorylation of Akt (Figure 37B).



**Scheme 4. ER stress and endothelial function.** ER, endoplasmic reticulum; hCAT-1, human cationic amino acid transporter 1; eNOS, endothelial nitric oxide synthase; P in green, activating phosphorylation; P in orange, inhibiting phosphorylation; NO, nitric oxide; HUVEC, human umbilical vein endothelial cell.

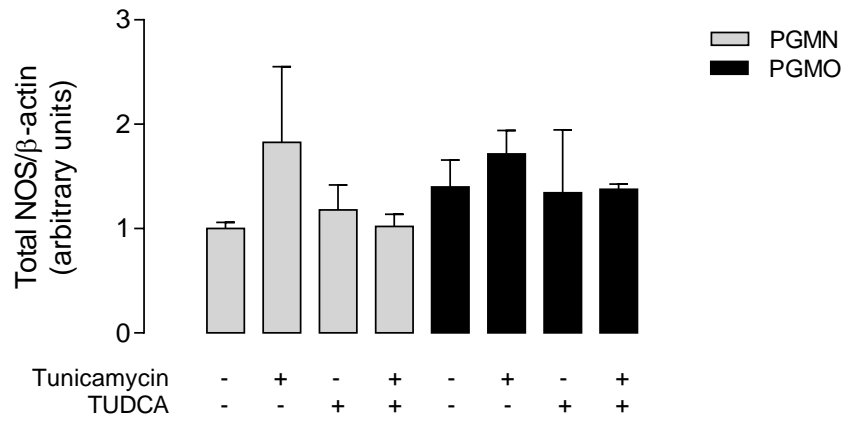
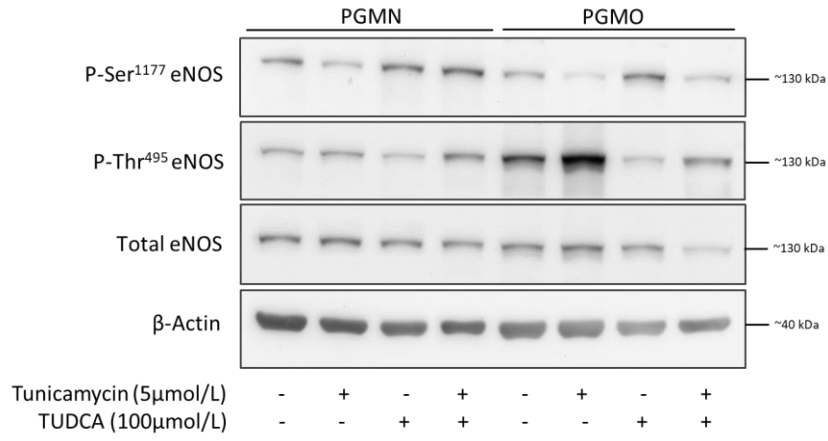


**Figure 34. ER stress modulation of NO generation in HUVECs.** The total and the NOS-dependent generation of NO were evaluated in HUVECS from pregnancies where the mother showed pre-gestational maternal normal weight (PGMN) or pre-gestational maternal obesity (PGMO). Cells were incubated without (-) or with (+) tunicamycin (5  $\mu$ M, 8 hours), TUDCA (100  $\mu$ M, 8 hours) and L-NAME (100  $\mu$ M, 30 minutes) and NO was detected by fluorescence lecture after loading the cells with the probe DAF-FM (1 hour, 5  $\mu$ M) (see Methods). **A**, Relative fluorescence units (RFU). **B**, The fraction of the RFU inhibited by L-NAME (i.e., dependent on NOS activity) derived from the data presented in A. Values are mean  $\pm$  S.E.M.  $P < 0.05$ . \* vs PGMN in basal condition. † vs PGMO in the baseline condition. (n = 9 PGMN, 9 PGMO).

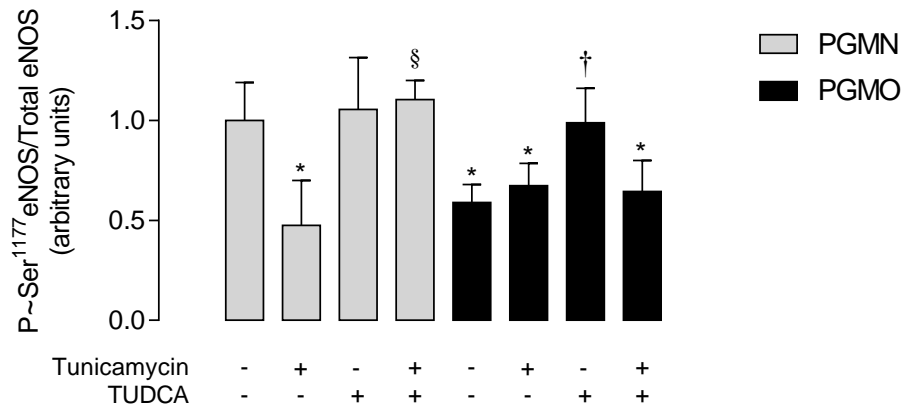
**A****B**

**Figure 35. ER stress modulation of L-citrulline content in HUVECs.** The intracellular content of L-citrulline was measured by h.p.l.c. in cells from pregnancies where the mother showed pre-gestational maternal normal weight (PGMN) or pre-gestational maternal obesity (PGMO). Cells were incubated with (-) or without (+) L-NAME (100  $\mu$ M, 30 minutes), tunicamycin (5  $\mu$ M, 8 hours) and TUDCA (100  $\mu$ M, 8 hours). **A**, Total L-citrulline content. **B**, The fraction of the L-citrulline content inhibited by L-NAME (i.e., dependent on NOS activity) derived from the data presented in A.  $P < 0.05$ . \* vs PGMN in basal condition. Values are mean  $\pm$  S.E.M. § vs PGMN + tunicamycin. † vs PGMO in the baseline condition. ‡ vs PGMO + tunicamycin. (n= 3 PGMN, 3 PGMO).

**A**



**B**



C

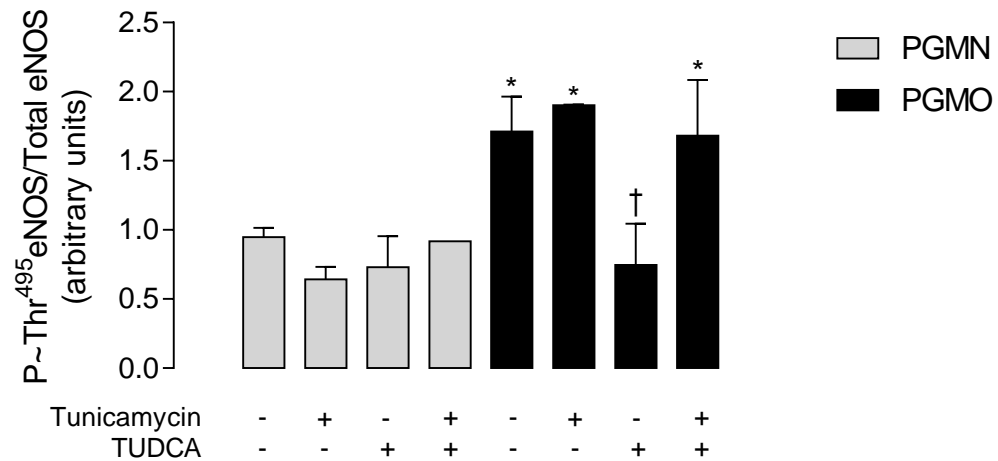


**Figure 36. Modulation of eNOS abundance and activation state by ER stress.** The protein abundance and the activating and inhibiting phosphorylation of eNOS were evaluated in HUVECS from pregnancies where the mother showed pre-gestational maternal normal weight (PGMN) or pre-gestational maternal obesity (PGMO). Cells were incubated without (-) or with (+) tunicamycin (5  $\mu$ M, 8 hours) and TUDCA (100  $\mu$ M, 8 hours) (see Methods). **A**, Western blot for the activating phosphorylation on serine 1177, the inhibiting phosphorylation in threonine 495, the total protein abundance and  $\beta$ -actin. The lower graph shows the densitometry for the total protein abundance of eNOS over  $\beta$ -actin. **B**, Densitometry of eNOS phosphorylated in serine 1177 over eNOS total. **C**, Densitometry for eNOS phosphorylated in threonine 495 over eNOS total. The densitometry was normalized to 1 with data in PGMN control. Values are mean  $\pm$  S.E.M.  $P < 0.05$ . \* vs PGMN in basal condition. § vs PGMN + tunicamycin. † P vs PGMO in the baseline condition. (n: PGMN = 9, PGMO = 9).

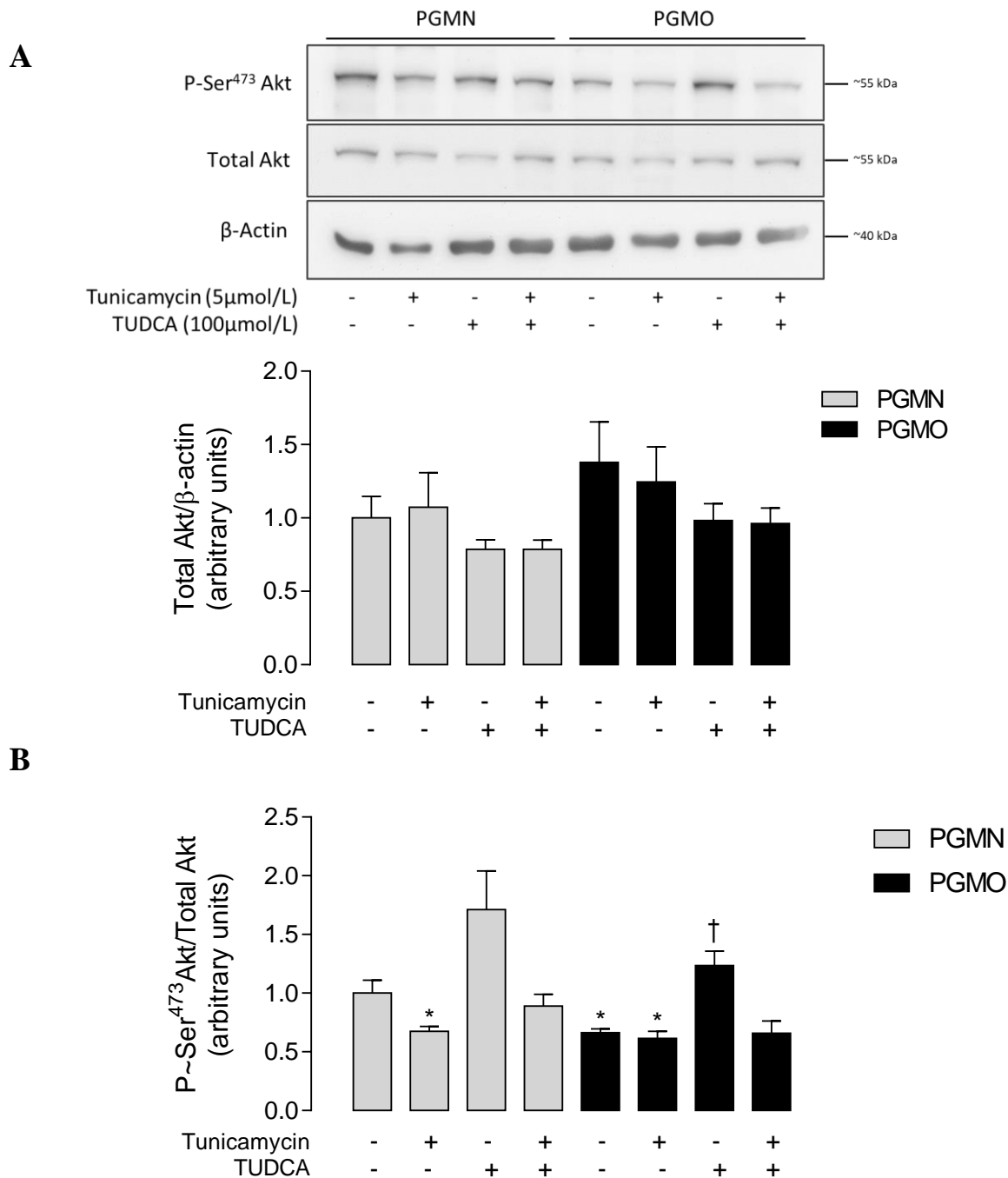


**Figure 37. Modulation of Akt abundance and activation state by ER stress.** The protein abundance and the activating phosphorylation of Akt were evaluated in HUVECS from pregnancies where the mother showed pre-gestational maternal normal weight (PGMN) or pre-gestational maternal obesity (PGMO). Cells were incubated without (-) or with (+) tunicamycin (5 μM, 8 hours) and TUDCA (100 μM, 8 hours) (see Methods). **A**, Western blot for the phosphorylation of Akt, the total protein abundance and β-actin. The lower graph shows the densitometry for the total protein abundance of Akt over β-actin. **B**, Densitometry of phosphorylated Akt over total Akt. The densitometry was normalized to 1 with data in PGMN control. Values are mean ± S.E.M.  $P < 0.05$ . \* vs PGMN in basal condition. † vs PGMO in the baseline condition. (n= 9 PGMN, 9 PGMO).

### *Arginase activity*

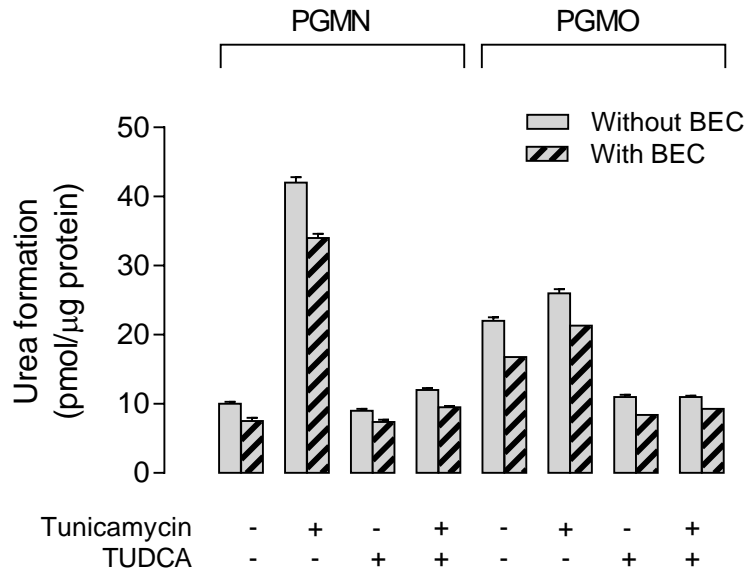
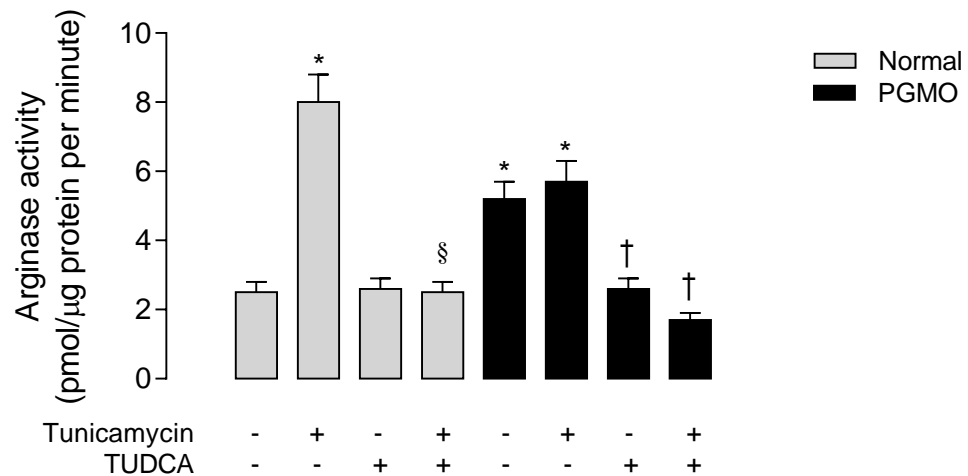
The activity of the arginases was measured since these enzymes compete with eNOS for the L-arginine, is associated with ER stress, and is involved in endothelial dysfunction. The arginases activity was determined by the formation of urea and the use of BEC, an inhibitor of arginases. The total urea formation was higher in HUVECs from PGMO than in PGMN pregnancies. Tunicamycin increased it in cells from PGMN and TUDCA reduced it in HUVECs from PGMO. BEC reduced the total urea formation in all the conditions (Figure 38A). The production of urea dependent on the arginases activity was higher (~2.1 fold) in HUVECs from PGMO compared with HUVECs from PGMN pregnancies (Figure 38B). Tunicamycin increased (~3.2 times) arginases activity in HUVECs from PGMN but did not changes it in HUVECs from PGMO. TUDCA reduced the level (~50%) in HUVECs from PGMO at similar levels than those seen in HUVECs from PGMN at basal conditions. The treatment with both molecules prevented the increase in arginases activity induced by tunicamycin in HUVECs from PGMN and did not alter the reduction caused by TUDCA in HUVECs from PGMO (Figure 38B).

### *L-Arginine transport and hCAT-1 expression*

Values for  $v_i$  were higher in cells from PGMO compared with PGMN (Table 10). Tunicamycin increased the  $v_i$  in cells from PGMN to values close to those from PGMO; however, did not alter this parameter in cells from PGMO. TUDCA reversed the increase seen in the  $v_i$  in cells from PGMO in the absence or presence of tunicamycin and in cells from PGMN incubated with tunicamycin. However, TUDCA did not alter the  $v_i$  in cells from PGMN in the absence of this ER stress inducer.

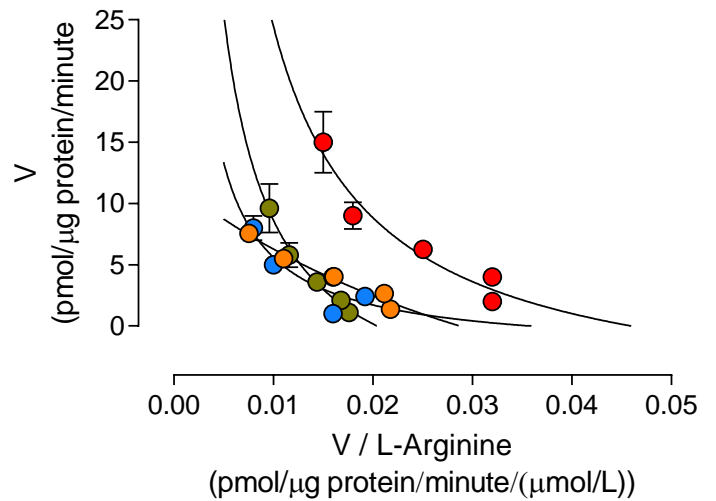
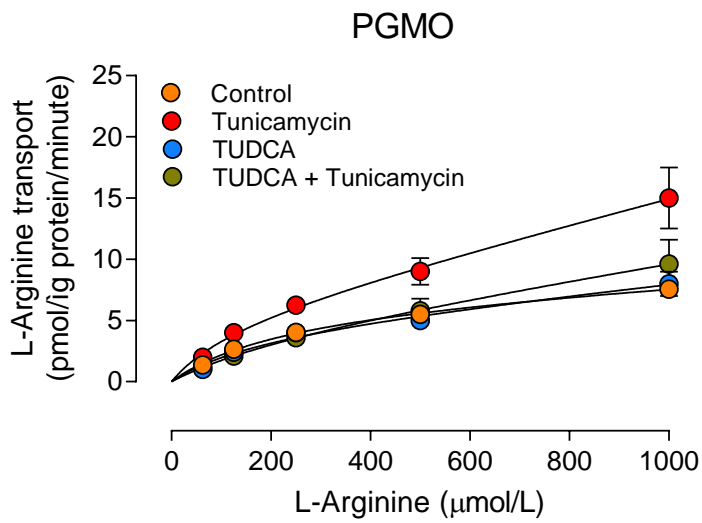
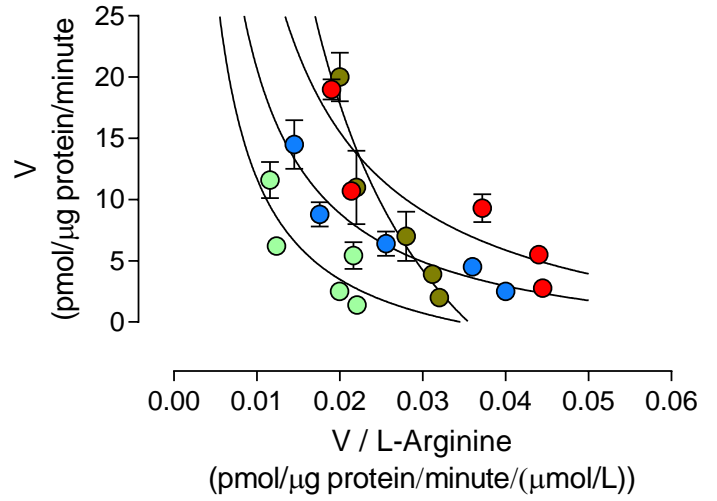
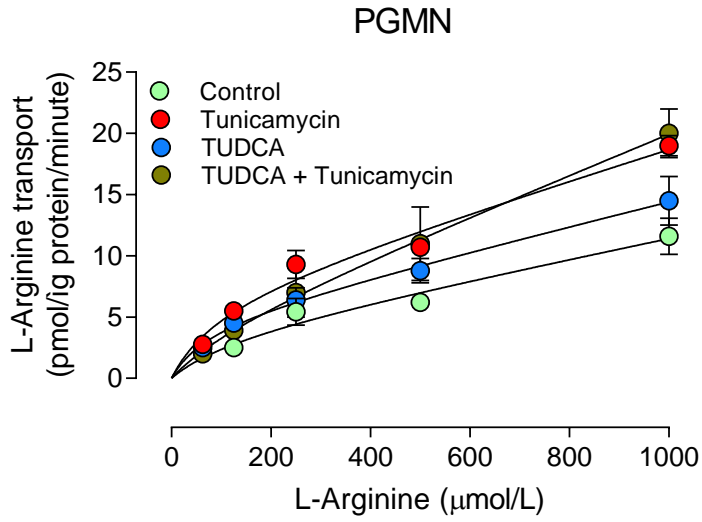
The treatment with tunicamycin increased the overall transport of L-arginine in HUVECs from PGMN and did not produce changes in HUVECs from PGMO (Figure 39A, Table 10). TUDCA treatment reduced the overall transport in cells from PGMO to values close to those detected in HUVECs from PGMN. The overall transport was adjusted to a semi-saturable transport system for all conditions. After subtracting the non-saturable component from total transport, the transport of L-arginine adjusted to the Michaelis-Menten equation (Figure 39B) and was linear in the of Eadie-Hofstee representation. The incubation with tunicamycin increased the  $V_{max}$  and the maximum transport capacity ( $V_{max}/K_m$ ) in HUVECs from PGMN pregnancies, an effect blocked by TUDCA (Table 10). The increased  $V_{max}$  and  $V_{max}/K_m$  seen in cells from PGMO was unaltered by tunicamycin but blocked by TUDCA in the absence or presence of tunicamycin. TUDCA did not change the parameters in HUVECs from PGMN. The apparent  $K_m$  values were not significantly altered in cells from these two study groups in all experimental conditions (Table 10).

The protein and mRNA abundance of hCAT-1 presented a similar behavior (Figure 40), increasing the protein abundance (~1.5 fold) and mRNA expression (~34 fold) in HUVECs from PGMN treated with tunicamycin and decreasing the protein abundance (~53%) and mRNA expression (~92%) after incubation with TUDCA in HUVECs from PGMO. The co-incubation of both compounds prevented the increase of mRNA and protein induced by tunicamycin in HUVECs from PGMN and blocked the reduction of mRNA produced by TUDCA in HUVECs from PGMO.

**A****B**

**Figure 38. ER stress effect on arginases activity.** The activity of arginases was assayed in lysates of HUVECs from pregnancies where the mother showed pre-gestational maternal normal weight (PGMN) or pre-gestational maternal obesity (PGMO). Cells were treated with tunicamycin (5  $\mu$ M, 8 hours), TUDCA (100  $\mu$ M, 8 hours) and S-(2-boronoethyl)-L-cysteine (BEC, arginase inhibitor, 20  $\mu$ M, 10 minutes) and the urea formation was determined by a colorimetric method (see Methods). **A**, total urea formation. **B**, the fraction of urea formation inhibited by BEC (i.e., dependent on the activity of arginase) derived from the data in A. Values are mean  $\pm$  S.E.M.  $P < 0.05$ . \* vs PGMN control. § vs PGMN + tunicamycin. † vs PGMO control. (n = 3 PGMN, 3 PGMO).

A



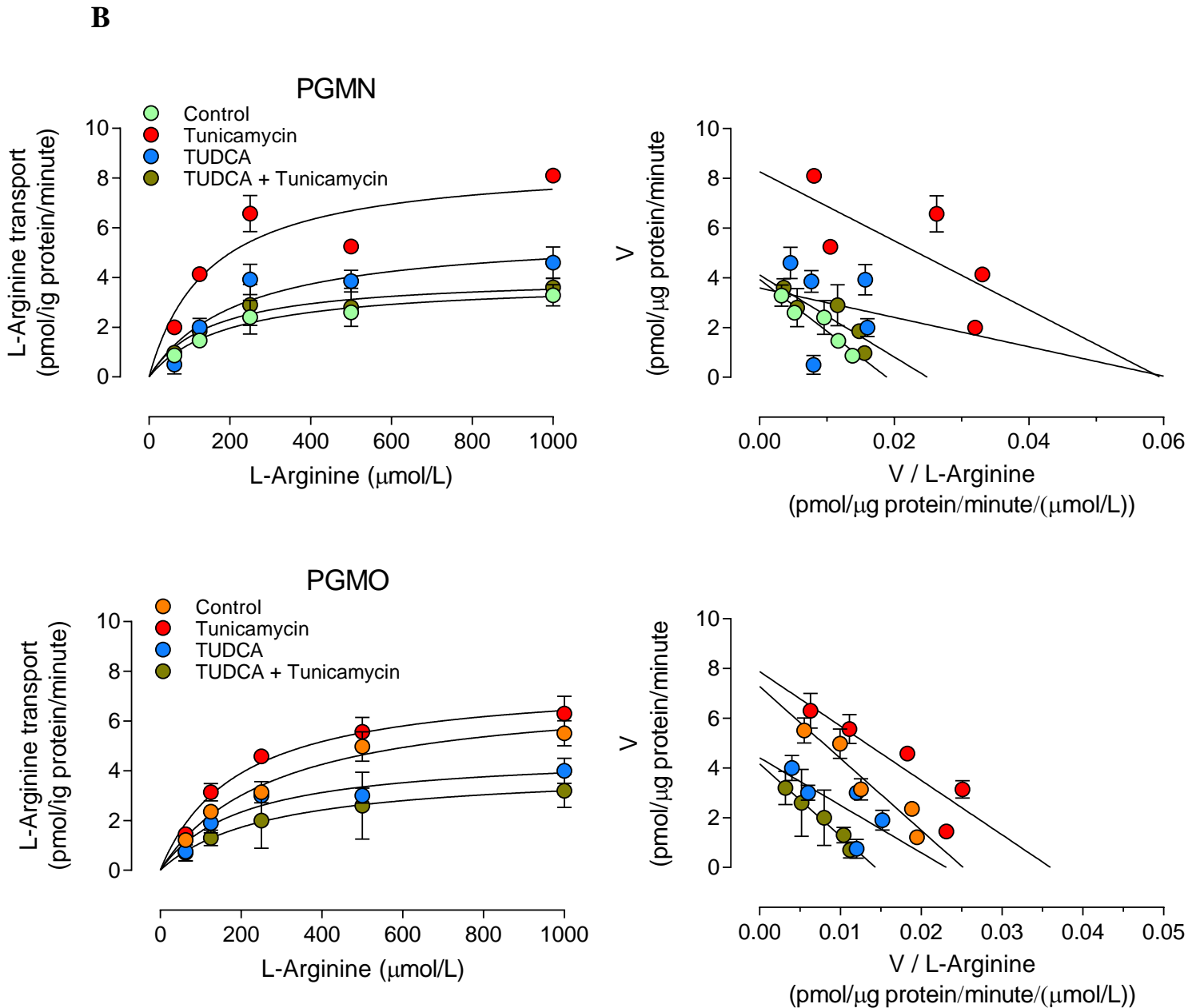


**Figure 39. ER stress effect on L-arginine transport.** The overall L-arginine transport was determined in from pregnancies where the mother showed pre-gestational maternal normal weight (PGMN) or pre-gestational maternal obesity (PGMO). Cells were incubated without or with tunicamycin (5  $\mu\text{M}$ , 8 hours), TUDCA (100  $\mu\text{M}$ , 8 hours) and L-arginine (0-1000  $\mu\text{M}$ , 3  $\mu\text{Ci/mL}$  of L-[ $^3\text{H}$ ]arginine, 37 $^{\circ}\text{C}$ , 1 minute) (see Methods). **A**, Left graphs show the overall transport of L-arginine. Right graphs show the representation of the Eadie-Hofstee plot of the data obtained in left graphs. **B**, Left graphs show the saturated transport resulting from the subtraction of the linear component of the data in A and adjusted to the Michaelis-Menten equation. Right graphs show the representation of the Eadie-Hofstee graph of the data obtained in left graphs. Values are mean  $\pm$  S.E.M. (n = 12 PGMN, 12 PGMO).

**Table 10. Kinetic parameters for the L-arginine transport in HUVECs**

	<i>Saturable transport</i>			<i>Overall transport</i>	
	$V_{\max}$ (pmol/ $\mu$ g protein/ minute)	$K_m$ ( $\mu$ M)	$V_{\max}/K_m$ (pmol/ $\mu$ g protein/ minute/ $(\mu$ M))	$K_D$ (pmol/ $\mu$ g protein/ minute/ $(\mu$ M))	$v_i$ (pmol/ $\mu$ g protein/ 0.5 s)
<i>PGMN</i>					
Control	3.86 $\pm$ 0.29	195 $\pm$ 42	0.0198 $\pm$ 0.0029	0.0081 $\pm$ 0.0042	0.0069 $\pm$ 0.0001
Tunicamycin	9.50 $\pm$ 0.30 *	220 $\pm$ 45	0.0432 $\pm$ 0.0094 *	0.0109 $\pm$ 0.0025	0.0150 $\pm$ 0.0001 *
TUDCA	4.85 $\pm$ 0.35	224 $\pm$ 35	0.0217 $\pm$ 0.0025	0.0099 $\pm$ 0.0013	0.0075 $\pm$ 0.0002
Tunicamycin + TUDCA	4.06 $\pm$ 0.43	152 $\pm$ 51	0.0267 $\pm$ 0.0058	0.0114 $\pm$ 0.0018	0.0088 $\pm$ 0.0001
<i>PGMO</i>					
Control	7.26 $\pm$ 0.59 *	253 $\pm$ 58	0.0287 $\pm$ 0.0043 *	0.0021 $\pm$ 0.0010 *	0.0099 $\pm$ 0.0001 *
Tunicamycin	7.67 $\pm$ 0.49 *	193 $\pm$ 36	0.0397 $\pm$ 0.0049 *	0.0102 $\pm$ 0.0031 †	0.0102 $\pm$ 0.0002 *
TUDCA	4.71 $\pm$ 0.63 †	203 $\pm$ 77	0.0230 $\pm$ 0.0025 †	0.0084 $\pm$ 0.0026 †	0.0070 $\pm$ 0.0002 †
Tunicamycin + TUDCA	4.06 $\pm$ 0.10 †	271 $\pm$ 18	0.0150 $\pm$ 0.0015 †	0.0064 $\pm$ 0.0005 †	0.0052 $\pm$ 0.0002 †

The overall L-arginine transport was determined in HUVECs from PGMN or PGMO pregnancies treated or not with tunicamycin (5  $\mu$ M, 8 hours) or TUDCA (100  $\mu$ M, 8 hours). The cells were incubated with L-arginine (0-1000  $\mu$ M, 3  $\mu$ Ci/mL of L-[<sup>3</sup>H]arginine, 37°C, 1 minute) as described in methods. The saturated transport resulted from the subtraction of the linear component to the overall transport.  $V_{\max}$ : maximum transport velocity;  $K_m$ : apparent constant of Michaelis-Menten;  $K_D$ : linear component;  $v_i$ : initial velocity;  $V_{\max}/K_m$ : maximal transport capacity. Values are mean  $\pm$  S.E.M.  $P < 0.05$ . \* vs the PGMN control. † vs PGMO in baseline condition. (n = 12 PGMN, 12 PGMO).

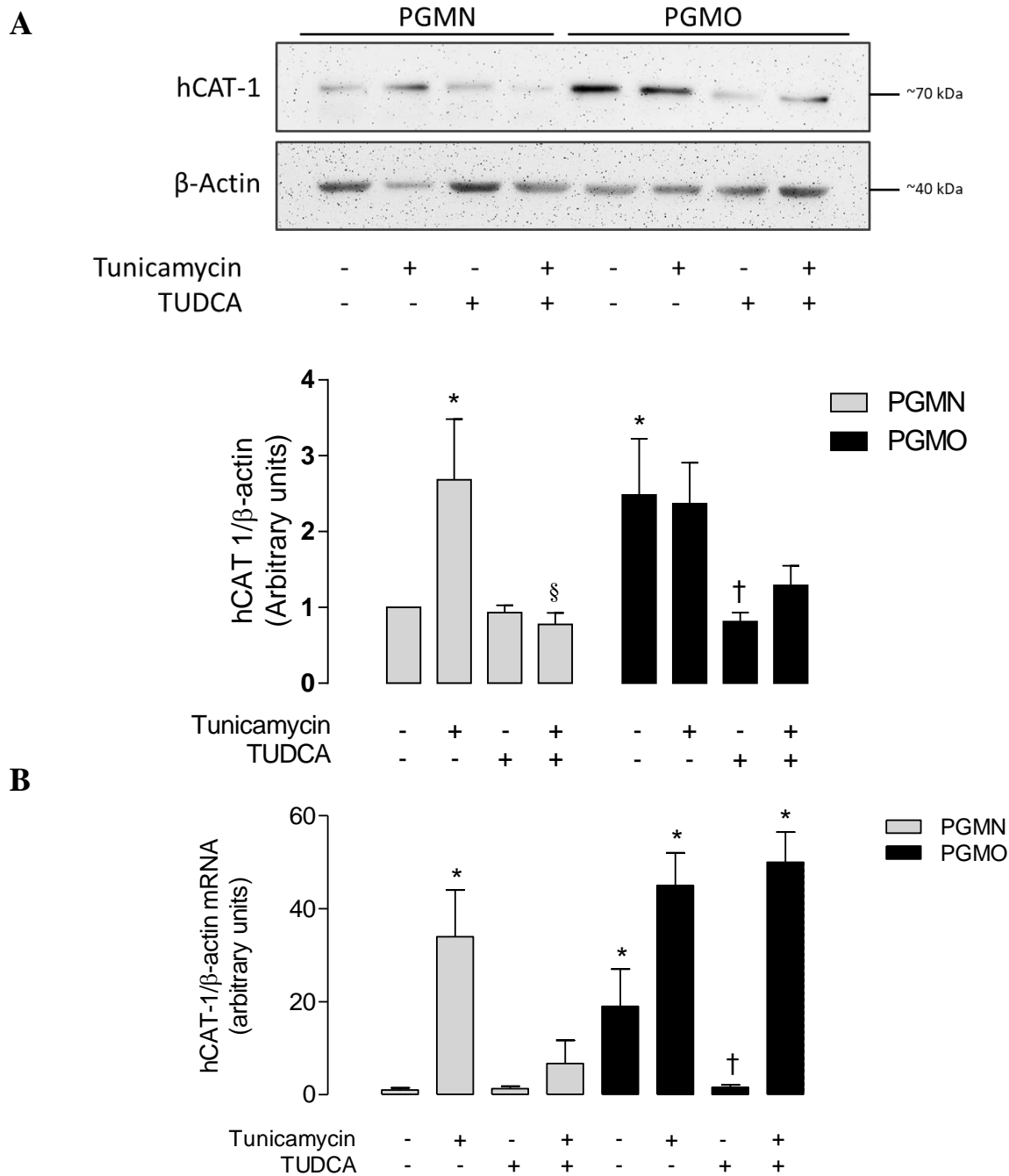


**Figure 40. Modulation of hCAT-1 expression in HUVECs by ER stress.** The protein and mRNA abundance of hCAT-1 were determined by western blot and RT-qPCR in HUVECS from pregnancies where the mother showed pre-gestational maternal normal weight (PGMN) or pre-gestational maternal obesity (PGMO) (see Methods). **A**, Representative western blot for hCAT-1. The graph shows the densitometry for hCAT-1 over  $\beta$ -actin. The densitometry was normalized to 1 with the data obtained in HUVECs PGMN at basal conditions. **B**, Relative abundance of hCAT-1 mRNA analyzed by the  $\Delta\Delta C_T$  method. Values are mean  $\pm$  S.E.M.  $P < 0.05$ . \* vs PGMN at basal conditions. † vs PGMO control. (n = 9 PGMN, 9 PGMO).

#### 5.4.2 *ER stress and insulin response*

The involvement of ER stress on the insulin response was evaluated by inducing or reducing ER stress and its effect on the activation of key proteins of the insulin signaling pathway, as represented in Scheme 5.

##### *Umbilical vein reactivity*

Tunicamycin reduced the insulin response in umbilical vein rings from PGMN and did not generate changes in vessels from PGMO pregnancies (Figure 41A,B). TUDCA increased the effect of insulin in vessels from PGMO pregnancies reducing the  $EC_{50}$  (~84%) and generating a  $R_{max}$  (~19%) similar to that determined in the untreated vessels from PGMN pregnancies. The incubation of vein rings with both compounds prevented the impairment in the insulin response induced by tunicamycin in umbilical veins from PGMN and blunted the sensitization induced by TUDCA in umbilical veins from PGMO pregnancies (Figure 41A,B, Table 10).

##### *ER stress and NO generation by HUVECs*

Tunicamycin blocked the relative fluorescence increased by insulin in HUVECs from PGMN pregnancies and did not induce changes in HUVECs from PGMO pregnancies incubated with insulin (Figure 42A) (see Scheme 5). TUDCA did not produce changes in the insulin response in both conditions. Regarding the NOS-dependent NO production, tunicamycin induced a similar effect to that seen for the relative fluorescence (Figure 42B). However, the incubation with TUDCA increased the effect of insulin in HUVECs from PGMO, leading to higher NOS-dependent NO production (~3.5 fold) compared with HUVECS from PGMO at basal conditions. The increased NO production in response to TUDCA was still lower than the insulin-induced NO production in HUVECs from PGMN

treated with TUDCA (Figure 42B). The co-incubation of TUDCA with tunicamycin blocked TUDCA-induced response in the HUVECs from PGMO.

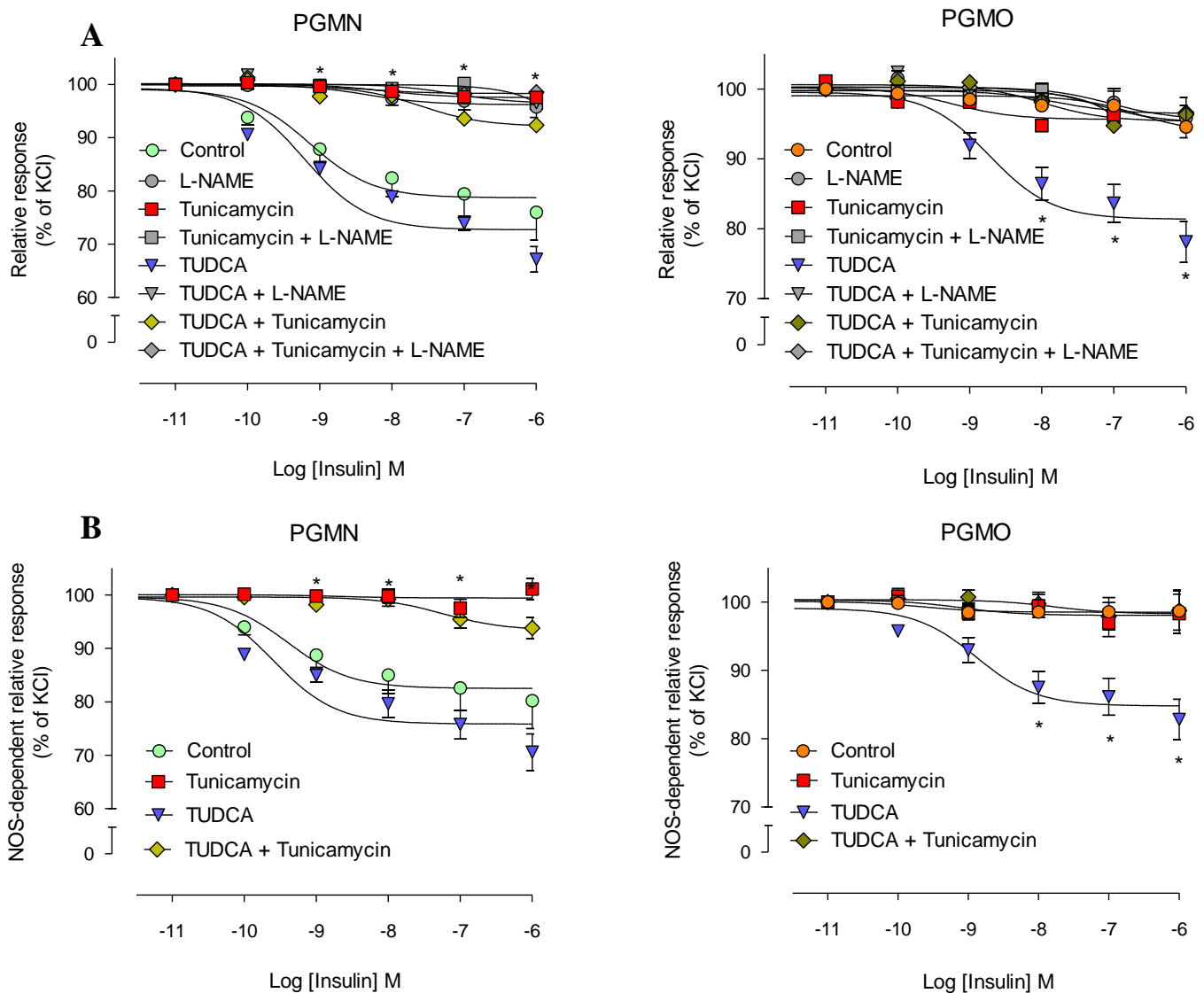
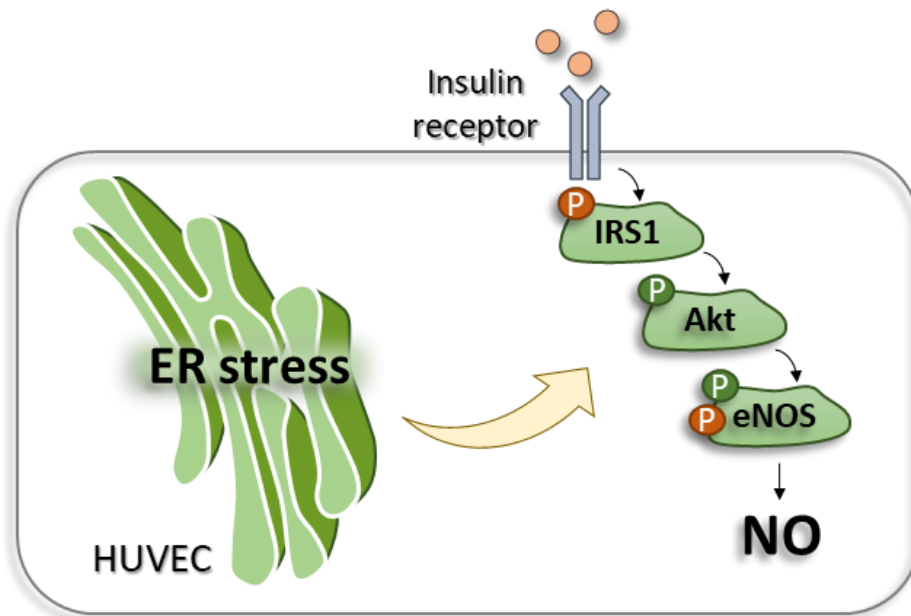


**Figure 41. Involvement of ER stress in the insulin-induced relaxation in umbilical vein rings.** Human umbilical vein rings from pregnancies where the mother showed pre-gestational maternal normal weight (PGMN) or pre-gestational maternal obesity (PGMO) were pre-contracted with KCl 32.5 mM and incubated without or with tunicamycin (5  $\mu$ M, 8 hours), TUDCA (100  $\mu$ M, 8 hours) and L-NAME (30 minutes, 100  $\mu$ M), and then exposed (5 minutes) to insulin. **A**, Vasodilation curves of vessels from PGMN (left graph) and PGMO (right graph) pregnancies in the absence or presence of L-NAME. **B**, NOS-dependent vasodilation determined by the subtraction of the total insulin response minus the response in the presence of L-NAME. Values are mean  $\pm$  S.E.M. \*  $P < 0.05$  vs the corresponding values in PGMN or PGMO at basal conditions. (n = 2-5 PGMN, 2-7 PGMO).

**Table 11. Parameters dose-response of relaxation in response to insulin in human umbilical vein rings treated with tunicamycin or TUDCA**

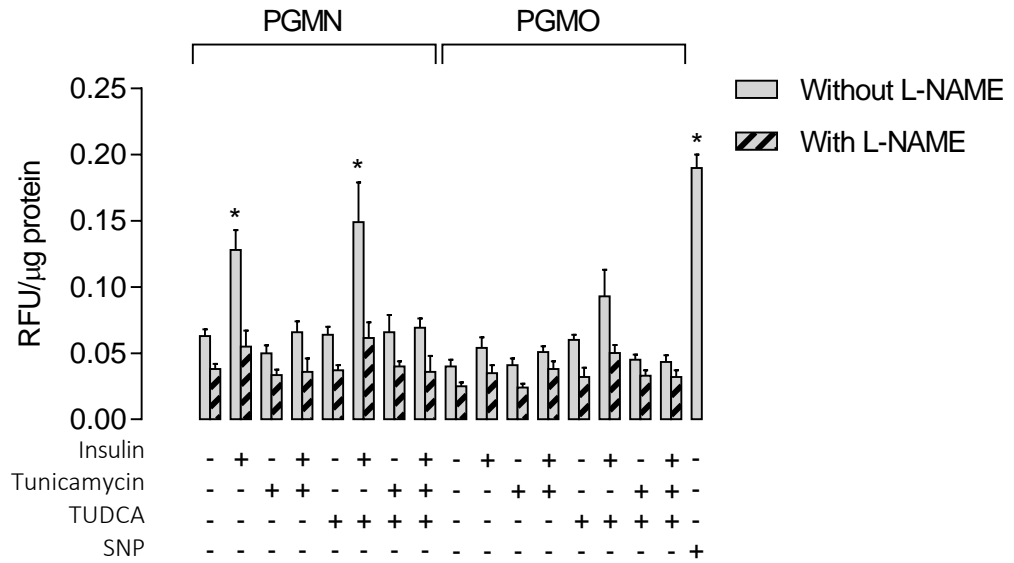
<i>Condition</i>	<i>Treatment</i>	<i>EC<sub>50</sub></i> <i>-Log [Ins] M</i>	<i>EC<sub>50</sub></i> <i>[Ins] nM</i>	<i>R<sub>max</sub></i>	<i>% Relaxation</i>	<i>R<sub>max</sub>/EC<sub>50</sub></i>
<b><i>PGMN</i></b>	Control	9.14 ± 0.29	0.72 ± 0.02	78.72 ± 1.88	21.28 ± 1.88	108.66 ± 6.04
	L-NAME	8.35 ± 0.60	4.47 ± 0.32 *	96.21 ± 0.81 *	3.79 ± 0.81 *	21.54 ± 1.073 *
	Tunicamycin	8.16 ± 0.15	6.92 ± 0.13	97.55 ± 0.14	2.45 ± 0.14	14.10 ± 0.28
	Tunicamycin + L-NAME	7.69 ± 0.10	20.42 ± 0.27	96.46 ± 0.14	3.54 ± 0.14	4.72 ± 0.07
	TUDCA	9.14 ± 0.43	0.72 ± 0.06	70.42 ± 3.56	29.58 ± 3.56	97.21 ± 9.49
	TUDCA + L-NAME	7.30 ± 0.71	50.12 ± 4.87	96.56 ± 1.29	3.44 ± 1.29	1.92 ± 0.21
	TUDCA + Tunicamycin	7.60 ± 0.37	25.12 ± 5.02	92.14 ± 1.20	7.86 ± 1.20	3.67 ± 0.23
	TUDCA + Tunicamycin + L-NAME	7.68 ± 0.56	20.89 ± 3.85	98.34 ± 0.40	1.66 ± 0.40	4.71 ± 0.36
<b><i>PGMO</i></b>	Control	8.13 ± 1.02	7.41 ± 0.93 *	93.99 ± 3.61 *	6.01 ± 3.61 *	12.68 ± 2.08 *
	L-NAME	7.05 ± 0.72	89.13 ± 9.10 *	95.61 ± 1.92 *	4.39 ± 1.92 *	1.07 ± 0.13 *
	Tunicamycin	8.15 ± 0.63	7.08 ± 0.55	95.65 ± 1.05	4.34 ± 1.05	13.51 ± 1.19
	Tunicamycin + L-NAME	7.42 ± 0.68	38.02 ± 3.48	96.06 ± 2.10	3.94 ± 2.10	2.53 ± 0.29
	TUDCA	8.92 ± 0.22	1.2 ± 0.03 †	81.37 ± 1.32 †	18.63 ± 1.32 †	67.68 ± 2.77 †
	TUDCA + L-NAME	7.23 ± 0.61	58.88 ± 4.97	95.20 ± 1.59	4.8 ± 1.59	1.62 ± 0.16
	TUDCA + Tunicamycin	8.0 ± 1.24	10.00 ± 1.55	95.39 ± 0.36	4.61 ± 0.36	9.54 ± 1.51
	TUDCA + Tunicamycin + L-NAME	7.80 ± 0.47	15.85 ± 0.95	96.48 ± 1.84	3.52 ± 1.84	6.09 ± 0.48

EC<sub>50</sub>, Half maximal effective concentration. R<sub>max</sub>, Maximum response. Values are mean ± S.E.M. *P*<0.05. \* vs PGMN control, † vs PGMO control. (n= PGMN control: 5, PGMO control: 7, PGMO + TUDCA: 4, all other treatments: 2)

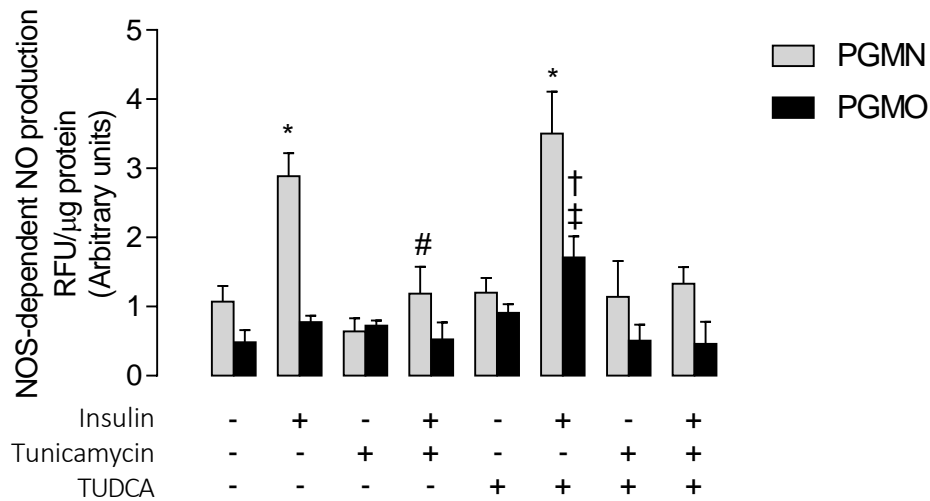


**Scheme 5. ER stress and insulin signaling pathway.** ER, endoplasmic reticulum; IRS1, insulin receptor substrate 1; eNOS, endothelial nitric oxide synthase; P in orange, inhibiting phosphorylation; P in green, activating phosphorylation; NO, nitric oxide; HUVEC, human umbilical vein endothelial cell.

**A**



**B**

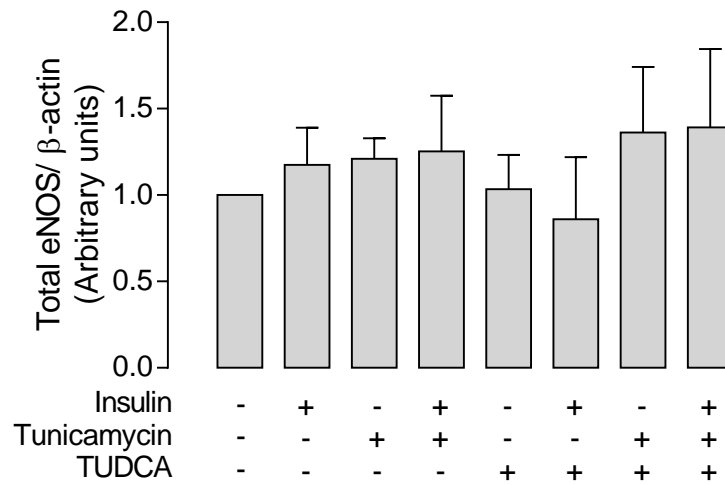
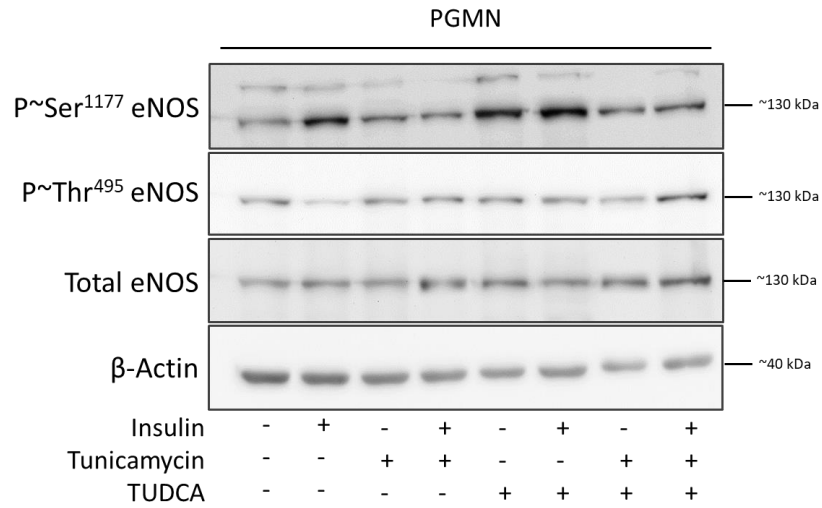
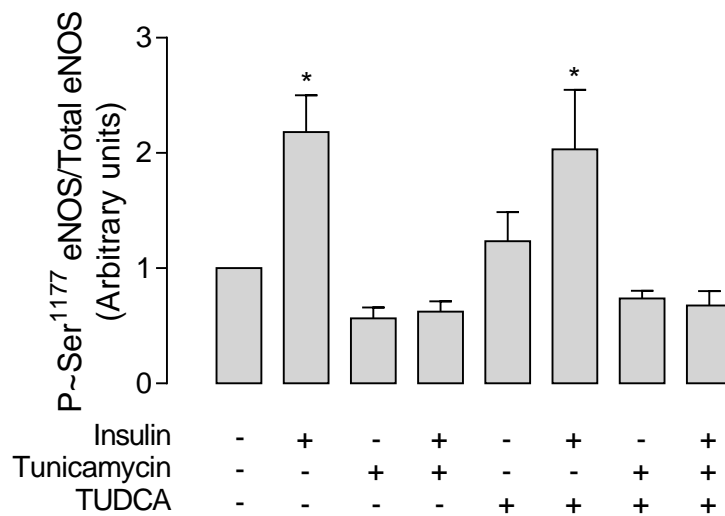


**Figure 42. ER stress modulation of NO generation in response to insulin by HUVECs.** The total (relative fluorescence) and the NOS-dependent generation of NO in HUVECS from pregnancies where the mother showed pre-gestational maternal normal weight (PGMN) or pre-gestational maternal obesity (PGMO) were evaluated by fluorescence lecture after loading the cells with the probe DAF-FM (1 hour, 5 μM). Cells were incubated without (-) or with (+) tunicamycin (5 μM, 8 hours), TUDCA (100 μM, 8 hours), L-NAME (100 μM, 30 minutes) and insulin (1nM) (see Methods). **A**, Relative fluorescence units (RFU). **B**, The fraction of the RFU inhibited by L-NAME (i.e., dependent on NOS activity) derived from the data presented in A. Values are mean ± S.E.M. *P*<0.05. \* vs PGMN in basal condition. # vs PGMN + insulin. † vs PGMO in the baseline condition. ‡ vs PGMN + TUDCA + insulin. (n = 5 PGMN, 6 PGMO).

### *eNOS and Akt activation*

Tunicamycin and TUDCA did not change the protein abundance for total eNOS and Akt in HUVECs from both conditions (Figures 43, 44, 45, and 46, section A). The incubation with tunicamycin blocked the increase in the activating phosphorylation of eNOS (Figure 43B) and Akt (Figure 45B) caused by insulin in HUVECs from PGMN pregnancies and did not change the levels of both protein phosphorylations in HUVECs from PGMO pregnancies treated with insulin. On the contrary, the incubation with insulin in cells treated with TUDCA increased the activating phosphorylation of eNOS and Akt (~2.3 fold, ~ 2.5 fold, respectively) in HUVECs from PGMO (Figures 44B, 46B), and did not alter the insulin-induced increase in HUVECs from PGMN pregnancies (Figures 43B, 45B). The co-incubation of TUDCA with tunicamycin prevented the effect of TUDCA on the insulin response in HUVECs from PGMO. Additionally, the treatment with TUDCA in the presence of tunicamycin did not revert the tunicamycin-induced impaired insulin-induced phosphorylation of both proteins in HUVECs from PGMN.

The inhibiting phosphorylation of eNOS in threonine 495 did not present changes after treatments with tunicamycin or TUDCA in HUVECs from PGMN pregnancies (Figure 43C). However, TUDCA reduced the PGMO-increased phosphorylation and were kept at the same level after insulin treatment (Figure 44C). The treatment with both compounds did not produce changes in HUVECs from PGMN and prevented the TUDCA-promoted reduction of the inhibiting phosphorylation in HUVECs from PGMO.

**A****B**

C

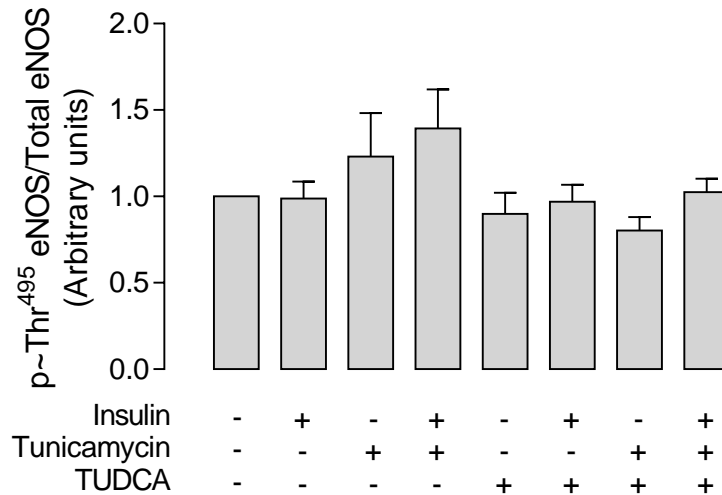
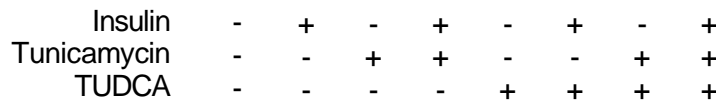
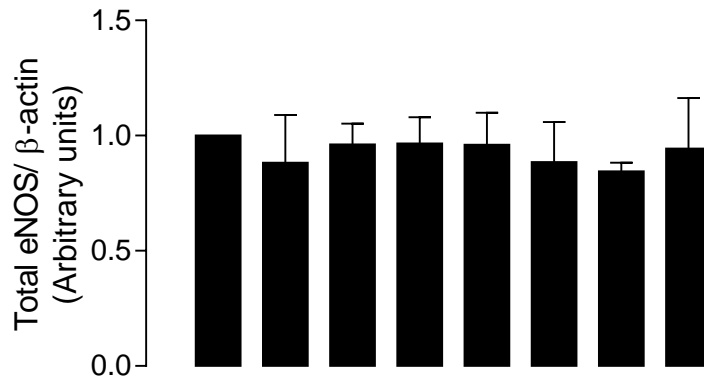
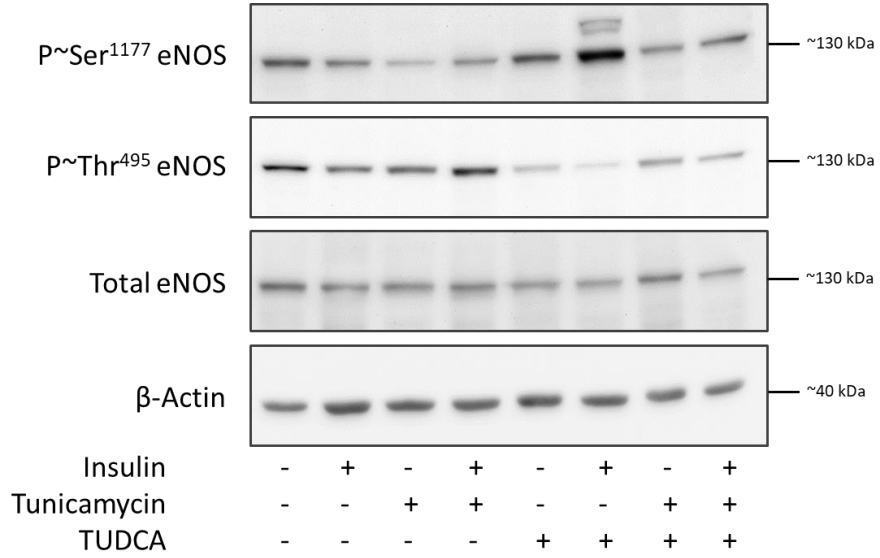
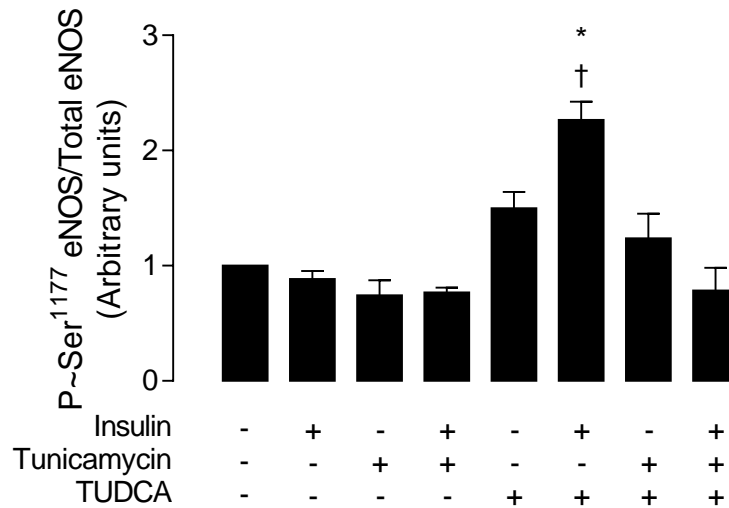


**Figure 43. Modulation of the abundance and activation state of eNOS in response to inulin by ER stress.** The protein abundance and the activating and inhibiting phosphorylation of eNOS were evaluated in HUVECS from pregnancies where the mother showed pre-gestational maternal normal weight (PGMN). Cells were incubated without (-) or with (+) tunicamycin (5  $\mu$ M, 8 hours), TUDCA (100  $\mu$ M, 8 hours) and insulin (1 nM, 20 minutes) (see Methods). **A**, Representative western blot for the activating and inhibiting phosphorylation of eNOS, the total protein abundance and  $\beta$ -actin. The graph shows the densitometry for the total protein abundance of eNOS over  $\beta$ -actin. **B**, Densitometry for eNOS phosphorylated in serine 1177 over total eNOS. **C**, Densitometry for eNOS phosphorylated in threonine 495 over total eNOS. The densitometry was normalized to 1 with data in PGMN control. Values are mean  $\pm$  S.E.M.  $P < 0.05$ . \* vs control. (n = 5).

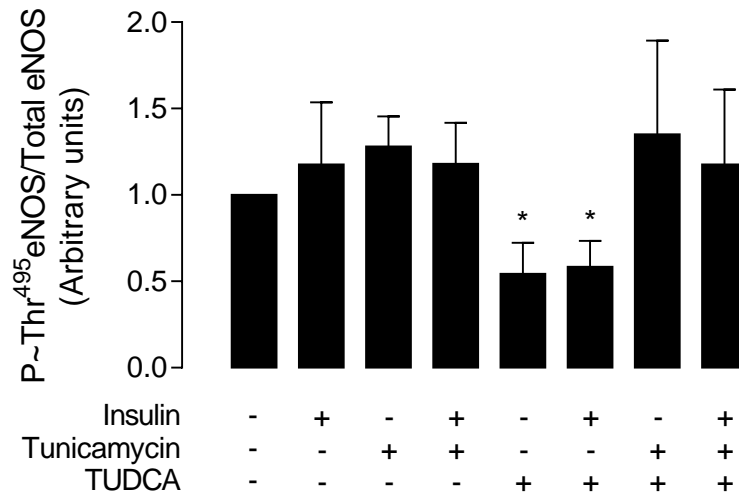
**A**



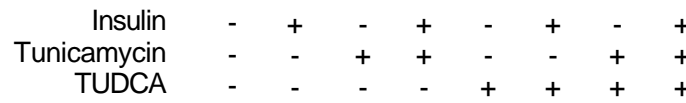
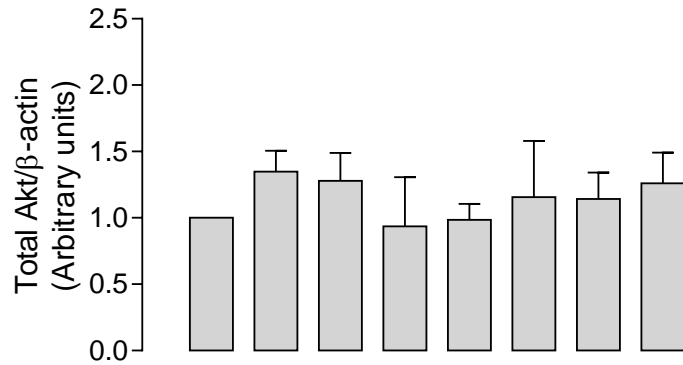
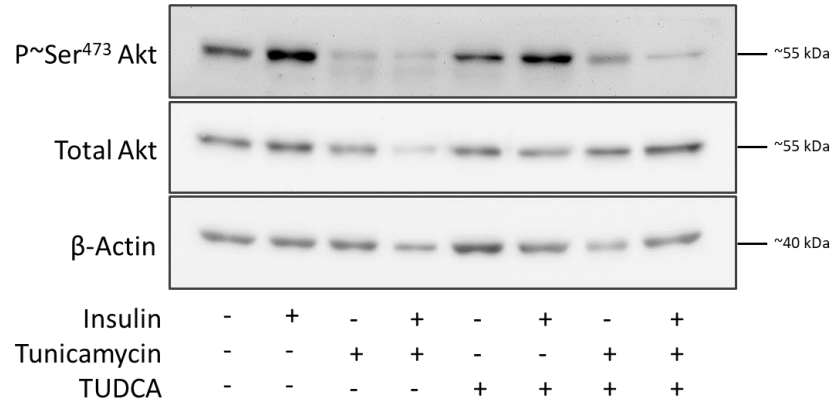
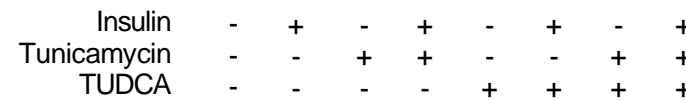
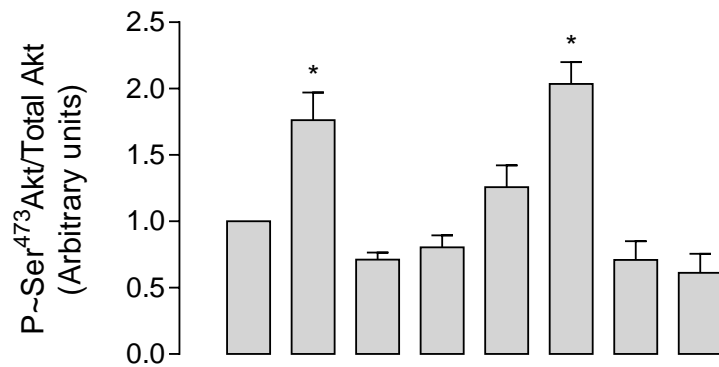
**B**



C



**Figure 44. Modulation of the abundance and activation state of eNOS in response to insulin by ER stress.** The protein abundance and the activating and inhibiting phosphorylation of eNOS were evaluated in HUVECS from pregnancies where the mother showed pre-gestational maternal obesity (PGMO). Cells were incubated without (-) or with (+) tunicamycin (5  $\mu$ M, 8 hours), TUDCA (100  $\mu$ M, 8 hours) and insulin (1 nM, 20 minutes) (see Methods). **A**, Representative western blot for the activating and inhibiting phosphorylation of eNOS, the total protein abundance and  $\beta$ -actin. The graph shows the densitometry for the total protein abundance of eNOS over  $\beta$ -actin. **B**, Densitometry for eNOS phosphorylated in serine 1177 over total eNOS. **C**, Densitometry for eNOS phosphorylated in threonine 495 over total eNOS. The densitometry was normalized to 1 with data in control. Values are mean  $\pm$  S.E.M.  $P < 0.05$ . \* vs control (n = 7).

**A****B**

**Figure 45. Modulation of Akt abundance and activation in response to insulin by ER stress.** The protein abundance and the phosphorylation of Akt were evaluated in HUVECS from pregnancies where the mother showed pre-gestational maternal normal weight (PGMN). Cells were incubated without (-) or with (+) tunicamycin (5  $\mu$ M, 8 hours), TUDCA (100  $\mu$ M, 8 hours) and insulin (1 nM, 20 minutes) (see Methods). **A**, Representative western blot for Akt phosphorylated, the total protein abundance and  $\beta$ -actin. The graph shows the densitometry for the total protein abundance of Akt over  $\beta$ -actin. **B**, Densitometry for Akt phosphorylated over total Akt. The densitometry was normalized to 1 with data in control. Values are mean  $\pm$  S.E.M.  $P < 0.05$ . \* vs control (n = 5).

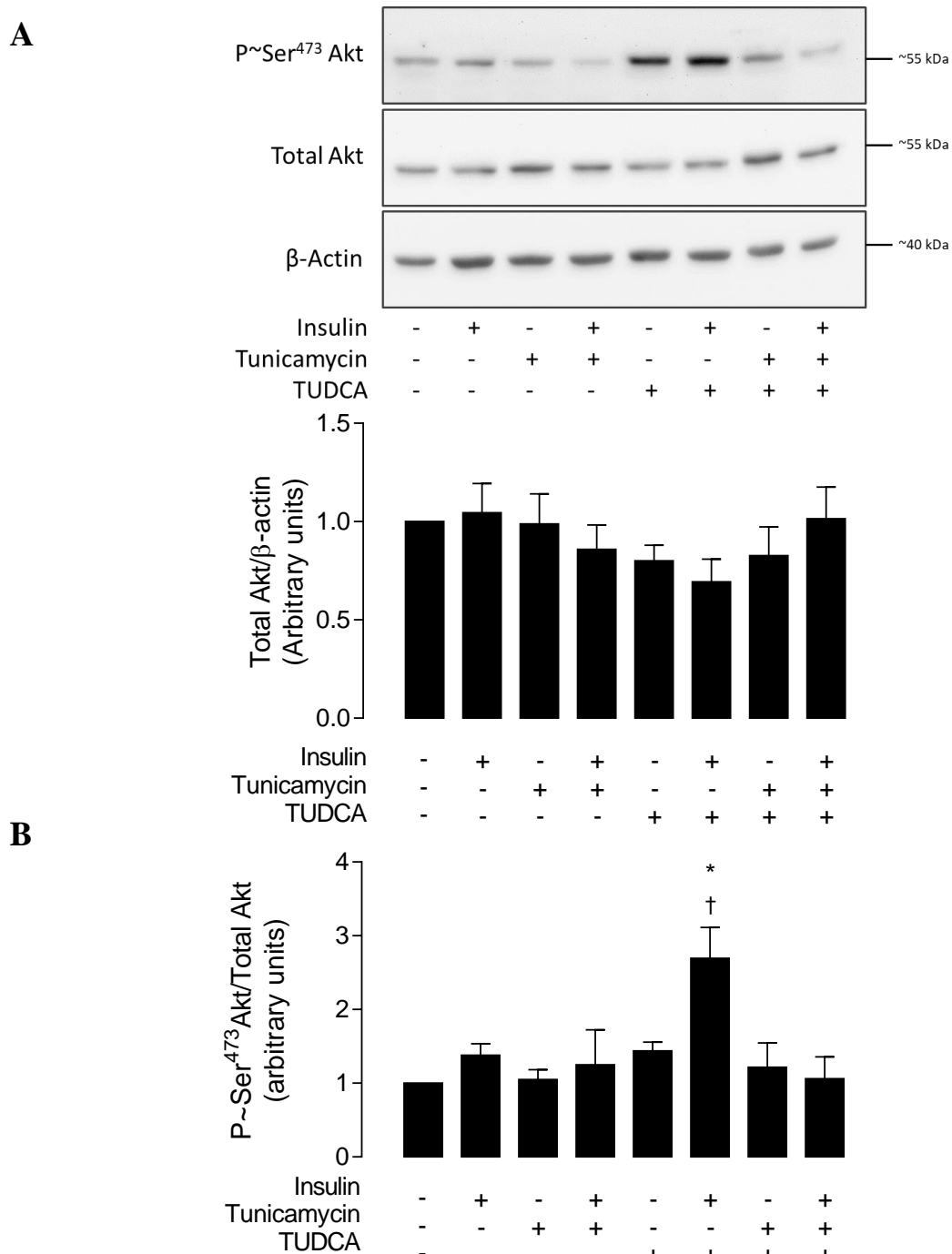


**Figure 46. Modulation of Akt abundance and activation state by ER stress.** The protein abundance and the phosphorylation of Akt were evaluated in HUVECS from pregnancies where the mother showed pre-gestational maternal obesity (PGMO). Cells were incubated without (-) or with (+) tunicamycin (5  $\mu$ M, 8 hours), TUDCA (100  $\mu$ M, 8 hours) and insulin (1 nM, 20 minutes) (see Methods). **A**, Representative western blot for Akt phosphorylated, the total protein abundance and  $\beta$ -actin. The graph shows the densitometry for the total protein abundance of Akt over  $\beta$ -actin. **B**, Densitometry for Akt phosphorylated over total Akt. The densitometry was normalized to 1 with data in control. Values are mean  $\pm$  S.E.M.  $P < 0.05$ . \* vs control. † vs TUDCA (n = 7).

#### 5.4.3 Pharmacological inhibition of PERK, IRE1 $\alpha$ , and knockdown of IRE1 $\alpha$

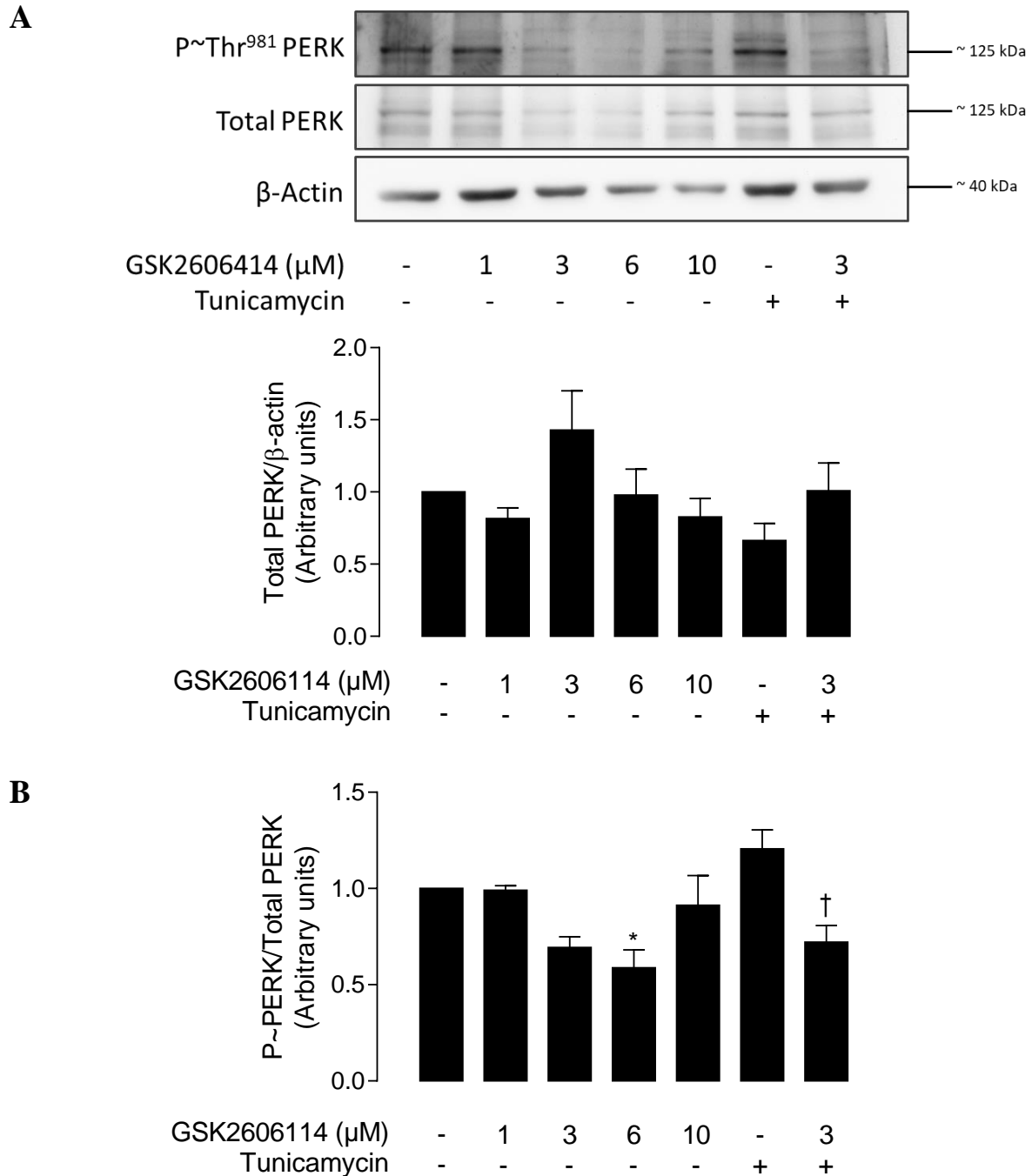
The inhibitor of PERK, GSK2606115, and the inhibitor of the kinase and endoribonuclease activity of IRE1 $\alpha$ , KIRA6, were used for the evaluation of the involvement of these proteins in the ER stress-associated endothelial dysfunction and insulin desensitization seen in HUVECs from PGMO. The incubation of HUVECs from PGMO with 6  $\mu$ M of GSK2606115 reduced the phosphorylation of PERK in the absence of tunicamycin, and at 3  $\mu$ M it reduced by  $\sim$ 40% in the presence of tunicamycin (Figure 47). A similar effect was observed for the inhibiting phosphorylation of eIF2 $\alpha$ , reaching a maximal reduction at 3  $\mu$ M even in the presence of tunicamycin (Figure 48). The inhibitor did not cause significant changes in the total abundance of PERK. Thus, the involvement of PERK in the insulin response was evaluated using GSK2606115 at 3  $\mu$ M.

The incubation of HUVECs from PGMN pregnancies with KIRA6 for 8 hours at a concentration of 3  $\mu$ M reduced the activating phosphorylation of IRE1 $\alpha$  ( $\sim$ 49%) in HUVECs from PGMN pregnancies treated with tunicamycin (Figure 49B), with an  $EC_{50}$  of  $1.1 \pm 1.3$   $\mu$ M. In concordance, KIRA6 at 3 and 6  $\mu$ M also reduced the activating phosphorylations of JNK (JNK1 and JNK2) in the presence of tunicamycin (Figure 50B). The inhibitor did not change the total abundance of IRE1 $\alpha$  and JNK. On the other hand, the increase of sXBP1 mRNA induced by tunicamycin in HUVECs from PGMN was prevented by the incubation of cells with 3  $\mu$ M and 6  $\mu$ M (Figure 50C). Therefore, with those data, it was decided to evaluate the involvement of IRE1 $\alpha$  in the insulin response using KIRA6 at 3  $\mu$ M.

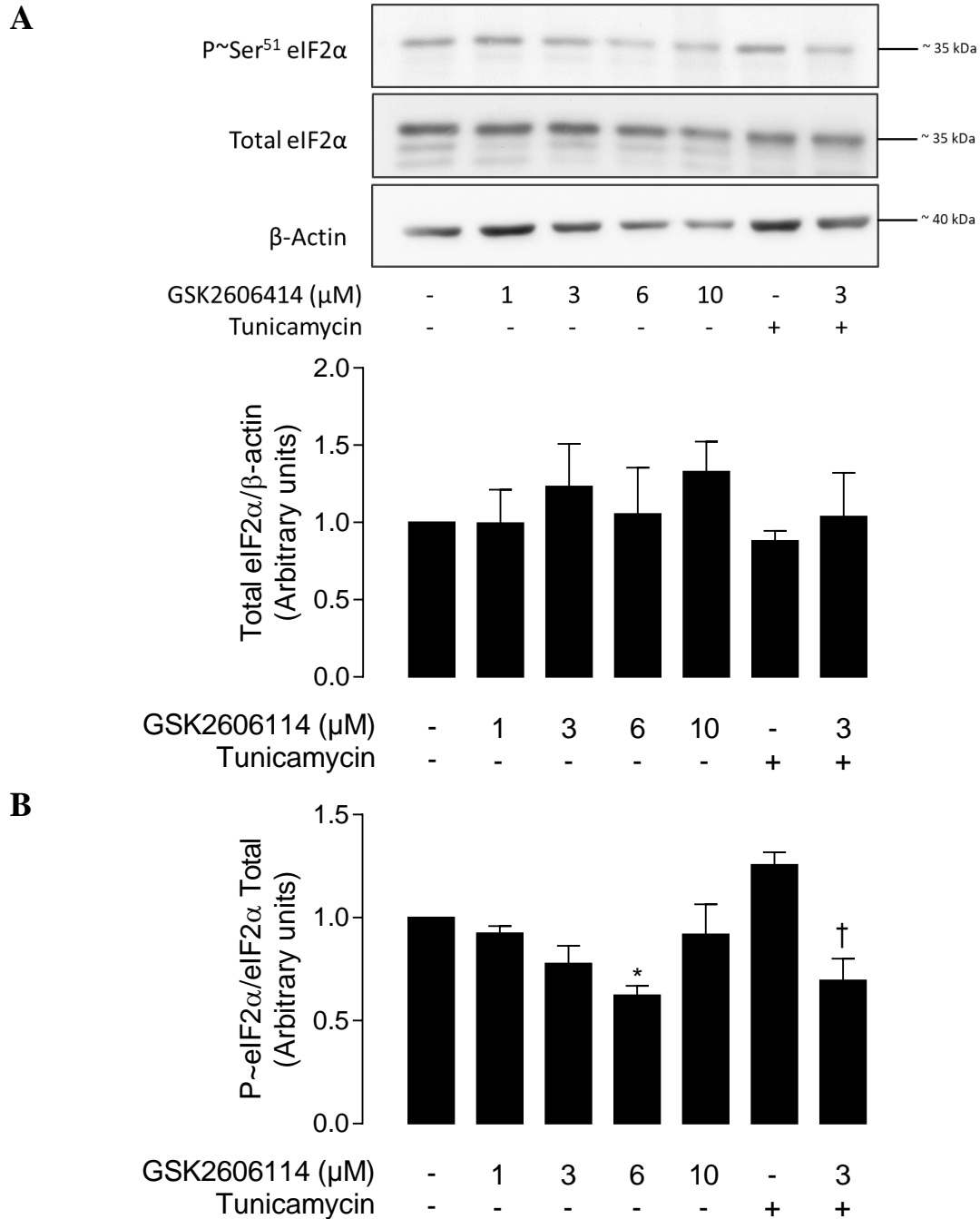
The participation of IRE1 $\alpha$  in HUVECs from PGMO was further evaluated by the use of a small interfering RNA against IRE1 $\alpha$ . The IRE1 $\alpha$  knockdown decreased ( $\sim$ 37%) the total expression of IRE1 $\alpha$  in comparison to control, which remained low ( $\sim$ 64%) when the

knockdown cells were treated with tunicamycin (Figure 51). IRE1 $\alpha$  knockdown showed a similar effect on the JNK phosphorylation, which decreased (~29%) in comparison to the control and remained low (~55%) in the presence of tunicamycin (Figure 52B). There were no changes in total JNK.

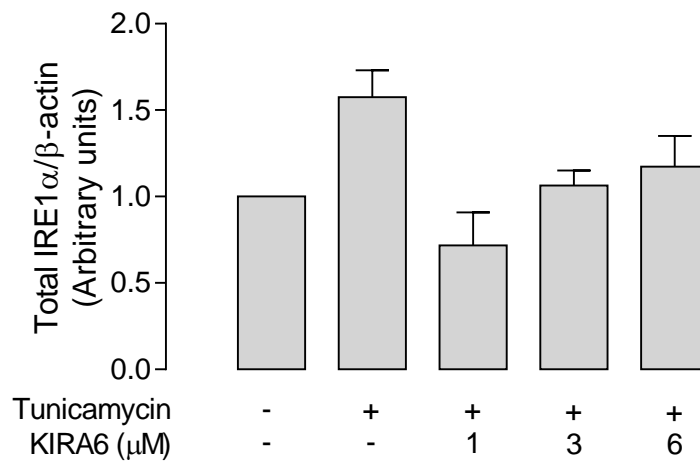
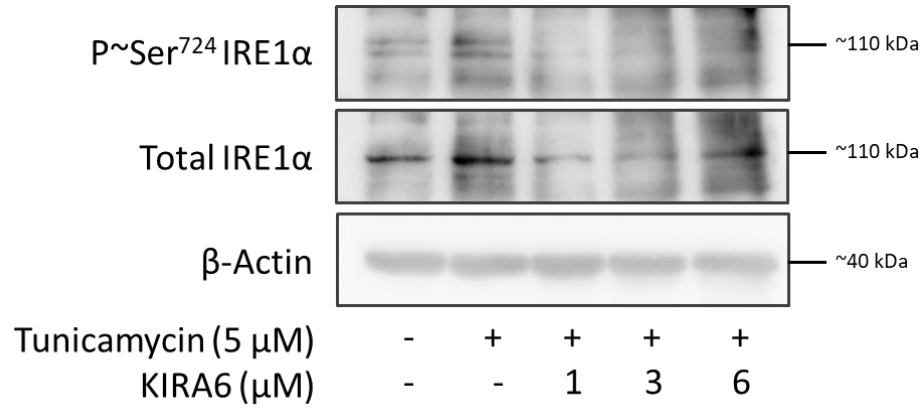
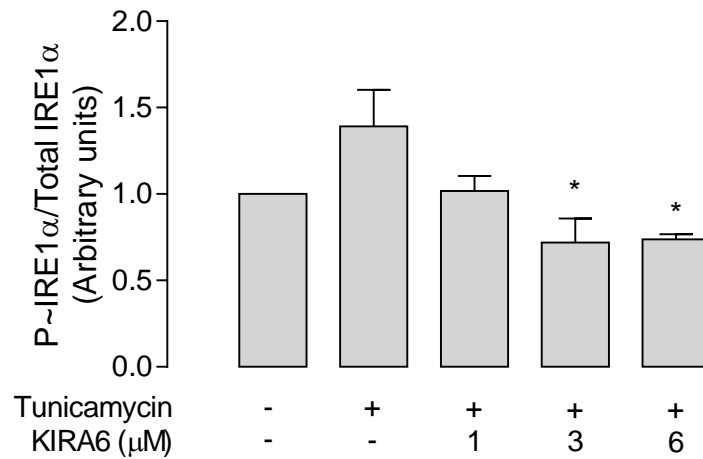
The involvement of JNK was evaluated by the use of the inhibitor SP600125. The incubation of HUVECs from PGMN pregnancies with SP600125 at 25  $\mu$ M for 8 hours reduced (~54%) the activating phosphorylations of JNK in the presence of tunicamycin (Figure 53B). SP600125 did not cause significant changes in the total abundance of JNK. Thus, the involvement of JNK was evaluated using SP600125 at 25  $\mu$ M.



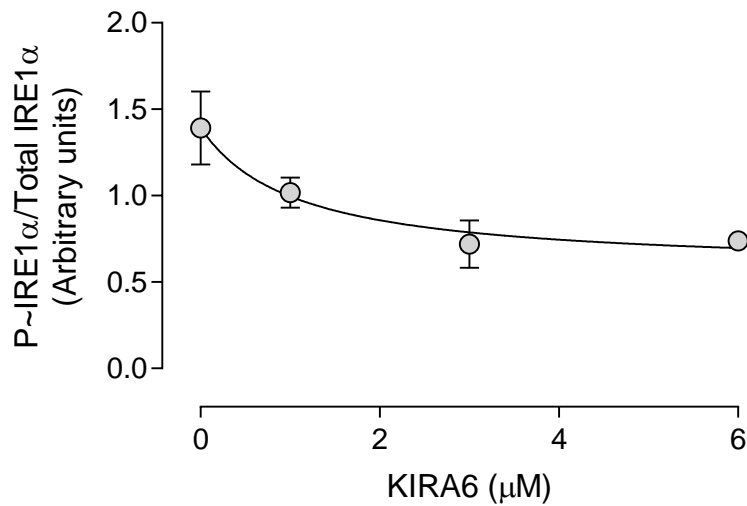
**Figure 47. Inhibition of PERK by GSK2606114.** The protein abundance and the phosphorylation of PERK were evaluated in HUVECS from pregnancies where the mother showed pre-gestational maternal obesity (PGMO). Cells were incubated without (-) or with (+) tunicamycin (5 μM, 8 hours) and GSK2606114 (8 hours at the indicated concentrations) (see Methods). **A**, Representative western blot for PERK phosphorylated, the total protein abundance and β-actin. The graph shows the densitometry for the total protein abundance of PERK over β-actin. **B**, Densitometry for PERK phosphorylated over total PERK. The densitometry was normalized to 1 with data in control. Values are mean ± S.E.M.  $P < 0.05$ . \* vs control. † vs TUDCA (n = 3).



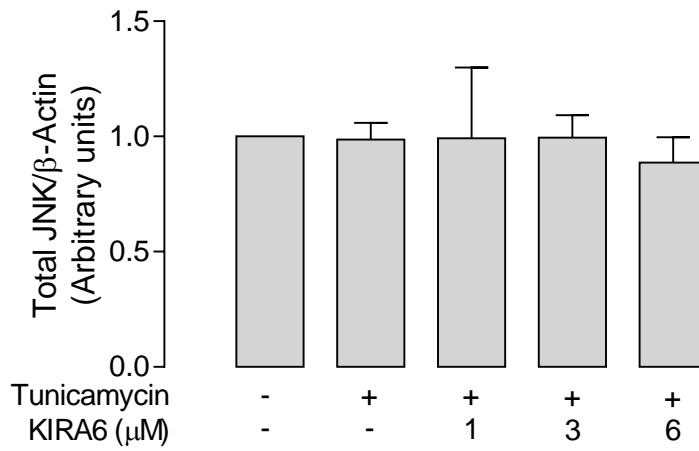
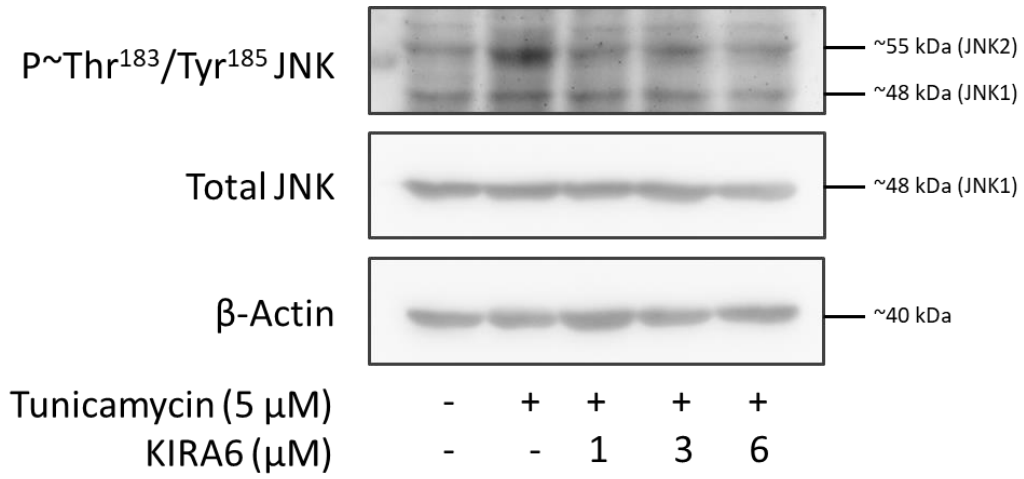
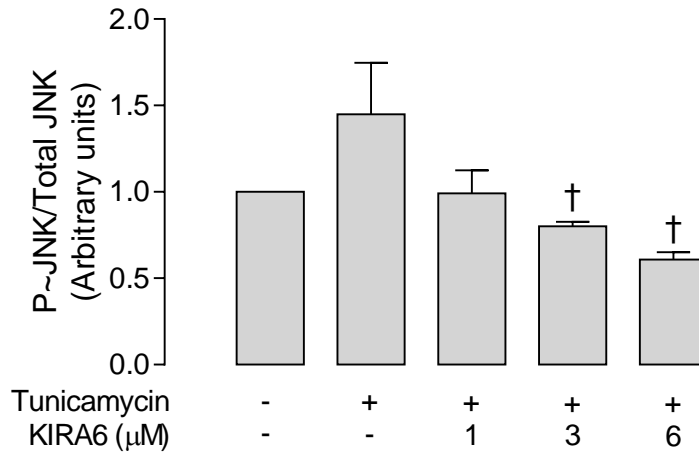
**Figure 48. PERK-induction of eIF2 $\alpha$  activation in HUVECs.** The protein abundance and the phosphorylation of eIF2 $\alpha$  were evaluated in HUVECS from pregnancies where the mother showed pre-gestational maternal obesity (PGMO). Cells were incubated without (-) or with (+) tunicamycin (5  $\mu$ M, 8 hours) and GSK2606114 (8 hours at the indicated concentrations) (see Methods). **A**, Representative western blot for eIF2 $\alpha$  phosphorylated, the total protein abundance and  $\beta$ -actin. The graph shows the densitometry for the total protein abundance of eIF2 $\alpha$  over  $\beta$ -actin. **B**, Densitometry for eIF2 $\alpha$  phosphorylated over total eIF2 $\alpha$ . The densitometry was normalized to 1 with data in control. Values are mean  $\pm$  S.E.M.  $P < 0.05$ . \* vs control. † vs TUDCA (n = 3).

**A****B**

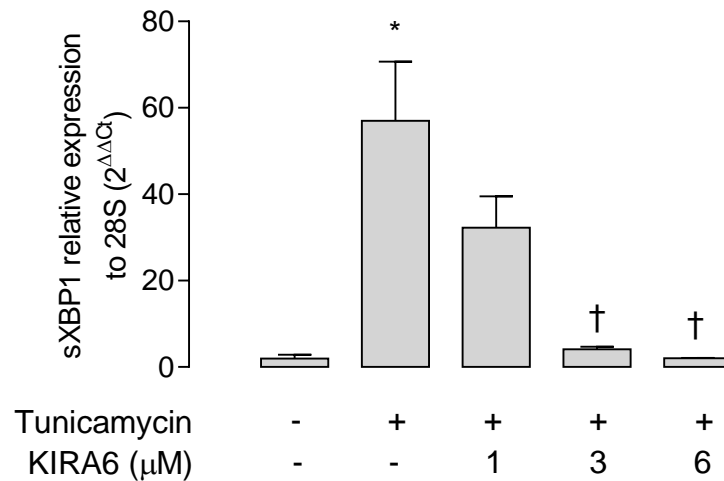
C



**Figure 49. Inhibition of IRE1 $\alpha$  by KIRA6.** The protein abundance and the phosphorylation of IRE1 $\alpha$  were evaluated in HUVECS from pregnancies where the mother showed pre-gestational maternal normal weight (PGMN). Cells were incubated without (-) or with (+) tunicamycin (5  $\mu$ M, 8 hours) and KIRA6 (8 hours at the indicated concentrations) (see Methods). **A**, Representative western blot for IRE1 $\alpha$  phosphorylated, the total protein abundance and  $\beta$ -actin. The graph shows the densitometry for the total protein abundance of IRE1 $\alpha$  over  $\beta$ -actin. **B**, Densitometry for IRE1 $\alpha$  phosphorylated over total IRE1 $\alpha$ . **C**, Inhibition curve of IRE1 $\alpha$  in cells treated with tunicamycin. The densitometry was normalized to 1 with data in control. Values are mean  $\pm$  S.E.M.  $P < 0.05$ . \* vs tunicamycin (n = 3).

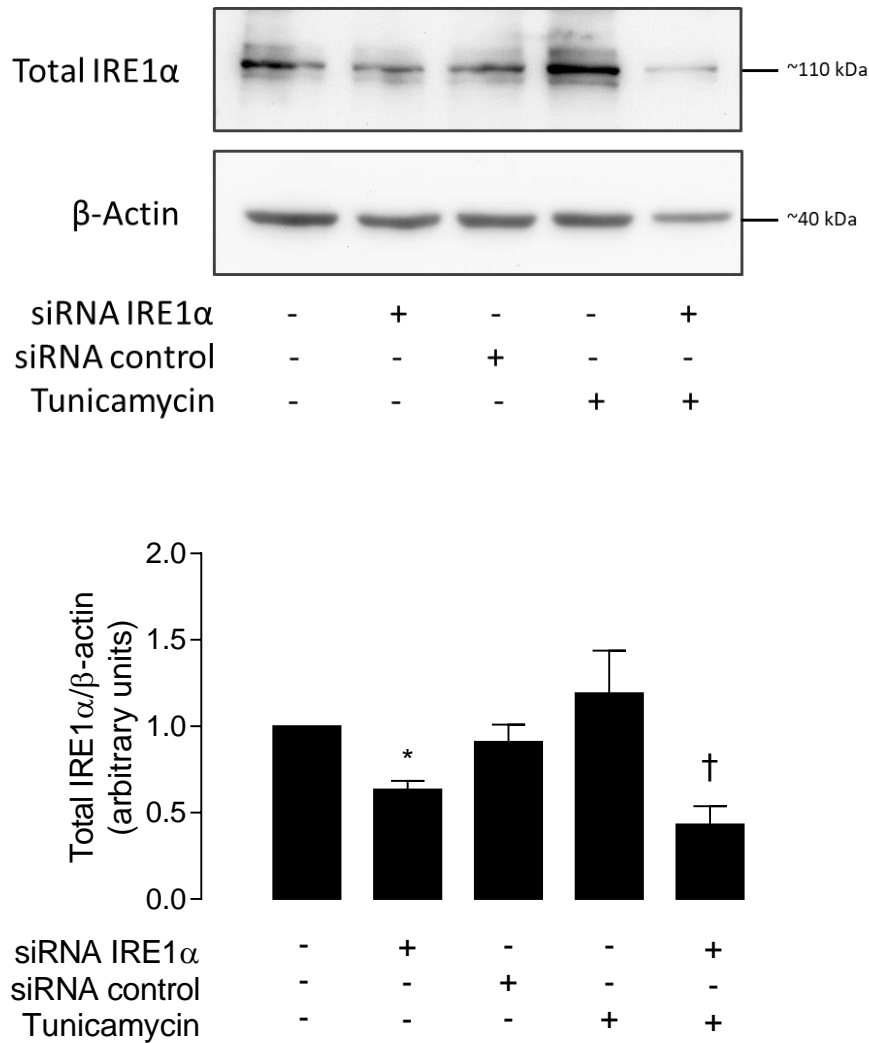
**A****B**

C

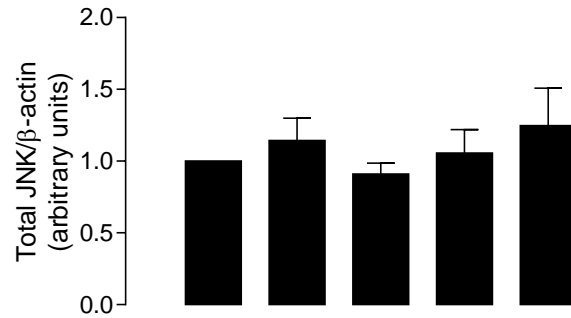
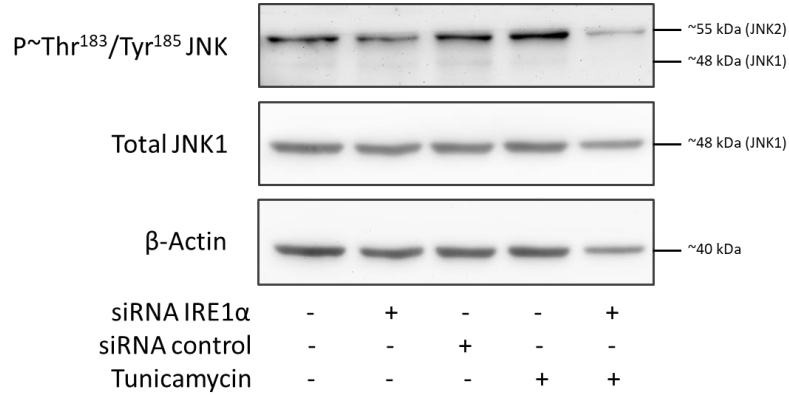
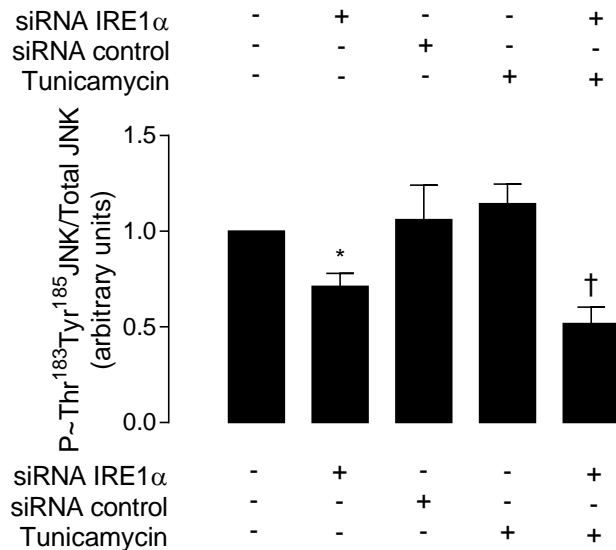


**Figure 50. IRE1 $\alpha$ -inhibition effect on JNK and XBP1 processing.** The protein abundance and the phosphorylation of JNK, and XBP1 mRNA levels, were evaluated in HUVECS from pregnancies where the mother showed pre-gestational maternal normal weight (PGMN). Cells were incubated without (-) or with (+) tunicamycin (5  $\mu$ M, 8 hours) and KIRA6 (8 hours at the indicated concentrations) (see Methods). **A**, Representative western blot for JNK phosphorylated, the total protein abundance and  $\beta$ -actin. The graph shows the densitometry for the total protein abundance of JNK over  $\beta$ -actin. **B**, Densitometry for JNK phosphorylated over total JNK. **C**, Relative abundance of XBP1s mRNA analyzed by the  $\Delta\Delta C_T$  method. The densitometry was normalized to 1 with data in control. Values are mean  $\pm$  S.E.M.  $P < 0.05$ . \* vs control, † vs tunicamycin (n = 3).

A



**Figure 51. Knockdown of IRE1α.** The protein abundance of IRE1α was evaluated by western blot in HUVECS from pregnancies where the mother showed pre-gestational maternal normal weight (PGMN) pre-treated (+) or not (-) with siRNA against IRE1α (According to the manufacturer indications) and tunicamycin (5 μM, 8 hours) (see Methods). The panel shows a representative western blot for the total protein abundance of IRE1α and β-actin. The graph shows the densitometry for the total protein abundance of IRE1α over β-actin. The densitometry was normalized to 1 with the data obtained in control. Values are mean ± S.E.M.  $P < 0.05$ . \* vs the basal condition- † vs tunicamycin. (n = 4).

**A****B**

**Figure 52. Effect of IRE1α Knockdown on the activation of JNK.** The protein abundance and phosphorylation of JNK were evaluated by western blot in HUVECS from pregnancies where the mother showed pre-gestational maternal normal weight (PGMN) pre-treated (+) or not (-) with siRNA against IRE1α (According to the manufacturer indications) and tunicamycin (5 μM, 8 hours) (see Methods). **A**, Representative western blot for the phosphorylation of JNK, the total protein abundance, and β-actin. The graph shows the densitometry for the total protein abundance of JNK over β-actin. **B**, Densitometry for JNK phosphorylated over total JNK. The densitometry was normalized to 1 with the data in control. Values are mean ± S.E.M.  $P < 0.05$ . \* vs the basal condition- † vs tunicamycin. (n = 4).

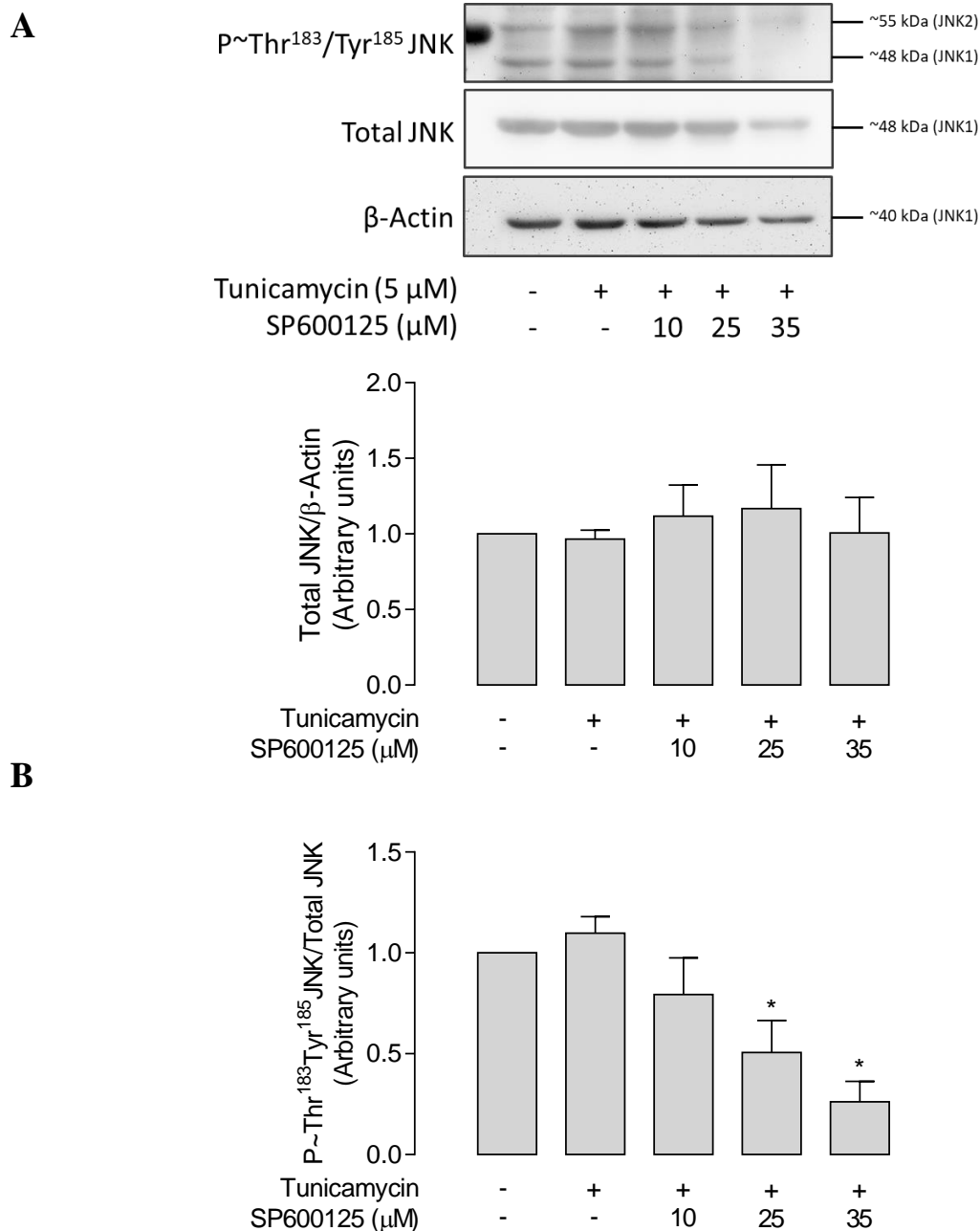


**Figure 53. Inhibition of JNK by SP600125.** The protein abundance and the phosphorylation of JNK were evaluated in HUVECS from pregnancies where the mother showed pre-gestational maternal normal weight (PGMN). Cells were incubated without (-) or with (+) tunicamycin (5  $\mu$ M, 8 hours) and SP600125 (8 hours at the indicated concentrations) (see Methods). **A**, Representative western blot for JNK phosphorylated, the total protein abundance and  $\beta$ -actin. The graph shows the densitometry for the total protein abundance of JNK over  $\beta$ -actin. **B**, Densitometry for JNK phosphorylated over total IRE1 $\alpha$ . The densitometry was normalized to 1 with data in control. Values are mean  $\pm$  S.E.M.  $P < 0.05$ . \* vs tunicamycin (n = 3).

#### 5.4.4 *PERK and IRE1 $\alpha$ involvement in the impairment of the insulin response*

##### *Insulin-induced NO generation*

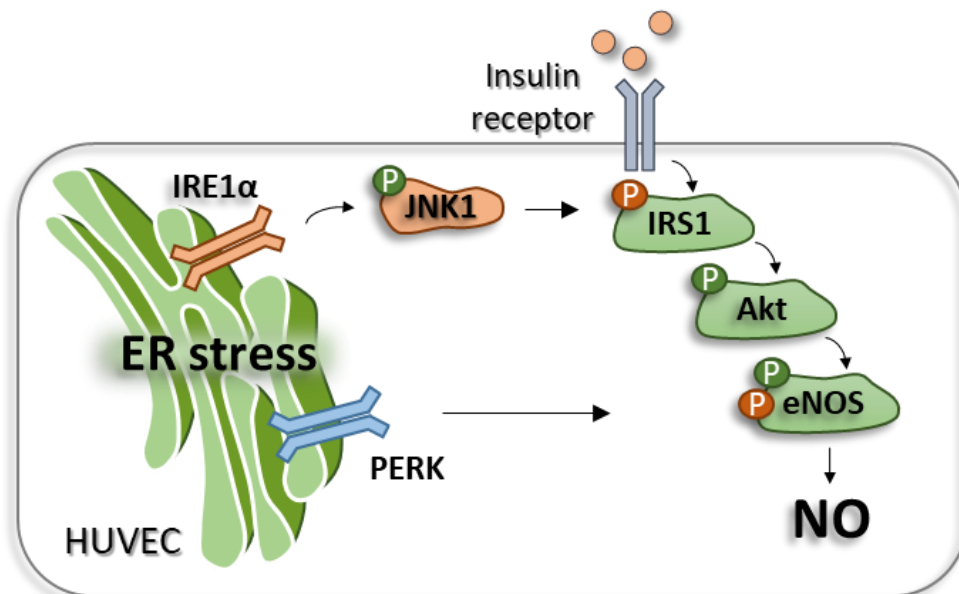
The participation of PERK and IRE1 $\alpha$  in the insulin response was evaluated by pharmacological inhibition of PERK and IRE1 $\alpha$ , and the knockdown of IRE1 $\alpha$  and their effects on the activation of key elements of the insulin signaling pathway, as represented in Scheme 6.

The inhibition of PERK with GSK2606414 did not generate changes either in the basal production of NO nor in response to insulin in HUVECs from PGMN and PGMO pregnancies (Figure 54A,B) (see Scheme 6). Furthermore, GSK2606414 did not prevent the tunicamycin-induced impairment of the NOS-dependent NO generation in HUVECs from PGMN. KIRA6 did not alter the NOS-dependent NO production in response to insulin in HUVECs from PGMN but this inhibitor prevented the impaired NO production caused by tunicamycin (Figure 55A). Furthermore, KIRA6 increased the NOS-dependent NO production in response to insulin in HUVECs from PGMO (Figure 55B). However, in the presence of tunicamycin, KIRA6 did not improve the insulin action in these cells. The co-incubation of GSK2606414 and KIRA6 showed a similar pattern than that presented by inhibition of IRE1 $\alpha$  (Figure 56).

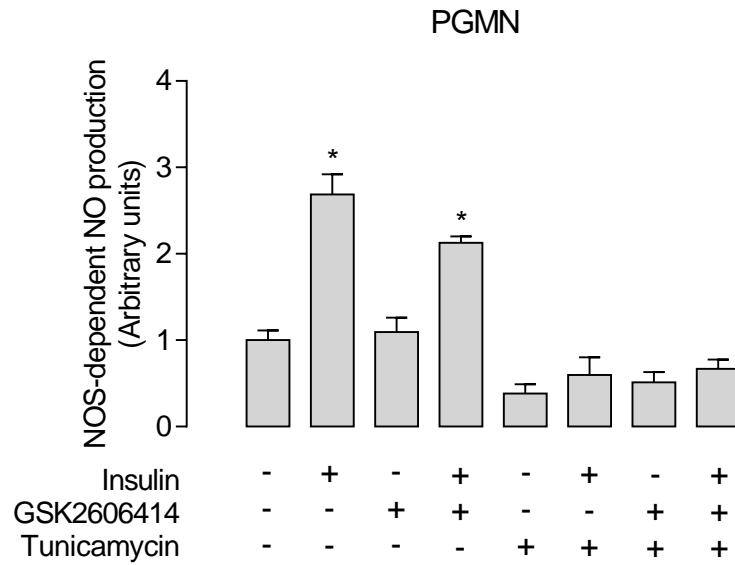
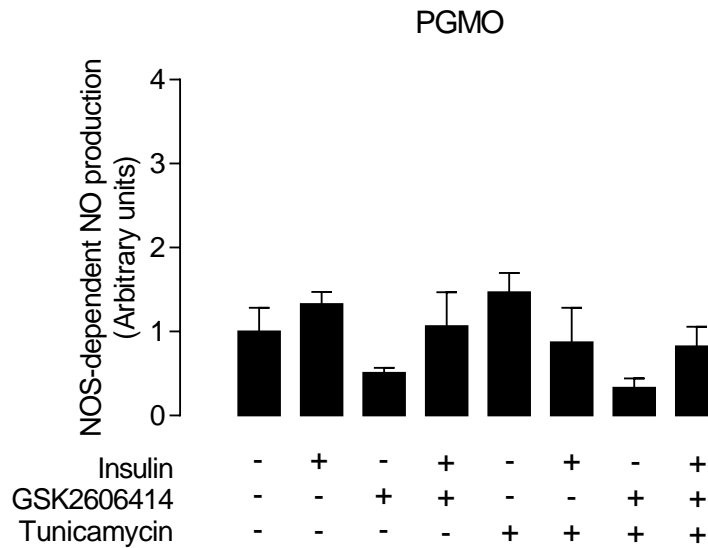
##### *Insulin signaling pathway*

The knockdown of IRE1 $\alpha$  reduced (~32%) the inhibiting phosphorylation of IRS1 in serine 307 in HUVECs from PGMO in comparison to the baseline condition, and decrease it (~53%) in knockdown cells treated with tunicamycin (Figure 57B). In addition, the inhibition of JNK reduced (~46%) the same phosphorylation in HUVECs from PGMN pregnancies treated with tunicamycin (Figure 58B). The knockdown and the inhibition of JNK did not

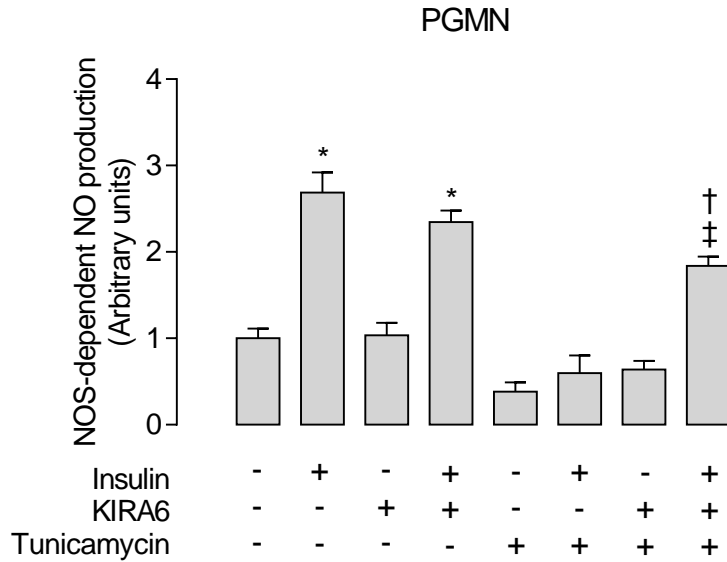
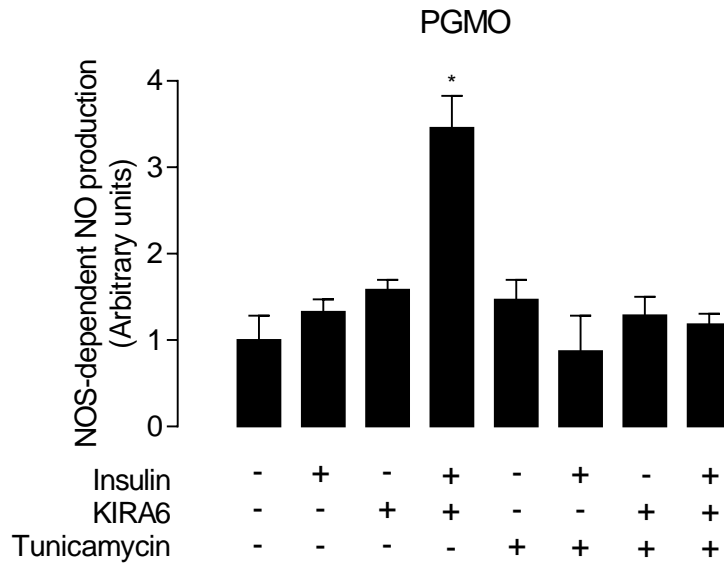
induce changes in the total protein abundance of IRS1 (Figure 57A, 58A). On the other hand, the inhibition of IRE1 $\alpha$ , but not PERK, caused insulin to increase (~2.4 fold) the activating phosphorylation of eNOS in HUVECs from PGMO pregnancies (Figure 59B). A similar effect was that presented by the activating phosphorylation of Akt, which increased (~3.0 fold) in response to insulin by the inhibition of IRE1 $\alpha$  but not PERK in cells from that condition (Figure 60B). The inhibition of both proteins did not generate significant changes in the total abundance of eNOS or Akt (Figure 59A, 60A).



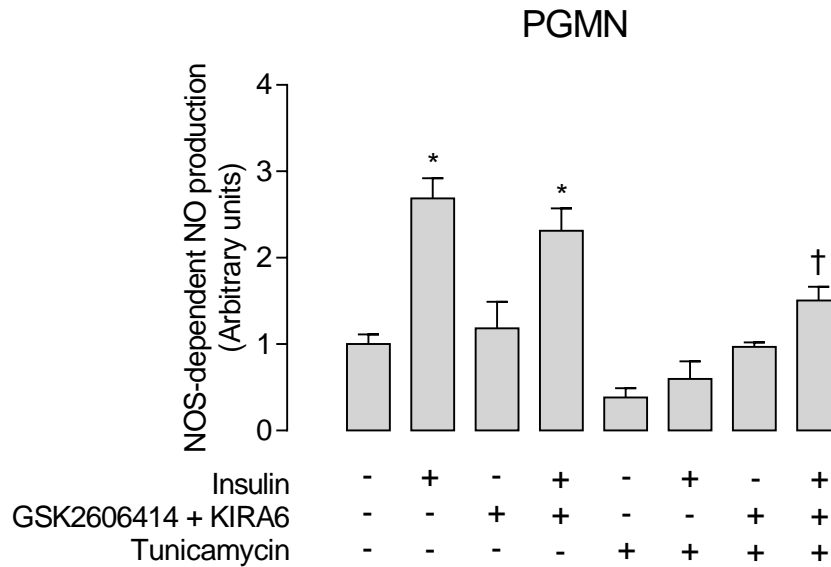
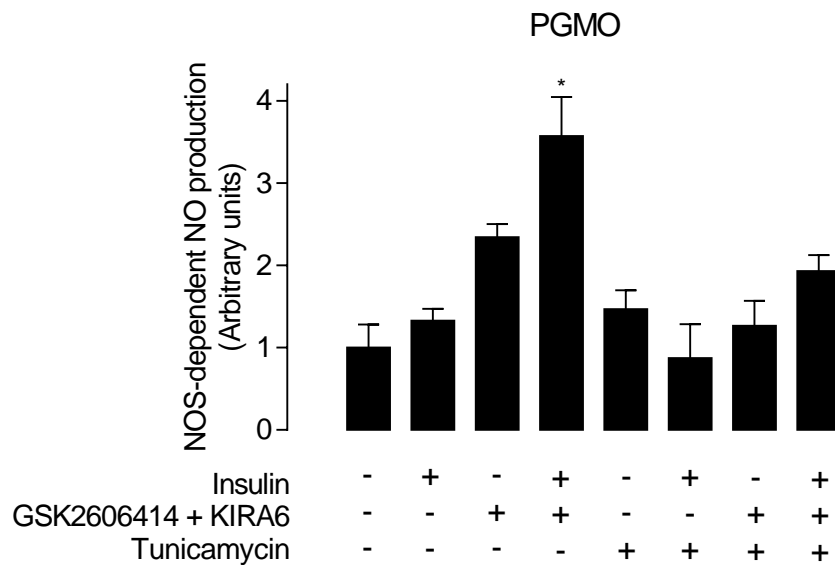
**Scheme 6. PERK and IRE1 $\alpha$  involvement in the insulin signaling pathway.** ER, endoplasmic reticulum; IRE1 $\alpha$ , Inositol-requiring enzyme 1 $\alpha$ ; JNK, c-jun N-terminal kinase 1; PERK, Protein kinase RNA-like endoplasmic reticulum kinase; IRS1, insulin receptor substrate 1; eNOS, endothelial nitric oxide synthase; P in green, activating phosphorylation; P in orange, inhibiting phosphorylation; NO, nitric oxide; HUVEC, human umbilical endothelial cell.

**A****B**

**Figure 54. PERK-inhibition effect on the NOS-dependent NO production in response to insulin.** HUVECs from pregnancies where the mother showed pre-gestational maternal normal weight (PGMN) (A) or pre-gestational maternal obesity (PGMO) (B) were incubated without (-) or with (+) GSK2606414 (3  $\mu$ M, 8 hours), tunicamycin (5  $\mu$ M, 8 hours), L-NAME (100  $\mu$ M, 30 minutes) and insulin (1nM) (see Methods). The NOS-dependent generation of NO was evaluated by fluorescence lecture after loading the cells with the probe DAF-FM (1 hour, 5  $\mu$ M) and subtracting the inhibitable fraction by L-NAME. Values are mean  $\pm$  S.E.M.  $P < 0.05$ . \* vs control. (n = 6 PGMN, 4 PGMO).

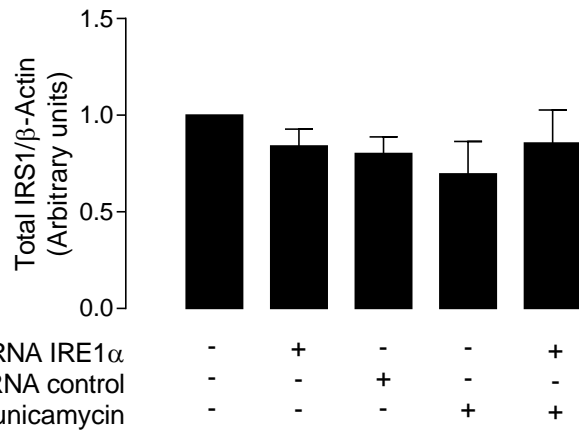
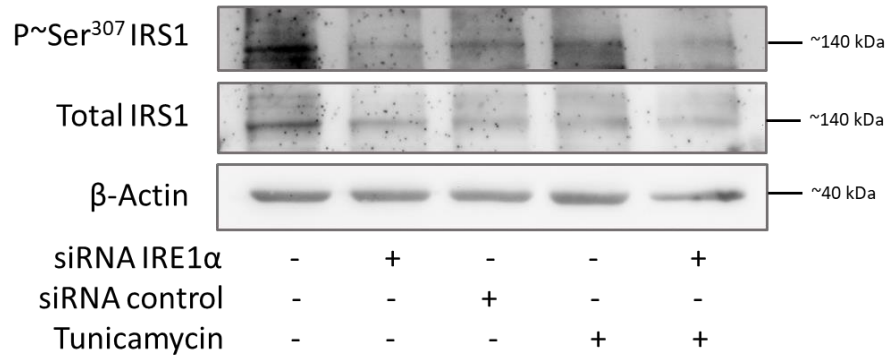
**A****B**

**Figure 55. Effect of IRE1 $\alpha$  inhibition on the NOS-dependent NO production in response to insulin.** HUVECs from pregnancies where the mother showed pre-gestational maternal normal weight (PGMN) (**A**) or pre-gestational maternal obesity (PGMO) (**B**) were incubated without (-) or with (+) KIRA6 (3  $\mu$ M, 8 hours), tunicamycin (5  $\mu$ M, 8 hours), L-NAME (100  $\mu$ M, 30 minutes) and insulin (1nM) (see Methods). The NOS-dependent generation of NO was evaluated by fluorescence lecture after loading the cells with the probe DAF-FM (1 hour, 5  $\mu$ M) and subtracting the inhibitable fraction by L-NAME. Values are mean  $\pm$  S.E.M.  $P < 0.05$ . \* vs control, † vs tunicamycin, ‡ vs tunicamycin plus KIRA6 (n = 6 PGMN, 4 PGMO).

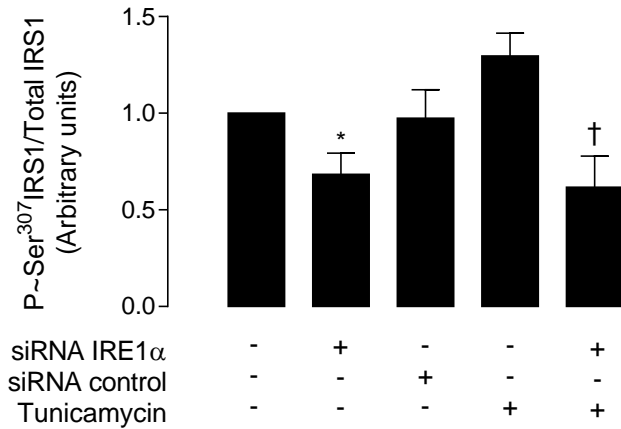
**A****B**

**Figure 56. Effect of IRE1 $\alpha$  inhibition on the NOS-dependent NO production in response to insulin.** HUVECs from pregnancies where the mother showed pre-gestational maternal normal weight (PGMN) (**A**) or pre-gestational maternal obesity (PGMO) (**B**) were incubated without (-) or with (+) a mixture of GSK2606414 plus KIRA6 (3  $\mu$ M each, 8 hours), and tunicamycin (5  $\mu$ M, 8 hours), L-NAME (100  $\mu$ M, 30 minutes) and insulin (1nM) (see Methods). The NOS-dependent generation of NO was evaluated by fluorescence lecture after loading the cells with the probe DAF-FM (1 hour, 5  $\mu$ M) and subtracting the inhibitable fraction by L-NAME. Values are mean  $\pm$  S.E.M.  $P < 0.05$ . \* vs control, † vs tunicamycin (n = 6 PGMN, 4 PGMO).

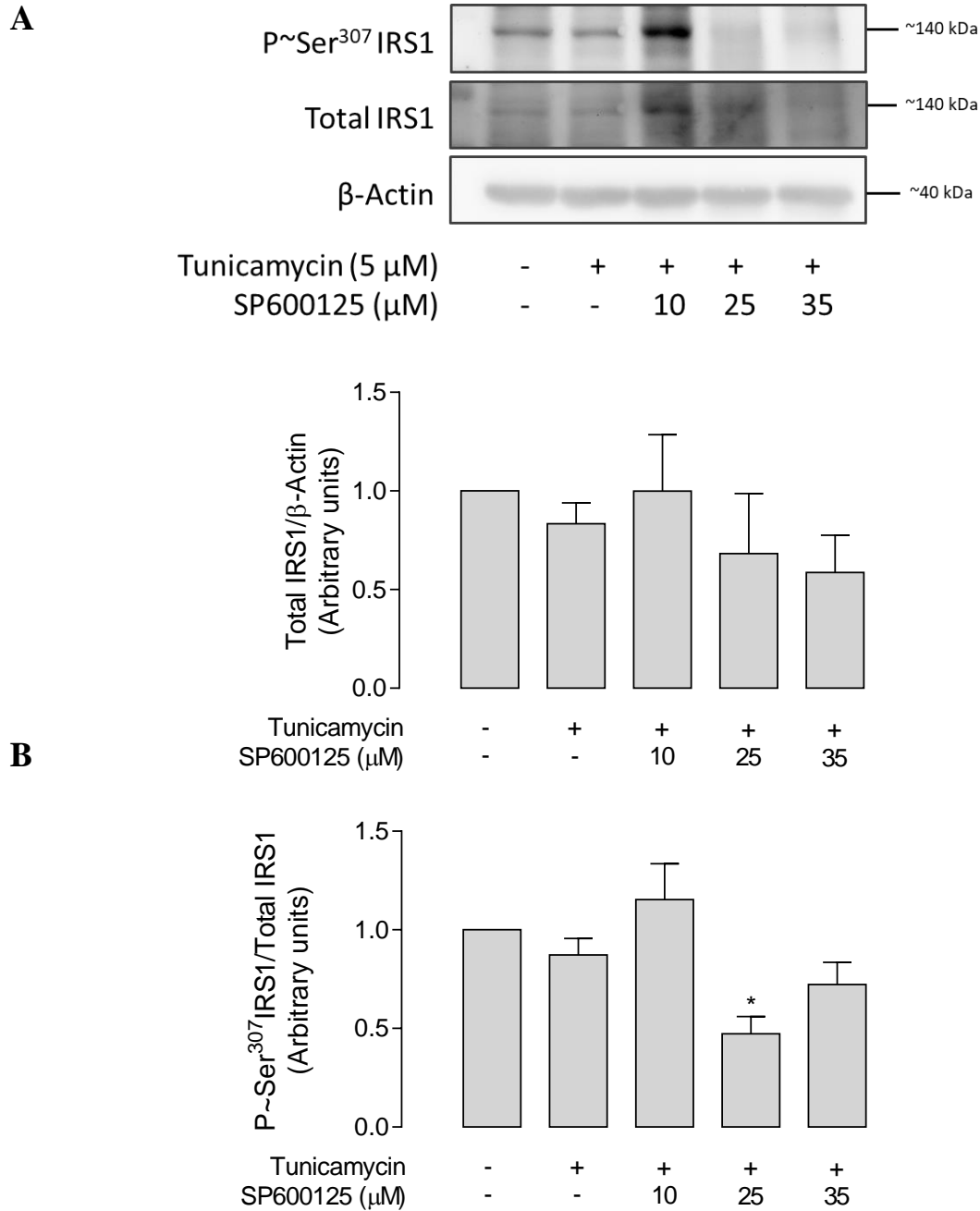
**A**



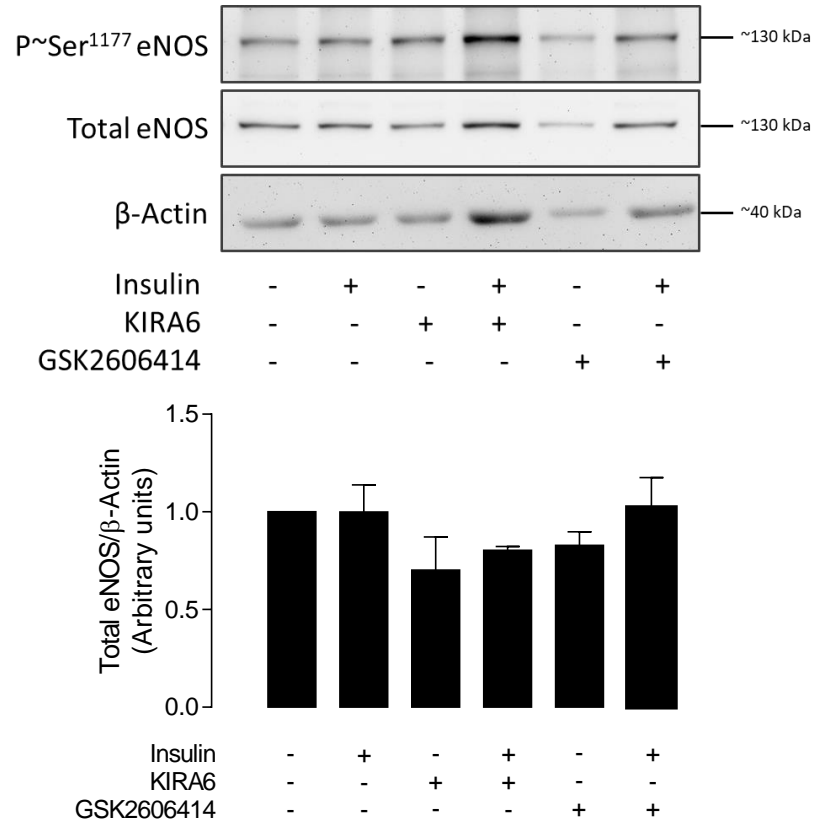
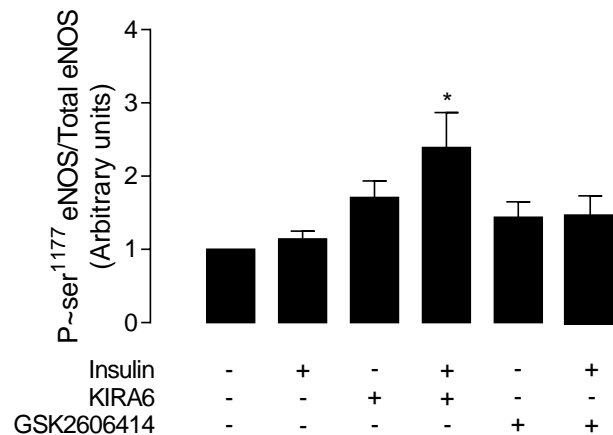
**B**



**Figure 57. Effect of IRE1α Knockdown on the activation of IRS1.** The protein abundance and phosphorylation of IRS1 were evaluated by western blot in HUVECS from pregnancies where the mother showed pre-gestational maternal normal weight (PGMN) pre-treated (+) or not (-) with siRNA against IRE1α (According to the manufacturer indications) and tunicamycin (5 μM, 8 hours) (see Methods). **A**, Representative western blot for the phosphorylation of IRS1, the total protein abundance, and β-actin. The graph shows the densitometry for the total protein abundance of IRS1 over β-actin. **B**, Densitometry for IRS1 phosphorylated over total IRS1. The densitometry was normalized to 1 with the data in control. Values are mean ± S.E.M. *P*<0.05. \* vs the basal condition- † vs tunicamycin. (n = 4).



**Figure 58. JNK-inhibition effect on the IRS1 activation state.** The protein abundance and the phosphorylation of IRS1 were evaluated in HUVECS from pregnancies where the mother showed pre-gestational maternal normal weight (PGMN). Cells were incubated without (-) or with (+) tunicamycin (5  $\mu$ M, 8 hours) and SP600125 (8 hours at the indicated concentrations) (see Methods). **A**, Representative western blot for IRS1 phosphorylated, the total protein abundance and  $\beta$ -actin. The graph shows the densitometry for the total protein abundance of IRS1 over  $\beta$ -actin. **B**, Densitometry for IRS1 phosphorylated over total IRS1. The densitometry was normalized to 1 with data in control. Values are mean  $\pm$  S.E.M.  $P < 0.05$ . \* vs tunicamycin (n = 3).

**A****B**

**Figure 59. IRE1 $\alpha$  involvement in the insulin-induced eNOS activation in HUVECs from PGMO.** The protein abundance and the activating and inhibiting phosphorylation of eNOS were evaluated in HUVECS from pregnancies where the mother showed pre-gestational maternal obesity (PGMO). Cells were incubated without (-) or with (+) KIRA6 (3  $\mu$ M, 8 hours), GSK260414 (3  $\mu$ M, 8 hours), and insulin (1 nM, 20 minutes) (see Methods). **A**, Representative western blot for the activating and inhibiting phosphorylation of eNOS, the total protein abundance and  $\beta$ -actin. The graph shows the densitometry for the total protein abundance of eNOS over  $\beta$ -actin. **B**, Densitometry for eNOS phosphorylated in serine 1177 over total eNOS. The densitometry was normalized to 1 with data in control. Values are mean  $\pm$  S.E.M.  $P < 0.05$ . \* vs control (n = 7).

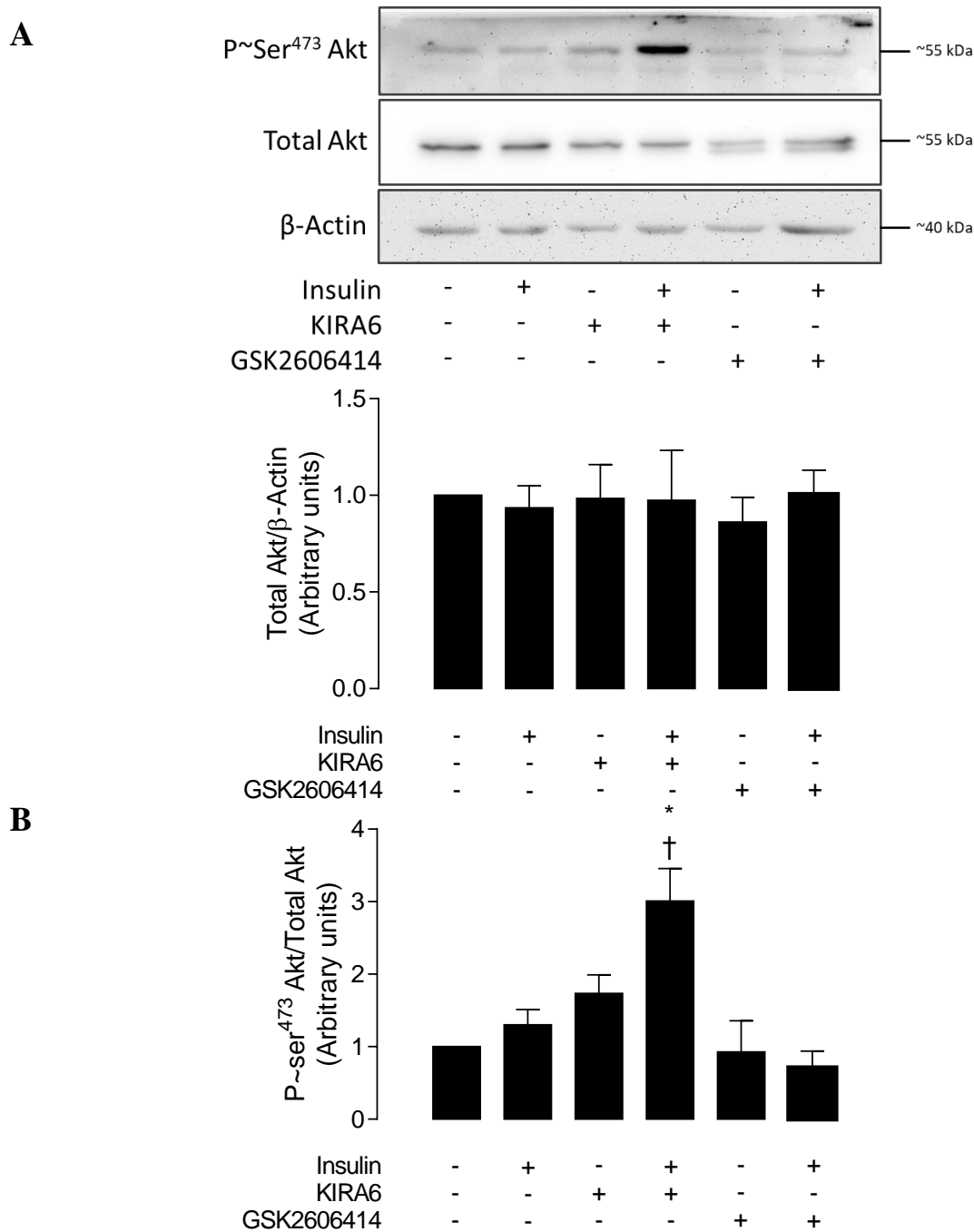


**Figure 60. IRE1 $\alpha$  involvement in the insulin-induced Akt activation in HUVECs from PGMO.** The protein abundance and the phosphorylation of Akt were evaluated in HUVECS from pregnancies where the mother showed pre-gestational maternal obesity (PGMO). Cells were incubated without (-) or with (+) KIRA6 (3  $\mu$ M, 8 hours), GSK260414 (3  $\mu$ M, 8 hours), and insulin (1 nM, 20 minutes) (see Methods). **A**, Representative western blot for Akt phosphorylated, the total protein abundance and  $\beta$ -actin. The graph shows the densitometry for the total protein abundance of Akt over  $\beta$ -actin. **B**, Densitometry for Akt phosphorylated over total Akt. The densitometry was normalized to 1 with data in control. Values are mean  $\pm$  S.E.M.  $P < 0.05$ . \* vs the control, † vs KIRA6 (n = 7).

## 6. Discussion

This thesis shows the occurrence of endothelial dysfunction and insulin resistance in the umbilical vein endothelium of PGMO mothers and how ER stress is involved in the development of both. The present findings evidence an abnormal response to insulin by umbilical veins from PGMO pregnancies, which was associated with reduced basal and insulin-induced NO generation in HUVECs. Further analysis showed a reduced basal and insulin-induced insulin signaling pathway and eNOS activation along with higher L-arginine transport. These results suggest a state of endothelial dysfunction and insulin desensitization in HUVECs that may explain the reduced vasodilation in umbilical vein rings from this condition. Furthermore, higher activation of key proteins of the UPR was found, evidencing the occurrence of ER stress in cells from PGMO. The treatment of PGMO cells with TUDCA, a chemical chaperone that reduces ER stress, reduced the PGMO-activated UPR markers evaluated. In addition, the treatment with TUDCA improved the basal generation of NO and activation state of eNOS, reduced the L-arginine transport and increased the insulin-induced activation of the insulin signaling pathway, eNOS and NO generation in HUVECs from PGMO pregnancies. Additionally, treatment with TUDCA reversed the PGMO-reduced insulin response in umbilical vein rings. Conversely, treatment with the ER stress inducer tunicamycin induced endothelial dysfunction and blocked the action of insulin in HUVECs and umbilical vein rings from PGMN pregnancies. On the other hand, the inhibition of IRE1 $\alpha$ , but not PERK, improved insulin-induced NO generation in HUVECs from PGMO and prevented the tunicamycin-induced blockade of the NO generation in response to insulin in HUVECs from PGMN pregnancies. Considering these findings altogether, and the fact that current literature shows the association of ER stress with endothelial dysfunction and

insulin resistance, the proposal of this thesis is that the pathological condition of PGMO induces ER stress in the human umbilical vein endothelium leading to endothelial dysfunction and insulin desensitization in the fetoplacental vasculature.

### **6.1 Pregestational maternal obesity**

Obesity is a worldwide epidemic that also affects pregnancy. The prevalence of women starting their pregnancy with obesity is increasing worldwide (WHO, 2018), reaching an estimated of 14.9 million obese pregnant women in 2014 (Chen et al., 2018). Countries with high and middle income showed the highest prevalence, which correlated with the income level, caloric supply, and urbanization. However, obesity is also increasing rapidly in areas with lower incomes, as in countries of central Africa, where the prevalence of women in childbearing age has doubled between 1991 and 2014 (Amugsi et al., 2017).

Obesity-associated complications during pregnancy include a higher risk to develop pregnancy hypertensive disorders, preeclampsia, GDM, cesarean delivery, fetal malformation, macrosomia, and fetal death (Fuchs et al., 2017; Shen et al., 2018; Yang et al., 2017), which are positively correlated with pregestational BMI (Fuchs et al., 2017; Stuebe et al., 2012). Also, PGMO is not only associated with pregnancy complications, but its consequences also affect the offspring's health later in life. The latter have a higher risk to develop obesity and metabolic syndrome in childhood and adulthood (Eriksson et al., 2015, 2014; Forsen et al., 1997; Gaillard et al., 2014; Godfrey et al., 2017; Hochner et al., 2012; Pirkola et al., 2010; Stuebe et al., 2009), and are associated with greater premature death while adults (Reynolds et al., 2013). Additionally, newborns born to PGMO mothers have shorter telomeres evidencing a lower biological age that could be associated with shorter life

expectancy (Martens et al., 2016). Thus, obesity during pregnancy is considered as a growing public health hazard for both the mother and the fetus.

According to the Institute of Medicine and the National Research Council (IOM and NRC, 2009), women that start their pregnancy with a normal BMI (BMI 18.5-24,9 kg/m<sup>2</sup>) should increase 11.5 to 16 kg of body weight during pregnancy, while those starting with obesity (BMI  $\geq$  30 kg/m<sup>2</sup>) should increase 5 to 9 kg. These ranges were established according to published literature at the time and considering a lower prevalence of the following factors: cesarean delivery, postpartum weight retention, preterm birth, small- or large-for-gestational-age birth, and childhood obesity. While IOM recommends a narrow range of GWG for PGMO mothers, they also emphasize that more studies should be performed to evaluate this interval, due to the little data available. As a matter of fact, potential cardiovascular effects induced by excessive GWG (eGWG) on the offspring were not considered. Additionally, since these guidelines were designed using data from people from North American, new studies considering ethnicity, geographical location, and demographic features are encouraged to establish adequate guidelines for other countries. Therefore, the use of these as a reference for Chilean population may not be the most appropriate. However, since there are no similar studies in Latin-American countries, this study considered the guidelines established by the IOM.

As predicted by the IOM, subsequent epidemiological studies have shown that eGWG is a risk factor for the development of cardiometabolic risk in the offspring of women starting pregnancy with normal BMI (Fraser et al., 2010; Yang et al., 2017). Nonetheless, there is not a clear consensus about whether eGWG exacerbates the problems induced by a PGMO state. Studies by Kaar and colleagues showed that in a group of 164 pre-pregnant overweight/obese

women the eGWG further increased cardiovascular risk induced by a pre-pregnancy overweight/obesity state on their children at the age of ~10 years old (Kaar et al., 2014). However, it is shown that independently of the GWG, a high pre-pregnancy BMI is enough to induce the worsening of long-term health in the offspring, and eGWG does not worsen that outcome in newborns (Hochner et al., 2012). Indeed, a recent meta-analysis performed with data from 162,129 women from 37 cohort studies from Australia, Europe, and North America, showed that eGWG in women with PGMO has not further effects on their offspring's overweight and obesity than that induced by only PGMO (Voerman et al., 2019). This apparent discrepancy with the findings reported by Kaar and colleagues could be explained by the fact that they did not discriminate between overweight and obese pregnant women; therefore, cardiovascular risk induced by eGWG in the descend in addition to that induced by BMI before pregnancy may demonstrate an effect of eGWG only in pre-pregnant overweight mothers rather than in PGMO mothers. Thus, unlike for the offspring from PGMN mothers, the PGMO-induced increase of cardiovascular risk on the offspring would predominate over the one induced by eGWG.

The present study included a group of PGMN women with an adequate GWG and a group of PGMO women where 46,2% had an eGWG. This finding is consistent with the fact that women with PGMO tend to have excessive gestational weight gain more frequently than PGMN women (IOM and NRC, 2009). Indeed, eGWG for North American population reached 55.8% in 2013 (Deputy et al., 2015) while in the studies used by IOM to elaborate the guidelines only one-third of the PGMO patients had a GWG within the ranges recommended by the IOM (IOM and NRC, 2009). As indicated above, because eGWG did not affect the cardiovascular risk in addition to that induced by the PGMO condition, the

results obtained in this study show evidence of the alterations induced only by PGMO that are unlikely to be affected by eGWG. However, a more in-depth study should be made in order to differentiate between PGMO with adequate GWG from those with eGWG.

The evaluation of the patient's data revealed a negative correlation between GWG and BMI in mothers with PGMN and PGMO, an association that has been reported in the literature (Fraser et al., 2010; IOM and NRC, 2009). On the other hand, most of the literature reported positive correlations between BMI and GWG of the mother and the weight and fat accumulation of the fetus (Catalano et al., 2009; Fraser et al., 2010; Stirrat and Reynolds, 2014). Despite the above, our study showed that birth weight and ponderal index were similar in fetuses from both conditions, and birth weight was not dependent on the pre-gestational BMI or GWG of the mother. The lack of effect of GWG on birthweight in PGMO is supported by a study performed in 4814 women with PGMO, which showed that GWG did not increase the percentage of large for gestational age newborns, even in those cases where women had a GWG over 20 kg (Nohr et al., 2008). Even though our findings showed neither a significant difference nor a tendency concerning the BMI, the small number of patients participating in this study could impede to observe a potential increase that may be more clearly evidenced with a higher number of patients.

Neonates from PGMO pregnancies showed higher umbilical vein blood levels of insulin and C-peptide, in agreement with the previously reported increase of these parameters in umbilical vein blood from PGMO mothers (Catalano et al., 2009). Furthermore, the increased C-peptide level associated with insulin resistance in preterm infants (Mitanchez-Mokhtari et al., 2004; Salis et al., 2017) along with higher umbilical blood C-peptide and insulin values suggest insulin desensitization in neonates from PGMO mothers. The latter is

supported by a ~10% reduction in the QUICKI (Katz et al., 2000) and a ~2.4 fold HOMA-IR increase (Matthews et al., 1985) in neonates born to PGMO mothers. Glycemia levels were similar in PGMO and PGMN umbilical vein blood. These findings suggest a potential state of insulin resistance in these individuals.

## **6.2 Insulin desensitization and endothelial dysfunction in fetoplacental vasculature**

Obesity is associated with endothelial dysfunction and vascular insulin resistance in the adult population (Janus et al., 2016; Prieto et al., 2014; Versari et al., 2009). It is also reported that pregnant women with PGMO present with endothelial dysfunction (Stewart et al., 2007). Endothelial dysfunction and insulin resistance are factors associated with the initiation, development, and perpetuation of cardiovascular pathologies (Breen and Giacca, 2011; Sandoo et al., 2015). Both conditions occur in the first steps that lead to cardiovascular disease, even decades before the clinical outcome (Davignon and Ganz, 2004). On the other hand, dysfunction of fetoplacental tissues is crucial in the fetal outcome, and its effects remain present for a lifetime in the offspring (Howell and Powell, 2017; Longtine and Nelson, 2011; Sobrevia et al., 2014). Therefore, the occurrence of endothelial dysfunction and insulin resistance in the fetoplacental vasculature from PGMO suggest a higher risk to develop cardiovascular disease later in life in the offspring.

Some studies suggest the occurrence of both phenomena in fetoplacental tissues or fetuses from PGMO mothers. Increased resistance to flow in the umbilical arteries from PGMO mothers was reported (Sarno et al., 2015), likely suggesting a state of endothelial dysfunction as an explanation for the vascular dysfunction. Additionally, insulin resistance in newborns (Catalano et al., 2009), a reduced response to insulin by trophoblastic cells (Lassance et al., 2015) and a transcriptome profile associated to insulin resistance in

umbilical cords (Thakali et al., 2014) has been reported. Thus, the available evidence suggests a probable state of endothelial dysfunction and insulin resistance in fetoplacental tissues from PGMO.

#### *6.2.1 PGMO effect on umbilical vein reactivity*

Null insulin-induced vasodilation in umbilical veins from PGMO compared with the response in vessels from PGMN pregnancies was observed in this study. These findings show that PGMO reduces insulin sensitivity in the fetal vasculature *ex vivo*. It is worth noting that similar results were obtained by Pardo and colleagues in a group of women that started pregnancy with normal BMI but had eGWG, reaching obesity at the third trimester (Pardo et al., 2015). Thus, eGWG, obesity in the third trimester, or a combination of both conditions may be enough to elicit a similar vascular dysfunction in the umbilical vein to that seen in the umbilical vein from women with PGMO.

Vasodilation induced by insulin is dependent on NO production by eNOS in the endothelium (Muniyappa et al., 2007). In this regard, L-NAME, a NOS inhibitor, blocked the insulin-induced vasodilation in umbilical veins from PGMN pregnancies. The results also showed that NOS activity is required for insulin-induced vasodilation in umbilical veins from PGMN. However, L-NAME did not change the response of umbilical vein rings to insulin in PGMO. These results suggest that the lack of response to insulin could be due to a reduced production of NO, which is characteristic of endothelial dysfunction (Tousoulis et al., 2012; Yuyun et al., 2018).

To further support the occurrence of endothelial dysfunction in the umbilical vein vessels, the endothelium-dependent vasodilator CGRP was assayed. CGRP's vasodilator effect is dependent on NOS activity (Brain, 2004; Dong et al., 2004). As expected, umbilical veins

from PGMO were insensitive to CGRP. However, vessels from PGMN dilated in response to CGRP, agreeing with similar findings in chorionic arteries from mothers with pre-pregnancy overweight and PGMO (Schneider et al., 2015). Similar to what was observed with insulin, the inhibition of NOS activity by L-NAME blocked the CGRP-induced vasodilation in vessels from PGMN showing that the effect of CGRP also depends on NOS activity in umbilical veins. Additionally, vascular response to SNP (spontaneous NO donor) remained intact in vessels from PGMN and PGMO, suggesting that the lack of effect of insulin and CGRP in PGMO might be due to an inadequate response of the vascular endothelium rather than a lack of response from the vascular smooth muscle. Altogether these findings suggest a significant role played by NOS activity in the insulin and CGRP response and evidence the likely occurrence of endothelial dysfunction in umbilical veins from PGMO. The latter is a phenomenon that might be involved in insulin desensitization of the human placental vasculature in this maternal metabolic alteration in pregnancy.

Because vascular reactivity in response to agonists depends on the initial conditions in which the vessel was set, it was necessary to define a common basal condition for the vessels studied. The vessels were normalized at the point where they generated the maximum active tension in response to KCl as described (Lew and McPherson, 1996). The procedure required stretching the vessel to the point where the myosin and actin fibers are in such a superposition that they reach their highest possible interaction, which was evidenced by the generation of the maximum contraction induced by KCl. The maximum contraction point is defined as the ideal baseline stretch or optimal diameter (Lew and McPherson, 1996). The stretch needed to reach the optimal diameter depends on the caliber of each vessel. Additionally, it is described that basal physiological tension of blood vessels in the organism

is closer to the optimal length (Burkholder and Lieber, 2001; Winters et al., 2011). Therefore, this parameter allows inferring differences in the diameter of each vessel under physiological conditions. The results in this study show that vessels from PGMO mothers required greater stretch than those from PGMN pregnancies, suggesting that the caliber of umbilical veins may be higher in PGMO than in those from PGMN pregnancies. On the other hand, the stretch-induced by KCl was lower in the PGMO vessels, which may suggest a lower number of smooth muscle cells (Lew and McPherson, 1996; Mulvany and Halpern, 1977) or a higher baseline precontraction state in those vessels. Since endothelial dysfunction is associated with vasoconstriction (De Artinano and Gonzalez, 1999), the last explanation is in line with the occurrence of endothelial dysfunction. Therefore, the lower vasoconstriction induced by KCl may suggest a state of endothelial dysfunction in umbilical veins from PGMO mothers.

#### *6.2.2 PGMO effect on endothelial function and insulin response in HUVECs*

In line with the endothelial dysfunction suggested by the results obtained with myography assays, primary cultures of HUVECs from PGMO showed lower basal NO production compared with HUVECs from PGMN pregnancies. These results suggest a state of endothelial dysfunction and may explain the lack of response to the vasodilatory factors insulin and CGRP in human umbilical vein rings with intact endothelium. Besides, insulin only increased NO generation in HUVECs from PGMN but not in PGMO cells. To further validate these findings, the activation state of eNOS was evaluated. Two main phosphorylation sites regulate the activity of eNOS, i.e. serine 1177, which activates eNOS, and threonine 495, which inhibits eNOS (Fleming, 2010). The results showed that in the absence of insulin HUVECs from PGMO showed lower levels of serine 1177 phosphorylation and higher levels of threonine 495 compared with cells from PGMN. Insulin

did not change the level of both phosphorylation sites in cells from PGMO. Thus, the reduced bioavailability of NO may be due to lower basal activity of eNOS and a reduced capacity of insulin to activate this enzyme. These results agree with those reported in HUVECs from PGMN mothers with eGWG where a reduced NO synthesis as well as reduced level of serine 1177 phosphorylation and a higher level of threonine 495 phosphorylation was reported (Pardo et al., 2015).

### 6.2.3 PGMO effect on L-arginine transport in HUVECs

The activity of eNOS is tightly dependent on L-arginine transport from the extracellular medium, even when the intracellular concentrations of L-arginine exceed the  $K_m$  of the enzyme for this amino acid. This apparent discrepancy is known as the ‘L-arginine paradox’ (Hardy and May, 2002), and the most acceptable explanation for this is the hypothesis of L-arginine compartmentalization (Casanello et al., 2007; Closs et al., 2004; Cynober, 2002), where eNOS would use the L-arginine taken up by hCAT and that contained in caveolae. L-arginine transport is mainly mediated by hCAT-1 and hCAT-2, but preferentially hCAT-1-mediated L-arginine transport has been associated with NO production by eNOS (García-Cardena et al., 1996; McDonald et al., 1997). Both proteins colocalized in caveolae and showed a direct structural interaction between them, which results in the activation of eNOS (Li et al., 2005). Thus, hCAT-1-mediated L-arginine transport is crucial to maintain a healthy endothelial function. Therefore, it is another characteristic that is altered in a state of endothelial dysfunction. The results showed that HUVECs from PGMO exhibit higher L-arginine transport than HUVECs from PGMN. The  $K_m$  values were in the range of hCAT-1  $K_m$  and the hCAT-1 expression was increased in these cells. Thus, it is likely that the increased L-arginine transport is due to a higher

availability of hCAT-1 in the cells from this condition. However, despite the increased L-arginine transport, NO production was lower. Therefore, it seems that the apparent compensation for the increase of the substrate is not sufficient to counteract the state of inactivation of eNOS. Interestingly, this phenomenon may be preventing higher damage in HUVECs from PGMO pregnancies. Other studies showed that higher extracellular concentrations of L-arginine associated with reduced plasma NOx in patients with obesity, a phenomenon proposed to result from lower L-arginine transport (Gruber et al., 2008; Sledzinski et al., 2010). Indeed, reduced CAT-1-mediated L-arginine transport in the endothelium of obese mice is also reported (Rajapakse et al., 2015, 2014). However, there is no information addressing this phenomenon in the endothelium of obese subjects nor the fetal endothelium from PGMO women. Besides, L-arginine plasma concentrations depend more on the diet, protein breakdown and hepatic metabolism than the endothelial L-arginine use (Luiking and Deutz, 2007). Thus, a higher L-arginine concentration may be reflecting other metabolic alterations and not necessarily changes in L-arginine transport, such as ER stress (Kilberg et al., 2009).

eNOS competes for the L-arginine substrate with arginases (Fleming, 2010; Prieto et al., 2011). Arginases metabolize L-arginine into urea and L-ornithine. Interestingly, endothelial dysfunction associated with higher abundance and activity of the arginases, resulting in taking away the substrate from eNOS and thus contributing to the reduced NO availability (Fleming, 2010; Prieto et al., 2011). Other pathologies of pregnancy presenting endothelial dysfunction in fetoplacental tissues, such as preeclampsia (Sankaralingam et al., 2010), maternal hypercholesterolemia (Leiva et al., 2013) or IUGR (Prieto et al., 2011), are shown to present increased arginases activity. In this regard, the results of this study show

that arginase activity was higher in HUVECs from PGMO, a phenomenon that may result in the higher metabolism of L-arginine available as the result of an increased transport via hCAT in these cells.

#### *6.2.4 PGMO effect on the insulin signaling pathway in HUVECs*

Insulin exerts a vasodilatory effect through the activation of the IR at the endothelium and the subsequent activation of the metabolic pathway (Muniyappa and Quon, 2007). Insulin binding to IR causes phosphorylation of IRS1 in tyrosine residues and downstream activation of Akt. Activation of Akt increases eNOS phosphorylation in serine 1177 leading to increased NO production and, ultimately, to vasodilation (Manrique et al., 2014; Muniyappa et al., 2007). Thus, insulin resistance in metabolic tissues as well as in the vasculature may occur by alterations in the metabolic pathway downstream of IR activation. This phenomenon is mainly modulated by inhibiting IRS1 phosphorylation on serine residues leading to reduced activation of the IR/PIK3/Akt pathway (Muniyappa and Sowers, 2013). In this regard, our results showed higher inhibiting phosphorylation of IRS1 in serine 307 in HUVECs from PGMO, suggesting an impairment of the metabolic pathway at the beginning of this insulin signaling branch. Also, the activating phosphorylation of Akt was reduced in basal conditions and in response to insulin, suggesting a reduced activation of this metabolic pathway in HUVECs from this condition. However, since Akt is also a target for other proteins (Hemmings and Restuccia, 2012), the reduction of Akt activation state could be affected by other inhibiting mechanisms. The impairment of the metabolic insulin signaling pathway seen in this study supports findings reporting an association between a gene expression profile with insulin resistance in umbilical cords from PGMO mothers by a higher expression of proinflammatory cytokines and reduced expression of PDK1 (Thakali et al.,

2014). The PDK1 is a kinase that activates Akt leading to increased activity of the IR/PI3K/Akt signaling pathway. Also, insulin changed the transcriptome of trophoblast cells from the first trimester of pregnancy in a lower proportion in cells from PGMO compared with PGMN pregnancies, a phenomenon likely resulting from insulin resistance in these cells (Lassance et al., 2015). Thus, evidence reported in the literature and the results obtained in this study show that, along with an endothelial dysfunction state, the fetoplacental endothelium from mothers with PGMO shows an impaired basal insulin signaling and response to this hormone which could explain the reduced insulin-induced vasodilation seen in the umbilical veins from this condition.

### **6.3 Endoplasmic reticulum stress in HUVECs from PGMO pregnancies**

ER stress is proposed as one of the causes of obesity-associated endothelial dysfunction and insulin resistance in metabolic tissues (Flamment et al., 2012; Lenna et al., 2014). Obese subjects show increased activity of UPR proteins in the liver, adipose tissue, skeletal muscle, and endothelial cells (Flamment et al., 2012; Villalobos-Labra et al., 2018b). Interestingly, the skeletal muscle from PGMO mothers showed increased activation of UPR proteins (Liong and Lappas, 2016). Also, women with PGMO show placentas with higher JNK activation (Saben et al., 2013) and elevated markers of inflammation (Saben et al., 2014, 2013), alterations that are described as closely related to the activation of UPR (Garg et al., 2012). Thus, altogether, this information suggests that pregnant mothers with obesity may present with ER stress in the fetoplacental tissues. The findings obtained in this study showed activation of the three canonical pathways of UPR in HUVECs from PGMO pregnancies, i.e., PERK, IRE1 $\alpha$ , and ATF6; supporting the presence of ER stress in the fetoplacental endothelium.

### *6.3.1 PERK signaling branch in HUVECs from PGMO pregnancies*

Activation of the three canonical pathways of UPR in HUVECs from PGMO pregnancies, i.e. PERK, IRE1 $\alpha$ , and ATF6, were found in this study. These findings support the presence of ER stress in the fetoplacental endothelium in pregnancies where the mother was with PGMO. PERK activation leads to the phosphorylation of the  $\alpha$  subunit of eIF2, causing its inactivation and leading to the overall attenuation of the cap-dependent protein translation. This selective inhibition of translation leads to the expression of specific proteins such as ATF4, which is a crucial transcription factor of the PERK-induced response. ATF4 induces the expression of CHOP, transcription factor involved in the triggering of ER-stress induced apoptosis and inflammation (Nishitoh, 2012) and that in association with ATF4, induces the expression of TRB3 (Ohoka et al., 2005). TRB3 plays a major role in the context of insulin resistance since it is a pseudokinase that prevents the activation of Akt (Du et al., 2003). Thus, ATF4 is proposed to disrupt the insulin signaling pathway and elicit insulin resistance.

TRB3 is linked to obesity-induction of insulin resistance in metabolic tissues such as liver, skeletal muscle, and adipose (Koh et al., 2013; Liu et al., 2010; Marinho et al., 2015; Prudente et al., 2012). Thus, TRB3 is a key protein linking ER stress and insulin resistance through the activation of PERK branch signaling (Cnop et al., 2012; Flamment et al., 2012). However, whether PERK signaling and TRB3 expression were increased in the fetoplacental endothelium from PGMO mothers is unknown. The results of this study showed that the HUVECs from PGMO pregnancies exhibit higher phosphorylation of PERK, eIF2 $\alpha$ , and the expression of CHOP and TRB3. These results support a higher activity of the PERK signaling branch in these cells. Also, a reduction of ER stress with TUDCA resulted in lowering all the

PGMO-induced changes supporting the involvement of ER stress in the activation of this signaling branch in PGMO cells. Since TRB3 involvement in the induction of insulin resistance, the greater TRB3 expression can be associated with reduced activity of the insulin signaling pathway in the cells from PGMO.

### *6.3.2 IRE1 $\alpha$ signaling branch in HUVECs from PGMO pregnancies*

IRE1 $\alpha$  is one of the most conserved UPR signaling branches (Dufey et al., 2014). It is activated by homodimerization-induced trans-autophosphorylation after being detached from BiP, which leads to its kinase and endoribonuclease activity at the cytosolic side. The domain with endoribonuclease activity catalyzes the unconventional splicing of XBP1 mRNA, which encodes a transcription factor called XBP1s. XBP1s function ameliorates the ER stress and associated with improving metabolic alterations induced by obesity in animal models (Cnop et al., 2012; Flamment et al., 2012; Jiang et al., 2015). On the other hand, the XBP1 kinase domain binds the adapter protein TRAF2, promoting the activation of other pathways, including JNK. The activation of the JNK signaling pathway leads to the expression of proinflammatory cytokines, apoptosis, and links to the impairment of the insulin signaling pathway (Flamment et al., 2012).

The results found in this study showed higher IRE1 $\alpha$  protein abundance in HUVECs from PGMO pregnancies, with no changes in the phosphorylation state of this protein. Despite the finding that the percentage of activated protein is unaltered in these cells, a greater abundance will result in a higher volume of activated protein, eventually leading to greater activation of the IRE1 $\alpha$ -mediated signaling pathway. Interestingly, the activating phosphorylation of JNK was higher in HUVECs from PGMO, a finding agreeing with the increased activity of this kinase reported in placentas (Saben et al., 2013) and the higher pro-

inflammatory state of fetoplacental tissues from PGMO women (Saben et al., 2014, 2013; Thakali et al., 2014). The induction of ER stress with tunicamycin increased IRE1 $\alpha$  total protein abundance and JNK phosphorylation in HUVECs PGMN, and the inhibition of IRE1 $\alpha$  prevented the tunicamycin-induced increase of JNK phosphorylation. These findings agree with the higher JNK activation shown to depend on IRE1 $\alpha$  activity (Ozcan et al., 2004). Besides, the lower ER stress caused by TUDCA reduced IRE1 $\alpha$  total protein abundance and JNK phosphorylation in HUVECs from PGMO. Thus, increased activity of IRE1 $\alpha$ /JNK signaling branch in HUVECs from PGMO pregnancies is likely.

Interestingly, the alternative splicing of XBP1 was unaltered in HUVECs from PGMO, but tunicamycin-induced ER stress resulted in higher processing at similar levels in HUVECs from PGMN and PGMO pregnancies. The higher JNK activation and unaltered XBP1 mRNA splicing suggest a higher IRE1 $\alpha$  kinase but not endonuclease activity in PGMO cells. The latter is plausible since IRE1 $\alpha$ /JNK activity is activated independently of the endoribonuclease activity of IRE1 $\alpha$  (Dufey et al., 2014). Indeed, XBP1s protein inhibits IRE1 $\alpha$ /JNK branch activity (Ozcan et al., 2004). Furthermore, the results agree with the increased activity of UPR proteins in the liver of ob/ob mice (HFD mice model) at 7, 12 and 16 week-old relative to lean controls (Yang et al., 2015). However, although an increase was observed in the first weeks, and despite a sustained activation of IRE1 $\alpha$  and JNK, the alternative splicing of XBP1 was gradually reduced, being even lower than in lean mice. Thus, it seems that in a chronic state of obesity the kinase activity of IRE1 $\alpha$  is maintained and likely enhanced by lower endoribonuclease activity.

XBP1 is involved in the resolution of ER stress and protects from the deleterious effects of ER stress on insulin desensitization (Jiang et al., 2015; Ozcan et al., 2004). Thus,

the reduced splicing of XBP1 despite the increased IRE1 $\alpha$  activity may contribute to the insulin resistance seen in HUVECs from PGMO pregnancies. The translocation mechanism of sXBP1 to the nucleus requires the disruption induced by insulin of the heterodimerization of the regulatory subunits of PI3K p85 $\alpha$  and p85 $\beta$ . The resulting monomers of p85 interact with sXBP1 promoting its translocation to the nucleus (Park et al., 2010). Reduced interaction between p85 subunits and sXBP1 and sXBP1 translocation to the nucleus was detected in the liver of ob/ob mice, which was restored by the overexpression of p85 $\alpha$  and p85 $\beta$  (Park et al., 2010). Thus, the insulin desensitization seen in HUVECs from PGMO could contribute to a reduction in the IRE1 $\alpha$ /XBP1 mediated effects exacerbating the ER stress and the impairment of the insulin signaling in these cells.

### *6.3.3 ATF6 activation in HUVECs from PGMO*

After BiP is displaced to interact with misfolded luminal proteins, ATF6 translocates from the ER membrane to the Golgi where it is cleaved by intramembrane proteolysis. The cleaved-off cytoplasmic domain acts as a transcriptional activator for several genes encoding ER chaperones, ERAD proteins, and protein foldases (Flamment et al., 2012), aimed to prevent ER stress-associated damage. ATF6 interacts with IRE1 $\alpha$  activity by binding directly to the promoter of XBP1 gene enhancing its expression (Guo et al., 2014), and it is associated with regulation of the PERK signaling branch (Yan et al., 2002). Thus, ATF6 acts as a regulator of PERK and IRE1 $\alpha$  resulting in a protective effect against ER stress (Wu et al., 2007). Studies in animal models of obesity showed that ATF6 is activated in target metabolic tissues (Flamment et al., 2012; Villalobos-Labra et al., 2018b), but in patients with obesity ATF6 activation has only been studied in the liver (Kumashiro et al., 2011) and endothelial cells (Kaplon et al., 2013). The findings obtained in this study showed higher activation of

ATF6 by increased nuclear localization in HUVECs from PGMO pregnancies. The PGMO-induced nuclear localization of ATF6 was reduced after the treatment with the chemical chaperone TUDCA, showing that ATF6 activation was due to the occurrence of ER stress in these cells. Besides, together with the activation of PERK and IRE1 $\alpha$ , the activation of ATF6 suggests that HUVECs from mother with PGMO present ER stress, activating the three canonical pathways of the UPR in HUVECs.

On the other hand, ATF6 is reported to have a beneficial effect against insulin resistance in the liver in the context of obesity. Lower expression of ATF6 is reported in the liver from obese subjects with insulin resistance compared with non-insulin resistant subjects (Kumashiro et al., 2011). Also, the overexpression of ATF6 in the liver of db/db and diet-induced obesity (DIO) mice protected from obesity-induced hyperglycemia; and conversely, ATF6 knockdown induced hyperglycemia (Wang et al., 2009), which is the result of systemic insulin resistance (Martyn et al., 2009). The ATF6-associated improvement of insulin sensitivity in the liver may result from inhibition of PERK branch caused by ATF6 in hepatocytes leading to lower TRB3 expression (Yan et al., 2002) and subsequent increase in the insulin response (Ozcan et al., 2013). Indeed, the overexpression of ATF6 in the liver of obese mice inhibited the PERK/TRB3 branch and protected the mice from obesity-induced insulin resistance not only in the liver but also at a systemic level (Ozcan et al., 2016). All these studies suggest an ATF6 protecting role of the obesity-associated insulin resistance. Thus, the increased activity of ATF6 could prevent a major alteration in the insulin response in HUVECs from PGMO mothers. However, whether ATF6 crosstalk with PERK signaling occurs and whether this mechanism improves insulin signaling pathway in the endothelium of the human placenta is still unknown.

## 6.4 PGMO-associated ER stress and endothelial dysfunction

Several studies show endothelial dysfunction as a result of ER stress in different vascular beds including the aorta (Cheang et al., 2015, 2014; Murugan et al., 2015), heart (Galán et al., 2014; Kassan et al., 2012), lung (Shah et al., 2017), mesenteric vessels (Hong et al., 2018) or HUVECs (Murugan et al., 2015). Also, murine models of obesity suggest a link between obesity-associated ER stress and the induction of endothelial dysfunction (Cheang et al., 2014; Lenna et al., 2014; Maamoun et al., 2019; Shah and Urbina, 2017; Shah et al., 2015). Thus, the involvement of ER stress in the endothelial dysfunction observed in HUVECs and fetoplacental vasculature from PGMO pregnancies is likely.

### 6.4.1 PGMO-associated ER stress and NO production

Our results showed that the reduction of ER stress by TUDCA improved the NOS-dependent NO availability in HUVECs from PGMO, and the induction of ER stress impaired it in cells from PGMN. Furthermore, the L-citrulline production (index of NOS activity), was also reduced in HUVECs from PGMO and restored after the treatment of cells with TUDCA. Also, TUDCA prevented the tunicamycin-induced impairment in HUVECs from PGMN, supporting the role of ER stress in the reduction of NO synthesis. On the other hand, the pre-incubation with TUDCA did not improve NO synthesis in the presence of tunicamycin in HUVECs from PGMO, suggesting that TUDCA at that concentration is ineffective against the ER stress which was already present in these cells in addition to that induced by an exogenous stressor. The association of ER stress with reduced NO generation was also reported in HUVECs where treatment with tunicamycin blunted the induction of NO production in response to calcium entrance (Murugan et al., 2015). The later was also reported in endothelial cells from mice (Cheang et al., 2014; Galán et al., 2014). The pre-

incubation with TUDCA also supported the involvement of ER stress, which prevented the effect induced by tunicamycin (Galán et al., 2014). Furthermore, *ex vivo* experiments in aortas from DIO mice showed that obesity impaired the vasodilation induced by the NOS-dependent vasodilator acetylcholine (Durand and Gutterman, 2013), a phenomenon prevented by the treatment of mice with a reducer of ER stress (Cheang et al., 2014). A similar impairment of the Ach response occurred in mouse mesenteric arteries when the isolated vessels (Hong et al., 2018) or mice (Galán et al., 2014; Kassan et al., 2012) were treated with tunicamycin. Thus, the literature shows a link between ER stress and endothelial dysfunction. Taken these findings together and in the context of this study, the ER stress detected in HUVECs from PGMO is involved in the PGMO-induced impairment of the NOS-dependent NO production by these cells. The latter may explain the reduced CGRP and insulin-induced vasodilation seen in umbilical veins from PGMO.

#### 6.4.2 *PGMO-associated ER stress and eNOS activation state*

Since eNOS mainly mediates NO production at physiological conditions in the endothelium, the next step was to evaluate whether the ER stress and its modulation altered the eNOS activation state in HUVECs from both conditions. It is described that obesity reduced eNOS activating phosphorylation on serine 1177 in aortas from DIO mice, an effect prevented by the reduction of ER stress after the treatment of mice with metformin (Cheang et al., 2014). In mouse aortas, coronary endothelial cells, and HUVECs, tunicamycin-induced ER stress resulted in lower eNOS activation (Galán et al., 2014; Murugan et al., 2015). Also, prevention of ER stress by TUDCA blocked the effect induced by tunicamycin (Galán et al., 2014). Since TUDCA reverted the inhibition of eNOS in PGMO increasing the activating phosphorylation and reducing the increased levels of the inhibitory phosphorylation on

threonine 495, a post-translational mechanism is involved. Also, the induction of ER stress in HUVECs from PGMN reduced the activating phosphorylation of this enzyme, a change prevented by pre-incubation of the cells with TUDCA. Thus, the involvement of ER stress in the reduction of serine 1177 phosphorylation is likely. Interestingly, the induction of ER stress by tunicamycin did not increase the level of the inhibiting phosphorylation of eNOS. The latter suggests that acute induction of ER stress may not alter the induction of phosphorylation on threonine 495, but impaired the phosphorylation on the activating site of eNOS. These findings suggest that the reduction of NO availability seen in HUVECs from PGMN may result from the inactivation of eNOS induced by the ER stress present in these cells.

#### *6.4.3 PGMN-associated ER stress and L-arginine transport*

ER stress is also associated with higher amino acids transport into the cells (Usuki et al., 2017). It is described that the activation of PERK branch signaling increases CAT-1 expression after ER stress (Kilberg et al., 2009). The inhibition of eIF2 $\alpha$  was shown as crucial for the increased protein abundance since CAT1 mRNA translation initiates in an IRES region and not by a cap-dependent mechanism (Fernandez et al., 2002b, 2002a). Furthermore, the transcription of *SLC7A1* (for hCAT-1) is increased by ATF4 due to the presence of a CARE region on its sequence (Kilberg et al., 2009; Lopez et al., 2007; Majumder et al., 2009). XBP1s is also shown to participate in the transcription regulation of this gene (Huang et al., 2010). Thus, the expression of CAT-1 depends on the levels of phosphorylated eIF2 $\alpha$ , ATF4, and XBP1s (Huang et al., 2010; Lopez et al., 2007). In the latter phenomenon, the PERK/eIF2/ATF4 and IRE1 $\alpha$ /XBP1s signaling mechanisms act as modulators of L-arginine transport via hCAT-1. Thus, ER stress could be linked to endothelial dysfunction not only

by affecting the state of eNOS activity but also altering the access of eNOS to its crucial substrate L-arginine. The results in this study show that the reduction of ER stress in HUVECs from PGMO reverted the PGMO-increased L-arginine transport, and conversely, the induction of ER stress in cells from PGMN increased this cell response. Also, the pre-incubation with TUDCA prevented tunicamycin-increased L-arginine transport in PGMN cells but did not change the increased transport seen in HUVECs from PGMO in the presence of tunicamycin. Altogether these results show that ER stress depends on L-arginine transport in HUVECs and explain the increased transport of this amino acid in cells from PGMO pregnancies. On the other hand, the expression of mRNA and protein of hCAT-1 followed a similar pattern than the one seen for L-arginine transport, revealing that the changes in L-arginine transport induced by ER stress depend on the ER stress modulation of hCAT-1 expression in HUVECs from PGMO pregnancies.

#### *6.4.4 PGMO-associated ER stress and arginases activity*

Although the increase in L-arginine uptake in cells from PGMO suggested an over-abundance of the substrate for the production of NO by eNOS, NO production is diminished by lower activation of the enzyme. The over-availability of L-arginine suggests its use in other metabolic routes in the cell. In this line, arginases compete with eNOS for the substrate L-arginine to synthesize urea in endothelial cells (Leiva et al., 2013; Prieto et al., 2011). Indeed, their increased activity was associated with endothelial dysfunction in HUVECs from pregnant women with hypercholesterolemia (Leiva et al., 2013) or IUGR (Krause et al., 2013, 2012). Other reports showed that ER stress is associated with higher arginases expression in mice immune cells (Lee et al., 2014; Mahadevan et al., 2011). The results in the present study showed that arginase activity was increased in HUVECs from PGMO and that ER stress

inhibition restored these alterations. Conversely, induction of ER stress increased arginases activity in HUVECs from PGMN. Thus, PGMO-induced ER stress in HUVECs from PGMO induced the activity of arginases. This alteration may lead to the reduced availability of L-arginine to eNOS despite the increased L-arginine uptake, and thus to contribute to the lower NO generation seen in cells from PGMO pregnancies.

## **6.5 PGMO-associated ER stress and desensitization to insulin**

The link between obesity-induced ER stress and insulin resistance in metabolic tissues is widely described (Flamment et al., 2012; Villalobos-Labra et al., 2018b; Yilmaz, 2017) but it is less explored in the vasculature. It is reported that plasma from obese children caused *in vitro* ER stress and insulin resistance in HUVECs by impairing insulin-stimulated NO production, a response prevented by reducing the ER stress after the incubation of the chemical chaperones sodium 4-phenylbutyrate (PBA) or TUDCA (Di Pietro et al., 2017). Moreover, the treatment of mice with palmitate, a free fatty acid in the human bloodstream that increases in obesity and induces insulin resistance in obesity (Sears and Perry, 2015), impaired the insulin-induced vasodilation in mesenteric arterioles by a mechanism that involves ER stress. Furthermore, the pre-treatment of these animals with TUDCA prevented the palmitate-induced insulin resistance state (Kim et al., 2015). Thus, ER stress is a plausible mechanism in the obesity-induced insulin resistance in the vasculature.

### *6.5.1 PGMO-associated ER stress and impaired insulin response*

The results of this study show that ER stress reduction by TUDCA sensitized the NOS-dependent vasodilation induced by insulin in umbilical veins from PGMO pregnancies. These findings suggest that ER stress was blocking the insulin response in these placental vessels. Conversely, the induction of ER stress by tunicamycin blocked the insulin response

in umbilical veins from PGMN pregnancies. Based on these results it is suggested that ER stress is involved in the impairment of the insulin response detected in umbilical veins from PGMO pregnancies. The evaluation of the intracellular mechanisms involved in this abnormal response of the umbilical veins revealed that ER stress inhibition improved the insulin signaling pathway by activating Akt and eNOS in HUVECs from PGMO. The latter resulted in a higher insulin-induced synthesis of NOS-dependent NO. Conversely, the induction of ER stress resulted in the opposite effect in HUVECs from PGMN pregnancies. These findings show that PGMO-associated ER stress in HUVECs is involved in the impairment of the insulin signaling pathway and supports the involvement of ER stress in the deficient insulin-induced vasodilation from PGMO umbilical veins.

#### *6.5.2 PERK and IRE1 $\alpha$ involvement in the impairment of the insulin response*

Studies in animals and humans showed two signaling pathways linking ER stress with the impairment of the insulin signaling pathway, i.e. IRE1 $\alpha$ /JNK and PERK/TRB3. The IRE1 $\alpha$ /JNK was first described in hepatocytes and liver of mice (Ozcan et al., 2004), where after ER stress induction, IRE1 $\alpha$  inhibited IRS1 through JNK activation. The latter resulted in deficient activation of Akt in response to insulin. Thus, IRE1 $\alpha$  activation of JNK impaired insulin signaling by inhibiting IRS1. Since IRE1 $\alpha$  also has endoribonuclease activity, the authors also evaluated the involvement of XBP1 processing in their results. The effect of XBP1s opposed to that seen for JNK, and XBP1s prevented IRE1 $\alpha$ -induced activation of JNK and protected from the obesity-associated insulin resistance in mice (Ozcan et al., 2004). Thus, IRE1 $\alpha$ /JNK branch activity may induce insulin resistance in obesity. Moreover, JNK activity is involved in the obesity-induction of insulin resistance in mice (Hirosumi et al., 2002), and mediates deficient vasodilation induced by insulin in visceral arterioles from

obese subjects (Farb et al., 2016). On the other hand, a study conducted in diabetic patients showed that greater activation of IRE1 $\alpha$  in endothelial cells was associated with lower FMD associating IRE1 $\alpha$  activity with endothelial dysfunction (Bretón-Romero et al., 2018). Therefore, IRE1 $\alpha$ /JNK is involved in vascular insulin resistance induced by obesity in humans. The results in this study show that the inhibition of IRE1 $\alpha$  improved the insulin-induced NO production in HUVECs from PGMO. Furthermore, the blocking action of tunicamycin on the insulin response in HUVECs from PGMN was abolished by pre-incubation of these cells with a pharmacological inhibitor of IRE1 $\alpha$ . Thus, IRE1 $\alpha$  was involved in the ER stress induction of the impaired insulin response seen in HUVECs from PGMO.

Other results suggested a potential role for JNK in the abnormal response of HUVECs from this metabolic condition of the mother. The inhibition of IRE1 $\alpha$  prevented the tunicamycin-induced increase of JNK phosphorylation in HUVECs from PGMN. Furthermore, the inhibiting phosphorylation of IRS1 was reduced by the inhibition of JNK in HUVECs from PGMN even in the presence of tunicamycin. Likewise, the IRE1 $\alpha$  knockdown reduced the JNK phosphorylation and serine 307 phosphorylation of IRS1 at the basal condition or at the presence of tunicamycin. Thus, ER stress-induced IRE1 $\alpha$  activation inhibited IRS1 following activation of JNK in HUVECs. The latter is proposed as a mechanism explaining the inactivation of the downstream signaling pathway and the concomitant inefficient insulin response seen in HUVECs from PGMO pregnancies. Since XBP1s prevented the IRE1 $\alpha$ -induced activation of JNK (Ozcan et al., 2004), a similar XBP1 processing between HUVECs from PGMN and PGMO despite the greater IRE1 $\alpha$  protein

abundance seen in HUVECs from PGM0, may result in improved activity of the IRE1 $\alpha$ /JNK branch by contributing to the deterioration of the insulin response in these cells.

TRB3 is a catalytically inactive pseudokinase (Boudeau et al., 2006; Hegedus et al., 2007) that inhibits activation of Akt, impairing the insulin signaling pathway and promoting insulin resistance (Du et al., 2003). Modulation of TRB3 expression by PERK activity was first described by Ohoka and colleagues (Ohoka et al., 2005), and since then several studies in obese mice have emerged linking ER stress with the induction of insulin resistance through the PERK/TRB3 pathway in cardiomyocytes and heart (Avery et al., 2010), skeletal muscle (Koh et al., 2013), liver (Ozcan et al., 2013), and adipose tissue (Du and Ding, 2009; Sun et al., 2017). Furthermore, TRB3 expression is higher in the skeletal muscle (Koh et al., 2013) and serum (Nourbakhsh et al., 2017) from obese patients. In addition, a polymorphism of TRB3 that gives the protein greater stability and affinity for Akt (Liew et al., 2010) was associated with higher risk for the development of insulin resistance in non-diabetic individuals and with the presence of a cluster of insulin resistance-related cardiovascular risk factors (Prudente et al., 2005). Therefore, TRB3 associates with the development of insulin resistance in obesity and other metabolic syndrome-associated diseases (Flamment et al., 2012; Marinho et al., 2015; Prudente et al., 2012).

A recent study showed that PERK inhibitor GSK2606114 and IRE1 $\alpha$  inhibitor KIRA6, also inhibit KIT receptor tyrosine kinase (Mahameed et al., 2019), a cell-surface receptor involved in cell survival, migration, and proliferation (Lennartsson and Rönstrand, 2012). Mature endothelial cells, including HUVECs, are shown to express this receptor (König et al., 1997; Matsui et al., 2004). Assays done in isolated KIT showed that its activity was blocked with a K<sub>d</sub> of ~600 nM for GSK2606114 and ~10  $\mu$ M for KIRA6. GSK2606114 and

KIRA6 inhibited KIT activity at nanomolar concentrations in MEL526 WT or MEL526 PERK KO cells, respectively (Mahameed et al., 2019). Since a concentration of 3  $\mu$ M of GSK2606114 and KIRA6 was used in this thesis, these inhibitors may also inhibit the activity of KIT. Thus, the results showing PERK and IRE1 $\alpha$  activity in the presence of these inhibitors may be affected by a potential inhibition of KIT in HUVECs.

The literature discussed above suggests that the increased activation of the PERK signaling branch and the consequent increase in the expression of TRB3 found in HUVECs from PGMO pregnancies participate in the insulin desensitization in these cells. However, our results showed that the inhibition of PERK did not improve the insulin-induced NO production in HUVECs from PGMO and did not prevent the tunicamycin-induced impairment of insulin response in HUVECs from PGMN. These findings suggest that despite having increased expression of TRB3 in HUVECs from PGMO, PERK inhibition for 8 hours did not change the level of TRB3 enough to see an effect on the response to insulin, needing perhaps a longer period of PERK inhibition to observe an effect on the level of TRB3. The latter is likely given that the stability of TRB3 protein has a half-life of around 9 hours (Liew et al., 2010), and the decrease of its expression by inhibition of the PERK pathway requires a previous decrease in the abundance of ATF4 and CHOP (Ohoka et al., 2005). Therefore, new experimental strategies are needed to confirm or rule out the participation of PERK in the deterioration of the insulin signaling pathway in HUVECs of PGMO pregnancies.

## **6.6 Final comments**

This study suggests that PGMO is a condition that causes endothelial dysfunction and reduced endothelial sensitivity to insulin in the umbilical vein endothelium as a result of the

occurrence of ER stress (Figure 61). This observation suggests a subclinical condition of insulin resistance in the fetus and a state of endothelial dysfunction of the umbilical vein, which could alter the local circulation in pregnancy. Also, considering the role played by the umbilical vein in the delivery of fresh blood to the arterial system of the fetus (Griffiths and Campbell, 2015) it may also affect the systemic hemodynamics of the fetus. Furthermore, even though fetoplacental tissues are a transient organ, its dysfunction is crucial in the fetal outcome, and altered functions in this tissue remain throughout the lifespan of the offspring (Howell and Powell, 2017; Longtine and Nelson, 2011; Sobrevia et al., 2014). Considering further the continuity of the endothelium of the umbilical vein with the endothelium of the arterial system of the fetus, the deleterious effects of pre-gestational obesity seen in the umbilical vein can occur in the fetal vasculature. Since endothelial dysfunction and insulin resistance are considered the first steps towards the development of cardiovascular diseases (Breen and Giacca, 2011; Sandoo et al., 2015), the potential occurrence of these alterations in the vasculature of the newborn suggest the possibility of developing serious consequences in their vascular system in young and adulthood. Indeed, the alterations shown in this thesis are in tune with the higher cardiovascular risk in the descendants of the PGMO mothers (Gaillard et al., 2014; Pirkola et al., 2010; Stuebe et al., 2009).

It is worth mentioning that the alterations presented by the HUVECs from PGMO pregnancies were maintained in culture after three passages and under the same conditions as the PGMN HUVECs. These observations suggest that the harmful effects of PGMO on the endothelium are intrinsic and lasting. Moreover, the endothelial dysfunction and the inadequate insulin response seen in HUVECs was in concordance with the alterations

presented by the *ex vivo* assays in umbilical vein rings. However, changes seen *in vitro* may result as an adaptation to culture and not necessarily reflecting a similar situation *in vivo*.

This study also presents ER stress as a cause of PGMO-induction of endothelial dysfunction and insulin resistance in fetoplacental umbilical vein, pointing to the modulation of ER stress as a potential treatment to improve the outcome of the newborn. Interestingly, TUDCA was used in clinical trials for the treatment of diseases associated with ER stress (Elia et al., 2016; Vang et al., 2014). The oral administration of TUDCA prevented endothelial dysfunction induced by the ingestion of a high glucose load in young humans (Walsh et al., 2016). Thus, these approaches showed that using ER stress blockers in humans is effective and safe. Unfortunately, there are not reports *in vivo* in human subjects regarding pregnant women with PGMO or other complication of pregnancy (Villalobos-Labra et al., 2018a). Considering these findings *in vivo*, we propose that adequate management of ER stress in the mother with PGMO may result in a better metabolic outcome of the newborn born to these women.

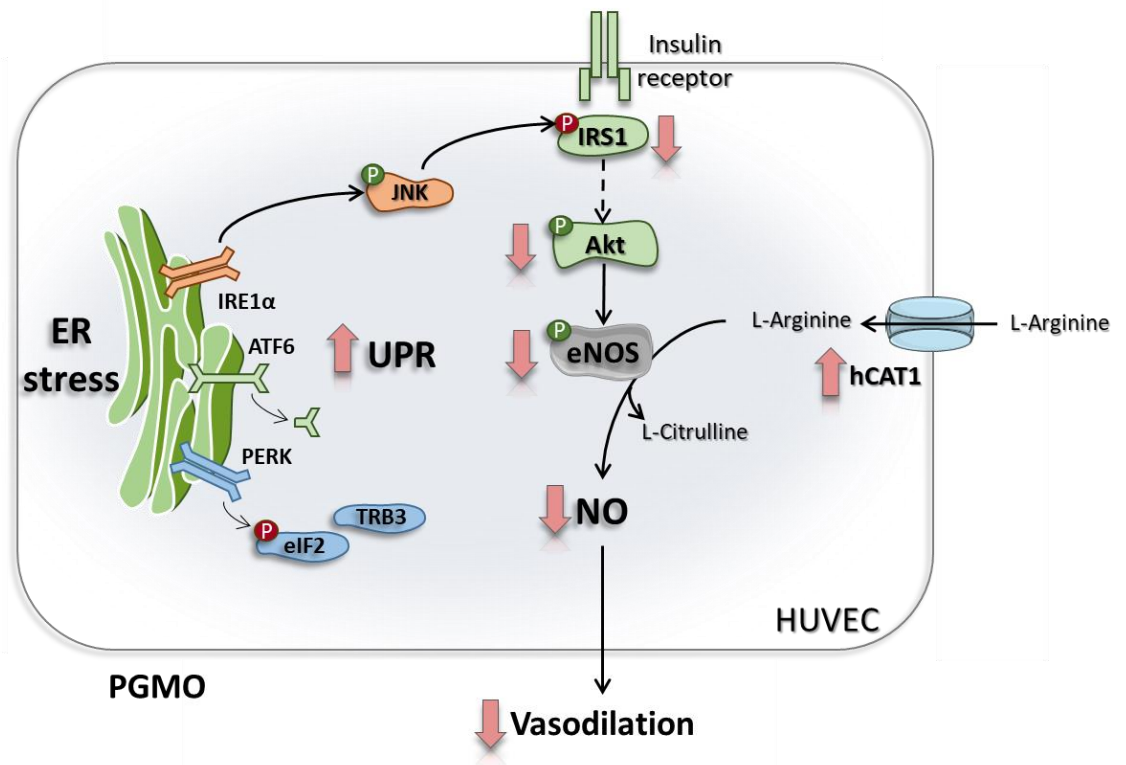


**Figure 61. The potential involvement of pre-pregnancy maternal obesity-induced endoplasmic** reticulum stress in human umbilical vein endothelial cell dysfunction and insulin desensitization. PGMO associated with increased activity of the UPR proteins in human umbilical vein endothelial cells. The activity of the signaling pathways activated by PERK and IRE1 $\alpha$  was found to be increased, as well as the translocation of ATF6 to the nucleus. On the other hand, despite presenting higher transport of L-arginine, the substrate for the production of NO by eNOS, NO production was lower due to a lower activation status of eNOS. Also, in these cells, insulin did not activate the post-IR metabolic signaling pathway, not activating eNOS and not increasing NO production in response to insulin. A lower endothelium-derived NO could explain the deficient vasodilation observed in the umbilical veins of PGMO pregnancies. ER stress reduction reduced the activity of the three pathways of the UPR and resulted in a reduction in L-arginine transport, increase in basal and insulin-induced eNOS activity, NO production, and in sensitization of the insulin signaling pathway in response to insulin. Thus, the PGMO-associated ER stress was related to the endothelial dysfunction and the insulin desensitization presented by HUVECs. Among the UPR proteins activated in HUVECs PGMO, the increased PERK-induced TRB3 expression, a pseudokinase that inhibits Akt, did not show to be part of the lower insulin response presented by these cells. However, the increase in IRE1 $\alpha$  activity and the consequent activation of JNK resulted in the inhibition of IRS1, reduction of Akt and eNOS activation, and reduction of NO production in response to insulin. Thus, the IRE1/JNK/IRS1 pathway is proposed as a probable mechanism in the deterioration of the insulin signaling pathway produced by the ER stress in the HUVECs from PGMO pregnancies.

## 7. Conclusions

This study suggests that obesity of the mother may be a potential deleterious condition for the newborn.

The metabolic alterations of the mother due to pre-gestational maternal obesity may result in:

1. Endothelial dysfunction and insulin resistance in the umbilical vein from PGMO pregnancies.
2. Increased activation of the UPR in HUVECs from PGMO, evidencing the occurrence of ER stress.
3. The induction of endothelial dysfunction and insulin resistance by PGMO-associated ER stress in HUVECs via activation of IRE1 $\alpha$ /JNK signaling branch.

## 8. Appendix



### **DOCUMENTO DE CONSENTIMIENTO PARA LA DONACIÓN DE PLACENTA, CORDÓN UMBILICAL Y SANGRE MATERNA PARA SU USO EN INVESTIGACIONES BIOMÉDICAS EN LA FACULTAD DE MEDICINA DE LA PONTIFICIA UNIVERSIDAD CATÓLICA DE CHILE**

El propósito de esta información es ayudarle a usted a tomar la decisión de donar -o no-, su placenta, el cordón umbilical y una muestra de su sangre para fines de investigación biomédica.

Tome todo el tiempo que necesite para decidirse, lea cuidadosamente este documento y hágale las preguntas que desee al médico.

#### **OBJETIVOS DE LA INVESTIGACIÓN BIOMÉDICA EN PLACENTA.**

La placenta es el tejido encargado de llevar los nutrientes y el oxígeno que el feto requiere para crecer mientras está en el útero de la madre.

La placenta y el cordón umbilical son expulsados del útero después del nacimiento de su hijo/hija (alumbramiento), ya sea que nazca por un parto normal o por medio de una operación cesárea. Después del alumbramiento la placenta no presta ninguna función, por lo que es eliminada como desecho biológico.

Diferentes investigadores de la Escuela de Medicina están interesados en estudiar la estructura y función de la placenta, el cordón umbilical y la sangre materna en variadas investigaciones biomédicas incluyendo investigaciones genéticas.

#### **PROCEDIMIENTO DE LA INVESTIGACIÓN.**

Estamos invitando a participar a todas las pacientes mayores de 18 años, que tengan su parto en la Maternidad del Hospital Clínico de la Pontificia Universidad Católica de Chile.

Si usted acepta participar, le solicitamos que done -a la Facultad de Medicina P. Universidad Católica de Chile- su placenta y cordón umbilical posterior a su parto y que nos permita acceder y usar los datos médicos contenidos en su ficha clínica. Adicionalmente, le solicitamos que autorice la obtención de una muestra de sangre materna no mayor de 6 ml (equivalente a una cucharada sopera) en el momento del ingreso a la maternidad.

La placenta, el cordón umbilical y la muestra de sangre, así como los datos clínicos relevantes obtenidos serán usados únicamente para los propósitos de las diferentes investigaciones biomédicas. La placenta, el cordón umbilical y la muestra de sangre serán guardados en el Laboratorio de Investigación en Perinatología en forma anónima por un tiempo indefinido y bajo la responsabilidad de la Dra. Paola Casanello.

La placenta, el cordón umbilical y la muestra de sangre donada no será comercializada.

### **BENEFICIOS.**

Usted no se beneficiará por la donación de su placenta, cordón umbilical o muestra de sangre materna. Sin embargo, la información científica que se obtenga será de utilidad para conocer más acerca del funcionamiento de la placenta humana y eventualmente en el largo plazo podría beneficiar a diferentes personas.

### **RIESGOS.**

La utilización de su placenta, cordón umbilical y sangre materna no involucra ningún riesgo para su hijo/hija o para usted, ya que la placenta y el cordón umbilical son tejidos que normalmente se desechan después del parto. Por su parte, la obtención de la muestra de sangre es un procedimiento habitual de mínimo riesgo que se realiza en toda paciente que ingresa a la maternidad, por lo que no se requerirá una punción venosa adicional.

### **COSTOS.**

Si usted decide donar su placenta, cordón umbilical y sangre materna, esta donación no tendrá ningún costo para usted.

## **COMPENSACIONES.**

No se le pagará por la donación de su placenta, cordón umbilical y sangre materna.

## **CONFIDENCIALIDAD DE LA INFORMACIÓN.**

Sus datos personales y los de su hijo/hija no serán conocidos y las muestras de placenta, cordón umbilical y sangre materna se guardarán en forma anónima. Los resultados obtenidos de las diferentes investigaciones biomédicas podrían ser presentados en congresos científicos o dados a conocer en revistas médicas y científicas, sin embargo, su nombre –ni el de su hijo/hija- no será dado a conocer.

## **VOLUNTARIEDAD.**

Su donación es completamente voluntaria. Usted tiene el derecho a no aceptar el donar su placenta, el cordón umbilical o una muestra de su sangre. Al hacerlo, usted y su hijo/hija no pierden ningún derecho que les asisten como pacientes de esta institución y no se verá afectada la calidad de la atención médica que merecen.

Si usted retira su voluntad de donar su placenta, cordón umbilical y sangre materna, estas muestras serán eliminadas y la información obtenida no será utilizada.

## **PREGUNTAS.**

Si tiene preguntas acerca de esta donación de su placenta, cordón umbilical y sangre materna para su uso en investigaciones biomédicas puede contactar a la Dra. Paola Casanello, al teléfono 2 354 8116.

Si tiene preguntas acerca de sus derechos como donante y participante en investigaciones biomédicas, puede llamar a la Dra. Beatriz Shand K., Presidente del Comité de Ética en Investigación de la Escuela de Medicina de la Pontificia Universidad Católica de Chile, al teléfono 2 354 8173, o enviar un correo electrónico a [etica.investigacion@med.puc.cl](mailto:etica.investigacion@med.puc.cl).

## **DECLARACIÓN DE DONACIÓN.**

- Se me ha explicado el propósito de la donación de placenta, cordón umbilical y sangre materna, los procedimientos, los riesgos, los beneficios y los derechos que me asisten.
- Firmo este documento voluntariamente, sin ser forzada a hacerlo.
- No estoy renunciando a ningún derecho que me asista.
- Se me ha informado que tengo el derecho a reevaluar mi participación según mi parecer, en cualquier momento.
- Yo autorizo el acceso y uso de los datos contenidos en mi ficha clínica, al investigador y sus colaboradores, para los propósitos de las diferentes investigaciones biomédicas.
- Al momento de la firma, se me entrega una copia firmada de este documento.

## **FIRMAS**

\_\_\_\_\_  
Nombre participante                      Firma                      Fecha

\_\_\_\_\_  
Nombre Investigador                      Firma                      Fecha

\_\_\_\_\_  
Nombre Director de la  
Institución o su Delegado                      Firma                      Fecha

## 9. References

- Alhusaini S, McGee K, Schisano B, Harte A, McTernan P, Kumar S, Tripathi G (2010). Lipopolysaccharide, high glucose and saturated fatty acids induce endoplasmic reticulum stress in cultured primary human adipocytes: Salicylate alleviates this stress. *Biochem Biophys Res Commun* 397:472–478. DOI:10.1016/j.bbrc.2010.05.138
- Amugsi DA, Dimbuene ZT, Mberu B, Muthuri S, Ezeh AC (2017). Prevalence and time trends in overweight and obesity among urban women: an analysis of demographic and health surveys data from 24 African countries, 1991 – 2014. *BMJ Open* 7:e017344. DOI:10.1136/bmjopen-2017-017344
- Antonov J, Goldstein DR, Oberli A, Baltzer A, Pirodda M, Fleischmann A, Altermatt HJ, Jaggi R (2005). Reliable gene expression measurements from degraded RNA by quantitative real-time PCR depend on short amplicons and a proper normalization. *Lab Invest* 85:1040–1050. DOI:10.1038/labinvest.3700303
- De Artinano AA, Gonzalez VLM (1999). Endothelial dysfunction and hypertensive vasoconstriction. *Pharmacol Res* 40:113–124. DOI:10.1006/phrs.1999.0481
- Avery J, Etzion S, DeBosch BJ, Jin X, Lupu TS, Beitinjaneh B, Grand J, Kovacs A, Sambandam N, Muslin AJ (2010). TRB3 function in cardiac endoplasmic reticulum stress. *Circ Res* 106:1516–1523. DOI:10.1161/CIRCRESAHA.109.211920
- Balligand J, Feron O, Dessy C (2009). ENOS activation by physical forces : From short-term regulation of contraction to chronic remodeling of cardiovascular tissues. *Physiol Rev* 89:481–534. DOI:10.1152/physrev.00042.2007.
- Bar J, Schreiber L, Saruhanov E, Ben-Haroush A, Golan A, Kovo M (2012). Placental histopathological findings in obese and nonobese women with complicated and uncomplicated pregnancies. *Arch Gynecol Obstet* 286:1343–1347. DOI:10.1007/s00404-012-2450-z
- Barker DJP (1998). In utero programming of chronic disease. *Clin Sci* 95:115–128. DOI:10.1042/cs0950115
- Battson ML, Lee DM, Gentile CL (2017). Endoplasmic reticulum stress and the development of endothelial dysfunction. *Am J Physiol - Hear Circ Physiol* 312:H355–H367. DOI:10.1152/ajpheart.00437.2016
- Boden G, Cheung P, Salehi S, Homko C, Loveland-Jones C, Jayarajan S, Stein TP, Jon Williams K, Liu ML, Barrero CA, Merali S (2014). Insulin regulates the unfolded protein response in human adipose tissue. *Diabetes* 63:912–922. DOI:10.2337/db13-0906
- Boden G, Duan X, Homko C, Molina EJ, Song W, Perez O, Cheung P, Merali S (2008). Increase in endoplasmic reticulum stress – related proteins and genes in adipose tissue of obese , insulin-resistant individuals. *Diabetes* 57:2438–2444. DOI:10.2337/db08-0604.

- Boudeau J, Miranda-Saavedra D, Barton GJ, Alessi DR (2006). Emerging roles of pseudokinases. *Trends Cell Biol* 16:443–452. DOI:10.1016/j.tcb.2006.07.003
- Bradford MM (1976). A rapid and sensitive method for the quantitation of microgram quantities of protein utilizing the principle of protein-dye binding. *Anal Biochem* 72:248–254. DOI:10.1016/0003-2697(76)90527-3
- Brain SD (2004). Vascular actions of calcitonin gene-related peptide and adrenomedullin. *Physiol Rev* 84:903–934. DOI:10.1152/physrev.00037.2003
- Bretón-Romero R, Weisbrod RM, Feng B, Holbrook M, Ko D, Stathos MM, Zhang JY, Fetterman JL, Hamburg NM (2018). Liraglutide treatment reduces endothelial endoplasmic reticulum stress and insulin resistance in patients with diabetes mellitus. *J Am Heart Assoc* 7. DOI:10.1161/JAHA.118.009379
- Burkholder TJ, Lieber RL (2001). Sarcomere length operating range of vertebrate muscles during movement. *J Exp Biol* 204:1529–1536.
- Casanello P, Escudero C, Sobrevia L (2007). Equilibrative nucleoside (ENTs) and cationic amino acid (CATs) transporters: implications in foetal endothelial dysfunction in human pregnancy diseases. *Curr Vasc Pharmacol* 5:69–84. DOI:10.2174/157016107779317198
- Casanello P, Krause B, Torres E, Gallardo V, González M, Prieto C, Escudero C, Farías M, Sobrevia L (2009). Reduced L-arginine transport and nitric oxide synthesis in human umbilical vein endothelial cells from intrauterine growth restriction pregnancies is not further altered by hypoxia. *Placenta* 30:625–633. DOI:10.1016/j.placenta.2009.04.010
- Catalano PM, Presley L, Minium J, Mouzon SH De (2009). Fetuses of obese mothers develop insulin resistance in utero. *Diabetes Care* 32:1076–1080. DOI:10.2337/dc08-2077
- Chambers JE, Marciniak SJ (2014). Cellular mechanisms of endoplasmic reticulum stress signaling in health and disease. 2. Protein misfolding and ER stress. *Am J Physiol Cell Physiol* 307:C657-C670. DOI:10.1152/ajpcell.00183.2014
- Cheang WS, Tian XY, Wong WT, Lau CW, Lee SST, Chen ZY, Yao X, Wang N, Huang Y (2014). Metformin protects endothelial function in diet-induced obese mice by inhibition of endoplasmic reticulum stress through 5' adenosine monophosphate-Activated protein kinase-peroxisome proliferator-Activated receptor  $\delta$  pathway. *Arterioscler Thromb Vasc Biol* 34:830–836. DOI:10.1161/ATVBAHA.113.301938
- Cheang WS, Wong WT, Zhao L, Xu J, Wang L, Lau CW, Chen ZY, Ma RCW, Xu A, Wang N, Tian XY, Huang Y (2017). PPAR $\delta$  is required for exercise to attenuate endoplasmic reticulum stress and endothelial dysfunction in diabetic mice. *Diabetes* 66:519–528. DOI:10.2337/db15-1657
- Cheang WS, Yuen Ngai C, Yen Tam Y, Yu Tian X, Tak Wong W, Zhang Y, Wai Lau C, Chen ZY, Bian ZX, Huang Y, Ping Leung F (2015). Black tea protects against hypertension-associated

endothelial dysfunction through alleviation of endoplasmic reticulum stress. *Sci Rep* 5:10340. DOI:10.1038/srep10340

Chen C, Xu X, Yan Y (2018). Estimated global overweight and obesity burden in pregnant women based on panel data model. *PLoS One* 13:e0202183. DOI:10.1371/journal.pone.0202183

Choi S-K, Lim M, Yeon S-I, Lee Y-H (2016). Inhibition of endoplasmic reticulum stress improves coronary artery function in type 2 diabetic mice. *Exp Physiol* 101:768–777. DOI:10.1113/EP085508

Clark MG, Wallis MG, Barrett EJ, Vincent MA, Richards SM, Clerk LH, Rattigan S (2003). Blood flow and muscle metabolism: a focus on insulin action. *Am J Physiol Endocrinol Metab* 284:E241–E258. DOI:10.1152/ajpendo.00408.2002

Clarkson P, Adams MR, Powe AJ, Donald AE, McCredie R, Robinson J, McCarthy SN, Keech A, Celermajer DS, Deanfield JE (1996). Oral L-arginine improves endothelial dysfunction in man rapid publication oral L-arginine improves endothelium-dependent dilation in hypercholesterolemic young adults. *J Clin Invest* 97:1989–1994.

Closs EI, Simon A, Vé N, Rotmann A (2004). Plasma membrane transporters for arginine. *J Nutr* 134:2752–2759.

Cnop M, Foufelle F, Velloso LA (2012). Endoplasmic reticulum stress, obesity and diabetes. *Trends Mol Med* 18:59–68. DOI:10.1016/j.molmed.2011.07.010

Cooke J, Dzau V (1997). Derangements of the nitric oxide synthase pathway, L-arginine, and cardiovascular diseases. *Circulation* 96:379–382.

Cooke JP, Singer AH, Tsao P, Zera P, Rowan RA, Billingham ME (1992). Antiatherogenic effects of L-arginine in the hypercholesterolemic rabbit. *J Clin Invest* 90:1168–1172. DOI:10.1172/JCI115937

Cynober LA (2002). Plasma amino acid levels with a note on membrane transport: Characteristics, regulation, and metabolic significance. *Nutrition* 18:761–766. DOI:10.1016/S0899-9007(02)00780-3

D’Oria R, Laviola L, Giorgino F, Unfer V, Bettocchi S, Scioscia M (2017). PKB/Akt and MAPK/ERK phosphorylation is highly induced by inositols: Novel potential insights in endothelial dysfunction in preeclampsia. *Pregnancy Hypertens* 10:107–112. DOI:10.1016/j.preghy.2017.07.001

Davignon J, Ganz P (2004). Role of endothelial dysfunction in atherosclerosis. *Circulation* 109:27–32. DOI:10.1161/01.CIR.0000131515.03336.f8

Deanfield J, Donald A, Ferri C, Giannattasio C, Halcox J, Halligan S, Lerman A, Mancina G, Oliver JJ, Pessina AC, Rizzoni D, Rossi GP, Salvetti A, Schiffrin EL, Taddei S, Webb DJ (2005). Endothelial function and dysfunction. Part I: Methodological issues for assessment in the different vascular beds: a statement by the Working Group on Endothelin and Endothelial

Factors of the European Society of Hypertension. *J Hypertens* 23:7–17. DOI:00004872-200501000-00004 [pii]

Denis RG, Arruda AP, Romanatto T, Milanski M, Coope A, Solon C, Razolli DS, Velloso LA (2010). TNF- $\alpha$  transiently induces endoplasmic reticulum stress and an incomplete unfolded protein response in the hypothalamus. *Neuroscience* 170:1035–1044. DOI:10.1016/J.NEUROSCIENCE.2010.08.013

Deputy NP, Sharma AJ, Kim SY (2015). Gestational Weight Gain — United States, 2012 and 2013. *MMWR Morb Mortal Wkly Rep* 64:1215–1220. DOI:10.15585/mmwr.mm6443a3

Desoye G (2018). The human placenta in diabetes and obesity: friend or foe? The 2017 Norbert Freinkel Award Lecture. *Diabetes Care* 41:1362–1369. DOI:10.2337/dci17-0045

Deves R, Boyd CAR (1998). Transporters for cationic amino acids in animal cells: Discovery, structure, and function. *Physiol Rev* 78:487–545. DOI:10.1016/0022-4804(91)90210-D

Díaz-Ruiz A, Guzmán-Ruiz R, Moreno NR, García-Rios A, Delgado-Casado N, Membrives A, Túnez I, El Bekay R, Fernández-Real JM, Tovar S, Diéguez C, Tinahones FJ, Vázquez-Martínez R, López-Miranda J, Malagón MM (2015). Proteasome dysfunction associated to oxidative stress and proteotoxicity in adipocytes compromises insulin sensitivity in human obesity. *Antioxid Redox Signal* 23:597–612. DOI:10.1089/ars.2014.5939

Dong YL, Vegiraju S, Chauhan M, Gangula PRR, Hankins GD V, Goodrum L, Yallampalli C (2004). Involvement of calcitonin gene-related peptide in control of human fetoplacental vascular tone. *Am J Physiol Hear Circ Physiol* 286:H230–H239. DOI:10.1152/ajpheart.00140.2003

Drexler H, Zeiher AM, Meinzer K, Just H (1991). Correction of endothelial dysfunction in coronary microcirculation of hypercholesterolaemic patients by L-arginine. *Lancet* 338:1546–1550. DOI:10.1016/0140-6736(91)92372-9

Du K, Ding J (2009). Insulin regulates TRB3 and other stress-responsive gene expression through induction of C/EBP $\beta$ . *Mol Endocrinol* 23:475–485. DOI:10.1210/me.2008-0284

Du K, Herzig S, Kulkarni RN, Montminy M (2003). TRB3: a tribbles homolog that inhibits Akt/PKB activation by insulin in liver. *Science* 300:1574–1577. DOI:10.1126/science.1079817

Dufey E, Sepúlveda D, Rojas-Rivera D, Hetz C (2014). Cellular mechanisms of endoplasmic reticulum stress signaling in health and disease. 1. An overview. *Am J Physiol Cell Physiol* 307:C582–C594. DOI:10.1152/ajpcell.00258.2014

Duncan ER, Crossey PA, Walker S, Anilkumar N, Poston L, Douglas G, Ezzat VA, Wheatcroft SB, Shah AM, Kearney MI (2008). Effect of endothelium-specific insulin resistance on endothelial function in vivo. *Diabetes* 57:3307–3314. DOI:10.2337/db07-1111

Durand MJ, Gutterman DD (2013). Diversity in mechanisms of endothelium-dependent vasodilation in health and disease. *Microcirculation* 20:239–247. DOI:10.1111/micc.12040

- Elia AE, Lalli S, Monsurr O MR, Sagnelli A, Taiello AC, Reggiori B, Bella V La, Tedeschi G, Albanese A (2016). Tauroursodeoxycholic acid in the treatment of patients with amyotrophic lateral sclerosis. *Eur J Neurol* 23:45–52. DOI:10.1111/ene.12664
- Eriksson JG, Sandboge S, Salonen M, Kajantie E, Osmond C (2015). Maternal weight in pregnancy and offspring body composition in late adulthood: Findings from the Helsinki Birth Cohort Study (HBCS). *Ann Med* 47:94–99. DOI:10.3109/07853890.2015.1004360
- Eriksson JG, Sandboge S, Salonen MK, Kajantie E, Osmond C (2014). Long-term consequences of maternal overweight in pregnancy on offspring later health: Findings from the Helsinki Birth Cohort Study. *Ann Med* 46:434–438. DOI:10.3109/07853890.2014.919728
- Esser N, Legrand-Poels S, Piette J, Scheen AJ, Paquot N (2014). Inflammation as a link between obesity, metabolic syndrome and type 2 diabetes. *Diabetes Res Clin Pract* 105:141–150. DOI:10.1016/j.diabres.2014.04.006
- Farb MG, Karki S, Park SY, Saggese SM, Carmine B, Hess DT, Apovian C, Fetterman JL, Breton-Romero R, Hamburg NM, Fuster JJ, Zuriaga MA, Walsh K, Gokce N (2016). WNT5A-JNK regulation of vascular insulin resistance in human obesity. *Vasc Med* 21:489–496. DOI:10.1177/1358863X16666693
- Félétou M (2011). *The Endothelium: Part 1: Multiple Functions of the Endothelial Cells—Focus on Endothelium-Derived Vasoactive Mediators*. Morgan & Claypool Life Sciences, San Rafael.
- Fernandez J, Yaman I, Merrick WC, Koromilas A, Wek RC, Sood R, Hensold J, Hatzoglou M (2002a). Regulation of internal ribosome entry site-mediated translation by eukaryotic initiation factor-2 $\alpha$  phosphorylation and translation of a small upstream open reading frame. *J Biol Chem* 277:2050–2058. DOI:10.1074/jbc.M109199200
- Fernandez J, Yaman I, Sarnow P, Snider MD, Hatzoglou M (2002b). Regulation of internal ribosomal entry site-mediated translation by phosphorylation of the translation initiation factor eIF2 $\alpha$ . *J Biol Chem* 277:19198–19205. DOI:10.1074/jbc.M201052200
- Ferretti G, Cester AM, Bacchetti T, Raffaelli F, Vignini A, Orici F, Martino C, Tranquilli A (2014). Leptin and paraoxonase activity in cord blood from obese mothers. *J Matern Neonatal Med* 27:1353–1356. DOI:10.3109/14767058.2013.858319
- Flamment M, Hajduch E, Ferré P, Foufelle F (2012). New insights into ER stress-induced insulin resistance. *Trends Endocrinol Metab* 23:381–390. DOI:10.1016/j.tem.2012.06.003
- Fleming I (2010). Molecular mechanisms underlying the activation of eNOS. *Pflugers Arch Eur J Physiol* 459:793–806. DOI:10.1007/s00424-009-0767-7
- Fleming I, Busse R (2003). Molecular mechanisms involved in the regulation of the endothelial nitric oxide synthase. *Am J Physiol Regul Integr Comp Physiol* 284:R1–R12. DOI:10.1152/ajpregu.00323.2002

- Forsen T, Eriksson JG, Tuomilehto J, Teramo K, Osmond C, Barker DJP (1997). Mother's weight in pregnancy and coronary heart disease in a cohort of Finnish men: follow up study. *BMJ* 315:837–840. DOI:10.1136/bmj.315.7112.837
- Förstermann U, Sessa WC (2012). Nitric oxide synthases: Regulation and function. *Eur Heart J* 33:829–837. DOI:10.1093/eurheartj/ehr304
- Fraser A, Tilling K, MacDonald-Wallis C, Sattar N, Brion MJ, Benfield L, Ness A, Deanfield J, Hingorani A, Nelson SM, Smith GD, Lawlor DA (2010). Association of maternal weight gain in pregnancy with offspring obesity and metabolic and vascular traits in childhood. *Circulation* 121:2557–2564. DOI:10.1161/CIRCULATIONAHA.109.906081
- Fuchs F, Senat MV, Rey E, Balayla J, Chaillet N, Bouyer J, Audibert F (2017). Impact of maternal obesity on the incidence of pregnancy complications in France and Canada. *Sci Rep* 7. DOI:10.1038/s41598-017-11432-5
- Gaillard R, Steegers EAP, Duijts L, Felix JF, Hofman A, Franco OH, Jaddoe VW V (2014). Childhood cardiometabolic outcomes of maternal obesity during pregnancy: The generation R study. *Hypertension* 63:683–691. DOI:10.1161/HYPERTENSIONAHA.113.02671
- Galán M, Kassan M, Kadowitz PJ, Trebak M, Belmadani S, Matrougui K (2014). Mechanism of endoplasmic reticulum stress-induced vascular endothelial dysfunction. *Biochim Biophys Acta - Mol Cell Res* 1843:1063–1075. DOI:10.1016/j.bbamcr.2014.02.009
- García-Cardena G, Oh P, Liu J, Schnitzer J, Sessa WC (1996). Targeting of nitric oxide synthase to endothelial caveolae via palmitoylation: Implications for nitric oxide signaling. *Proc Natl Acad Sci U S A* 93:6448–6453. DOI:10.1073/pnas.93.13.6448
- Garg AD, Kaczmarek A, Krysko O, Vandenabeele P, Krysko D V, Agostinis P (2012). ER stress-induced inflammation: Does it aid or impede disease progression? *Trends Mol Med* 18:589–598. DOI:10.1016/j.molmed.2012.06.010
- Georgescu A, Popov D, Constantin A, Nemezc M, Alexandru N, Cochior D, Tudor A (2011). Dysfunction of human subcutaneous fat arterioles in obesity alone or obesity associated with Type 2 diabetes. *Clin Sci (Lond)* 120:463–472. DOI:10.1042/CS20100355
- Ghemrawi R, Battaglia-Hsu S-F, Arnold C (2018). Endoplasmic reticulum stress in metabolic disorders. *Cells* 7:63. DOI:10.3390/cells7060063
- Ghoshal P, Rajendran M, Odo N, Ikuta T (2014). Glycosylation inhibitors efficiently inhibit P-selectin-mediated cell adhesion to endothelial cells. *PLoS One* 9:e99363. DOI:10.1371/journal.pone.0099363
- Giam B, Kuruppu S, Head G, Kaye D, Rajapakse N (2016). Effects of dietary L-arginine on nitric oxide bioavailability in obese normotensive and obese hypertensive subjects. *Nutrients* 8:364. DOI:10.3390/nu8060364
- Gimbrone MA, García-Cardena G (2016). Endothelial cell dysfunction and the pathobiology of atherosclerosis. *Circ Res* 118:620–636. DOI:10.1161/CIRCRESAHA.115.306301

- Gluckman PD, Hanson MA, Cooper C, Thornburg KL (2008). Effect of in utero and early-life conditions on adult health and disease. *N Engl J Med* 359:61–73. DOI:10.1056/NEJMra0708473
- Godfrey KM, Reynolds RM, Prescott SL, Nyirenda M, Jaddoe VWV, Eriksson JG, Broekman BFP (2017). Influence of maternal obesity on the long-term health of offspring. *Lancet Diabetes Endocrinol* 5:53–64. DOI:10.1016/S2213-8587(16)30107-3
- González M, Flores C, Pearson JD, Casanello P, Sobrevia L (2004). Cell signalling-mediating insulin increase of mRNA expression for cationic amino acid transporters-1 and -2 and membrane hyperpolarization in human umbilical vein endothelial cells. *Pflugers Arch* 448:383–394. DOI:10.1007/s00424-004-1261-x
- González M, Gallardo V, Rodríguez N, Salomón C, Westermeier F, Enrique G-G, Abarzúa F, Leiva A, Casanello P, Sobrevia L (2011). Insulin-stimulated L-arginine transport requires SLC7A1 gene expression and is associated with human umbilical vein relaxation. *J Cell Physiol* 226:2916–2924. DOI:10.1002/jcp.22635
- Gregor MF, Yang L, Fabbrini E, Mohammed BS, Eagon JC, Hotamisligil GS, Klein S (2009). Endoplasmic reticulum stress is reduced in tissues of obese subjects after weight loss. *Diabetes* 58:693–700. DOI:10.2337/db08-1220
- Griffiths SK, Campbell JP (2015). Placental structure, function and drug transfer. *Contin Educ Anaesthesia, Crit Care Pain* 15:84–89. DOI:10.1093/bjaceaccp/mku013
- Gruber H, Mayer C, Mangge H, Fauler G, Grandits N, Wilders-Truschnig M (2008). Obesity reduces the bioavailability of nitric oxide in juveniles. *Int J Obes (Lond)* 32:826–831. DOI:10.1038/sj.ijo.0803795
- Guenard F, Deshaies Y, Cianflone K, Kral JG, Marceau P, Vohl M (2013). Differential methylation in glucoregulatory genes of offspring born before vs. after maternal gastrointestinal bypass surgery. *Proc Natl Acad Sci* 110:11439–11444. DOI:10.1073/pnas.1216959110
- Guo FJ, Xiong Z, Lu X, Ye M, Han X, Jiang R (2014). ATF6 upregulates XBP1S and inhibits ER stress-mediated apoptosis in osteoarthritis cartilage. *Cell Signal* 26:332–342. DOI:10.1016/j.cellsig.2013.11.018
- Guzmán-Gutiérrez E, Armella A, Toledo F, Pardo F, Leiva A, Sobrevia L (2016). Insulin requires A1 adenosine receptors expression to reverse gestational diabetes-increased L-arginine transport in human umbilical vein endothelium. *Purinergic Signal* 12:175–190. DOI:10.1007/s11302-015-9491-2
- Hardy OT, Czech MP, Corvera S (2012). What causes the insulin resistance underlying obesity? *Curr Opin Endocrinol Diabetes Obes* 19:81–87. DOI:10.1097/MED.0b013e3283514e13
- Hardy T a, May JM (2002). Coordinate regulation of L-arginine uptake and nitric oxide synthase activity in cultured endothelial cells. *Free Radic Biol Med* 32:122–131. DOI:10.1159/000353883

- Hegedus Z, Czibula A, Kiss-Toth E (2007). Tribbles: A family of kinase-like proteins with potent signalling regulatory function. *Cell Signal* 19:238–250. DOI:10.1016/j.cellsig.2006.06.010
- Hellermann GR, Solomonson LP (1997). Calmodulin promotes dimerization of the oxygenase domain of human endothelial nitric-oxide synthase. *J Biol Chem* 272:12030–12034. DOI:10.1074/jbc.272.18.12030
- Hemmings BA, Restuccia DF (2012). PI3K-PKB/Akt pathway. In: *Cold Spring Harbor Perspectives in Biology*. Cantley L, Hunter T, Sever R, Thorner J (eds) Cold Spring Harbor Laboratory Press, p 4:a011189 DOI:10.1101/cshperspect.a011189
- Hetz C, Chevet E, Oakes SA (2015). Proteostasis control by the unfolded protein response. *Nat Cell Biol* 17:829–838. DOI:10.1038/ncb3184
- Hirosumi J, Tuncman G, Chang L, Görgün CZ, Uysal KT, Maeda K, Karin M, Hotamisligil GS (2002). A central role for JNK in obesity and insulin resistance. *Nature* 420:333–336. DOI:10.1038/nature01137
- Hochner H, Friedlander Y, Calderon-Margalit R, Meiner V, Sagy Y, Avgil-Tsadok M, Burger A, Manor O, Savitsky B, Siscovick DS, Manor O (2012). Associations of maternal prepregnancy body mass index and gestational weight gain with adult offspring cardiometabolic risk factors: the Jerusalem perinatal family follow-up study. *Circulation* 125:1381–1389. DOI:10.1161/circulationaha.111.070060
- Hong J, Kim K, Park E, Lee J, Markofski MM, Marrelli SP, Park Y (2018). Exercise ameliorates endoplasmic reticulum stress-mediated vascular dysfunction in mesenteric arteries in atherosclerosis. *Sci Rep* 8:7938. DOI:10.1038/s41598-018-26188-9
- Howell KR, Powell TL (2017). Effects of maternal obesity on placental function and fetal development. *Reproduction* 153:R97–R108. DOI:10.1530/REP-16-0495
- Hu P, Han Z, Couvillon AD, Kaufman RJ, Exton JH (2006). Autocrine tumor necrosis factor alpha links endoplasmic reticulum stress to the membrane death receptor pathway through IRE1 - mediated NF- $\kappa$ B activation and down-regulation of TRAF2 expression. *Mol Cell Biol* 26:3071–3084. DOI:10.1128/MCB.26.8.3071-3084.2006
- Huang CC, Li Y, Lopez AB, Chiang C-M, Kaufman RJ, Snider MD, Hatzoglou M, Huang C, Lopez A (2010). Temporal regulation of Cat-1 (cationic amino acid transporter-1) gene transcription during endoplasmic reticulum stress. *Biochem J* July 1:215–224. DOI:10.1042/BJ20100286
- Huang PL (2009). ENOS, metabolic syndrome and cardiovascular disease. *Trends Endocrinol Metab* 20:295–302. DOI:10.1016/j.tem.2009.03.005
- Huang X, Liu G, Guo J, Su Z (2018). The PI3K/AKT pathway in obesity and type 2 diabetes. *Int J Biol Sci* 14:1483–1496. DOI:10.7150/ijbs.27173
- Institute of Medicine (IOM), National Research Council (NRC) (2009). *Weight Gain During Pregnancy: Reexamining the Guidelines*. Washington, DC Natl Acad Press. DOI:10.17226/12584

- Jaffe EA, Nachman RL, Becker CG, Minick CR (1973). Culture of human endothelial cells derived from umbilical veins. Identification by morphologic and immunologic criteria. *J Clin Invest* 52:2745–2756. DOI:10.1172/JCI107470
- Janus A, Szahidewicz-Krupska E, Mazur G, Doroszko A (2016). Insulin resistance and endothelial dysfunction constitute a common therapeutic target in cardiometabolic disorders. *Mediators Inflamm* 2016. DOI:10.1155/2016/3634948
- Jiang D, Niwa M, Koong AC (2015). Targeting the IRE1 $\alpha$ -XBP1 branch of the unfolded protein response in human diseases. *Semin Cancer Biol* 33:48–56. DOI:10.1016/j.semcancer.2015.04.010
- Kaar JL, Crume T, Brinton JT, Bischoff KJ, McDuffie R, Dabelea D (2014). Maternal obesity, gestational weight gain, and offspring adiposity: The exploring perinatal outcomes among children study. *J Pediatr* 165:509–515. DOI:10.1016/j.jpeds.2014.05.050
- Kaplon RE, Chung E, Reese L, Cox-York K, Seals DR, Gentile CL (2013). Activation of the unfolded protein response in vascular endothelial cells of nondiabetic obese adults. *J Clin Endocrinol Metab* 98:E1505–E1509. DOI:10.1210/jc.2013-1841
- Kassan M, Galán M, Partyka M, Saifudeen Z, Henrion D, Trebak M, Matrougui K (2012). Endoplasmic reticulum stress is involved in cardiac damage and vascular endothelial dysfunction in hypertensive mice. *Arterioscler Thromb Vasc Biol* 32:1652–1661. DOI:10.1161/ATVBAHA.112.249318
- Kassan M, Vikram A, Li Q, Kim YR, Kumar S, Gabani M, Liu J, Jacobs JS, Irani K (2017). MicroRNA-204 promotes vascular endoplasmic reticulum stress and endothelial dysfunction by targeting Sirtuin1. *Sci Rep* 7:9308. DOI:10.1038/s41598-017-06721-y
- Katz A, Nambi SS, Mather K, Baron AD, Follmann DA, Sullivan G, Quon MJ (2000). Quantitative insulin sensitivity check index: A simple, accurate method for assessing insulin sensitivity in humans. *J Clin Endocrinol Metab* 85:2402–2410. DOI:10.1210/jcem.85.7.6661
- Kilberg MS, Shan J, Su N (2009). ATF4-dependent transcription mediates signaling of amino acid limitation. *Trends Endocrinol Metab* 20:436–443. DOI:10.1016/j.tem.2009.05.008
- Kim J, Jang HJ, Hwang DH (2015). Toll-like receptor 4-induced endoplasmic reticulum stress contributes to impairment of vasodilator action of insulin. *Am J Physiol - Endocrinol Metab* 309:E767–E776. DOI:10.1152/ajpendo.00369.2015
- Kim J, Montagnani M, Koh KK, Quon MJ (2006). Reciprocal relationships between insulin resistance and endothelial dysfunction: molecular and pathophysiological mechanisms. *Circulation* 113:1888–1904. DOI:10.1161/CIRCULATIONAHA.105.563213
- Kim NN, Cox JD, Baggio RF, Emig FA, Mistry SK, Harper SL, Speicher DW, Morris SM, Ash DE, Traish A, Christianson DW (2001). Probing erectile function: S-(2-boronoethyl)-L-cysteine binds to arginase as a transition state analogue and enhances smooth muscle relaxation in human penile corpus cavernosum. *Biochemistry* 40:2678–2688. DOI:10.1021/bi002317h

- Koh HJ, Toyoda T, Didesch MM, Lee MY, Sleeman MW, Kulkarni RN, Musi N, Hirshman MF, Goodyear LJ (2013). Tribbles 3 mediates endoplasmic reticulum stress-induced insulin resistance in skeletal muscle. *Nat Commun* 4:1871. DOI:10.1038/ncomms2851
- Komar AA, Hatzoglou M (2011). Cellular IRES-mediated translation: The war of ITAFs in pathophysiological states. *Cell Cycle* 10:229–240. DOI:10.4161/cc.10.2.14472
- König A, Corbacioglu S, Ballmaier M, Welte K (1997). Downregulation of c-kit expression in human endothelial cells by inflammatory stimuli. *Blood* 90:148–155.
- Kothari H, Pendurthi UR, Rao LVM (2013). Tissue factor purified from different cellular sources and non-glycosylated tissue factor show similar procoagulant activity. *J Thromb Haemost* 11:2066–2068. DOI:10.1111/jth.12407
- Kral JG, Biron S, Simard S, Hould FR-S, Fane Lebel S, Marceau S, Marceau P (2006). Large Maternal Weight loss from obesity surgery prevents transmission of obesity to children.pdf. *Pediatrics* 118:e1644–e1649. DOI:10.1542/peds.2006-1379
- Kraskiewicz H, Fitzgerald U (2012). InterfERing with endoplasmic reticulum stress. *Trends Pharmacol Sci* 33:53–63. DOI:10.1016/j.tips.2011.10.002
- Krause BJ, Carrasco-Wong I, Caniguir A, Carvajal J, Farías M, Casanello P (2013). Endothelial eNOS/arginase imbalance contributes to vascular dysfunction in IUGR umbilical and placental vessels. *Placenta* 34:20–28. DOI:10.1016/j.placenta.2012.09.015
- Krause BJ, Prieto CP, Muñoz-Urrutia E, San Martín S, Sobrevia L, Casanello P (2012). Role of arginase-2 and eNOS in the differential vascular reactivity and hypoxia-induced endothelial response in umbilical arteries and veins. *Placenta* 33:360–366. DOI:10.1016/j.placenta.2012.02.006
- Kumashiro N, Erion DM, Zhang D, Kahn M, Beddow SA, Chu X, Still CD, Gerhard GS, Han X, Dziura J, Petersen KF, Samuel VT, Shulman GI (2011). Cellular mechanism of insulin resistance in nonalcoholic fatty liver disease. *Proc Natl Acad Sci* 108:16381–16385. DOI:10.1073/pnas.1113359108
- Kurz S, Harrison D (1997). Insulin and the arginine paradox. *J Clin Invest* 99:369–370.
- Lassance L, Haghiac M, Leahy P, Basu S, Minium J, Zhou J, Reider M, Catalano PM, Hauguel-De Mouzon S (2015). Identification of early transcriptome signatures in placenta exposed to insulin and obesity. *Am J Obstet Gynecol* 212:647.e1–11. DOI:10.1016/j.ajog.2015.02.026
- Lee BR, Chang SY, Hong EH, Kwon BE, Kim HM, Kim YJ, Lee J, Cho HJ, Cheon JH, Ko HJ (2014). Elevated endoplasmic reticulum stress reinforced immunosuppression in the tumor microenvironment via myeloid-derived suppressor cells. *Oncotarget* 5. DOI:10.18632/oncotarget.2589
- Leiva A, De Medina CD, Salsoso R, Sáez T, San Martín S, Abarzúa F, Farías M, Guzmán-Gutiérrez E, Pardo F, Sobrevia L (2013). Maternal hypercholesterolemia in pregnancy associates with

umbilical vein endothelial dysfunction: Role of endothelial nitric oxide synthase and arginase II. *Arterioscler Thromb Vasc Biol* 33:2444–2453. DOI:10.1161/ATVBAHA.113.301987

Lenna S, Han R, Trojanowska M (2014). Endoplasmic reticulum stress and endothelial dysfunction. *IUBMB Life* 66:530–537. DOI:10.1002/iub.1292

Lennartsson J, Rönstrand L, 2012. Stem cell factor receptor/c-Kit: From basic Science to clinical implications. *Physiol Rev* 92:1619–1649. DOI:10.1152/physrev.00046.2011

Lew MJ, McPherson GA (1996). Isolated tissue techniques. In: *The Pharmacology of Vascular Smooth Muscle*. Garland CJ, Angus J (eds) Oxford University Press, Oxford, p 25–41 DOI:10.1093/acprof:oso/9780192623874.003.0002 Abstract

Li C, Huang W, Harris MB, Goolsby JM, Venema RC (2005). Interaction of the endothelial nitric oxide synthase with the CAT-1 arginine transporter enhances NO release by a mechanism not involving arginine transport. *Biochem J* 386:567–574.

Liew CW, Bochenski J, Kawamori D, Hu J, Leech CA, Wanic K, Malecki M, Warram JH, Qi L, Krolewski AS, Kulkarni RN (2010). The pseudokinase tribbles homolog 3 interacts with ATF4 to negatively regulate insulin exocytosis in human and mouse  $\beta$  cells. *J Clin Invest* 120:2876–2888. DOI:10.1172/JCI36849

Lima AF, Ropelle ER, Pauli JR, Cintra DE, Frederico MJS, Pinho RA, Velloso LA, De Souza CT (2009). Acute exercise reduces insulin resistance-induced TRB3 expression and amelioration of the hepatic production of glucose in the liver of diabetic mice. *J Cell Physiol* 221:92–97. DOI:10.1002/jcp.21833

Liong S, Lappas M (2015). Endoplasmic reticulum stress is increased in adipose tissue of women with gestational diabetes. *PLoS One* 10:e0122633. DOI:10.1371/journal.pone.0122633

Liong S, Lappas M (2016). Endoplasmic reticulum stress regulates inflammation and insulin resistance in skeletal muscle from pregnant women. *Mol Cell Endocrinol* 425:11–25. DOI:10.1016/j.mce.2016.02.016

Liu J, Wu X, Franklin JL, Messina JL, Hill HS, Moellering DR, Walton RG, Martin M, Garvey WT (2010). Mammalian Tribbles homolog 3 impairs insulin action in skeletal muscle: role in glucose-induced insulin resistance. *Am J Physiol Metab* 298:E565–E576. DOI:10.1152/ajpendo.00467.2009

Longtine MS, Nelson DM (2011). Placental dysfunction and fetal programming: The importance of placental size, shape, histopathology, and molecular composition. *Semin Reprod Med* 29:187–196. DOI:10.1055/s-0031-1275515

Lopez AB, Wang C, Huang CC, Yaman I, Li Y, Chakravarty K, Johnson PF, Chiang CM, Snider MD, Wek RC, Hatzoglou M (2007). A feedback transcriptional mechanism controls the level of the arginine/lysine transporter cat-1 during amino acid starvation. *Biochem J* 402:163–173. DOI:10.1042/BJ20060941

- Luiking YC, Deutz NEP (2007). Biomarkers of arginine and lysine excess. *J Nutr* 137:1662S-1668S. DOI:10.1093/jn/137.6.1662S
- M. Breen D, Giacca A (2011). Effects of Insulin on the Vasculature. *Curr Vasc Pharmacol* 9:321–332. DOI:10.2174/157016111795495558
- Maamoun H, Abdelsalam S, Zeidan A, Korashy H, Agouni A (2019). Endoplasmic Reticulum Stress: A Critical Molecular Driver of Endothelial Dysfunction and Cardiovascular Disturbances Associated with Diabetes. *Int J Mol Sci* 20:1658. DOI:10.3390/ijms20071658
- Mahadevan NR, Rodvold J, Sepulveda H, Rossi S, Drew AF, Zanetti M (2011). Transmission of endoplasmic reticulum stress and pro-inflammation from tumor cells to myeloid cells. *Proc Natl Acad Sci* 108:6561–6566. DOI:10.1073/pnas.1008942108
- Mahameed M, Wilhelm T, Darawshi O, Obiedat A, Tommy WS, Chintha C, Schubert T, Samali A, Chevet E, Eriksson LA, Huber M, Tirosh B (2019). The unfolded protein response modulators GSK2606414 and KIRA6 are potent KIT inhibitors. *Cell Death Dis* 10:300. DOI:10.1038/s41419-019-1523-3
- Mahoney WC, Duksin D (1980). Separation of tunicamycin homologues by reversed-phase high-performance liquid chromatography. *J Chromatogr* 198:506–510.
- Majumder M, Yaman I, Gaccioli F, Zeenko V V, Wang C, Caprara MG, Venema RC, Komar AA, Snider MD, Hatzoglou M (2009). The hnRNA-binding proteins hnRNP L and PTB are required for efficient translation of the Cat-1 arginine/lysine transporter mRNA during amino acid starvation. *Mol Cell Biol* 29:2899–2912. DOI:10.1128/mcb.01774-08
- Mamun AA, O’Callaghan M, Callaway L, Williams G, Najman J, Lawlor DA (2009). Associations of gestational weight gain with offspring body mass index and blood pressure at 21 years of age: evidence from a birth cohort study. *Circulation* 119:1720–1727. DOI:10.1161/CIRCULATIONAHA.108.813436
- Mandal S, Causevic A, Dzudzevic-Cancar H, Semiz S (2017). Free fatty acid profile in Type 2 diabetic subjects with different control of glycemia. In: *CMBEBIH 2017*. Springer, Singapore, p 781–786 DOI:10.1007/978-981-10-4166-2\_117
- Mann GE, Yudilevich DL, Sobrevia L (2003). Regulation of amino acid and glucose transporters in endothelial and smooth muscle cells. *Physiol Rev* 83:183–252. DOI:10.1152/physrev.00022.2002
- Manrique C, Lastra G, Sowers JR (2014). New insights into insulin action and resistance in the vasculature. *Ann N Y Acad Sci* 1311:138–150. DOI:10.1111/nyas.12395
- Marinho R, Mekary RA, Muñoz VR, Gomes RJ, Pauli JR, de Moura LP (2015). Regulation of hepatic TRB3/Akt interaction induced by physical exercise and its effect on the hepatic glucose production in an insulin resistance state. *Diabetol Metab Syndr* 7:67. DOI:10.1186/s13098-015-0064-x

- Martens DS, Plusquin M, Gyselaers W, De Vivo I, Nawrot TS (2016). Maternal pre-pregnancy body mass index and newborn telomere length. DOI:10.1186/s12916-016-0689-0
- Martyn JAJ, Kaneki M, Yasuhara S (2009). Obesity-induced insulin resistance and hyperglycemia. *Anesthesiology* 109:137–148. DOI:10.1097/aln.0b013e3181799d45
- Mas M (2009). A close look at the endothelium: Its role in the regulation of vasomotor tone. *Eur Urol Suppl* 8:48–57. DOI:10.1016/j.eursup.2008.10.011
- Mather KJ, Steinberg HO, Baron AD (2013). Insulin resistance in the vasculature. *J Clin Invest* 123:1003–1004. DOI:10.1172/JCI67166
- Matsushita E, Asai N, Enomoto A, Kawamoto Y, Kato T, Mii S, Maeda K, Shibata R, Hattori S, Hagikura M, Takahashi K, Sokabe M, Murakumo Y, Murohara T, Takahashi M (2011). Protective role of Gipiie, a Girdin family protein, in endoplasmic reticulum stress responses in endothelial cells. *Mol Biol Cell* 22:736–747. DOI:10.1091/mbc.E10-08-0724
- Matsui J, Wakabayashi T, Asada M, Yoshimatsu K, Okada M (2004). Stem cell factor/c-kit signaling promotes the survival, migration, and capillary tube formation of human umbilical vein endothelial cells. *J Biol Chem* 279, 18600–18607. DOI:10.1074/jbc.M311643200
- Matthews DR, Hosker JP, Rudenski AS, Naylor BA, Treacher DF, Turner RC (1985). Homeostasis model assessment: insulin resistance and  $\beta$ -cell function from fasting plasma glucose and insulin concentrations in man. *Diabetologia* 28:412–419. DOI:10.1007/BF00280883
- McArdle MA, Finucane OM, Connaughton RM, McMorrow AM, Roche HM (2013). Mechanisms of obesity-induced inflammation and insulin resistance: Insights into the emerging role of nutritional strategies. *Front Endocrinol (Lausanne)* 4. DOI:10.3389/fendo.2013.00052
- Mcdonald KK, Zharikov S, Block ER, Kilberg MS (1997). A caveolar complex between the cationic amino acid transporter 1 and endothelial nitric-oxide synthase may. *J Biol Chem* 272:31213–31216. DOI:10.1074/jbc.272.50.31213
- Mendizábal Y, Llorens S, Nava E (2013). Hypertension in metabolic syndrome: Vascular pathophysiology. *Int J Hypertens* 2013. DOI:10.1155/2013/230868
- Michel JB, Feron O, Sase K, Prabhakar P, Michel T (1997). Caveolin versus calmodulin. Counterbalancing allosteric modulators of endothelial nitric oxide synthase. *J Biol Chem* 272:25907–25912. DOI:10.1074/JBC.272.41.25907
- Mingrone G, Manco M, Mora ME, Guidone C, Iaconelli A, Gniuli D, Leccesi L, Chiellini C, Ghirlanda G (2008). Influence of maternal obesity on insulin sensitivity and secretion in offspring. *Diabetes Care* 31:1872–1876. DOI:10.2337/dc08-0432.
- Ministerio de Salud (MINSAL), Gobierno de Chile,. (2015). *Guia Perinatal 2015*.
- Ministerio de Salud (MINSAL), Gobierno de Chile. (2017). *Encuesta Nacional de Salud 2016-2017: Primeros resultados*.

- Mirmiran P, Bahadoran Z, Ghasemi A, Azizi F (2016). The association of dietary L-arginine intake and serum nitric oxide metabolites in adults: A population-based study. *Nutrients* 8. DOI:10.3390/nu8050311
- Mitanchez-Mokhtari D, Lahlou N, Kieffer F, Magny J-F, Roger M, Voyer M (2004). Both relative insulin resistance and defective islet beta-cell processing of proinsulin are responsible for transient hyperglycemia in extremely preterm infants. *Pediatrics* 113:537–541. DOI:10.1542/PEDS.113.3.537
- Mukherjee A, Morales-Scheihing D, Butler PC, Soto C (2015). Type 2 diabetes as a protein misfolding disease. *Trends Mol Med* 21:439–449. DOI:10.1016/j.molmed.2015.04.005
- Mulvany MJ, Halpern W (1977). Contractile properties of small arterial resistance vessels in spontaneously hypertensive and normotensive rats. *Circ Res* 41:19–26.
- Muniyappa R, Montagnani M, Koh KK, Quon MJ (2007). Cardiovascular actions of insulin. *Endocr Rev* 28:463–491. DOI:10.1210/er.2007-0006
- Muniyappa R, Quon MJ (2007). Insulin action and insulin resistance in vascular endothelium. *Curr Opin Clin Nutr Metab Care* 10:523–530. DOI:10.1097/MCO.0b013e32819f8ecd
- Muniyappa R, Sowers JR (2013). Role of insulin resistance in endothelial dysfunction. *Rev Endocr Metab Disord* 14:5–12. DOI:10.1007/s11154-012-9229-1
- Murugan D, Lau YS, Lau WC, Mustafa MR, Huang Y (2015). Angiotensin 1-7 protects against angiotensin II-induced endoplasmic reticulum stress and endothelial dysfunction via Mas receptor. *PLoS One* 10. DOI:10.1371/journal.pone.0145413
- Naruse K, Rask-madsen C, Takahara N, Ha S, Suzuma K, Way KJ, Jacobs JRC, Clermont AC, Ueki K, Ohshiro Y, Zhang J, Goldfine AB, King GL (2006). Function in obesity-associated insulin resistance. *Diabetes* 55:691–698.
- Nishitoh H (2012). CHOP is a multifunctional transcription factor in the ER stress response. *J Biochem* 151:217–219. DOI:10.1093/jb/mvr143
- Noakes TD (2018). So what comes first: The obesity or the insulin resistance? And which is more important? *Clin Chem* 64:7–9. DOI:10.1373/clinchem.2017.282962
- Nohr EA, Vaeth M, Baker JL, Sørensen TI, Olsen J, Rasmussen KM (2008). Combined associations of prepregnancy body mass index and gestational weight gain with the outcome of pregnancy. *Am J Clin Nutr* 87:1750–1759.
- Nourbakhsh M, Sharifi R, Ghorbanhosseini SS, Javad A, Ahmadpour F, Razzaghy Azar M, Larijani B (2017). Evaluation of plasma TRB3 and sestrin 2 levels in obese and normal-weight children. *Child Obes* 13:409–414. DOI:10.1089/chi.2017.0082
- O'Reilly JR, Reynolds RM (2013). The risk of maternal obesity to the long-term health of the offspring. *Clin Endocrinol (Oxf)* 78:9–16. DOI:10.1111/cen.12055

- Ohoka N, Yoshii S, Hattori T, Onozaki K, Hayashi H (2005). TRB3, a novel ER stress-inducible gene, is induced via ATF4–CHOP pathway and is involved in cell death. *EMBO J* 24:1243–1255. DOI:10.1038/sj.emboj.7600596
- Osowski CM, Urano F (2011). Measuring ER stress and the unfolded protein response using mammalian tissue culture system. *Methods Enzymol* 490:71–92. DOI:10.1016/B978-0-12-385114-7.00004-0
- Ozcan L, Cristina De Souza J, Harari AA, Backs J, Olson EN, Tabas I (2013). Activation of calcium/calmodulin-dependent protein kinase II in obesity mediates suppression of hepatic insulin signaling. *Cell Metab* 18:803–815. DOI:10.1016/j.cmet.2013.10.011
- Ozcan L, Ghorpade DS, Zheng Z, de Souza JC, Chen K, Bessler M, Bagloo M, Schrope B, Pestell R, Tabas I (2016). Hepatocyte DACH1 is increased in obesity via nuclear exclusion of HDAC4 and promotes hepatic insulin resistance. *Cell Rep* 15:2214–2225. DOI:10.1016/j.celrep.2016.05.006
- Ozcan U, Cao Q, Yilmaz E, Lee A-H, Iwakoshi NN, Ozdelen E, Tuncman G, Görgün C, Glimcher LH, Hotamisligil GS (2004). Endoplasmic reticulum stress links obesity, insulin action, and type 2 diabetes. *Science* 306:457–461. DOI:10.1126/science.1103160
- Pardo F, Silva L, Sáez T, Salsoso R, Gutiérrez J, Sanhueza C, Leiva A, Sobrevia L (2015). Human supraphysiological gestational weight gain and fetoplacental vascular dysfunction. *Int J Obes* 39:1264–1273. DOI:10.1038/ijo.2015.57
- Park SW, Zhou Y, Lee J, Lu A, Sun C, Chung J, Ueki K, Ozcan U (2010). The regulatory subunits of PI3K, p85 $\alpha$  and p85 $\beta$ , interact with XBP-1 and increase its nuclear translocation. *Nat Med* 16:429–437. DOI:10.1038/nm.2099
- Penfold NC, Ozanne SE (2015). Developmental programming by maternal obesity in 2015: Outcomes, mechanisms, and potential interventions. *Horm Behav* 76:143–152. DOI:10.1016/j.yhbeh.2015.06.015
- Di Pietro N, Marcovecchio ML, Di Silvestre S, de Giorgis T, Cordone VGP, Lanuti P, Chiarelli F, Bologna G, Mohn A, Pandolfi A (2017). Plasma from pre-pubertal obese children impairs insulin stimulated Nitric Oxide (NO) bioavailability in endothelial cells: Role of ER stress. *Mol Cell Endocrinol* 443:52–62. DOI:10.1016/j.mce.2017.01.001
- Pirkola J, Pouta A, Bloigu A, Hartikainen AL, Laitinen J, Järvelin MR, Väärasmäki M (2010). Risks of overweight and abdominal obesity at age 16 years associated with prenatal exposures to maternal prepregnancy overweight and gestational diabetes mellitus. *Diabetes Care* 33:1115–1121. DOI:10.2337/dc09-1871
- Prieto CP, Krause BJ, Quezada C, Martin RS, Sobrevia L, Casanello P (2011). Hypoxia-reduced nitric oxide synthase activity is partially explained by higher arginase-2 activity and cellular redistribution in human umbilical vein endothelium. *Placenta* 32:932–940. DOI:10.1016/j.placenta.2011.09.003

- Prieto D, Contreras C, Sanchez A (2014). Endothelial dysfunction, obesity and insulin resistance. *Curr Vasc Pharmacol* 12:412–426. DOI:10.2174/1570161112666140423221008
- Prudente S, Hribal ML, Flex E, Turchi F, Morini E, De Cosmo S, Bacci S, Tassi V, Cardellini M, Lauro R, Sesti G, Dallapiccola B, Trischitta V (2005). The functional Q84R polymorphism of mammalian tribbles homolog TRB3 is associated with insulin resistance and related cardiovascular risk in Caucasians from Italy. *Diabetes* 54:2807–2811. DOI:10.2337/diabetes.54.9.2807
- Prudente S, Sesti G, Pandolfi A, Andreozzi F, Consoli A, Trischitta V (2012). The mammalian tribbles homolog TRIB3, glucose homeostasis, and cardiovascular diseases. *Endocr Rev* 33:526–546. DOI:10.1210/er.2011-1042
- Rafikov R, Fonseca F V, Kumar S, Pardo D, Darragh C, Elms S, Fulton D, Black SM (2011). eNOS activation and NO function: Structural motifs responsible for the posttranslational control of endothelial nitric oxide synthase activity. *J Endocrinol* 210:271–284. DOI:10.1530/JOE-11-0083
- Rajapakse NW, Head GA, Kaye DM (2016). Say NO to obesity-related hypertension: Role of the L-arginine–nitric oxide pathway. *Hypertension*:1–8. DOI:10.1161/HYPERTENSIONAHA.116.06778
- Rajapakse NW, Karim F, Evans RG, Kaye DM, Head GA (2015). Augmented endothelial-specific L-arginine transport blunts the contribution of the sympathetic nervous system to obesity induced hypertension in mice. *PLoS One* 10:e0131424. DOI:10.1371/journal.pone.0131424
- Rajapakse NW, Karim F, Straznicki NE, Fernandez S, Evans RG, Head GA, Kaye DM (2014). Augmented endothelial-specific L-arginine transport prevents obesity-induced hypertension. *Acta Physiol* 212:39–48. DOI:10.1111/apha.12344
- Reynolds RM, Allan KM, Raja EA, Bhattacharya S, McNeill G, Hannaford PC, Sarwar N, Lee AJ, Bhattacharya S, Norman JE (2013). Maternal obesity during pregnancy and premature mortality from cardiovascular event in adult offspring: Follow-up of 1 323 275 person years. *BMJ* 347:f4539. DOI:10.1136/bmj.f4539
- Roberts VHJ, Frias AE, Grove KL (2015). Impact of maternal obesity on fetal programming of cardiovascular disease. *Physiology (Bethesda)* 30:224–231. DOI:10.1152/physiol.00021.2014
- Saben J, Lindsey F, Zhong Y, Thakali K, Badger TM, Andres A, Gomez-Acevedo H, Shankar K (2014). Maternal obesity is associated with a lipotoxic placental environment. *Placenta* 35:171–177. DOI:10.1016/j.placenta.2014.01.003
- Saben J, Zhong Y, Gomez-Acevedo H, Thakali KM, Borengasser SJ, Andres A, Shankar K (2013). Early growth response protein-1 mediates lipotoxicity-associated placental inflammation: role in maternal obesity. *Am J Physiol Endocrinol Metab* 305:E1-14. DOI:10.1152/ajpendo.00076.2013

- Sáez PJ, Shoji KF, Retamal MA, Harcha PA, Ramírez G, Jiang JX, von Bernhardt R, Sáez JC (2013). ATP is required and advances cytokine-induced gap junction formation in microglia in vitro. *Mediators Inflamm* 2013:216402. DOI:10.1155/2013/216402
- Salis ER, Reith DM, Wheeler BJ, Broadbent RS, Medicott NJ (2017). Insulin resistance, glucagon-like peptide-1 and factors influencing glucose homeostasis in neonates. *Arch Dis Child Fetal Neonatal Ed* 102:F162–F166. DOI:10.1136/archdischild-2015-309174
- Salsoso R, Guzmán-Gutiérrez E, Sáez T, Bugueño K, Ramírez MA, Farías M, Pardo F, Leiva A, Sanhueza C, Mate A, Vázquez C, Sobrevia L (2015). Insulin restores L-arginine transport requiring adenosine receptors activation in umbilical vein endothelium from late-onset preeclampsia. *Placenta* 36:287–296. DOI:10.1016/j.placenta.2014.12.007
- Sandoo A, Veldhuijzen van Zanten JJCS, Metsios GS, Carroll D, Kitas GD (2015). The endothelium and its role in regulating vascular tone. *Open Cardiovasc Med J* 4:302–312. DOI:10.2174/1874192401004010302
- Sankaralingam S, Xu H, Davidge ST (2010). Arginase contributes to endothelial cell oxidative stress in response to plasma from women with preeclampsia. *Cardiovasc Res* 85:194–203. DOI:10.1093/cvr/cvp277
- Sarno L, Maruotti GM, Saccone G, Morlando M, Sirico A, Martinelli P (2015). Maternal body mass index influences umbilical artery Doppler velocimetry in physiologic pregnancies. *Prenat Diagn* 35:125–128. DOI:10.1002/pd.4499
- Savage DB, Petersen KF, Shulman GI (2005). Mechanisms of insulin resistance in humans and possible links with inflammation. *Hypertension* 45:828–833. DOI:10.1161/01.HYP.0000163475.04421.e4
- Schneider D, Hernández C, Farías M, Uauy R, Krause BJ, Casanello P (2015). Oxidative stress as common trait of endothelial dysfunction in chorionic arteries from fetuses with IUGR and LGA. *Placenta* 36:552–558. DOI:10.1016/j.placenta.2015.02.003
- Sears B, Perry M (2015). The role of fatty acids in insulin resistance. *Lipids Health Dis* 14:121. DOI:10.1186/s12944-015-0123-1
- Shah AS, Urbina EM (2017). Vascular and endothelial function in youth with type 2 diabetes mellitus. *Curr Diab Rep* 17:36. DOI:10.1007/s11892-017-0869-0
- Shah D, Romero F, Duong M, Wang N, Paudyal B, Suratt BT, Kallen CB, Sun J, Zhu Y, Walsh K, Summer R (2015). Obesity-induced adipokine imbalance impairs mouse pulmonary vascular endothelial function and primes the lung for injury. *Sci Rep* 5:11362. DOI:10.1038/srep11362
- Shah D, Romero F, Guo Z, Sun J, Li J, Kallen CB, Naik UP, Summer R (2017). Obesity-induced endoplasmic reticulum stress causes lung endothelial dysfunction and promotes acute lung injury. *Am J Respir Cell Mol Biol* 57:204–215. DOI:10.1165/rcmb.2016-0310OC

- Sharma NK, Das SK, Mondal AK, Hackney OG, Chu WS, Kern PA, Rasouli N, Spencer HJ, Yao-Borengasser A, Elbein SC (2008). Endoplasmic reticulum stress markers are associated with obesity in nondiabetic subjects. *J Clin Endocrinol Metab* 93:4532–4541. DOI:10.1210/jc.2008-1001
- Shen J, Zhang Z, Chen K, Lu M, Qian Q, Liu P, Gao Q, Zhang C (2018). Prepregnancy obesity status and risks on pregnancy outcomes in Shanghai. *Medicine (Baltimore)* 97:e12670. DOI:10.1097/md.00000000000012670
- Sledzinski T, Sledzinski MI, Smolenski RT, Swierczynski J (2010). Increased serum nitric oxide concentration after bariatric surgery—a potential mechanism for cardiovascular benefit. *Obes Surg* 20:204–210. DOI:10.1007/s11695-009-0041-2
- Smith J, Cianflone K, Biron S, Hould FS, Lebel S, Marceau S, Lescelleur O, Biertho L, Simard S, Kral JG, Marceau P (2009). Effects of maternal surgical weight loss in mothers on intergenerational transmission of obesity. *J Clin Endocrinol Metab* 94:4275–4283. DOI:10.1210/jc.2009-0709
- Smith PK, Krohn RI, Hermanson GT, Mallia AK, Gartner FH, Provenzano MD, Fujimoto EK, Goeke NM, Olson BJ, Klenk DC (1985). Measurement of Protein Using Bicinchoninic Acid'. *Anal Biochem* 150:76–85.
- Sobrevia L, Myatt L, Rice G (2014). Diseases of pregnancy and fetal programming: Cell and molecular mechanisms. *Biomed Res Int* 2014. DOI:10.1155/2014/937050
- Soriano A, Pipitone N, Salvarani C (2017). Behçet's Disease. In: *The Heart in Rheumatic, Autoimmune and Inflammatory Diseases*. Academic Press, p 505–526 DOI:10.1016/B978-0-12-803267-1.00021-1
- Stewart FM, Freeman DJ, Ramsay JE, Greer IA, Caslake M, Ferrell WR (2007). Longitudinal assessment of maternal endothelial function and markers of inflammation and placental function throughout pregnancy in lean and obese mothers. *J Clin Endocrinol Metab* 92:969–975. DOI:10.1210/jc.2006-2083
- Stirrat L, Reynolds R (2014). Effects of maternal obesity on early and long-term outcomes for offspring. *Res Reports Neonatol* 4:43–53. DOI:10.2147/rn.s46783
- Stuebe AM, Forman MR, Michels KB (2009). Maternal-recalled gestational weight gain, pre-pregnancy body mass index, and obesity in the daughter. *Int J Obes (Lond)* 33:743–752. DOI:10.1038/ijo.2009.101
- Stuebe AM, Landon MB, Lai Y, Spong CY, Carpenter MW, Ramin SM, Casey B, Wapner RJ, Varner MW, Rouse DJ, Sciscione A, Catalano P, Harper M, Saade G, Sorokin Y, Peaceman AM, Tolosa JE, Eunice Kennedy Shriver National Institute of Child Health and Human Development Maternal-Fetal Medicine Units Network, Bethesda, MD (2012). Maternal BMI, glucose tolerance, and adverse pregnancy outcomes. *Am J Obstet Gynecol* 207:62.e1–7. DOI:10.1016/j.ajog.2012.04.035

- Suganya N, Bhakkiyalakshmi E, Suriyanarayanan S, Paulmurugan R, Ramkumar KM (2014). Quercetin ameliorates tunicamycin-induced endoplasmic reticulum stress in endothelial cells. *Cell Prolif* 47:231–240. DOI:10.1111/cpr.12102
- Sun X, Song M, Wang H, Zhou H, Wang F, Li Y, Zhang Y, Zhang W, Zhong M, Ti Y (2017). TRB3 gene silencing activates AMPK in adipose tissue with beneficial metabolic effects in obese and diabetic rats. *Biochem Biophys Res Commun* 488:22–28. DOI:10.1016/j.bbrc.2017.04.154
- Symons JD, McMillin SL, Riehle C, Tanner J, Palionyte M, Hillas E, Jones D, Cooksey RC, Birnbaum MJ, McClain DA, Zhang QJ, Gale D, Wilson LJ, Abel ED (2009). Contribution of insulin and Akt1 signaling to endothelial nitric oxide synthase in the regulation of endothelial function and blood pressure. *Circ Res* 104:1085–1094. DOI:10.1161/CIRCRESAHA.108.189316
- Tan HC, Roberts J, Catov J, Krishnamurthy R, Shypailo R, Bacha F (2015). Mother's pre-pregnancy BMI is an important determinant of adverse cardiometabolic risk in childhood. *Pediatr Diabetes* 16:419–426. DOI:10.1111/pedi.12273
- Thakali KM, Saben J, Faske JB, Lindsey F, Gomez-Acevedo H, Lowery CL, Badger TM, Andres A, Shankar K (2014). Maternal pregravid obesity changes gene expression profiles toward greater inflammation and reduced insulin sensitivity in umbilical cord. *Pediatr Res* 76:202–210. DOI:10.1038/pr.2014.72
- Toral M, Jimenez R, Montoro-Molina S, Romero M, Wangensteen R, Duarte J, Vargas F (2018). Thyroid hormones stimulate L-arginine transport in human endothelial cells. *J Endocrinol* 239:49–62. DOI:10.1530/JOE-18-0229
- Tousoulis D, Kampoli A-M, Tentolouris C, Papageorgiou N, Stefanadis C (2012). The role of nitric oxide on endothelial function. *Curr Vasc Pharmacol* 10:4–18. DOI:10.2174/157016112798829760
- Uemura A, Oku M, Mori K, Yoshida H (2009). Unconventional splicing of XBP1 mRNA occurs in the cytoplasm during the mammalian unfolded protein response. *J Cell Sci* 122:2877–2886. DOI:10.1242/jcs.040584
- Usuki F, Fujimura M, Yamashita A (2017). Endoplasmic reticulum stress preconditioning modifies intracellular mercury content by upregulating membrane transporters. *Sci Rep* 7:12390. DOI:10.1038/s41598-017-09435-3
- Vang S, Longley K, Steer CJ, Low WC (2014). The unexpected uses of urso- and tauroursodeoxycholic acid in the treatment of non-liver diseases. *Glob Adv Heal Med* 3:58–69. DOI:10.7453/gahmj.2014.017
- Vásquez G, Sanhueza F, Vásquez R, González M, San Martín R, Casanello P, Sobrevia L (2004). Role of adenosine transport in gestational diabetes-induced L-arginine transport and nitric oxide synthesis in human umbilical vein endothelium. *J Physiol* 560:111–122. DOI:10.1113/jphysiol.2004.068288

- Vendrell J, Maymó-Masip E, Tinahones F, García-España A, Megia A, Caubet E, García-Fuentes E, Chacón MR (2010). Tumor necrosis-like weak inducer of apoptosis as a proinflammatory cytokine in human adipocyte cells: Up-regulation in severe obesity is mediated by inflammation but not hypoxia. *J Clin Endocrinol Metab* 95:2983–2992. DOI:10.1210/jc.2009-2481
- Versari D, Daghini E, Viridis A, Ghiadoni L, Taddei S (2009). Endothelial dysfunction as a target for prevention of cardiovascular disease. *Diabetes Care* 32:S314–S321. DOI:10.2337/dc09-S330
- Villalobos-Labra R, Sáez P, Subiabre M, Silva L, Toledo F, Westermeier F, Pardo F, Farías M, Sobrevia L (2018a). Pre-pregnancy maternal obesity associates with endoplasmic reticulum stress in human umbilical vein endothelium. *Biochim Biophys Acta - Mol Basis Dis* 1864:3195–3210. DOI:10.1016/J.BBADIS.2018.07.007
- Villalobos-Labra R, Subiabre M, Toledo F, Pardo F, Sobrevia L (2018b). Endoplasmic reticulum stress and development of insulin resistance in adipose, skeletal, liver, and foetoplacental tissue in diabetes. *Mol Aspects Med* 2019:49-61. DOI:10.1016/j.mam.2018.11.001
- Voerman E, Santos S, Patro Golab B, Amiano P, Ballester F, Barros H, Bergström A, Charles M-A, Chatzi L, Chevrier C, Chrousos GP, Corpeleijn E, Costet N, Crozier S, Devereux G, Eggesbø M, Ekström S, Fantini MP, Farchi S, Forastiere F, Georgiu V, Godfrey KM, Gori D, Grote V, Hanke W, Hertz-Picciotto I, Heude B, Hryhorczuk D, Huang R-C, Inskip H, Iszatt N, Karvonen AM, Kenny LC, Koletzko B, Küpers LK, Lagström H, Lehmann I, Magnus P, Majewska R, Mäkelä J, Manios Y, McAuliffe FM, McDonald SW, Mehegan J, Mommers M, Morgen CS, Mori TA, Moschonis G, Murray D, Chaoimh CN, Nohr EA, Nybo Andersen A-M, Oken E, Oostvogels AJJM, Pac A, Papadopoulou E, Pekkanen J, Pizzi C, Polanska K, Porta D, Richiardi L, Rifas-Shiman SL, Ronfani L, Santos AC, Standl M, Stoltenberg C, Thiering E, Thijs C, Torrent M, Tough SC, Trnovec T, Turner S, van Rossem L, von Berg A, Vrijheid M, Vrijkotte TGM, West J, Wijga A, Wright J, Zvinchuk O, Sørensen TIA, Lawlor DA, Gaillard R, Jaddoe VW V. (2019). Maternal body mass index, gestational weight gain, and the risk of overweight and obesity across childhood: An individual participant data meta-analysis. *PLOS Med* 16:e1002744. DOI:10.1371/journal.pmed.1002744
- Walsh LK, Restaino RM, Neuringer M, Manrique C, Padilla J (2016). Administration of tauroursodeoxycholic acid prevents endothelial dysfunction caused by an oral glucose load HHS Public Access. *Clin Sci* 130:1881–1888. DOI:10.1042/CS20160501
- Wang CF, Yuan JR, Qin D, Gu JF, Zhao BJ, Zhang L, Zhao D, Chen J, Hou XF, Yang N, Bu WQ, Wang J, Li C, Tian G, Dong ZB, Feng L, Jia X Bin (2016). Protection of tauroursodeoxycholic acid on high glucose-induced human retinal microvascular endothelial cells dysfunction and streptozotocin-induced diabetic retinopathy rats. *J Ethnopharmacol* 185:162–170. DOI:10.1016/j.jep.2016.03.026
- Wang Y, Vera L, Fischer WH, Montminy M (2009). The CREB coactivator CRTC2 links hepatic ER stress and fasting gluconeogenesis. *Nature* 460:534–537. DOI:10.1038/nature08111

- Winters TM, Takahashi M, Lieber RL, Ward SR (2011). Whole muscle length-tension relationships are accurately modeled as scaled sarcomeres in rabbit hindlimb muscles. *J Biomech* 44:109–115. DOI:10.1016/j.jbiomech.2010.08.033
- World Health Organization (WHO) (2018). Obesity and Overweight. Fact sheet 311. World Health Organization. Geneva, Switzerland.
- Wu J, Rutkowski DT, Dubois M, Swathirajan J, Saunders T, Wang J, Song B, Yau GDY, Kaufman RJ (2007). ATF6 $\alpha$  Optimizes Long-Term Endoplasmic Reticulum Function to Protect Cells from Chronic Stress. *Dev Cell* 13:351–364. DOI:10.1016/j.devcel.2007.07.005
- Wu S, Gao X, Yang S, Meng M, Yang X, Ge B (2015). The role of endoplasmic reticulum stress in endothelial dysfunction induced by homocysteine thiolactone. *Fundam Clin Pharmacol* 29. DOI:10.1111/fcp.12101
- Wyatt AW, Steinert JR, Wheeler-Jones CP, Morgan AJ, Sugden D, Pearson JD, Sobrevia L, Mann GE (2002). Early activation of the p42/p44MAPK pathway mediates adenosine-induced nitric oxide production in human endothelial cells: a novel calcium-insensitive mechanism. *FASEB* 16:1584–1594. DOI:10.1096/fj.01-0125com
- Xue X, Piao JH, Nakajima A, Sakon-Komazawa S, Kojima Y, Mori K, Yagita H, Okumura K, Harding H, Nakano H (2005). Tumor necrosis factor  $\alpha$  (TNF $\alpha$ ) induces the unfolded protein response (UPR) in a reactive oxygen species (ROS)-dependent fashion, and the UPR counteracts ROS accumulation by TNF $\alpha$ . *J Biol Chem* 280:33917–33925. DOI:10.1074/jbc.M505818200
- Yan W, Frank CL, Korth MJ, Sopher BL, Novoa I, Ron D, Katze MG (2002). Control of PERK eIF2 $\alpha$  kinase activity by the endoplasmic reticulum stress-induced molecular chaperone P58IPK. *Proc Natl Acad Sci U S A* 99:15920–15925. DOI:10.1073/pnas.252341799
- Yang L, Calay ES, Fan J, Arduini A, Kunz RC, Gygi SP, Yalcin A, Fu S, Hotamisligil GS (2015). S-Nitrosylation links obesity-associated inflammation to endoplasmic reticulum dysfunction. *Science* (80- ) 349:500–506. DOI:10.1126/science.aaa0079
- Yang W, Han F, Gao X, Chen Y, Ji L, Cai X (2017). Relationship Between Gestational Weight Gain and Pregnancy Complications or Delivery Outcome. *Sci Rep* 7:12531. DOI:10.1038/s41598-017-12921-3
- Yang Y, Shang J, Liu H (2013). Role of endoplasmic reticular stress in aortic endothelial apoptosis induced by intermittent/persistent hypoxia. *Chin Med J (Engl)* 126:4517–4523.
- Yanguas-Casás N, Barreda-Manso MA, Nieto-Sampedro M, Romero-Ramírez L (2014). Tauroursodeoxycholic acid reduces glial cell activation in an animal model of acute neuroinflammation. *J Neuroinflammation* 11. DOI:10.1186/1742-2094-11-50
- Yilmaz E (2017). Endoplasmic reticulum stress and obesity. In: *Advances in Experimental Medicine and Biology*. Springer, Cham, p 261–276 DOI:10.1007/978-3-319-48382-5\_11

- Yoon YM, Lee JH, Yun SP, Han YS, Yun CW, Lee HJ, Noh H, Lee SJ, Han HJ, Lee SH (2016). Tauroursodeoxycholic acid reduces ER stress by regulating of Akt-dependent cellular prion protein. *Sci Rep* 6:39838. DOI:10.1038/srep39838
- Yung H wa, Alnæs-Katjavivi P, Jones CJP, El-Bacha T, Golic M, Staff AC, Burton GJ (2016). Placental endoplasmic reticulum stress in gestational diabetes: the potential for therapeutic intervention with chemical chaperones and antioxidants. *Diabetologia* 59:2240–2250. DOI:10.1007/s00125-016-4040-2
- Yuyun MF, Ng LL, Ng GA (2018). Endothelial dysfunction, endothelial nitric oxide bioavailability, tetrahydrobiopterin, and 5-methyltetrahydrofolate in cardiovascular disease. Where are we with therapy? *Microvasc Res* 119:7–12. DOI:10.1016/j.mvr.2018.03.012
- Zeng G, Quon MJ (1996). Insulin-stimulated production of nitric oxide is inhibited by Wortmannin: Direct measurement in vascular endothelial cells. *J Clin Invest* 98:894–898. DOI:10.1172/JCI118871